THE APPLICATION OF NUMERICAL MODELLING TECHNIQUES TO THE MECHANISMS OF RESERVOIR- AND MINING-INDUCED SEISMICITY

R. A. Beale

A thesis presented for the degree of
Doctor of Philosophy in the
University of Keele

January 1981

ABSTRACT

A survey of the 31 case histories of reservoir-induced seismicity has failed to indicate any relationships between the geology of an area and the induced tremors. The occurrence of induced seismicity is however related to the water height and, to a lesser extent, the water volume. Reservoir load stresses have been modelled by finite element technique, considering both pre-existing topographic and tectonic stress fields, and been found to result in stabilisation in all cases. The presence of hard, thin layers of rock has been found, however, to significantly increase the effect of both topographic and reservoir loads, and pre-impoundment stress relief due to fracture and creep can then result in reservoir load stress destabilisation. Consideration of the subsequent pore pressure diffusion away from the reservoir using a finite difference technique can explain the induced rock failure by reduction of effective stress. This is particularly so if allowance for initial pore compression is made, but the effect of fractures can be to considerably reduce the pore pressure effect.

The use of numerical modelling in practical examples of reservoir-induced seismicity is subject to a variety of limitations. Lack of field information is the main problem, but lack of computer storage and of an understanding of the mechanism(s) involved also contribute. The stored strain energy due to the water load at Koyna is found to be sufficient to account for most of the induced seismic activity, but tectonic stress must be utilised to a large extent. A triggering mechanism is invoked to account for the majority of cases of reservoir-induced seismicity.

Finite element technique has also been applied to the study of stress interactions between adjacent mines, with particular reference to the mining-induced seismicity in N.Staffordshire. Certain configurations of longwall panels have been found to significantly increase the induced stress field.

ACKNOWLEDGEMENTS

I should particularly like to thank Dr. Nick Kusznir and Dr. Chris Browitt for their support over the past three years. The former has been a never-ending source of guidance and, most importantly, encouragement along the road to that mysterious realm of finite element philosophy. The latter provided the initial inspiration for this research topic, and has been continuously helpful since, particularly regarding the financial aspects of my enjoyable stays in Keele and, especially, Edinburgh. I would also like to mention Dr. Paul Collis and other members of the computing staff at Keele, for their assistance and advice concerning the endless problems generated by the computer programs. Recently, too, the final pains of thesis completion have been considerably eased by the keyboard skills of Mrs. Carolyn Parnell, for whom, it seems, even typing miracles can be done at once.

Finally, I should like to thank my parents for their generous supply of money which ensured my survival over the past few months. Most of this work, however, was financed by a grant from the Natural Environmental Research Council.

CONTENTS

I do not know what I may appear to the world; but to myself I seem to have been only like a boy playing on the seashore, and diverting myself now and then finding a smoother pebble or a prettier shell than ordinary, whilst the great ocean of truth lay all undiscovered before me.

Isaac Newton

CHAPTER 1

INDUCED SEISMICITY

1.1 Introduction

It is now well known that some of man's activities can affect the occurrence of earthquakes, and it is generally accepted that these activities include the establishment of large reservoirs and the pumping of liquid down wells. Much of the evidence in support of this has been clearly set out by Gupta and Rastogi (1976). However, despite the fact that part of this evidence was available over thirty years ago (Carder, 1945, in connection with the Hoover Dam), this influence has only recently been recognised by most earth scientists, having been brought to their attention in the 1960's by the seismicity which occurred at Kariba (Gough and Gough, 1970b), Kremasta (Galanopoulos, 1967) and Koyna (Gupta et al., 1969) dams. These reservoirs all suffered damaging shallow-focus shocks in their vicinity, of magnitudes greater than 6, and in the case of Koyna this resulted in the loss of almost 200 lives.

Rothé (1968) was the first to bring the cases of several seismic reservoirs together. He cited the above mentioned dams, together with those at Marathon, first described by Papazachos (1968), and Monteynard, at both of which shocks of magnitude 5 had occurred, and he also mentions the 1962 earthquake at Canelles which was centred on the dam itself. Rothé immediately considered a triggering process to be responsible for at least some artificial earthquakes, but also proposed that the origin of the energy "derives from the mass of the stored water". In papers in 1969 and 1970 he brought the number of examples up to twelve, and discussed how the association of pressurised injection of waste fluid into the ground at the Denver well with the subsequent seismicity (Evans, 1966) showed the importance of considering underground water pressures when explaining the induction mechanism at

reservoirs. Carder had already considered this aspect in 1968 when he presented again the case at Hoover Dam. By 1970 the reality of the phenomenon was almost totally accepted, and in that year about 15 possible cases were referred to at a UNESCO Working Group meeting on the subject. Also in 1969 and 1970, three important papers were published by Gough and Gough presenting the first attempts to put a quantative basis behind the study of the effects of reservoir imposition. Firstly, calculations of the theoretical elastic crustal depression were found to agree with field measurements. Secondly, they dealt with the resulting stresses and strains, and the transformation of these into seismic energy. The shear and normal stresses at a fault plane were also considered quantitatively. In 1972 Gupta et al. published studies of the seismological aspects of induced seismicity and established several important relationships concerning the occurrence and magnitudes of induced earthquakes. Several more case histories were brought to light in the succeeding years, and Simpson (1976) cited 29 cases of induced seismicity, with magnitudes ranging from 6.5 down to just above the general seismic noise level. Since then two other cases have been reported, at the Manicagouan 3 dam in Quebec (Leblanc and Anglin, 1978) and at Lake Keowee, S.Carolina (Talwani, 1979). The geographical distribution of all these reservoirs is shown in Figs. 1.1 and 1.2. Also plotted are the positions of the large aseismic reservoirs listed in Table 1.2. Gough (1976) calculated that at least 10% of large reservoirs (i.e. those which exceed 100 m in depth or 1 km^3 in volume) suffer induced seismicity of magnitude greater than 2.

However, the installation of seismometers prior to the filling of the reservoir has occurred in only one or two cases, and there have not yet been any instances published of a pre-impoundment survey examining the regional seismicity, crustal stresses, hydrology, structural and stratigraphic geology in order to assess the possibility of induced seismicity. Indeed, there is no established framework into which the results could be introduced, as the interaction of all these complicated and poorly-known parameters is

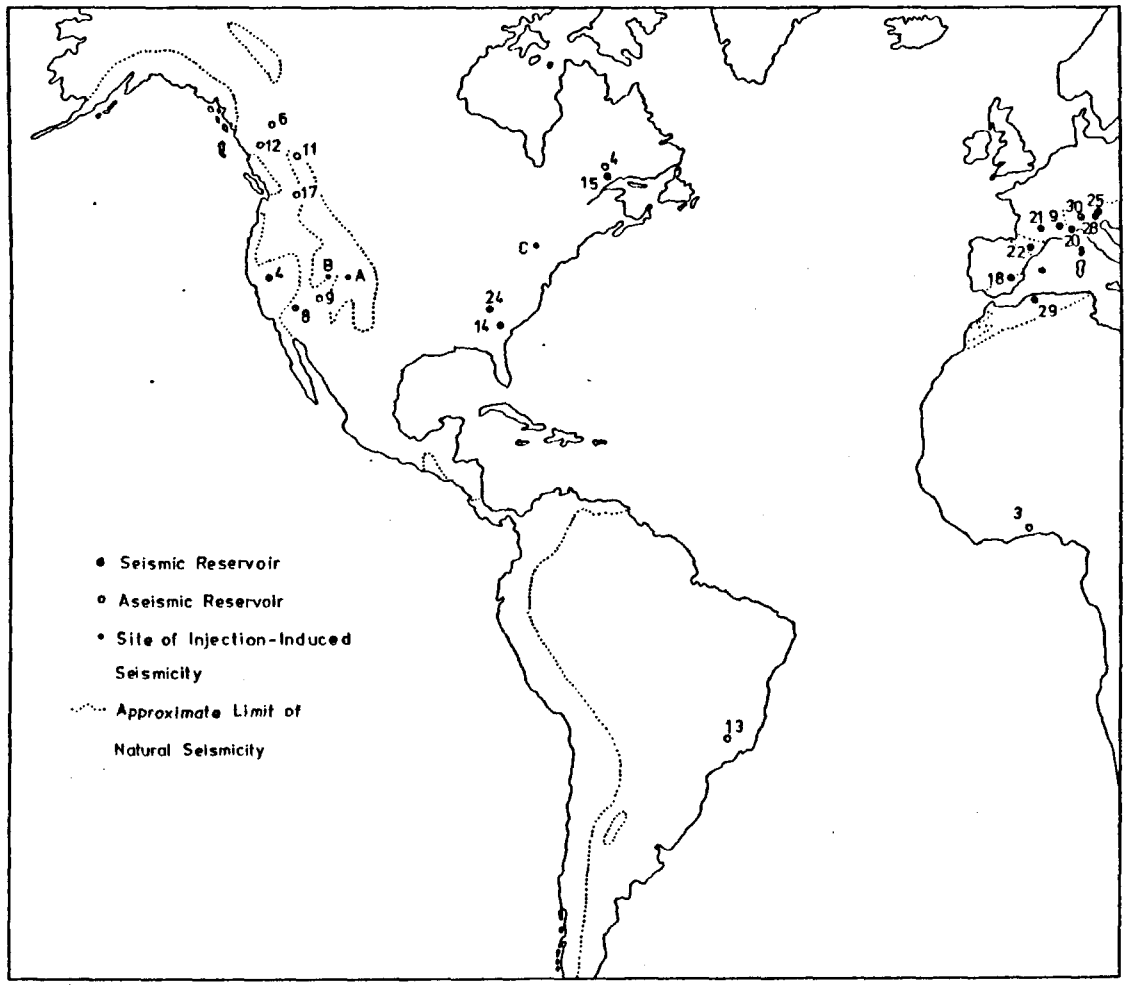

Figure 1.1 Geograpical Distribution of Large and Seismic Reservoirs - Western Hemisphere

SEISMIC : 4 OROVILLE, 8 HOOVER, 9 MONTEYNARD, 14 CLARK HILL, 15 MANIC 3, 18 CAMARILLAS, 20 PIASTRA, 21 GRANDVAL, 22 CANALLES, 24 KEOWEE, 25 PIEVE DI CADORE, 28 VAIONT, 29 OUED FODDA, 30 CONTRA.

ASEISMIC : 3 AKOSOMBO, 4 MANIC 5, 6 W.A.C.BENNETT, 10 GLEN CANYON, 11 MICA, 12 KENNEY, 13 FURNAS, 17 GRAND COULEE.

INJECTION SITES : A DENVER, B RANGELEY, C DALE.

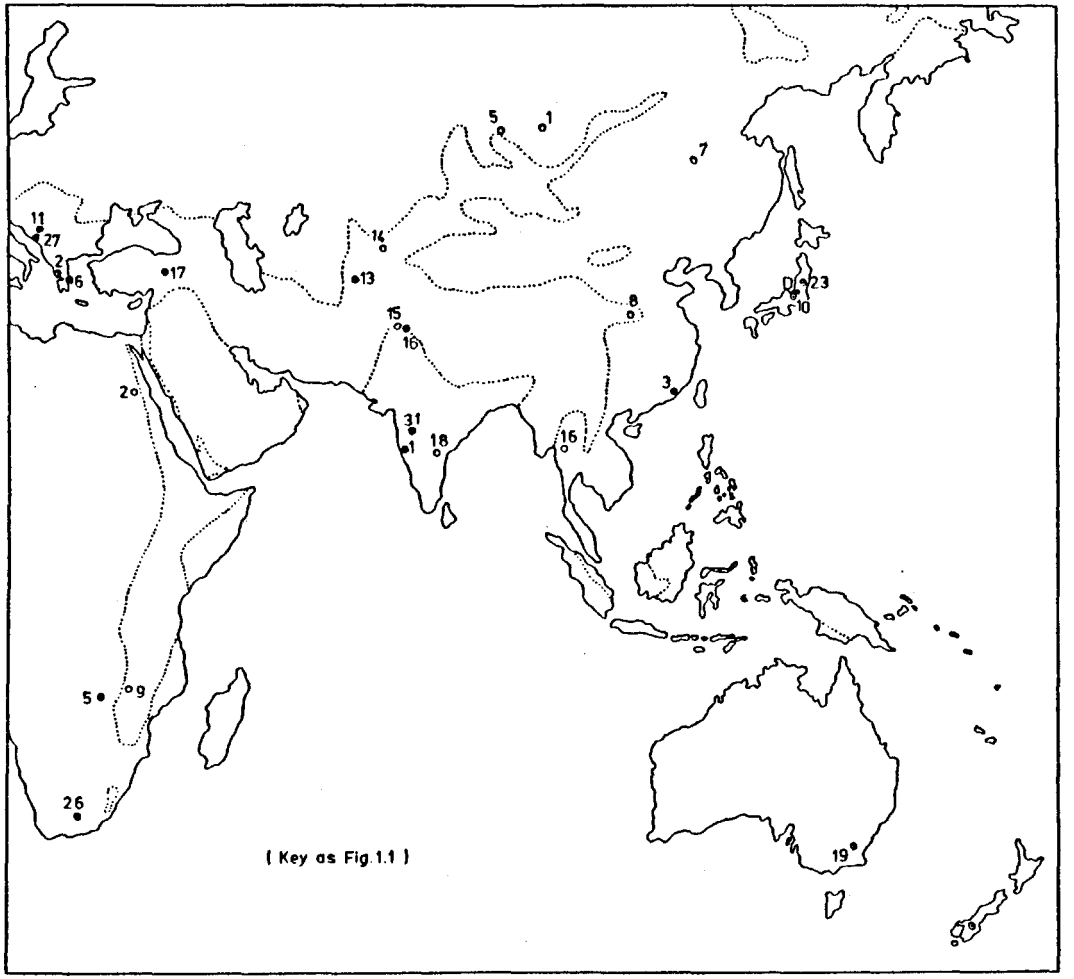

Figure 1.2 Geographical Distribution of Large and Seismic Reservoirs - Eastern Hemisphere

SEISMIC : 1 KOYNA , 2 KREMASTA , 3 HSINFENKIANG , 5 KARIBA , 6 MARATHON , 7 BENMORE , 10 KUROBE , 11 BAJINA BASTA , 13 NUREK , 16 MANGLA , 17 KEBAN , 19 TALBINGO , 23 KAMAFUSA , 26 HENDRIK VERWOERD , 27 GRANCAREVO , 31 MULA.

ASEISMIC : 1 BRATSK , 2 ASWAN , 5 KRASNOYARSK , 7 ZEYA , 8 SANMEN HSIA , 9 CABORA BASSA , 14 TOKTOGUL , 15 TARBELA , 16 BHUMIPHOL , 18 NAGARJUNA SAGAR.

INJECTION SITE : D MATSUSHIRO.

scarcely predictable by the analytical procedures available. One of the aims of this thesis is to provide the outlines of such a framework, by combining the finite-element technique, which is capable of processing the highly variable data involved, with the present-day knowledge about the induction processes acquired from past case histories. Using this method, the thesis also examines the individual effects of the many parameters involved in order to provide a semi-quantitative basis for assessing their relevance in each case. Sections 2 and 3 of this chapter are devoted to the extraction of data from the literature for the purposes of determining the factors that are most important and which should be investigated in the remainder of the thesis.

1.2 Reservoir Characteristics

Some recent data concerning all known seismic reservoirs and eighteen of the largest aseismic reservoirs are given in Tables 1.1 and 1.2.

(i) Topography

It might be expected that irregularities in the nearby topography, especially the reservoir valley itself, would produce concentrations of stresses likely to be exploited by the additional stresses due to reservoir imposition.

Tables 1.1a and 1.2 show that in common with aseismic reservoirs, there is a tendency for the immediate valley to be steep and the surrounding region to be hilly or mountainous. However, the values of the known maximum slopes of the valley side at the dam site range from 15° at the Henrik Verwoerd dam up to 75° for Vaiont. The maximum height contrast within 30 km of each seismic reservoir is on average 1.3 km, but this varies between 100 m (Clark Hill) and 2.8 km (Nurek). These figures are very similar to those deduced from the large aseismic reservoirs. Also, Fig. 1.3b shows no noticeable correlation between the average maximum height contrast and the maximum earthquake magnitude. Thus it cannot be stated on the basis of this data that topographic factors either contribute noticeably to the induction of seismicity

Dam (Lake)	Constr. Date	Dam Ht. (Water Ht. at Main Shock)(m)	Max. Water Vol. ($x10^6 m^3$)	Main Shock (Intens.)	Date of Main Shock	Topog. Ht. (m)	Max. Valley Slope	Topog. Ht Contr. Within 30 Km. (m)
1 Koyna	1962	100	2780	6.5	Dec. 1967	800	20°	600
2 Kremasta	1965	165	4750	6.3	Feb. 1966	200	35+°	2000
3 Hsinfenkiang	1959	105	10500	6.1	Mar. 1962	200	35°	800
4 Oroville	1968	236	4300	5.9	Aug. 1975	200		800
5 Kariba	1959	128	160370	5.8	Sep. 1963	800	30°	500
6 Marathon	1930	63	40	5.0	1938	300		1100
7 Benmore	1964	96	2040	5.0	1966,1971	400		1400
8 Hoover (Mead)	1936	221	36700	5.0	May 1939	400		1100
9 Monteynard	1962	130	240	4.9	Apr. 1963	500	55+°	2300
10 Kurobe	1960	186(102)	149	4.9	Aug. 1961	1400		1800
11 Bajina Bašta	1966	89	340	4.7	Jul. 1967	400		1000
12 Vouglans	1968	130	600	4.5	Jun. 1971			
13 Nurek	1969	315(105)	10400	4.4	Nov. 1972	1000		2800
14 Clark Hill	1952	67	2500	4.3	Aug. 1974	100		100
15 Manic 3	1975	108(50)	10400	4.1	Oct. 1975	200		500
16 Mangla (?)	1967	135	7250	3.6	Sep. 1967	400		1000
17 Keban	1973	207	31000	3.5	Jun. 1974	900		2100
18 Camarillas	1960	44(30)	40	3.5	Dec. 1961	400		1000
19 Talbingo	1971	162	935	3.5	Jul. 1971	900	35+°	900
20 Piastra	1965	93	13	VI-VII	Apr. 1966	1000		2400
21 Grandval	1959	78	290	V	Aug. 1963	800	30°	1000
22 Canelles	1960	150	680	V	Jun. 1962	900		800
23 Kamafusa	1970	46	45	2.5		400		1400
24 Keowee	1969	40		2.2	Jan. 1978	400		200
25 Pieve Di Cadore	1949	112	68	2.0		800	65°	2300
26 Hendrik Verwoerd	1970	66	5000	2.0	1971	1200	15+°	300
27 Grančarevo	1967	123	1280	1.5		400		1500
28 Vaiont	1961	266	150		Sep. 1962	1000	75°	2200
29 Oued Fodda	1932	89	230		1933	300	60°	1300
30 Contra (Vogorno)	1964	220(100)	100		1965	500	50°	2700
31 Mula	1972	11		<1.0	1972	400		300

Table 1.1a

Dam (Lake)	Tectonic Regime	Principal Rock Types (Others) /Peculiarities/	Time Lags (Mnths) (major shocks underlined)	Epicentre-Lake Distance (Km)	Focal Depth (Km)	Main Sequence Mogi Type
1 Koyna	Pre-Cambrian	Volcanics, sediments, (bole clay)	8, 4, 7, (2, 60?)	0-20, 4	1-20	II
2 Kremasta	Alpine	Flysch, limestone, (shales) /Springs/	1	0-45, 14	20, shallow crustal	II
3 Hsinfenkiang	Mesozoic	Granite, sediments, (volcanics)	12?, 1	0-5, 1	1-11, 5	II
4 Oroville	Mesozoic		<5	11	0-9	II
5 Kariba	Pre-Cambrian	Sediments, gneisses /Hot springs/	1, 1, 1, 1	0-20(60?), 5?	5?	II
6 Marathon	Alpine	Schists, sediments	2, 0, 3, 4, 3, 0, 0	0-18		II
7 Benmore	Alpine	Sediments, schists	2, 9, 1, 1	0-50, 10, 1		
8 Hoover (Mead)	Mesozoic	Volcanics, intrusives, (m'morphics)	18?	0-20, 5	1-9	II
9 Monteynard	Alpine	Limestone, (schist, marl)	(1?, 11?)	0	v. shallow	II
10 Kurobe	Alpine	Granite	1, 1, 1, 1, 6?	5	10?	II
11 Bajina Bašta	Alpine	Limestone, (sediments, volcanics)		0	7	III
12 Vouglans	Alpine	Limestone	2			I
13 Nurek	Alpine	Sediments /Salt fmn./	1	0-15, 6	0-10, 5	II
14 Clark Hill	Hercynian	Schist, gneiss	(4, 6, 9?), 0	0-3, 2	shallow	II
15 Manic 3	Pre-Cambrian	Gneiss, intrusives	2	0-3	0-2	II
16 Mangla (?)	Alpine	Sediments	1, 1	5-25?	crustal	III
17 Keban	Alpine	Sediments, metamorphics	3			III
18 Camarillas	Alpine	Limestone /Salt dome/	2		v. shallow	
19 Talbingo	Hercynian	Volcanics, granite, (sediments)	1	0-10	v. shallow	III
20 Piastra	Alpine		~6	<5	v. shallow	III
21 Grandval	Hercynian	Schists		0	v. shallow	II
22 Canelles	Hercynian			0		
23 Kamafusa	Alpine	Volcanics /Hot springs/	1, 1	2	0-3	III
24 Keowee	Hercynian	Gneiss	6, 6	0-1	0-3	III
25 Pieve Di Cadore	Alpine	Dolomite	1	<5		III
26 Hendrik Verwoerd	Pre-Cambrian	Sediments, dykes	5?	0-1	1-6	III
27 Grančarevo	Alpine	Limestone		<15		
28 Vaiont	Alpine	Limestone, sediments	3, 3, 4	0-4		III
29 Oued Fodda	Alpine	Limestone, (marl) /Salt fmn./				
30 Contra (Vogorno)	Alpine	Gneisses	1, 1			
31 Mula	Pre-Cambrian	Volcanics, (sediments)	2	0-1		III

Table 1.1b

	Name	Constr. Date	Water Height Ht.(m)	Water Volume ($\times 10^6 m^3$)	Topog. Ht.(m)	Height Contr.(m)	Tectonic Regime
1	Bratsk	1964	125	169270	400	200	Pre-Cambrian
2	Aswan	1970	111	164000	100	200	Pre-Cambrian
3	Akosombo	1965	141	148000	100	200	Pre-Cambrian
4	Manic 5	1968	214	141850	100	800	Pre-Cambrian
5	Krasnoyarsk	1967	124	73300	200	600	Caledonian
6	W.A.C. Bennett	1967	183	70310	900	1300	Mesozoic
7	Zeya	1976+	115	68400	200	200	Hercynian
8	Sanmen Hsia	1962	107	65000	300	1500	Pre-Cambrian
9	Cabora Bassa	1974	171	63000	400	700	Pre-Cambrian
10	Glen Canyon	1964	216	33300	1500	1500	Pre-Cambrian
11	Mica	1974	242	24670	900	2700	Mesozoic
12	Kenney	1952	104	22200	800	1400	Mesozoic
13	Furnas	1962	127	20860	800	400	Pre-Cambrian
14	Toktogul	1976+	215	19500	800	3300	Hercynian
15	Tarbela	1975	143	13690	400	1300	Pre-Cambrian
16	Bhumiphol	1964	154	12200	200	1600	Mesozoic
17	Grand Coulee	1942	168	11970	400	1500	Mesozoic
18	Nagarjuna Sagar	1976+	124	11315	100	600	Pre-Cambrian

Table 1.2

or that they influence its magnitude. A more detailed and quantitative investigation of this matter is presented in Chapter 4.

(ii) Geology

Table 1.1b gives the broad lithological types found at the surface in contact with each lake, along with other main rock types in the immediate seismic area. It may not always include the actual rock(s) in which the slippage occurred, but it does show that seismicity has been attributed to reservoirs founded upon a wide variety of lithologies. All the main rock types expected to be associated with reservoir sites are present and, moreover, they occur in many of the possible combinations. Thus, for example, the foundation of the Monteynard reservoir in the French Alps is almost entirely limestone, whilst that of Kurobe is biotite granite and that of Lake Benmore is evenly divided between greywackes and chlorite schist. However, the presence of particular geologies in cases of induced seismicity was pointed to by Rothé (1970), and he referred to heterogeneous strata in the case of Koyna, to strong faulting with water leakage in the cases of Oued Fodda and Monteynard, and to the presence of old faults in many other cases. It seems likely that these are specific examples of the three geological factors that contribute to the likelihood of seismicity or its spatial or temporal distribution. These factors are:

(a) the mechanical, especially elastic, properties of the rock types present, and their contrasts,

(b) the hydrological properties of the rocks, and

(c) their structural properties, especially the amount and nature of faulting.

The presence of rocks of differing elastic properties subject to external and body forces will result in an uneven distribution of stress, possibly with stress concentrations in local areas of weakness. The greater the contrast in properties, the more heterogeneous the stresses will be.

Table 1.1b shows many possible cases where this might happen, for example at Koyna, Hsinfenkiang, Kariba and Marathon, where relatively deformable sedimentary layers are in contact with hard igneous or metamorphic rocks. On the other hand, in an extreme case, where a soft and thick salt formation is present in the Virgin-Detrital Trough of Lake Mead, the ductility of this layer has been proferred as an explanation for the relative stability of this basin as compared to its seismic neighbour, the Boulder Basin (Anderson, 1973). The salt would deform by slow creep, preventing the build-up of stresses to a critical level.

Water has been cited to be a prime factor in inducing seismicity, in three different ways. Two of these were attempts to explain the shocks that occurred at Oued Fodda, the earliest known case of induced seismicity, and were prompted by the presence of underlying evaporite deposits (Gourinard, 1952). Firstly, it was thought the additional water might have caused swelling of an anhydrous layer, and secondly that increased rates of solution of the salts might have created unstable underground cavities. However, the principal effect of increased underground water pressure is the reduction of effective stresses, probably in the manner proposed by Hubbert and Rubey (1959). The hydrological factor which has the greatest bearing on the occurrence of seismicity is permeability, as this governs the time taken for the pressure front to travel from the main water body to the positions that are susceptible to failure. In most rock masses the permeability is largely dependent upon the amount of jointing and fracturing,these being dependent on the structural history of the rock. In sedimentary rocks, permeability is also contributed to by interconnected primary or secondary pores, the presence of which is a function of the rock's post-depositional history. Intergranular porosity is also a contributing factor in non-sedimentary rocks. Hence, a simply compiled Table cannot clearly show the geological factors relevant to the internal behaviour of water, although in general igneous rocks and pelites can be assumed to have low permeabilities (although the

former are often susceptible to jointing). Areas protected by low permeability shales or high-grade metamorphic formations would not receive the radiating pore pressure front until long after the surrounding rock, and the water may be compelled to accumulate preferentially in adjacent regions where it would greatly weaken potential fault planes. For these reasons one might expect localised high pore pressure regions in, for example, the cases of Kremasta, Keban, Marathon and Benmore.

Few rock masses lack a network of planes of weakness, but the extent of any faulting and the past history of activity on these faults varies considerably. In shallow regions large increases in differential stress cause elastic and brittle responses such as dilatancy and faulting, whereas at depths greater than about 15 km the higher temperatures often lead to ductile closure of any fissures, although directional, possibly tectonic, stress at depth does result in the formation of planes of cleavage and foliations. On elevation to near-surface positions, the release of mainly vertical stress may result in further jointing (Price, 1959). Thus the present structural condition of a rock mass is a result of the set of conditions it has experienced, and the order in which it did so, and is not a function merely of rock type. The amount and direction of faulting, the age(s) when it occurred and the present state of the fault planes are usually an important part of any pre-construction geological survey. Ideally a reservoir would not be constructed in an area where significant faults exist, but often it is decided that the risk of slippage is 'reasonably' small or else is underestimated. Seismic reservoir sites exhibit the whole range of degree of fracturing, for instance, although the damsite of Monteynard is formed of hard and mechanically competent limestones, these are dissected by numerous faults and joints (Rothé, 1970), and yet in the case of Hendrik Verwoerd no major faults are present in the area (Green, 1974). Many of the reservoirs in Table 1 have large faults, shear zones or joint systems within a distance normally associated with induced seismicity, and this seems to be especially

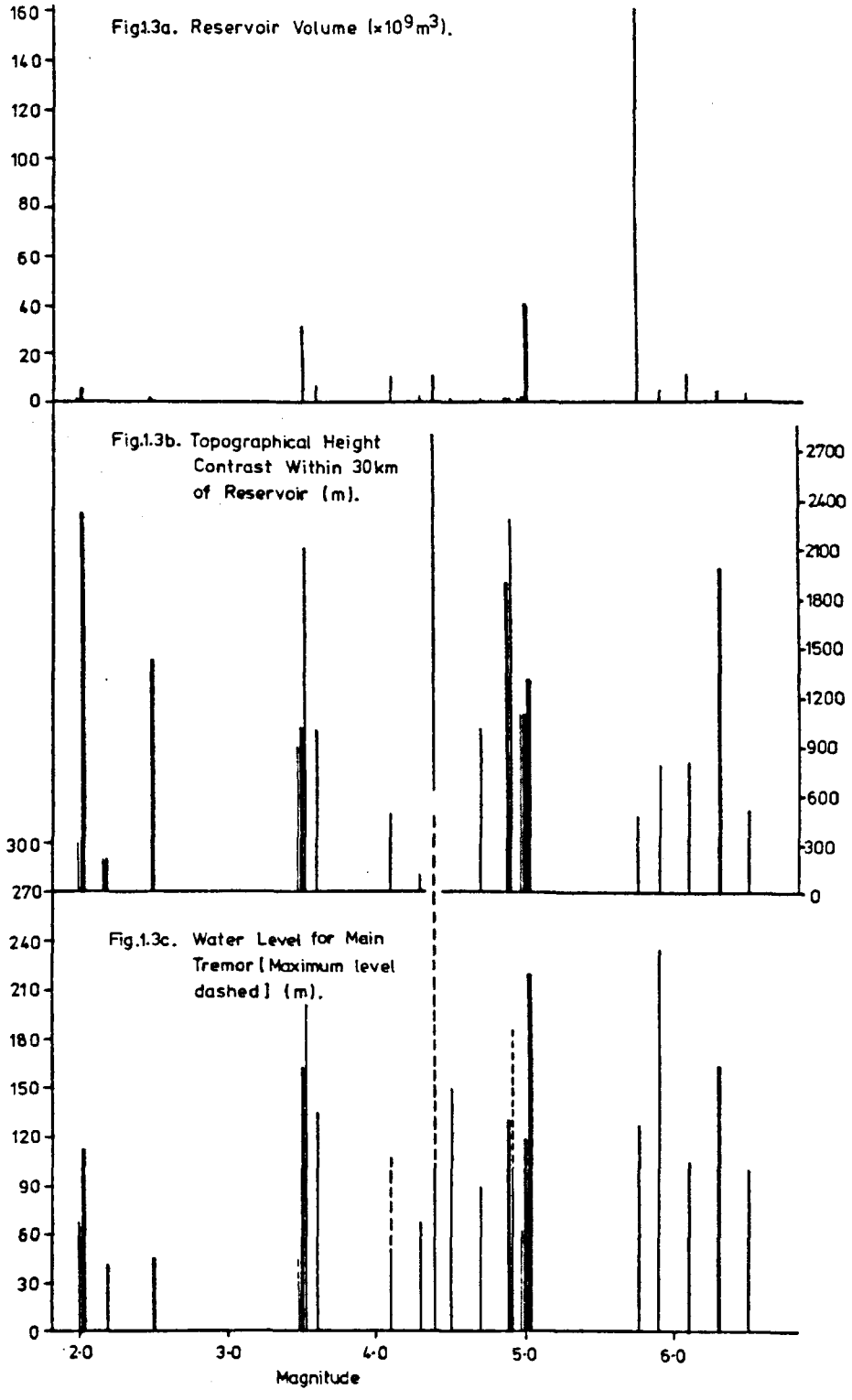
Fig1.3a. Reservoir Volume (×10⁹m³).
160
140
120
100
80
60
40
20
0
Fig.1.3b. Topographical Height Contrast Within 30km of Reservoir (m).
2700
2400
2100
1800
1500
1200
900
600
300
0
300
270
Fig.1.3c. Water Level for Main Tremor [Maximum level dashed] (m).
240
210
180
150
120
90
60
30
0
2·0
3·0
4·0
5·0
6·0
Magnitude

true where the larger shocks have been recorded, with the possible, but notable, exception of Koyna. However, it does not seem to be the case that seismic reservoirs exhibit a significantly greater degree of fracturing than do aseismic reservoirs.

In general, there are no particular geological features common to all seismic reservoirs, nor even features common to most which do not also frequent aseismic reservoir regions. Any geological factors which are relevant in determining the occurrence of reservoir-induced seismicity are therefore neither necessary nor sufficient. However, this does not mean that the factors discussed above cannot individually play a vital role in determining the induction of seismicity in the different tectonic and morphological circumstances of each case. The effects of geology, in so far as this affects the mechanical and hydrological properties of the media, are investigated quantitatively in Chapters 4 and 5.

(iii) Tectonic Setting

Table 1.1b shows clearly the tendency for seismic reservoirs to occur in regions of the most recent major tectonic events. 60% occur in areas affected by orogeny during Alpine times whereas only 15% occur on Pre-Cambrian shields. This inbalance might be expected anyway, as the naturally more rugged terrain and higher precipitation normally associated with recent orogenic regions are suitable for the siting of a large dam. However, when a comparison between the distributions of the large aseismic reservoirs and the seismic reservoirs of a similar size ($> 10{,}400 \times 10^6$ m^3) is made, a certain discrepancy is observed (Fig.1.4). The bias here towards more ancient foundations is probably the result of the fact that the water content of reservoirs in steep regions is limited by the narrowness of the valleys, and that more eroded areas are needed to contain the lakes of greatest volume. Thus the discrepancy between the two histograms would perhaps not show up so well if a largernumber of (necessarily smaller volume) reservoirs were included. The relative concentration of seismic reservoirs in the younger

CHRONOLOGICAL DISTRIBUTION OF FOUNDATIONS OF LARGE DAMS

(H<100m and V< 10,400 x 10^6 m^3)

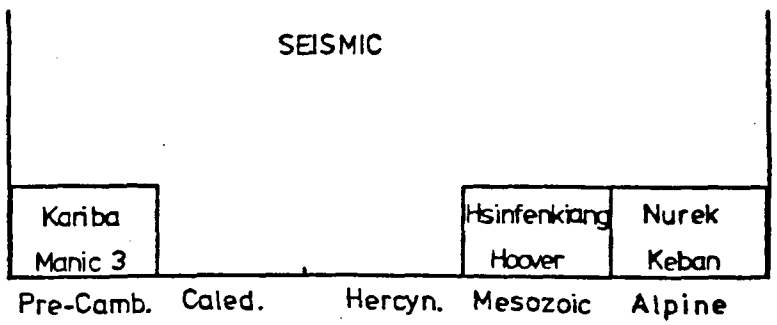

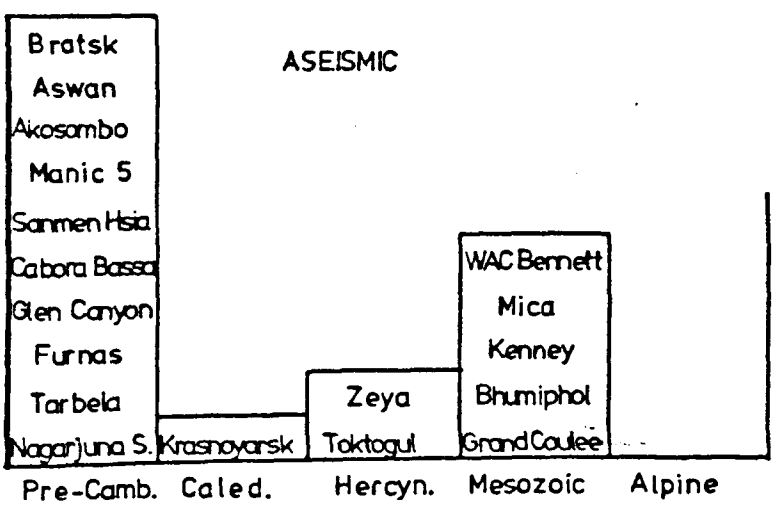

Figure 1.4

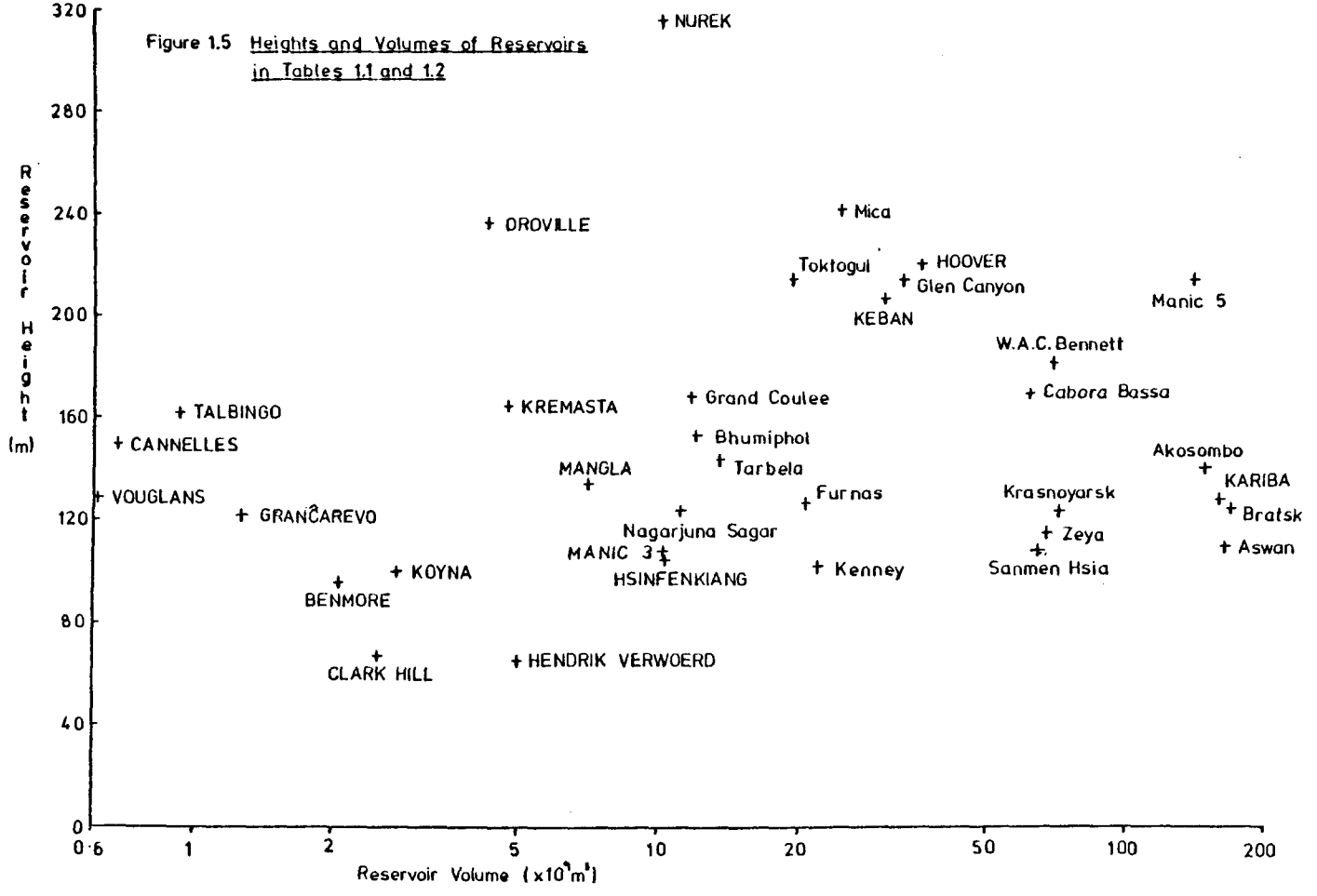

Figure 1.5 Heights and Volumes of Reservoirs in Tables 1.1 and 1.2

orogenic belts can be explained by accepting that the induction process is merely a triggering effect and that near-critical stresses must already be present for this to take place. This is supported by Gough's (1976) calculations showing that the shear stresses due to the weight of a reservoir are at least an order of magnitude too small to induce earthquakes ($M > 3.5$) directly. Recently active regions contain the higher and more heterogeneous stresses required (Nikolaev, 1974) whereas the older regions of the crust have had time for the stresses to equilibrate. Nikolaev also points to the relevance of later Tertiary and Quaternary ('neotectonic') activity, the distribution of which is indicated in Figs. 1.1 and 1.2 , and which is seen to coincide with many seismic reservoir sites.

(iv) Reservoir Dimensions

Although the situation is improving, the present set of seismic reservoirs is a non-random selection and comprises both cases brought to light by the obvious nature of the tremors and also those sites where a deliberate examination of all levels of seismicity has been undertaken. Ideally, any statistics should be restricted to those reservoirs where an equivalent amount of surveillance has taken place, with 'seismicity' being defined by a prespecified magnitude or energy-release. This is impossible at present since these standards have not yet been met, and even some of the statistics in this section based on all known induced seismicity cases have had to be discarded when sets restricted to large dimensions are examined. One factor which must be borne in mind is that many of the ratios quoted below may be too low due to shocks remaining undetected at inadequately monitored reservoirs, a circumstance that Božović (1974) considered likely to be common.

Rothé (1973) suggested that the height of the water column plays a more important role than the volume of the reservoir, and also that seismic activity is particularly pronounced when the depth of the reservoir is greater than 100 m. The histograms in Fig. 1.6 are based upon the Tables (III and IV) compiled by Simpson (1976), and these indeed indicate that the

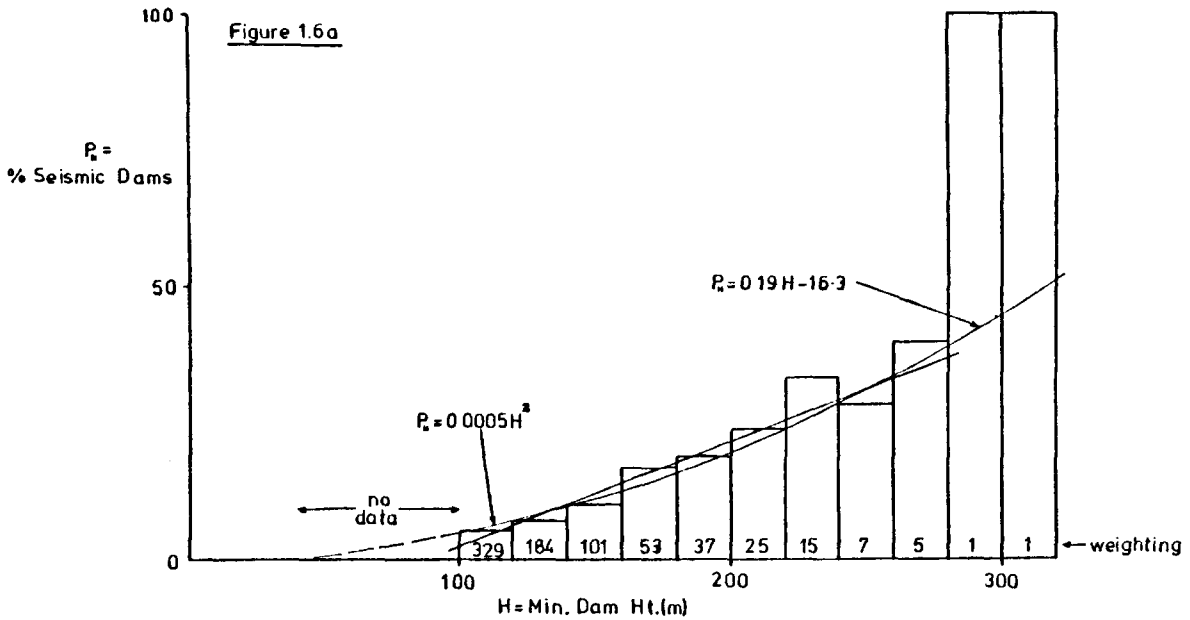
Figure 1.6a
100
50
0
P_s =
% Seismic Dams
$P_s = 0.19H - 16.3$
$P_s = 0.0005H^2$
no data
329
184
101
53
37
25
15
7
5
1
1
weighting
100
200
300
H = Min. Dam Ht.(m)

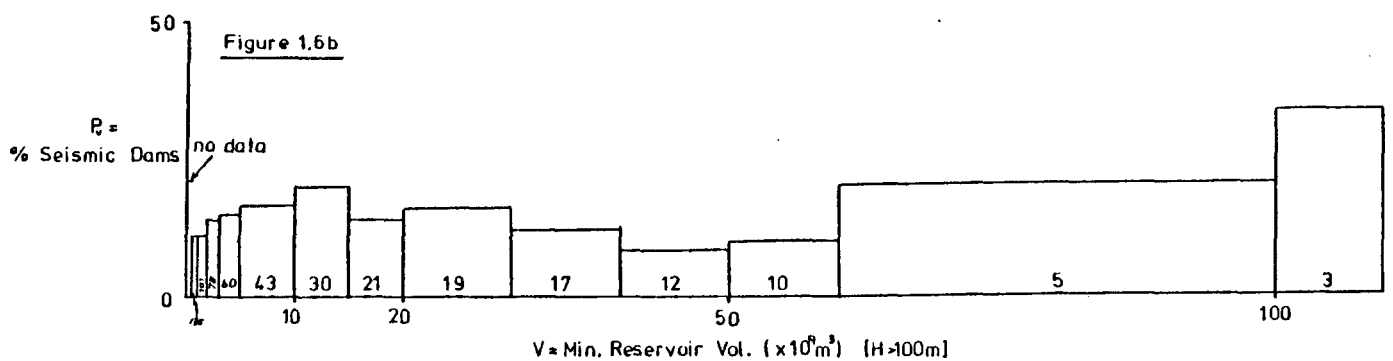
Figure 1.6b
50
0
P_s =
% Seismic Dams
no data
43
30
21
19
17
12
10
5
3
10
20
50
100
V = Min. Reservoir Vol. ($\times 10^6 m^3$) (H>100m)

occurrence of seismicity is more sensitive to the depth of the reservoir than to its volume.

The relationship between the percentage 'P' of dams producing seismicity and the minimum height 'H' of the set of reservoirs being considered is given by a least-squares fit to the histogram, using values weighted in proportion to the total number of dams considered in their derivation:

$$P = 0.19H - 16.3 \qquad (H > 88 \text{ m})$$

A better fit when including near-zero percentages for $H < 40$ m is given by:

$$P = 0.0005H^2$$

although this cannot be extrapolated far as it gives unreasonable behaviour for large percentages. Fig. 1.6b shows a positive correlation between the reservoir volume and seismic induction for all reservoirs less than 10 km^3. Above this value only three seismic reservoirs exist and so the subsequent fall and rise of the histogram need not be interpreted as meaningful, although a levelling off might be surmised. This relation is certainly not as powerful as that for the heights, and hence the combined percentages in Fig. 1.7 are almost wholly height-dependent. This is surprising in the light of Gough and Gough's (1970b) paper which demonstrated how the reservoir volume is more closely related to the incrementally stressed volume of rock than is the depth. For an approximate evaluation of the statistical risk for a reservoir of a particular depth and volume, Figs. 1.8 and 1.9 have been compiled.

The second part of the statement by Rothé is shown to be unfounded by Table 1.1a and Fig. 1.3c. Over a third of the maximum heights shown in Table 1.1a are below 100 m, and in many cases earthquakes occurred before these were reached, as at Manic 3 and Nurek. The shallowest reservoir to have induced seismicity, Camarillas, was only 30 m deep at the time, and the lakes at Kamafusa and Marathon were not much deeper. Also, no particular

Figure 1.7 % Dams Seismic = $\sqrt{P_x P_y}$

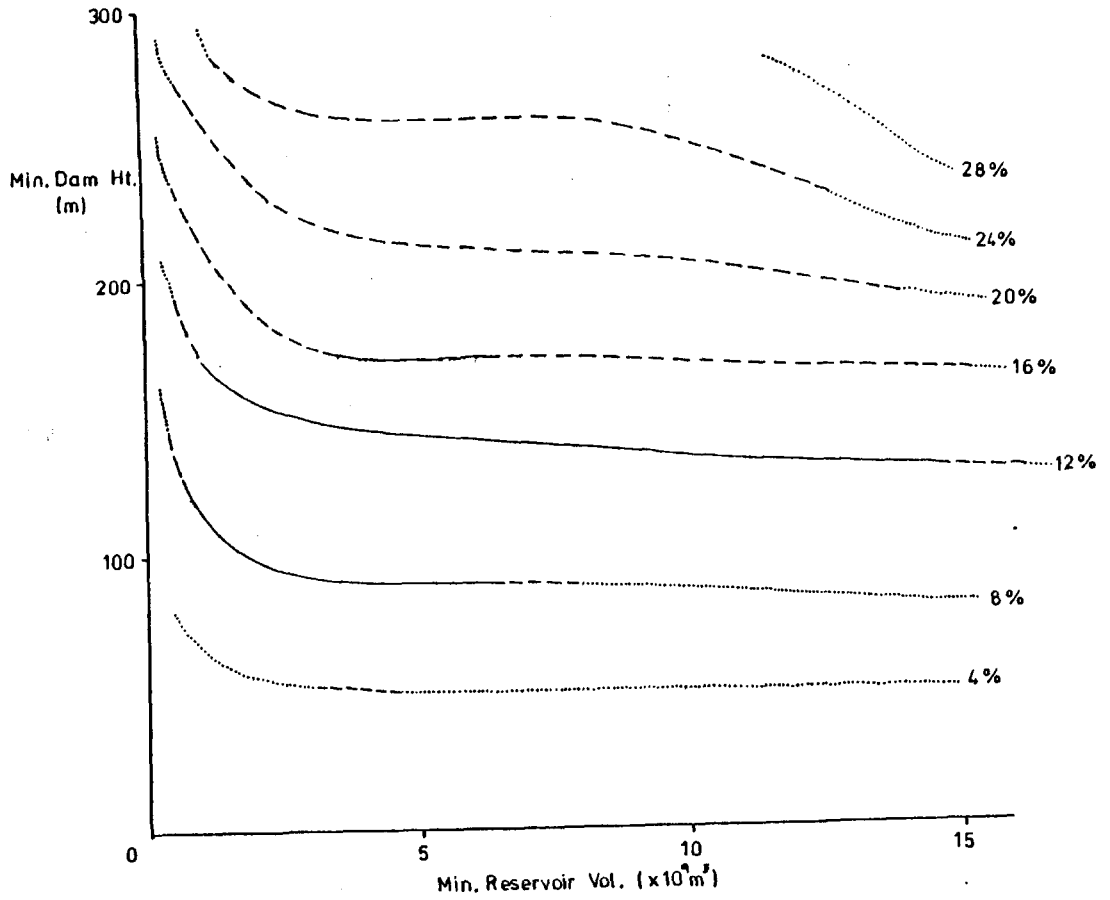

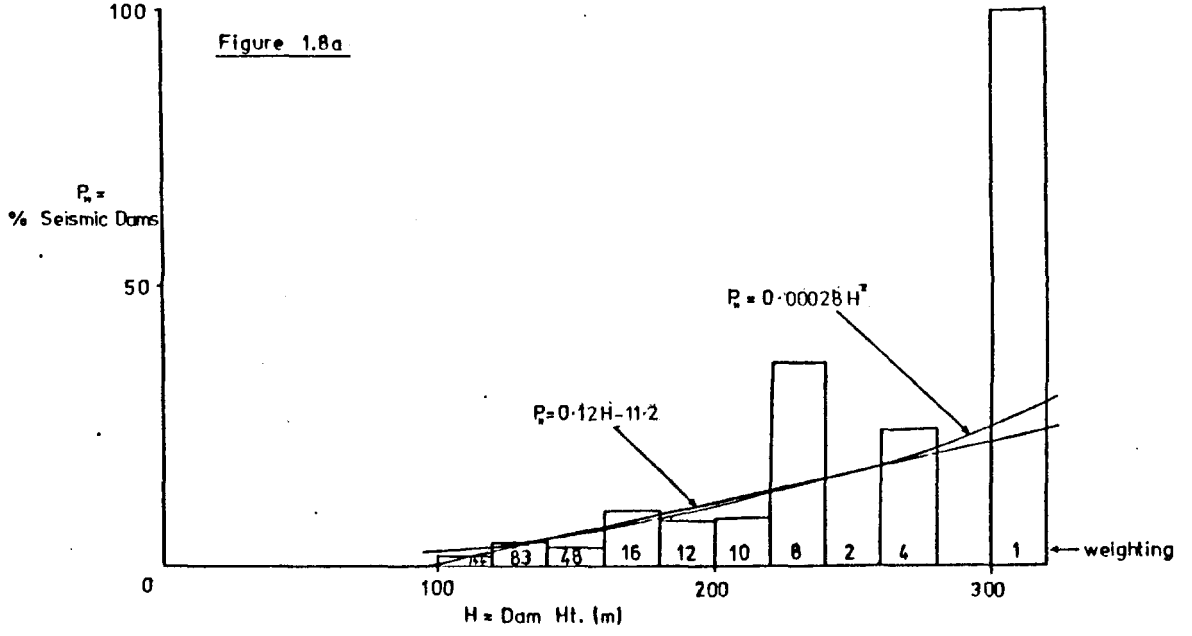

Figure 1.8a

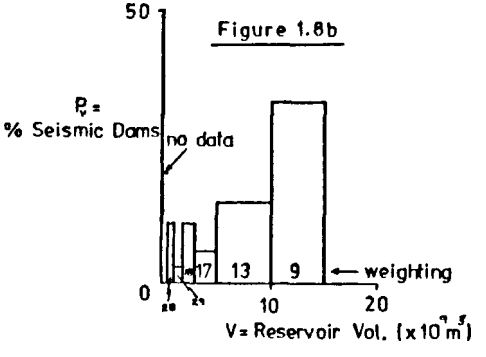

Figure 1.8b

Figure 1.9 $\%\ \text{DAMS SEISMIC} = \sqrt{P(h).P(v)}$

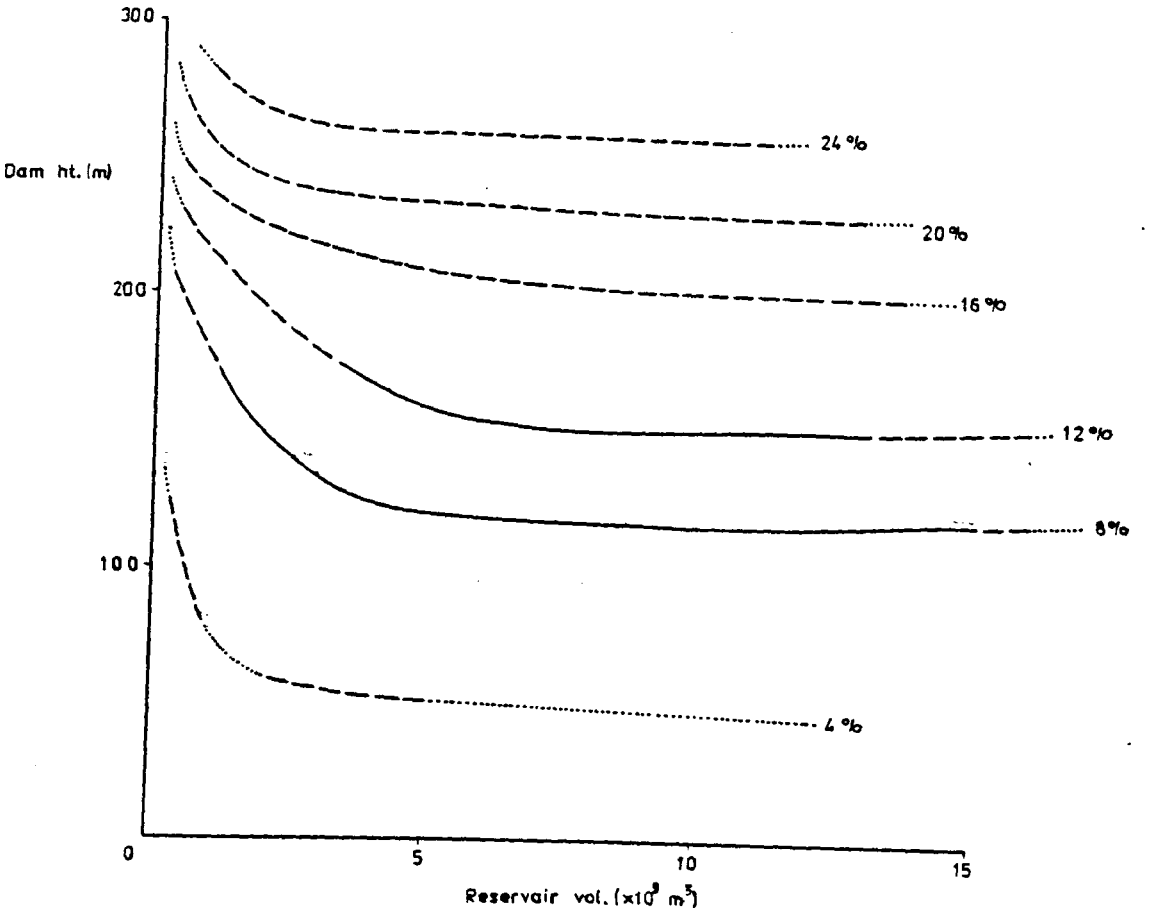

'threshold' depth is evident in Fig. 1.6a, although data for dams of less than 100 m are absent.

Despite the relationships noted above, Figs. 1.3a and 1.3c show a lack of correlation between either the heights or volumes of the lakes and the largest induced earthquake magnitude. This suggests that different factors may be behind the initiation of seismicity (e.g. closeness of the initial stresses in the rock to the initial rock strength) and the eventual magnitude (e.g. the initial rock strength itself).

1.3 Seismic Characteristics

(i) Temporal Variations

It has been observed that the main shocks induced do not often coincide in time with any parameter describing the initial filling of the reservoirs. Usually the increase in seismicity, or main shock, is delayed by a period of several months or years after the impoundment. The time lag obviously cannot be due to any one elastic factor. There are two possible reasons for its existence. Firstly, the loading of the water may not have actually brought the underlying rock directly to failure, which is consequently delayed until the natural build-up of tectonic stress is sufficient. Secondly, it may represent the time taken for the pore water pressure to increase sufficiently to reduce the effective strength of a fault at a distance from the reservoir to a critical level. The first reason will not often apply, but it does show that a time-lag need not necessarily be indicative of triggering by reduction of effective stress.

The most commonly used measure of this time-lag has been the period between the commencement of filling of the reservoir, or first attainment of maximum height, and the time of the largest shock (e.g. Gough, 1976). However, there are often induced tremors before this, and there will also be several, usually annual, water level maxima occurring within this period. Some of these variations in seismicity and water level have been extensively

examined by Gupta and Rastogi (1972, 1974) and Mickey (1971), and they demonstrated the high level of correlation that exists between them for several important cases of induced seismicity. In order to determine a meaningful value for the time-lag it has to be decided which of these variations in water level is linked with each particular bout of seismicity. Usually it must be assumed that it is the one immediately preceding it but, especially when it is the first onset of seismicity, the relevant initial time may well date back to the very first water level rise, and estimating the value of the time-lag in such cases becomes a rather subjective process. Many of the reservoirs, then, have several, probably different, discernible 'time-lags' associated with them, and these are listed in Table 1b.

Gough and Gough (1970b) showed that, in the case of Kariba, a parameter intuitively much more relevant than water height - the reservoir-induced volume of rock stressed above a chosen value (1 bar) - varies in a highly non-linear way with the water depth. This parameter is shown to increase sharply at a critical value of the depth, for example by 29% between 128 m and 131 m at Kariba, and thus the time when this occurs would be a much better estimate of the 'initial' time of the time-lag period. Unfortunately this stressed volume has been calculated for few other seismic reservoirs (except see Gupta et al., 1974; and Green, 1974), and so for convenience a steep rise in water level has to be used to mark this point. The value of the water level for each seismically-associated steep water rise will vary somewhat, even for the same reservoir due, for example, to the rock strength and threshold level of stress changing with time. The variation in the stress threshold, which has been observed in some cases of induced seismicity, is usually a rise. In other words, greater water levels are required to induce tremors with each passing year. As a best practical, but not entirely satisfactory, estimate of time-lag then, the period between a steep rise in water level and the most probable associated main shock has been used in Table 1.1b .

The values range from zero, as conclusively shown by Hagiwara and Ohtake (1972) for Kurobe, up to possibly twelve or more months in the case of Hsinfenkiang. However, the shortness of these time-lags in some cases may just be due to the uncertainty in picking the associated pairs of times from the water level and seismicity variations, and periods of five years (as suggested for Koyna) may be quite plausibly obtained in a few cases. However, it is most usual for at least a low level of activity to commence within a month of the first significant water rise. Unfortunately, no particular pattern is evident from the time-lag data in Table 1.1.

There is also little regularity about the distribution of the tremors in time. Most commonly they occur almost randomly spaced over a period which begins a few months after impounding, become more concentrated with some larger magnitude shocks over a further very variable period and then, usually more gradually, fade away over an equally variable period. Often, within the first two or three years, there will be a higher frequency correlation with water level superimposed upon this. Important examples were at Koyna and Kariba. A second type of activity is where there is a sharp increase in the number of tremors, usually following a sharp rise (or fall, in the case of Pieve Di Cadore) in water level, which includes a main shock, followed by a return to normal background activity within a few months. This occurred, for example, at Manic 3 in 1975. The other form of activity is a swarm of shocks, usually of quite low magnitudes, lasting a few days or months, with no well-defined main shock. This was the case at the Vaiont dam for instance.

Any subsequent activity seems to depend on the degree of activity in the main phase. In some cases where large shocks occurred, there may still be spurts of seismic activity occurring, as at Koyna in October 1973 and at Kariba in November 1971, several years after the principal sequence. At Kremasta, Lake Mead, Hsinfenkiang and Marathon, a low level of seismicity continued for many years afterwards, although three of these are in

naturally seismic areas. In contrast, reservoirs with less severe associated seismicity seem to be limited to a transient seismic phase which is usually completed within a year.

(ii) Spatial Distribution

One, intuitively obvious, characteristic of the reservoir-associated shocks is their proximity to the lake itself. Very frequently they are within five kilometres of the lake. This is especially true of the smaller activities (not necessarily the smaller reservoirs), but also of Hsinfenkiang for instance, where the magnitude 6.1 shock was only 1 km from the lake. The seismicity associated with larger shocks is however more often at a distance of up to 20 km, and statistical studies at Lake Benmore (Adams, 1974) indicate influence on seismicity up to 50 km from the dam, although the main activity was much closer than that.

The hypocentral depths are also characterised by their extreme shallowness, as indicated by the underground noises heard at Contra (Susstrunk, 1968) and Grandval (Rothé, 1969) amongst others, as well as by instrumental observations. There is again a suggestion that greater depths are associated with the larger shocks (Table 1.1b), as lower crustal hypocentres are reported at Koyna and Kremasta only.

The shocks are usually found clustered in a group near or under the reservoir (e.g. Talbingo, Hendrik Verwoerd) or, in the cases with a greater epicentral distance, spread around rather randomly (e.g. Benmore, Marathon). Sometimes however, they are clearly concentrated along a major fault line, as at Oroville.

Unfortunately, the data are not sufficient to show up any relationship that might exist between the reliable time-lag estimates and distance of the shock from the reservoir (Table 1.1b). For some individual reservoirs the epicentral locations are known to have shifted with time (e.g. Kariba, Hsinfenkiang), but a general exodus from the reservoir has not been known to occur. This would have indicated an important role for pore pressure,

by analogy with the situation at Denver where the migration of the epicentres is believed to have been due to the expanding pore pressure front (Healy et al., 1968). In one case however, a migratory trend has been observed, at Nurek, but in a direction towards the lake (Soboleva, 1976). As this is a region of thrust faulting however, an expanding pressure front can be invoked to explain this also (Simpson, 1976).

(iii) Seismic Characteristics

It is a remarkable fact that almost all the parameters concerning the magnitudes and frequencies of induced earthquakes are in complete contrast to those of normal earthquakes. Unfortunately, the statistical basis of some of these parameters means that they have been able to be meaningfully calculated in only a few cases. A summary of these well-established characteristics is presented in Table 1.3. A complete physical interpretation of the situation represented by these figures has not yet been achieved, but it is generally agreed that they are related to the mechanical properties of the rock, which have been affected by the reservoir. Moreover, the interpretation by Mogi (1963b) of the differing nature of foreshock sequences of normal earthquakes has been applied to induced activity (Gupta et al., 1972b), where his conclusions are supported by all the characteristics outlined in Table 1.3. These conclusions are that the Type II and III distributions, typical of induced seismicity, indicate heterogeneous media and/or non-uniform applied stress. Thus it is inferred from the seismic characteristics that the addition of the reservoir load with the attendant time-dependent pore pressure variations results in a decrease in the homogeneity of the rock properties and an increase in the number and degree of concentrations of stress.

1.4 Mining Induced Seismicity

In contrast to those earthquakes triggered by reservoirs, the tremors and rockbursts associated with mining have been studied, in some mining

KEY

b_F = foreshock 'b' value
b_A = aftershock 'b' value
M_o = magnitude of main shock
M_A = magnitude of main aftershock

	Seismic Parameter	INDUCED EARTHQUAKES	NORMAL EARTHQUAKES
1	b_F value	High, 1·1 – 1·9 [9]	Low 0·3 – 0·6 [1]
2	b_A value	High, 1·0 – 1·5 [9]	0·7 – 1·2 [1]
3	$b_F : b_A$	>1·0 [9]	<1·0 [1]
4	$b : M_o$	High b ⇒ med./small M_o [11]	High b ⇒ Large M_o Low b ⇒ Small M_o [11]
5	M_o/M_A $M_o - M_A$	High ~ 0·9 [8] Small ~ 0·6 [4]	0·6 – 0·7 [11] ~1·2 [2,3]
6	$b : M_o/M_A$	High b (0·7–1·4) ⇒ High M_o/M_A (0·9) [8,11]	Low b (0·4–0·5) ⇒ High M_o/M_A (0·9) High b (0·6–0·8) ⇒ Low M_o/M_A (0·6–0·7) [5,6,7,10]
7	A'shock 'h' [$n = ct^{-h}$]	Low 0·7 – 1·0 [9,12,13,14]	0·9 – 1·8 [16]
8	Mogi Type [15]	II, III [9]	I (for same region) [9]

Table 1.3

References :

1 Berg , 1968
2 Båth , 1965
3,4 Papazachos , 1971,1974
5 Utsu , 1969
6 McEvilly & Cassaday , 1967
7 McEvilly et al. , 1967
8,9,10 Gupta et al. , 1972a,b,c
11 Gupta & Rastogi , 1976
12 Comninakis et al. , 1968
13 Guha et al. , 1974
14 Hagiwara & Ohtake , 1972
15,16 Mogi , 1962a,1963b

regions, since near the beginning of the century. These tremors also differ in that they have no obvious relation to underground water pressures, and their origins can be explained easily in many cases, by simple recourse to elasticity theory and rock mechanics. Another difference is perhaps the 'b' values associated with the activity. In the few cases where these have been studied (e.g. Gibowicz, 1963; Al-Saigh, 1981), values typical of normal seismicity have been obtained. However, the larger events do tend to be of Mogi Type II, as aftershocks are often reported (lasting up to two days in the case of large tremors), and it has been found in Czech mines that the amount of noise increases from one to five days before the rockburst.

There are other similarities with reservoir earthquakes however. The shocks may take all magnitudes up to M = 5 (Buckle, 1965), and they frequently cause casualties and damage, both on the surface and underground. They also occur irrespective of geologies, although each kind of rock combination has its particular way of accumulating and releasing the additional stresses. For example, the coal mines of Britain and West Germany are situated in near-horizontally bedded variable sediments, whereas the near-vertical ore mines in India and Czechoslovakia which are developed in schists and dolerites respectively, are equally prone.

Despite mining-induced tremors being a well-accepted phenomenon, there have sometimes been long debates over their origins in naturally seismic areas where poor seismic control was available from the arrays present. For example, in the U. Silesia (Poland) coalfield, Janczewski (1950) stated that many of the earthquakes that he had studied in the preceding years were in fact natural, as they had hypocentres rather deeper than the mining, and he concluded that rockbursts observed to be coincident with the felt shocks had in fact been triggered off by them. Wierzchowska (1962) disputed the focal depths, and cited the small felt area, the correlation with bounces and with blasting as evidence of a mining origin. Kulpinski et al. (1966) finally located the hypocentres accurately, and found them to be mostly within the extraction zone.

The evidence given by Wierzchowska is in fact very typical of many cases of mining-induced seismicity. Correlations with periods just after blasting times have been noted in, amongst other places, Witwatersrand, Central Pensylvania, and Kirkland Lake (Canada), by Hodgson (1958), where the shifts were arranged to avoid this. Actually, although it would appear natural for underground workers to feel or observe many of the events, this is often not the case and, moreover, occasions when they did not notice shocks which were sensed by local residents or surface workers are not at all infrequent. This has been noted, for example, in the gold mines at Kirkland Lake, at Kolar in India (Isaacson, 1957), and in the coal mines of the Midland Valley of Scotland. This can be explained perhaps by Baule and Rao's (1979) observations of particle velocities which show that most of the energy transmitted is refracted towards the roadways rather than the face. Usually though, it is attributed to the rock bursting in an old worked-out seam. Sometimes, however, the opposite is the case, and visible rock movements do not coincide with traces recorded at the surface (e.g. S.Africa; Gane et al., 1946).

(i) Spatial Characteristics

Where sufficient resolution is available, it is possible to obtain the relative position of the hypocentres and the working face(s). A very close relation between the two is common, and investigations in the Ruhr coalfield which showed the shocks coming up to 40 m from the face, provide only one of the weaker examples. For instance, in a longwall mine in Pensylvania, Hardy and Mowney (1976) found the events clustered within 20 m of the face positions. Gane et al. (1952) and Cook (1962) placed seismicity in a Witwatersrand mine very accurately just at, and slightly above, the reef face. In the Donbass mine in Russia, Kagan and Lavrov (1966) found the seismic sources to be up to 16 m from the face, but mostly only 2 m - 10 m. Variations do exist however: Sebor et al. (1976) found that most of the shocks occurred in the overlying sandstone bed in a coal mine in the

Kladno district of Czechoslovakia. At Little Park Wash in Utah, the hypocentres are substantially below the working mines. Smith et al. (1974) could find no subsurface fault there, but showed that the fault plane solutions agreed with the geologically determined regional thrust-faulting regime. They concluded that the removal of pillars and barriers in the lower mines was reducing the vertical stresses due to the overburdon in the underlying rocks, thus exacerbating the natural stress system there.

It is also very frequently found that the presence of a nearby fault increases the instability, especially where two sets of faults intersect (e.g. Barnes et al., 1969). In the Kolar gold mines in India, the interaction with the Mysore North fault has proved significant in the location of the tremors (Taylor, 1963). Pillars have proved also to be particularly hazardous, particularly where the orebody is in steep, branching veins, as in Canada (Robson, 1946). Ivanov and Parshikov (1966) showed a large increase in noise to occur as faces pass underneath remnant pillars, with lag and lead anomalies due to its crushed ends.

(ii) Temporal Characteristics

There are several features which are commonly found to increase the level of activity, in addition to those mentioned above. The incidence of rockbursts is almost always greater at greater depths: in S.Staffordshire there are few problems until 300 m is reached (Phillips, 1944).

In the Wright-Hargreaves mines in Canada, the number of rockbursts and the depth have even been found to be proportional to one another (Buckle, 1965). Thus as the mines in a particular area become deeper as the coal or ore is worked out, there tends to be an increase in seismic activity throughout the history of the mining operation, as there was in S.Africa (Gane et al., 1946) where the energy released increased by 6% over the period 1911-1937. In Silesia, however, it is a different story. Neyman (1955) showed that the more violent rockbursts occurred when a level is being mined at first. This seems to trigger the stress of tectonic origin in this naturally seismic area, and the subsequent mining has weaker and fewer bursts.

The extraction itself also has an important effect; the rate at which it takes place is usually positively correlated with the level of seismicty, and it has been found in S.Staffordshire that this is particularly so when driving headings, or when two roadways are approaching each other. In Pensylvania, Hardy and Mowney (1976) found that the number of tremors dropped dramatically during shift changes - the microseismicity recommenced about twenty minutes after the following shift had begun. Many places in fact have markedly greater seismicity during week days, sometimes building up to a maximum on Thursday or Friday, and then dropping off till a minimum on Sunday (e.g. Cazalet, 1920; Kusznir et al., 1980). In central Scotland hardly any tremors occur during summer holiday periods or when there are strikes.

Apart from the temporal variations due to the mining activity itself, periodic variations of unexplained origin may occur. Isaacson (1957) has suggested a secular variation of mining tremors in S.India, and Osterwald and Dunrud (1966) report a maximum every five to nine days in the Sunnyside mines, Utah, along with sessional maxima twice a year, where fewer, but larger, bumps occur.

CHAPTER 2

THE NUMERICAL CALCULATION OF STRESSES AND THEIR RELATION TO ROCK FAILURE

2.1 Introduction

The complexities involved in the generation of reservoir-induced seismicity can be surmised from the frequently patternless nature of all the disparate parameters described in the preceding chapter. To tackle the problem in anything like a quantitative fashion requires that several simplifying assumptions be made. Initial attempts used Mohr Circle notation to describe the relative effects of water load and pore pressure superimposed upon various stress fields, or else calculated load stresses by analytical means (Gough and Gough, 1970b). The assumption of a homogeneous rock mass implicit in these approaches means that their results are hardly more relevant to practical examples of the phenomenon than are qualitative methods, although Gough and Gough did obtain good field agreement with their calculated displacements.

Considering the whole problem, it can firstly be noted that the following departures from the simplest models used by Gough and Gough are present: the medium may be heterogeneous, anisotropic, porous, cracked and pre-stressed. The first two properties might refer to any of the elastic constants, the viscosity, strength, permeability, specific heat, etc., many of which are also liable to vary in the time dimension. Fortunately, it is almost beyond question that the list of parameters having a direct bearing on the initiation of seismicity has only one member - the stress state of the rock. This is so if we imply that the term 'stress' here is relative to certain other mechanical properties of the rock, e.g. its strengths, friction coefficients, etc. If we then assume that it is a straightforward matter to predict seismicity after the stress state has been discovered, and that these last-

mentioned properties do not affect that state, then they can for the moment be neglected.

Thus the determination of the total space-and time-dependent stress field is the goal to be sought for. However, even if the important step is taken, of illiminating from consideration the space that lies outside what is assumed to be the region of interest, it is immediately obvious that solution of the problem either by analytical or numerical techniques still requires an infinity of data to be taken into account, and that further simplification is therefore necessary. The reduction to a finite number of variables can be attained by dividing the dimensions into separate 'sections', within the bounds of each of which the material is assumed to have constant properties. Although this is equivalent to opting for a numerical solution, it does still not necessarily imply that the stress-state is also constant within each section. This achieved, what remains to be tackled is the mathematical relationship between the variables and the resultant state of stress. Here it is necessary to be guided by the results of rock mechanics experiments under the equivalent of shallow crustal conditions. These results show that rock material behaves linearly elastically and/or in a brittle way during the short time periods encountered in induced seismicity (Jaeger and Cook, 1979), but they rarely take account of macroscopic structures, such as fissures and joints, which would partially invalidate the results of large-scale elastic modelling. Despite this latter reservation this is encouraging, because elasticity theory is straightforward and well documented, even for anisotropic media. If adequate allowance can then be made in the mathematics for initial stress, thermally induced stress and the effects of microscopic pores and cracks, it remains only to account for large fractures, the general heterogeneity and the effects of interstitial water.

Regarding the water, an assumption will now be made that its chemical and erosional effects are not sufficiently relevant, despite some suggestions

to the contrary (e.g. Gourinard, 1952; Murrell, 1965), to be worth tackling the appreciable difficulties involved in their quantification. The physical behaviour of water being well-known, it then becomes feasible to describe mathematically the relationship between its presence and the stress-state in the rock by using the principle of effective stress (Hubbert & Rubey, 1959; or Nur, 1971). It is propitious that the water must be dealt with separately from those points assigned to an elastic treatment in the previous paragraph, as this provides one means for introducing the time domain into the calculations.

If, for the moment, large-scale fractures are regarded as an extreme form of heterogeneity, then the one difficulty that remains is dealing with the mechanical irregularity. This problem is of a completely different type to those discussed above. The mathematical solution for each 'section' can of course be calculated analytically using the premisses and observations already mentioned, but each solution will have been derived independently from the others - in other words it will have ignored the heterogeneity we are trying to take into account. This can be overcome by in some way allying adjacent 'sections', so that we return in effect to a continuum similar to the original, but one partitioned by means of discontinuities in physical properties. The mathematics must now be performed in terms of pairs, or small groups, of sections, and a valid method of combination when dealing with the variables involved in elasticity is simply one of addition (Zienkiewicz, 1977 #1.3). If all the groups could then solve their particular sets of equations simultaneously, an overall solution would be obtained in which each section is at equilibrium with its neighbours, meaning in turn that equilibrium of the rock mass as a whole has been achieved. Fortunately, the method of finite-elements, which can deal with problems of exactly this kind, has been well-developed for some time, having first been exploited for solving similar problems in engineering (Turner et al., 1956). Finite element can conveniently work with problems in up to three dimensions, and

extensions to the theory can deal with changes in the time domain, and also with certain deviations from strictly elastic behaviour. The technique can and has been put to several disparate uses in earth science (e.g. Service and Douglas, 1973; Gale, 1974; Sturgul et al., 1976), after its potential for solving problems of this sort was pointed out by Voight and Samuelson (1968). Diab (1976) has in fact used finite-element for obtaining an approximate value for the energy that reservoir loading could contribute to an induced earthquake.

The earthquake can be regarded as a catastrophic response to relative changes in the pertinent parameters discussed above: the induction process can be regarded as an acceleration in the rate of change of some of these parameters. The mathematical nature of the final response is the subject of a later section in this chapter, but here we want to investigate the nature and causes of the original changes in the parameters themselves. As these changes are the consequences of the disturbance of the previous equilibrium, caused by the artificial imposition of the water load, they can be treated as the physical results of the natural readjustment to minimum overall energy.

2.2 Finite Element Theory

The theory given in this section is based on that of Zienkiewicz (1977, Chs. 1-4), but is presented here in a way that is specifically relevant to those aspects of finite element used in this thesis. For the greatest simplicity in the mathematics, the two-dimensional rock continuum will be divided into triangular elements which are, for the purposes of the analysis, only joined at their coincident nodes. They must of course also be contiguous along their common boundaries. The nodes are in fact the points which are directly subject to the calculations. As we are concerned with forces, the aggregate components dealt with at the nodes are obtained merely by adding the relevant contributions from each of the adjoining elements.

Since this is so, it is then possible to apply the following equations, which will be derived for an individual element, to the structure as a whole. Matrix notation will be used throughout.

Within any element (see Fig. 2.1), the displacements {f} at any point are determined in terms of the nodal displacements {δ} by means of shape functions [N] whose components are functions of position. These functions are chosen to be linear (thus ensuring good displacement continuities across element boundaries) so that:

$$\{f\} = [N]\{\delta\} \qquad (2.2.1)$$

where $[N] = [IN_i', IN_j', IN_m']$

$[N_i'] = (a_i + b_i x + c_i y)/2\Delta$,

$[I]$ is an identity matrix,

Δ is the area of the element $= \frac{1}{2}\begin{vmatrix} 1 & x_i & y_i \\ 1 & x_j & y_j \\ 1 & x_m & y_m \end{vmatrix}$

$a_i = x_j y_m - x_m y_i$

$b_i = y_j - y_m$

$c_i = x_m - x_j$

and the other coefficients are obtained by cyclic permutation of the subscripts.

From the displacements, the strains can be obtained:

$$\{\varepsilon\} = \begin{Bmatrix} \partial u/\partial x \\ \partial v/\partial y \\ \partial v/\partial y + \partial v/\partial x \end{Bmatrix}$$

Strain is usually given in terms of the nodal displacements, so that,

using 2.2.1: $\{\varepsilon\} = [B]\{\delta\}$ (2.2.2)

where $[B] = \frac{1}{2\Delta}\begin{bmatrix} b_i & 0 & b_j & 0 & b_m & 0 \\ 0 & c_i & 0 & c_j & 0 & c_m \\ c_i & b_i & c_j & b_j & c_m & b_m \end{bmatrix}$

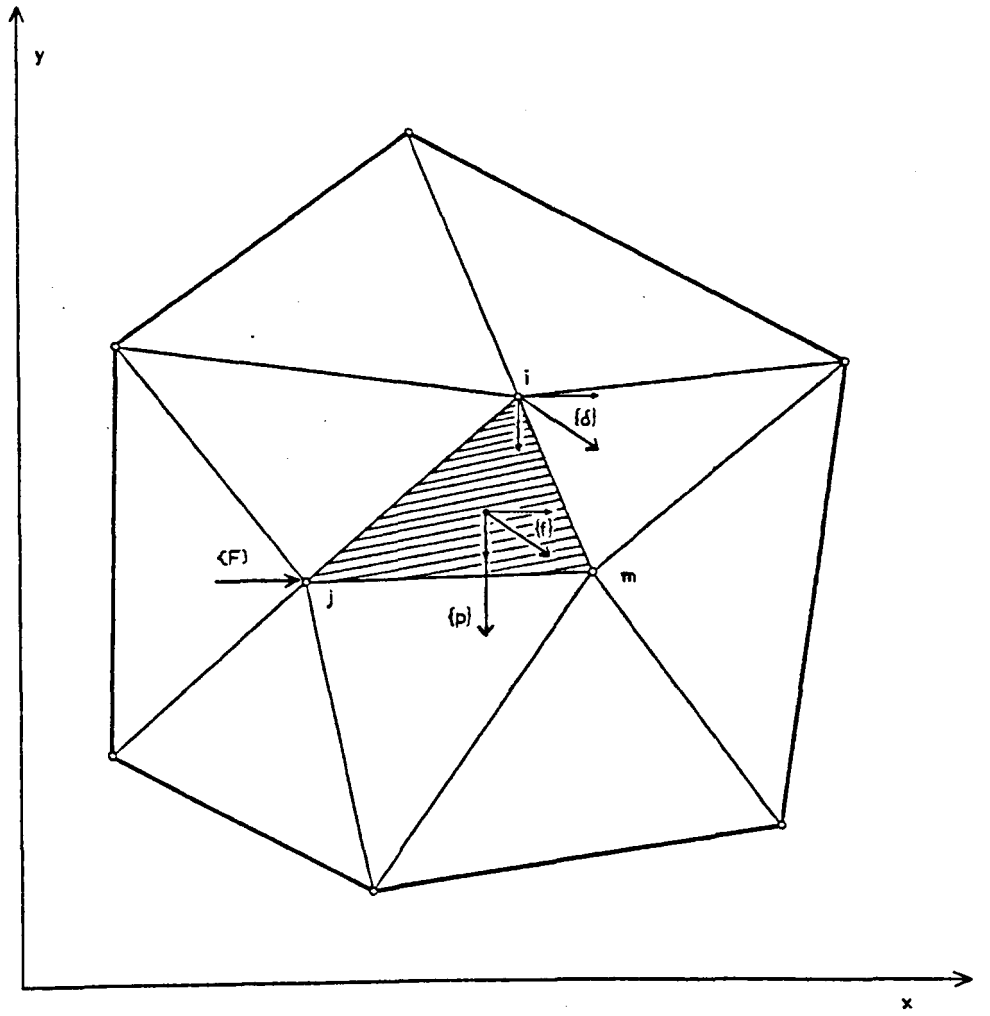

Figure 2.1 A plane stress region divided into finite elements showing representative nodal forces $\{F\}$, body force $\{p\}$, internal displacements $\{f\}$ and nodal displacements $\{\delta\}$, for one element.

Then it is a simple matter to obtain the internal stresses from the nodal displacements, if the analysis is confined to linear elastic behaviour (Jaeger and Cook, 1979). Taking into account any initial tectonic or residual stresses $\{\sigma_o\}$, and/or strain $\{\varepsilon_o\}$, the relationship will be:

$$\{\sigma\} = [D]\,(\{\varepsilon\} - \{\varepsilon_o\}) + \{\sigma_o\} \qquad (2.2.3)$$

where, if plane-strain conditions are assumed:

$$[D] = \frac{E(1-\nu)}{(1+\nu)(1-2\nu)} \begin{bmatrix} 1 & \nu/(1-\nu) & 0 \\ \nu/(1-\nu) & 1 & 0 \\ 0 & 0 & (1-2\nu)/2(1-\nu) \end{bmatrix}$$

or for plane-stress:

$$[D] = \frac{E}{1-\nu^2} \begin{bmatrix} 1 & \nu & 0 \\ \nu & 1 & 0 \\ 0 & 0 & (1+\nu)/2 \end{bmatrix}$$

where E is the Young's Modulus and ν the Poisson's ratio of the rock.

In treating induced seismicity problems, two main sources of potential and strain energy are present:

(a) gravity (represented by a body force {p} integrated over the area of each element and then partitioned off to the nodes), and

(b) external stresses, e.g. those due to the water load, or to the confining effects of adjacent regions of the crust. These are incorporated as equivalent nodal forces {F}, whose values are calculated by inspection.

These energies must be partially redistributed about the grid in such a way that their total is at a minimum. In other words the stresses in the rock change to values that provide a resistance equal to the final potential energy of the rock mass. Mathematically, the total internal strain energy is given by:

$$U = \tfrac{1}{2} \int \{\varepsilon\}^T \{\sigma\}\, d(vol) \quad *$$

* $[M]^T$ denotes the transpose of [M].

and the total potential energy by:

$$W = - \{\delta\}^T \{F\} - \int \{f\}^T \{p\} \, d(vol)$$

The total elastic energy χ (= U + W) is given by:

$$\chi = \tfrac{1}{2} \int \{\varepsilon\}^T \{\sigma\} \, d(vol) - \int \{f\}^T \{p\} \, d(vol) - \{\delta\}^T \{F\} \qquad (2.2.4)$$

Using equations 2.2.3, 2.2.2 and 2.2.1 respectively in 2.2.4, an expression for the total energy is obtained in terms of displacements and the matrices [D], [B] and [N] which have been defined above:

$$\chi = \tfrac{1}{2} \int [B]^T \{\delta\}^T [D][B]\{\delta\} d(vol) + \int [B]^T \{\delta\}^T \{\sigma_o\} d(vol) -$$

$$\int [B]^T \{\delta\}^T [D]\{\varepsilon_o\} d(vol) - \{\delta\}^T \{F\} - \int [N]^T \{\delta\}^T \{p\} d(vol)$$

To find the values of the nodal displacements equivalent to minimum total energy, we put

$$\frac{\partial \chi}{\partial \{\delta\}} = 0$$

i.e. $\int [B]^T [D][B]\{\delta\} d(vol) + \int [B]^T \{\sigma_o\} d(vol) - \int [B]^T [D]\{\varepsilon_o\} d(vol) -$

$$\{F\} - \int [N]^T \{p\} d(vol) = 0$$

Rearranging:

$$\{F\} = \left(\int [B]^T [D][B] d(vol)\right)\{\delta\} + \int [B]^T \{\sigma_o\} d(vol) - \int [B]^T [D]\{\varepsilon_o\} d(vol)$$

$$- \int [N]^T \{p\} d(vol)$$

Usually the stiffness matrix [K] is put equal to $\int [B]^T [D][B] d(vol)$. Initial strains $\{\varepsilon_o\}$ are not physically important to elastic analyses of induced seismicity, but have been included up to now because they become relevant when viscous effects have to be used, as in Section 2.3. The gravitational forces are converted directly, as described above, to nodal forces, $\{F\}_p$, and the initial stress term is evaluated $\{F\}\sigma_o$ and also added to the nodal values. Thus the final form of the simultaneous finite-element equations,

to be solved for nodal displacements, is:

$$\{F\}_{TOT} = [K]\{\delta\} \qquad (2.2.5)$$

where $$\{F\}_{TOT} = \{F\} + \{F\}_p - \{F\}\sigma_o$$

The displacements are then converted to internal strains and stresses using relationships similar to 2.2.2 and 2.2.3, and these are then delivered as results in the form of the principal stresses at the centroid of each element. Where a plane-strain assumption has been made, the stress perpendicular to the plane of the grid is then calculated separately using:

$$\sigma_y = \nu(\sigma_x + \sigma_z) = \nu(\sigma_1 + \sigma_2) \qquad (2.2.6)$$

Displacement boundary conditions are applied before the solution of the basic equation 2.2.5 by making the stiffness matrix extremely stiff for the nodes in question. This is accomplished by multiplying the diagonal element of the stiffness matrix that corresponds to the node by a very large number (10^{12}). At the same time the corresponding force vector is replaced by the prescribed displacement multiplied by the new diagonal element.

2.3 Problems of the Application of Finite Element Theory

(i) Confusion of Gravitational and Elastic Perturbation Stress Fields

Finite element is a powerful technique, but is at the same time very susceptible to misuse. Both careful consideration of the assumptions that have been made, and a clear insight into the nature of the stress sources involved, must be realised if misleading results are to be avoided. A common error in elastic analyses similar to those in induced seismicity, is to neglect the differing time-spans over which the two main sources of stress act: the gravitational energy in producing the main stress field acts over periods during which significant non-elastic processes occur. Thus, if a straightforward elastic program run is carried out to investigate simultaneously both the gravitational and artificial stress effects, a model with

very large deviatoric stresses (with $\sigma_v \simeq 3\sigma_H$ ($\nu = 0.25$)) is produced, to which the artificially induced deviatoric stresses may not contribute to an extent much greater than the numerical error involved. These large deviatoric stresses are of course purely a result of the mathematics assumed when treating the body forces elastically, and do not bear any resemblance to the vast majority of stress fields measured in real rocks (Ch. 3). Obviously only the induced component is adequately catered for by an elastic assumption, and hence must be calculated separately from the body stresses. There are two ways in which these body stresses can be included. Firstly, they can be assumed to be lithostatic, calculated analytically and then added to the induced perturbation. Secondly, they can be calculated by means of a finite-element visco-elastic run, in which creep effects over long time periods are taken into account.

This second method obviously requires an extension to the theory presented in the first section of this chapter. A further decision, concerning the particular rheological properties of the rock, must be made before the creep behaviour can be calculated. As this behaviour is being utilised merely for determining the long-term, locked stress-state, its exact nature is not critical, and it has been assumed here that it is like that of a Maxwellian substance. This means that the creep rate is simply given by:

$$\dot{\varepsilon} = \dot{\sigma}/E + \sigma/\eta \qquad \text{(Jaegar and Cook, 1979)} \qquad (2.3.1)$$

(η is the rock viscosity) which represents the combination in series of Hookian and Newtonian substances. Thus the strains at any given time are dependent upon the creep history of the rock, and the numerical computation must proceed through time by a succession of small increments. Hence the simulation of continuous creep behaviour is accomplished by approximating it to a series of elastic strains, where the creep occurring during each time-step is incorporated in the following step as an initial strain in the finite-element equation. Details of the process are given in Appendix 5.

Once this stable stress-state has been determined, it becomes quite simple to feed it into the elastic run as an initial state of stress, hence producing the required combined stress state (N.B. Appendix 6). If the effects of the artificial perturbation need to be examined, then subtraction of the visco-elastic stress field from that of the elastic can be carried out. However, it is usually simpler, and more meaningful, just to calculate the deviatoric or shear stresses.

If however the first method is used, and the natural stress field is assumed lithostatic (and this can only be done easily with regular homogeneous models), then it has to be added after direct determination of the stresses due to the perturbation. Deviatoric stresses can of course in this case either be derived from the elastic stress field or from the total stress field.

The calculation of the stress field due solely to the artificial disturbance is then accomplished by removing the rock property that results in the body forces. This may be easily accomplished by subtracting the maximum rock density from the whole model. Around areas of air and water, which consequently have negative density contrasts, the predominantly tensional perturbation stresses are seen directly.

The numerical error in a finite-element solution is related to the maximum stress present, and so this latter method has inherently greater accuracy. The combined visco-elastic method described above, however, appears physically more realistic in that it simulates the build-up and/or relaxation of stresses over geologic time, and them imposes an instantaneous 'load' such as might be provided by erosion or a reservoir.

In practise, simple homogeneous models are most easily handled by the density contrast method. A slight modification of this, density stripping, can be used to advantage in a similar way, when horizontal layers of differing density occur. In this method the appropriate densities are subtracted from each layer in order that the densities at the boundaries are zero (see

next section), and the equivalent lithostatic stresses may be added to the solution afterwards.

More complicated models have to make use of a visco-elastic run to establish the initial stress state. It is still possible, however, to take advantage of the improved numerical accuracy afforded by partial removal of the density. The greatest improvement is obtained by subtracting the maximum density from the whole model. Little, if any, advantage can be derived from a more complicated density stripping procedure in this case.

(ii) Application of Boundary Conditions

One of the most unrealistic steps taken in the finite-element formulation was the isolation of the vertical rectangular grid from the surrounding rock. The conditions at the boundaries must be such that they produce results similar to those that would be arrived at without the isolation. Since these latter results are not known, it is necessary to make assumptions concerning the displacements and/or forces it might be necessary to impose on the boundaries by inspection and some ad hoc assumptions. Firstly, it must be noted that the more remote are the boundaries from the stress concentrations around the disturbance being investigated, the less effect these artificial limits will have.

However, boundaries cannot usually be put at infinity in finite-element models, and so the problem cannot be totally overcome. Indeed, for one method of application of boundary conditions, distant boundaries hinder the attempted compensation. This is the case when the bottom boundary is restrained for zero vertical movement, and resists the effective moment produced by lithostatic forces applied at the vertical sides. The use of calculated lithostatic forces to restrain the boundaries might be thought an apt way to treat the model. The problematical affect here is an example of St. Venant's Principle, which results in lateral stress gradients decreasing with distance from their source. This means often that distinctly meaningless non-lithostatic stresses are being combined with those calculated in the region of interest, grossly distorting the true stress field there.

For visco-elastic runs, constraining the boundaries for zero movement (while the nodes themselves can move along them) is a reasonable strategy, for this produces the gradual compaction required, so that the horizontal stresses increase to a near-lithostatic state. The use of the same boundary conditions for the subsequent elastic runs is not as defendable, but should have little effect on the solution since in this case only relatively small local changes around the disturbance are occurring.

In the case of density-contrast runs though, it is perfectly feasible, providing boundary densities are zero, to simulate exactly lithostatic boundary conditions without having to worry about St. Venant's Principle. This is achieved by not constraining displacement in any way, and applying zero forces at the boundary nodes.

(iii) Computer Storage

With matrices often containing several hundred elements, the actual finite-element calculations have to be carried out by computer. Even so, limitations are imposed by the storage space available in the largest computers, and hence the number of nodes used to form the grid is usually limited to approximately 200-300, even if the bandwidth is minimised (Appendix 3). A way of reducing the effective number of nodes is to take advantage of any lines of symmetry in the model, and using only the non-repeated areas. Thus for example when examining V-notch valleys, only the area on one side of the vertical plane of symmetry passing down its centre has to be examined. The boundary condition along this line is always one of zero movement perpendicular to the boundary. Further aspects of the computation are discussed in Chapter 6, and a program test is described in Appendix 7.

2.4 Computation of Rock Failure

In the present study, two main methods of predicting failure have been used, one for motion along a pre-existing fault plane, and one for fracture of intact rock. Brace (1974) reports that the effects of fracture strength

and friction upon rock failure up to 4 kbar (∿15 km) and 500°C (∿40 km), remain similar to those under near-surface conditions, and this will be especially so where pore pressures contribute to the brittle fracture process. Consideration of ductile effects in the analysis of rock fracture for reservoir-related earthquakes is thus unnecessary. Along pre-existing fault planes, either stick-slip or stable sliding must occur, the mechanism depending on the rock mineralogy (especially the presence of serpentine), confining pressure (Byerlee and Brace, 1968), and rock stiffness. Strain rate appears to have no effect in differentiating between the two mechanisms. Indeed, no convenient criterion has yet been established for determining which will occur. There is also considerable debate concerning the processes that lead to the original formation of a macroscopic fracture in rock: these no doubt depend on a very large number of factors. Sobolev et al. (1978) look into several different, recently presented, treatments, but none of these have been stated quantitatively. Failure of a rock continuum has thus been treated using the traditional Griffith's theory.

There are also, however, several factors which complicate the simple criteria, which must be borne in mind when using them. Rock strength has been shown (Brace, 1961) to be dependent on grain size (and, in an unknown way, to grain shape as well), but in general:

$$S \propto D^{-m} \qquad (2.4.1)$$

where S is the strength, D the maximum grain diameter, and $0.28 < m < 0.56$ (m is greater for stronger rocks). The coefficient of static friction is found to vary negligably within the low pressures and temperatures involved here (Edmond and Murrell, 1971).

Failure, either of intact rock, or along a pre-formed plane, is usually assumed to be governed by the maximum and minimum principal stresses. Several (mainly theoretical) studies have found the effect of the intermediate stress, σ_2, to be negligible in the case of homogeneous, compressive

conditions (e.g. Brady, 1970; Murrell, 1970a). Mogi (1967) does however find that strength at failure increases with σ_2 by a small amount that is proportional to σ_3 - an effect which is much more pronounced for brittle material. He gives in fact, as a failure criterion for some sedimentary rocks:

$$\tau \geq f[(\sigma_1 + \sigma_3 + \sigma_2/10)/2] \qquad (2.4.2)$$

where the function is dependent on rock type. The angle between faults and σ_1 is thus markedly reduced as σ_2 increases.

Phenomena such as pre-seismic slip, dilatancy and strain-softening are not considered here, as they have not yet been developed sufficiently quantitatively to be included. Other factors, such as increase in frictional stress with depth are accounted for intrinsically in the nature of the analysis. However, it remains true that no allowance has been made for the effects of many of the above variables on parts of the fault plane some distance away: each element is tested individually. Similarly no account is taken of changes in strength due to vertical or horizontal curvature of the fault plane, or stress distributions caused by previous fault slippage. In general these factors increase the strength and may be roughly simulated by the use of higher than normal shear strengths: their quantitative effects are not at all well known.

(i) The Modification of Griffith's Theory

Griffith (1920) put forward a theory describing the conditions necessary for the failure of a brittle substance containing microscopic flaws, such as rock. These conditions are (stresses in dynes/cm^2):

$$\sigma_2 \leq To \text{ in the region } \sigma_1 + 3\sigma_2 \leq 0 \quad \text{[Tensional failure]} \qquad (2.4.3)$$

or

$$(\sigma_1 - \sigma_2)^2 + 8\,To\,(\sigma_1 + \sigma_2) \geq 0 \text{ in the region } \sigma_1 + 3\sigma_2 \geq 0$$

$$\text{[Open Crack Failure]} \qquad (2.4.4)$$

where σ_1 and σ_2 are the maximum and minimum principal stresses respectively,

and To is the uniaxial tensile strength. These are shown in graphical form in Fig. 2.2. Equation 2.4.4 has been shown to be equivalent to a parabolic Mohr envelope (Murrell, 1958). Compressional stresses are taken as positive throughout this section. Murrell (1964) went on to consider the failure criterion for the case when all cracks are closed. This occurs when (by definition) σ_y, the stress across the crack, is greater than σ', the normal stress needed to close the crack. This will be the case for all cracks of any orientation when $\sigma_2 > \sigma'$ (Murrell, 1970b). In this region failure occurs when:

$$(\sigma_1 + \sigma_2) + \alpha\,(\sigma_2 - \sigma_1) - \beta \leq 0 \qquad (2.4.5)$$

where $\alpha = \frac{\sqrt{1+\mu^2}}{\mu}$ and $\beta = \frac{4To}{\mu}\left(1 - \frac{\sigma'}{To}\right) + 2\sigma'$, and μ is the coefficient of internal friction. This form is analagous to a linear Mohr envelope. Rearranging 2.4.5 gives:

$$\sigma_1 \leq \frac{\beta}{1-\alpha} - \sigma_2\left(\frac{1+\alpha}{1-\alpha}\right) \qquad (2.4.6)$$

which is more suitable for computation. This criterion, however, will also apply in part of the intermediate region, $\sigma_1 > \sigma' > \sigma_2$ (Murrell, 1970b) where only some of the cracks are closed. In this subregion cracks will be closed if:

$$\sigma_y = \sigma_1 \cos^2\theta + \sigma_2 \sin^2\theta \geq \sigma' \qquad (2.4.7)$$

or

$$\cos\theta \geq \sqrt{\frac{\sigma'-\sigma_2}{\sigma_1-\sigma_2}} \qquad (2.4.8)$$

or

$$\sigma_1 \geq \sigma' \sec^2\theta - \sigma_2 \tan^2\theta \qquad (2.4.9)$$

where θ is the maximum angle between σ_y and σ_1, and is equal to $\frac{1}{2}\tan^{-1}(1/\mu)$ at failure. The situation is represented in terms of the stress ellipse in Fig. 2.3. If we take $\sigma' = 4.19T_o$, $\mu = 1.09$ (Murrell, 1965) and $T_o = -0.5\times10^9$

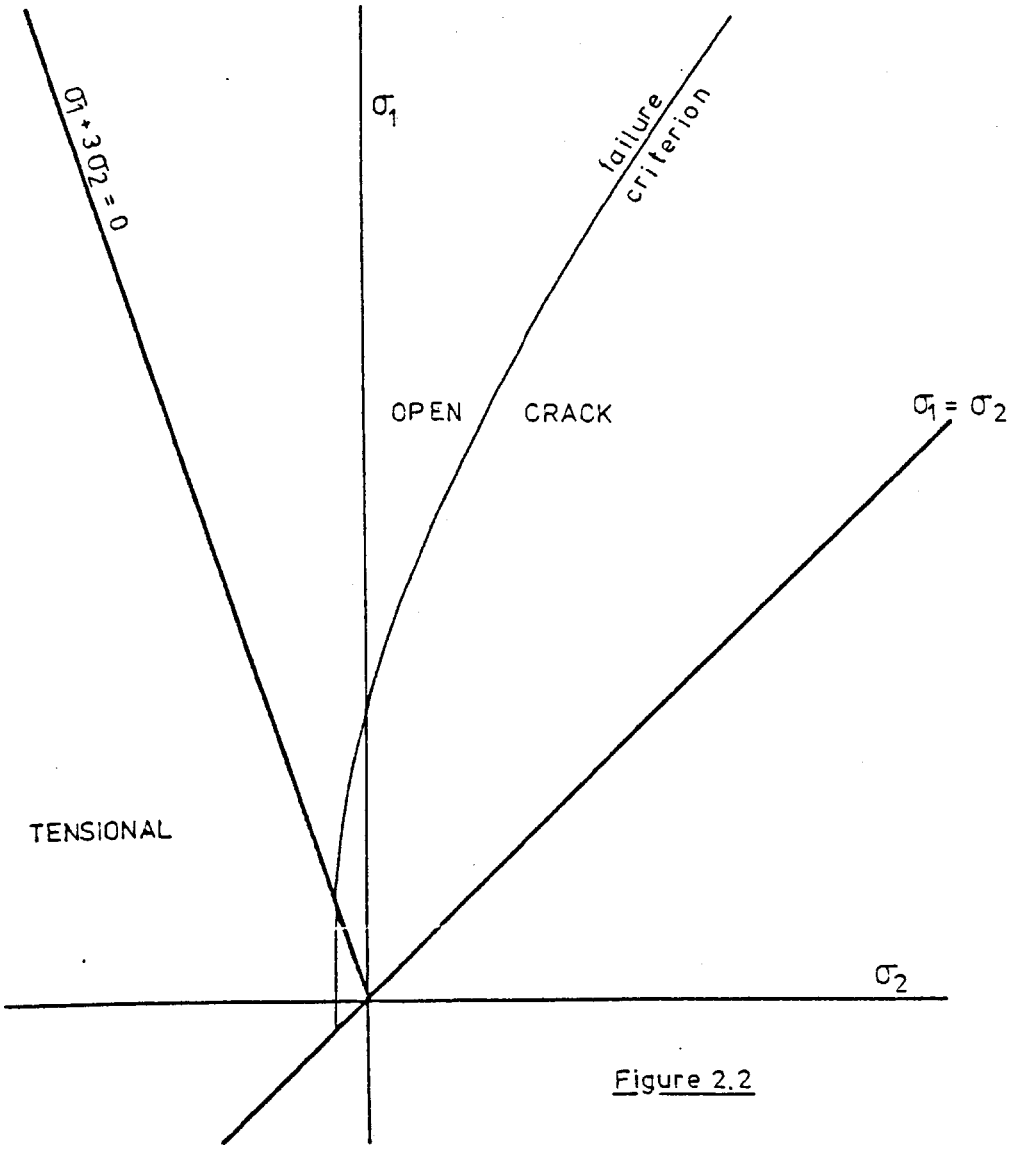

Figure 2.2

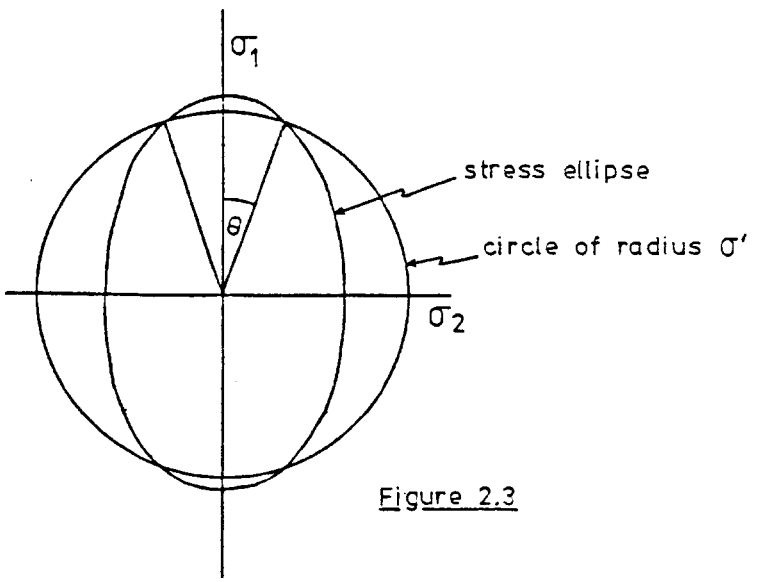

Figure 2.3

(For explanation of these figures see text.)

(Brace, 1961), this means $\beta = 0.01 \times 10^9$ (i.e. very small compared to the stresses), $\alpha = -1.357$ and $\theta = 21.3^\circ$. Equations 2.4.6 and 2.4.9 then mean that failure occurs when:

$$\sigma_1 \leq 6.6\ \sigma_2 \qquad (2.4.10)$$

in the subregion

$$\sigma_1 \geq 2.41 \times 10^9 - 0.15\ \sigma_2 \qquad (2.4.11)$$

which of course includes the region of completely closed cracks. Thus, equation 2.4.10 only applies to the region 2.4.11 in which all cracks, which are at angles likely to fail under the closed crack failure criterion, are closed. No account is taken of the fact that in this intermediate region, open crack failure might still occur in subregions Q1 and Q2 (Fig. 2.4), where closed cracks have not failed. Whether it does or not can be decided by comparing the angles of cracks closed in each region with the angles at which open crack failure would take place. The maximum orientation, θ, of the cracks that have closed is given by 2.4.8. $\sigma_1 = \sigma_2 = \sigma'$ satisfies this equation for all values of θ, and so the locus of all pairs of stress values for a particular angle is a straight line 2.4.9 of slope $-\tan^2\theta$, passing through (σ', σ'). The slope, ϕ, of these loci can be found from Fig. 2.5. The angle, γ, at which cracks fail under open crack conditions is given by:

$$\cos 2\gamma = -\tfrac{1}{2}\left(\frac{\sigma_1-\sigma_2}{\sigma_1+\sigma_2}\right) \qquad \text{(Murrell, 1964)} \qquad (2.4.12)$$

or

$$\sigma_1/\sigma_2 = (1-2\cos 2\gamma)/(1+2\cos 2\gamma) \qquad (2.4.13)$$

Equation 2.4.13 is plotted in Fig. 2.6. Thus, for example, along the tensional/open crack boundary where the stress ratio is -3, failure will occur at 90° to σ_1, and for the closed crack failure stress ratio of 6.6, at 56.5°.

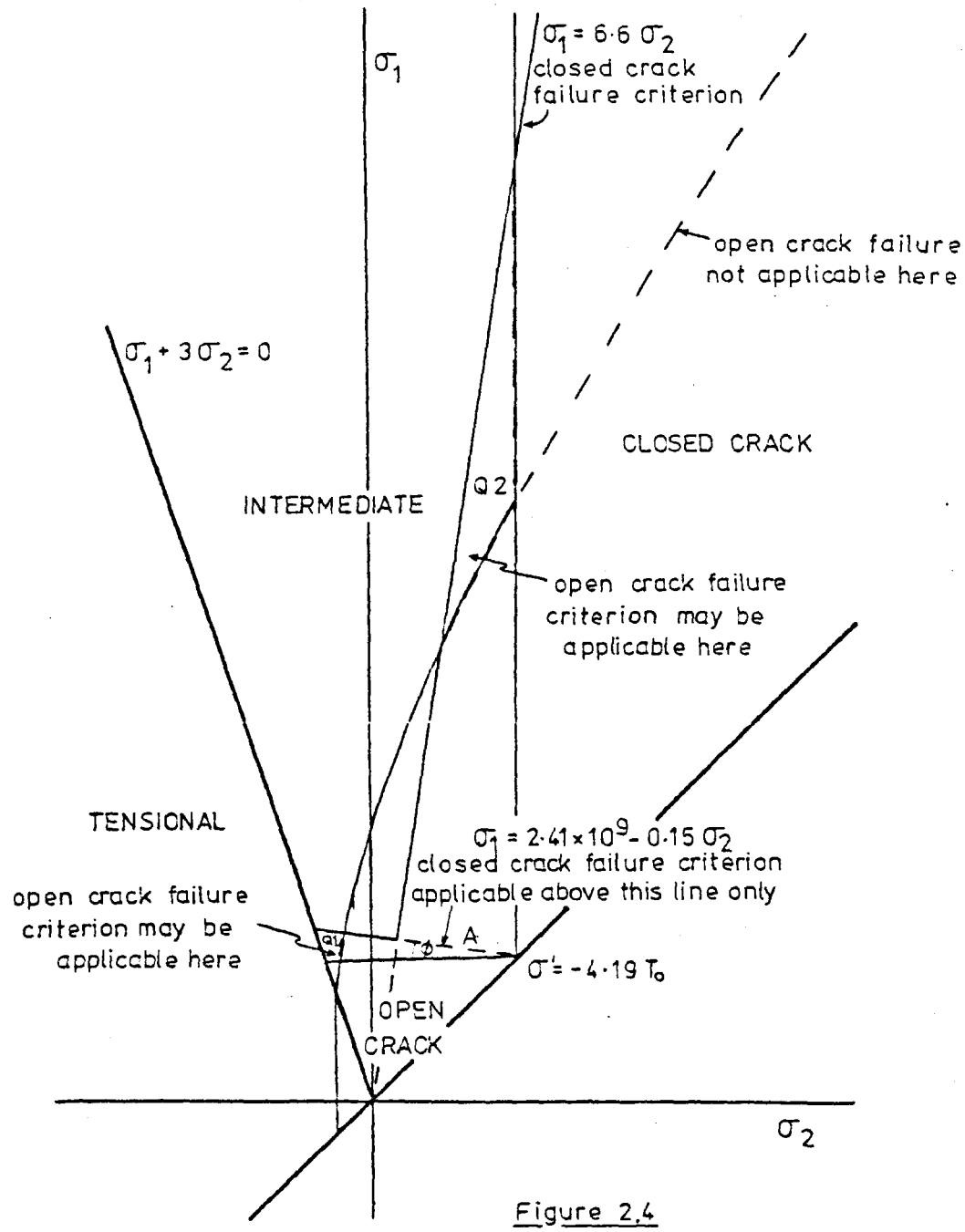

Figure 2.4

(for explanation see text)

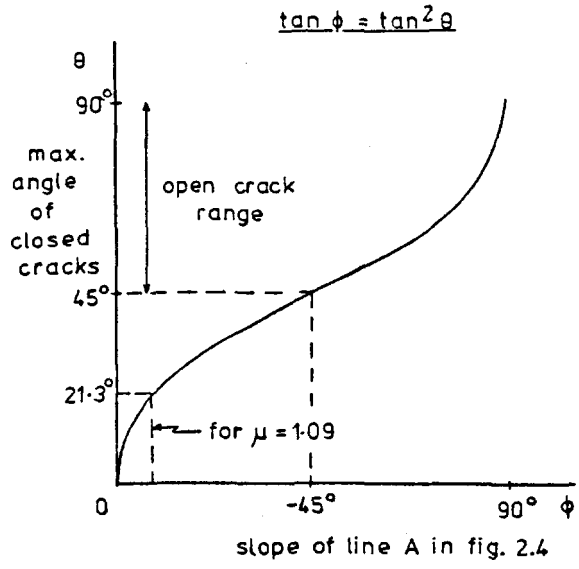

Figure 2.5

Variation of Open Crack Failure Angle with Stresses

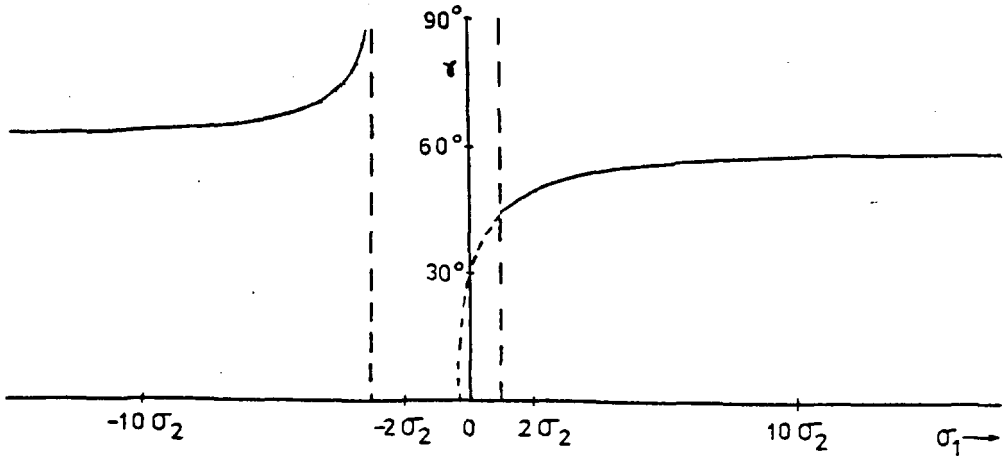

Figure 2.6

For the region Q1 in Fig. 2.7, reference to Fig. 2.6 will show that the corresponding failure angles range between 66.5° and 90°, and reference to Fig. 2.5 will then show that the region corresponding to these cracks being closed does not coincide with Q1, and lies above it. Thus, open crack failure is possible throughout the whole area of Q1 in this case, and in fact this must always be so, since θ must always be less than 45°, ($\mu > 0$), and γ is always greater than 45°. However, for Q2, the range of open-crack failure angles is from 54.5° to 56.5° and so the relevant cracks are now closed and open crack failure cannot occur.

The final overall criterion resulting from the above considerations is shown as a heavy line in Fig. 2.7. However, the value of σ' chosen so far, ($= -4.19T_o$) has the illogical effect of decreasing the strength of the rock when passing from open to closed crack criteria. By inspection of Fig. 2.7 it can be seen that, for a value of $\mu \leq 1.09$, this will occur for all values σ' given by:

$$\sigma' \leq 5.69 \times 10^9 \text{ dynes/cm}^2 \quad (= -11.4T_o) \qquad \text{(Fig. 2.8)} \qquad (2.4.14)$$

Murrell (1964) suggested that $\sigma' \simeq -40T_o$ ($= 20 \times 10^9$ dynes/cm^2), from theoretical work. When this value is used it is found that only in part of region Q2 are the cracks closed (Fig. 2.8). The potential crack failure angle, γ, for the stress ratios encountered in Q2 are between 56.5° and 49.5°. Using Fig. 2.5 to plot the corresponding values of θ, we find that above line A all the relevant cracks are closed and the closed-crack criterion applies. However, above point B only some of the relevant cracks are open. By combining equations 2.4.7 and 2.4.12 the locus of the points at which an incipiently failing crack just closes can be found:

$$\sigma_1^2 + \sigma_1 (6\sigma_2 - 4\sigma') + (\sigma_2^2 - 4\sigma_2 \sigma') = 0 \qquad (2.4.15)$$

or

$$(\sigma_1 + \sigma_2)^2 - 4\sigma' (\sigma_1 + \sigma_2) + 4\sigma_1 \sigma_2 = 0$$

[Intermediate Failure Criterion]

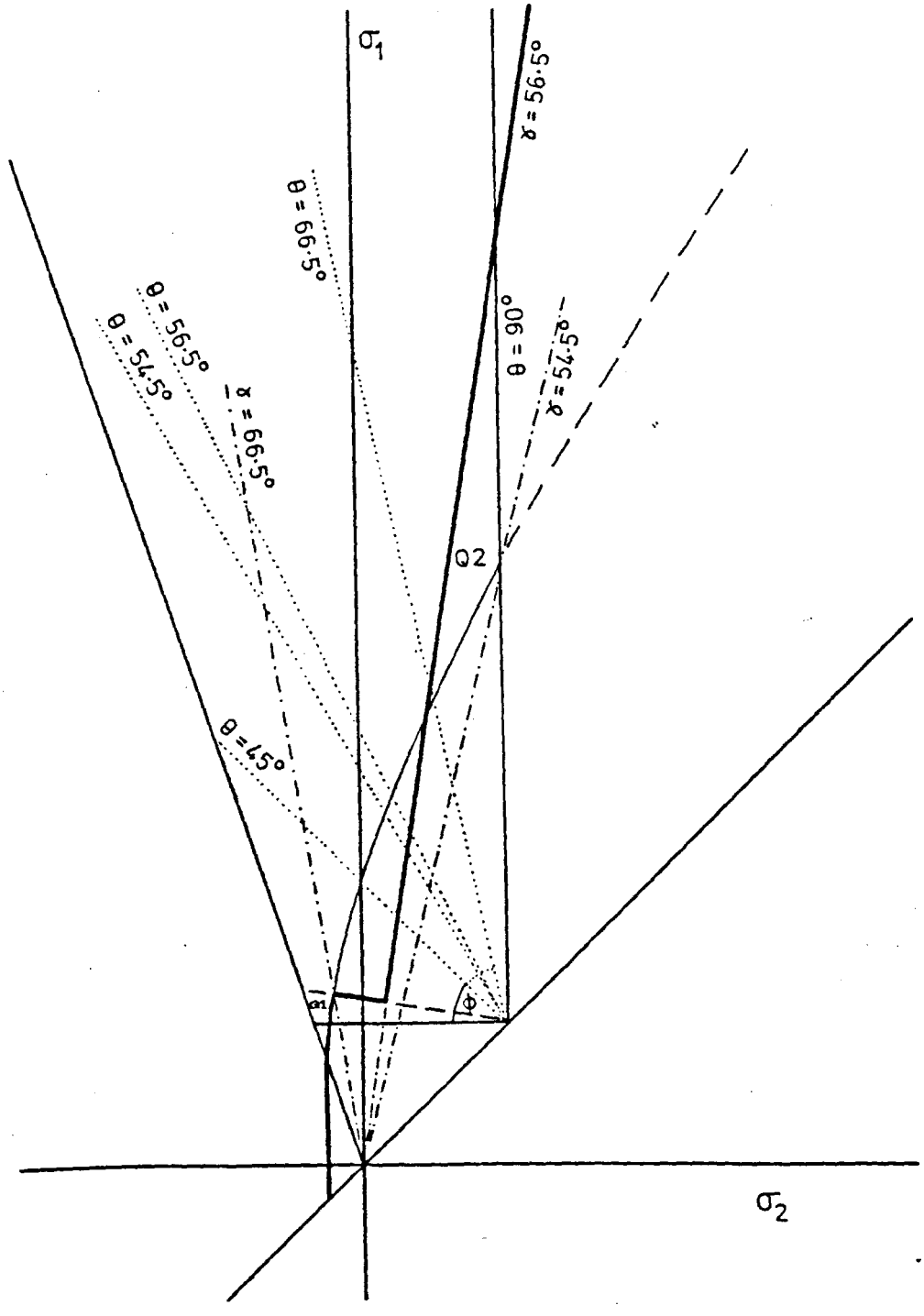

Figure 2.7 . (for explanation see text)

Intermediate construction lines are shown in Fig. 2.8, for θ and $\gamma = 51.5^{\circ}$, 53.5°. This criterionis effectively a version of the open crack criterion modified to take into account the cracks that have closed. Since equation 2.4.14 is satisfied, the transition from open crack to closed crack failure represents an increase in rock strength. Failure can still however be brought about on occasion by reduction of σ, as this opens up some cracks, releasing the frictional constraints.

The value of σ_1 at point B can be found by combin ing equations 2.4.4 and 2.4.15.

$$\sigma_1 = \sigma' - 2T_o + 2\sqrt{T_o(2T_o - \sigma')} \qquad (2.4.16)$$

and the value of σ_1 at D can be found by combining equations 2.4.6, 2.4.7 and 2.4.12:

$$\sigma_1 = \sigma' \left(\frac{2\alpha(\alpha+1)}{2\alpha^2-1} \right) \qquad (2.4.17)$$

The above criteria have been used in subroutine FAIL in the main finite-element program to test the final stress state in each element, with the failure regions denoted as in Fig. 2.9. Region 3B exists only if equation 2.4.14 holds. In fact, Murrell and Digby (1970) proposed for theoretical and experimental reasons, that $\sigma' \simeq -10T_o$, which is close to that given by equation 2.4.14. Thus in practice it is convenient to use a value of $\sigma' = 11.4T_o$ in the subroutine.

Murrell (1965) gave an empirical criterion, based on experiments with sandstone:

$$\tau \geq \sqrt{4T_o}\,(\sigma_n)^{0.61} \qquad (2.4.18)$$

where σ_n is the normal stress across the plane of fracture, and τ the shear stress in its direction. This criterion has been included in the pore pressure program as a failure subroutine SAFAIL.

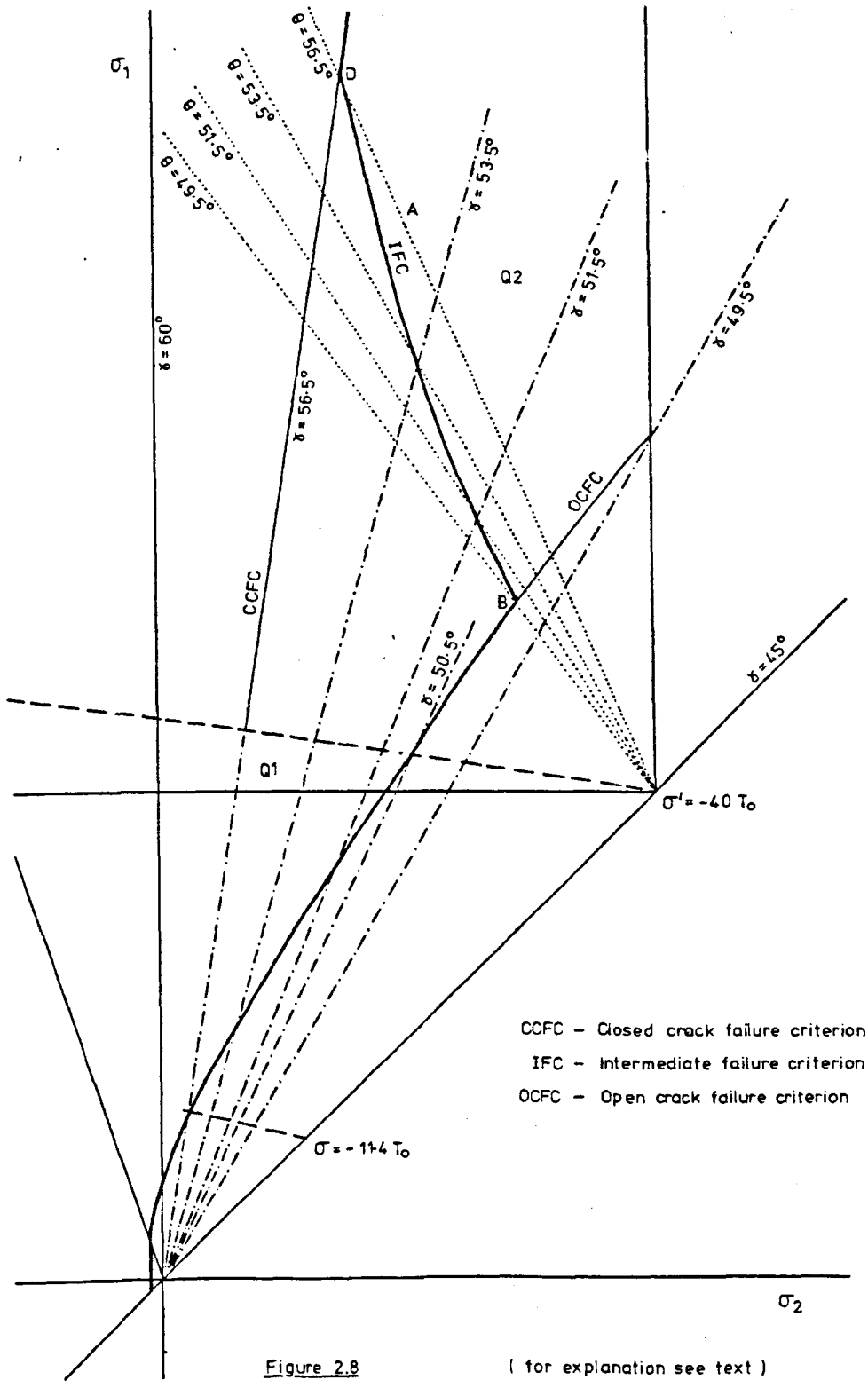

Figure 2.8 (for explanation see text)

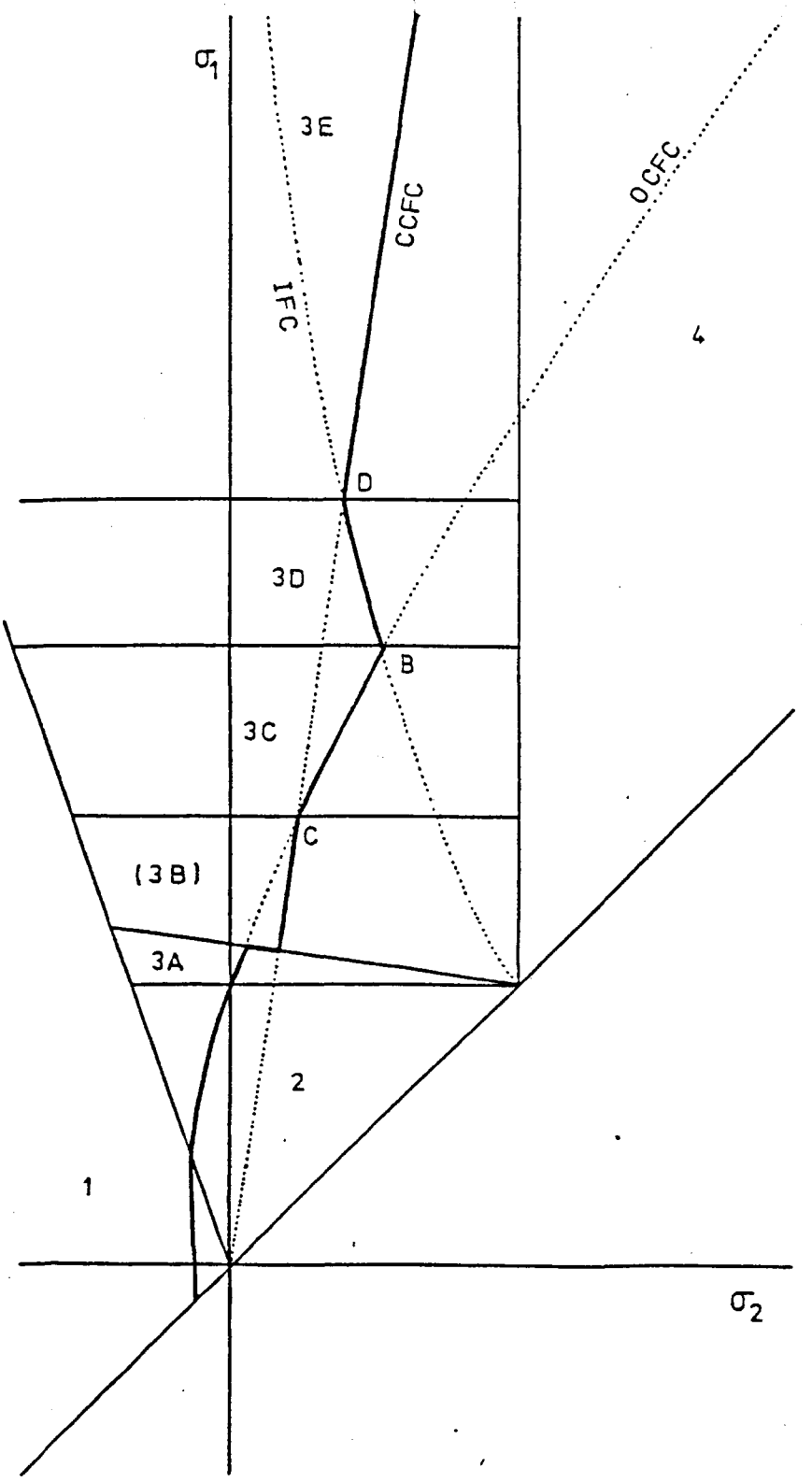

Figure 2.9 Computer designation of failure regions

(ii) Determination of Fault Slippage

Griffith's criterion applies to intact rock. The upper few kilometres of the crust, however, usually contains many fractures, and failure will tend to occur along these ready-formed planes as little energy is required to overcome their cohesive strength. Fortunately there is less controversy concerning the conditions necessary for slippage to occur in these circumstances. A subroutine SLIPS is used to test for failure by means of the Coulomb-Navier failure criterion:

$$\tau \geq S_o + \mu\sigma_{eff.} \qquad (2.4.19)$$

where S_o is the shear strength and has a value appropriately small compared to T_o. The subroutine determines the intersections (if any) of 2.4.19 and the Mohr circle defined by the principal stresses, and gives an approximate value for the maximum fault angle, with respect to σ_2, that will cause slip. This criterion, with small S_o, is almost exactly the same as the Modified Griffith closed crack criterion 2.4.5, as both were based on essentially the same assumptions. Equation 2.4.19 is, in principal stress space:

$$\sigma_1 = \sigma_2 \left(\frac{1 + \sin\phi}{1 - \sin\phi}\right) + \left(\frac{2T_o \cos\phi}{1-\sin\phi}\right) \qquad (2.4.20)$$

where $\phi = \tan^{-1}\mu$. Where there exists a plane of weakness, at an angle β to σ_2, unity in the above formula is replaced by the expression $\sin(\phi+2\beta)$. For smaller stresses, where Griffith's open crack criterion would apply, the effect of fracture planes is to produce relief of stress by slippage along these faults before the 'intact' rock begins to fail. At higher stresses ($\gtrsim$ 5 kbar) there is little difference between Griffith's and the Coulomb-Navier criteria, but if the latter were set to be a (more realistic) parabolic shape, then it would take precedence again. These sorts of stress magnitudes rarely concern the present study however.

In fact, Murrell (1965) has given an empirical failure criterion, which represents a stage part way between a linear and the near-parabolic Mohr

envelope usually encountered in practice (Edmond and Murrell, 1971):

$$\tau \geq 2(\sigma_n)^{0.9} \qquad (2.4.21)$$

- a condition which is also tested for in subroutine SAFAIL, for various fault angles.

The arithmetic

Of cause and effect I've never understood.

How many beans make five is an immense

Question, depending on how many

Preliminary beans preceeded them.

Christopher Fry

CHAPTER 3

STRESSES IN THE UPPER CRUST

As the initial state of stress is so critical to the prediction of failure, a study has been made in this chapter of the likely stress behaviours down to the depths associated with induced seismic hypocentres.

3.1 Theoretical Stress Fields and their Magnitudes

Voight (1967) proposed a genetic classification of in situ forces of natural origin in rock. He uses the term 'tectonic' in a very liberal sense, and so a slightly modified version of his scheme is presented here:

1. Current stresses - (a) Gravitational (b) Tectonic
2. Residual stresses - (a) Gravitational (b) Tectonic
   (c) Thermal (d) Inherent

1a. Gravitational stresses are those resulting from the weight of the overburden. Howard (1966) showed that the vertical stress component, σ_z, at a depth z, due to gravity, is given by:

$$\sigma_z(z) = g \int_0^z \rho(z)dz - \int_0^z \frac{\delta\tau_{xy}}{\delta x}\,\delta z - \int_0^z \frac{\delta\tau_{yz}}{\delta y}\,\delta z \qquad (3.1.1)$$

where ρ is the rock density, g is the gravitational acceleration (assumed constant), and τ_{xy} and τ_{yz} are the vertical shear stresses. The contributions from the shear stresses are often neglected, but deviations of measured values of σ_z from the frequently used theoretical value (= ρgz) may well be partly due to their presence, where σ_z is not a principal stress. Hence in rock of density 2.7 gcm^{-3}, σ_z should increase at a rate of $\sim$270 bars/km provided that vertical shear stresses are negligible. These shear stresses are likely to be more common in regions of large topographic irregularities and/or geological inhomogeneities.

Elasticity theory predicts that in the case of a continuous, homogeneous and isotropic rock mass, the gravitationally-induced horizontal stresses will be one third of the vertical, if a Poisson's ratio of 0.25 is assumed. They will therefore increase at approximately 90 bars/km depth.

1b. Current tectonic forces are evidenced by the plate motions known to be occurring at present, and the concomitant earthquake activity. Turcotte and Oxburgh (1976) give a summary of the various origins of tectonic stress. In rocks less deep than, say, 20 km, forces associated with plate tectonics will be fundamentally horizontal, except where crustal inhomogeneities cause deflections, and where local folding increases the vertical component. Also, high horizontal shearing stresses may exist in regions near plate boundaries. More localised sources of 'tectonic' movement, such as salt diapirs, may produce relatively large vertically-orientated stresses in the immediate area. The magnitudes of tectonic stresses are not subject to mathematical analysis or isolation in field measurements, and hence these can only be derived by a process of elimination, if at all.

2. The definition of the term 'residual stresses' used here is that given by Voight (1967), where they are regarded as potentially recoverable, self-equilibrating stress components which would exist without external loads across their boundaries . Orowan (1948) distinguishes two types:

I - stresses produced in a (possibly homogeneous), usually macroscopic, material because of an inhomogeneous external operation. These are often equivalent to the 'locking-in' stresses of Friedman (1972).

II - stresses produced in a material because of structural inhomogeneities within the material, usually on microscopic scales. According to Voight (op.cit.) these stresses cannot be 'separated' from the material without altering its physical and/or chemical behaviour.

Residual stresses of types (a), (b) and (c) above are all of Type I, and may well have been developed during past anelastic deformations, although they are usually all capable of elastic recovery.

(a) Stresses due to a pre-existing overburden often provide a significant contribution to residual horizontal compressive stress (Voight, 1966). Assuming a relatively rapid rate of erosion at the surface, such that creep effects are insignificant, the release of pressure will result in approximately elastic changes in stress. The reduction in horizontal pressures will only take place at one third the rate of the vertical stress, and hence relative horizontal compression will be increased by ∿180 bars/km of denudation.

(b) Geological evidence such as that obtained by petrofabric analysis indicates that past tectonic activities have occurred, and also that the intensity and direction of the stress field involved can change significantly in geologic time. This fact is confirmed by the results of stress measurements which show disagreement between the orientations of present-day stresses and the orientations of those which are inferred to have produced the structures observed in the rock. Past tectonic stresses may or may not have existed in presently stable areas (Voight, 1966).

(c) Voight and St. Pierre (1974) and Haxby and Turcotte (1967) have both considered the effect of the reduction in temperature associated with overburden removal - see (a) above. The tensional horizontal stresses which result from this are found to exceed the effects of the other factors, including Voight's gravitationally-based mechanism, if a typical geothermal gradient is assumed. This means that erosion will usually result in an overall elastic reduction in horizontal stress.

(d) Inherent residual stresses are those defined as Type II by Orowan (above), and correspond in some cases to the 'locked-in' stresses of Friedman (1972).

The magnitudes of the horizontal residual stresses of types 2(b) and 2(d) are even more difficult to estimate than are the magnitudes of the forces that caused them. It is possible that they become very large in circumstances where the orientations of successive stress fields are such

that they have a cumulative effect. The magnitudes of types 2(a) and 2(c), however, can be quantified by the use of the relationships given by Haxby and Turcotte (1976):

$$(a)\quad \delta\sigma_H\ (\text{Eros.}) = \frac{E}{1-\nu} \cdot \frac{\rho_s}{\rho_m} \cdot \frac{\delta H}{a} \qquad (3.1.2)$$

and

$$(c)\quad \delta\sigma_H\ (\text{Therm.}) = \frac{\alpha E, \delta T}{1-\nu} \qquad (3.1.3)$$

where ρ_s = density of overburden

ρ_m = density of mantle at compensation depth

α = coefficient of thermal expansivity

a = radius of the earth

and δH and δT are the depth of erosion and the corresponding temperature drop respectively.

3.2 Field Measurement of Stress Fields

Due to the existence of the different categories of in situ stress, and their differing origins and modes of containment, it is possible to use different techniques to measure, both in the field and in the laboratory, various combinations of these 'partial' stresses. Unfortunately, it is rarely clear which is the combination that a particular technique in a particular circumstance is measuring, and there have been several misunderstandings in the past, partly due to the lack of a standard nomenclature. A short summary of the presently used methods is therefore presented, primarily with the aim of indicating the relevance of each and the reliability of the results quoted.

(i) Soft Stress-Relief Methods

These involve measuring the change in strain that occurs after the artificial relief of the ambient stress acting on the rock, by means of single or multiple overcoring, either at the surface, or at the bottom of a borehole. This of course necessitates accurate laboratory determination of

the Young's Modulus and Poisson's ratio of the rock at the relevant pressure and temperature (McGarr and Gay, 1978). The results may contain contributions from stress concentrations induced by the underground working from which the borehole may be driven, and/or the borehole itself, if these are not properly compensated for by analytic methods.

(ii) Hard Stress-Relief and Stress-Compensation Methods

Hard instruments such as the borehole inclusion stressmeters used by Hast (1958) and Abel and Lee (1973) are rigid devices with Young's Moduli at least double that of the rock. The displacements of the instruments are small so that they essentially measure stress directly. Stress compensating techniques such as the flatjack method (Habib and Marchand, 1952) first allow the deformation due to relief to occur, and then measure the stress required to return the rock to its original position. These methods are still influenced by visco-elastic and hysteresis effects, but are free from the errors introduced by the necessity of determining elastic constants. Photoelastic methods also have this advantage, but are temperature dependent, and small stresses can be difficult to read from the fringe patterns (Kotze, 1970).

The assumption of elastic behaviour has been discredited in several instances (e.g. Price, 1970; Nichols, 1971), where not only do the changes in strain take place over several hours, but a reversal of the sense of strain occurs after a period of time. One reason for the time delay in the response of the rock specimens may well be the formation of microcracks in extension, leading to further internal strain relief. Crack formation is of course not accounted for by using elasticity theory in calculation of the stresses involved, and it gives rise to overestimation of the magnitude of compressional stresses.

Nichols (op.cit.) also noted the effect on the data of the size and shape of any isolated blocks being used. There is no way at present of quantitatively taking account of this. The geometry and distance of free surfaces in field measurements are a similar complicating factor.

Obviously, in in-situ measurements the value of the current tectonic stress field at the point of measurement will be fully sensed by the instrument, but the residual components will have an undetermined, yet important, influence. Two scales of residual stress will be relieved, and hence detected, by strain relief measurement. Firstly, those acting over a region larger than the core diameter will obviously be isolated from the core. Secondly, those smaller-scale stresses that are cut by the core-circumference, or whose locking-in stresses are cut, will be at least partially relieved. Tullis (1977) treats this phenomenon in a more quantitative fashion. The relatively small regions over which the unrelieved residual stresses inside the core act does not preclude their possessing large magnitudes. When considering failure over a 'large' area, for example an entire pre-existing fault plane, the residual stresses which act over an area large enough to be relevant to the criticality of the rock system, will have been relieved, and hence will form part of the measurement. However, on the microscopic scale usually encountered when considering the initiation of crack formation and propagation (e.g. Griffiths, 1920), the important residual stresses are not wholly taken into account by stress-relief methods on the usual scale.

Multiple (usually double) overcoring, or single overcoring of an isolated block, produces measurements of residual stresses only. These stresses are mainly those acting over a domain of a few centimetres, but there will also be relief of granular residual stresses around the circumference of the overcore or original borehole. Multiple overcoring experiments have demonstrated the inefficiency of single overcoring, as the subsequent measurements record ever increasing relief of strain (e.g. Nichols, 1971).

(iii) Hydrofracture

This technique is illustrated in Fig. 3.1. Two basic assumptions are made in order to calculate the complete stress state:

(a) the stress field induced by the borehole can be calculated elastically,

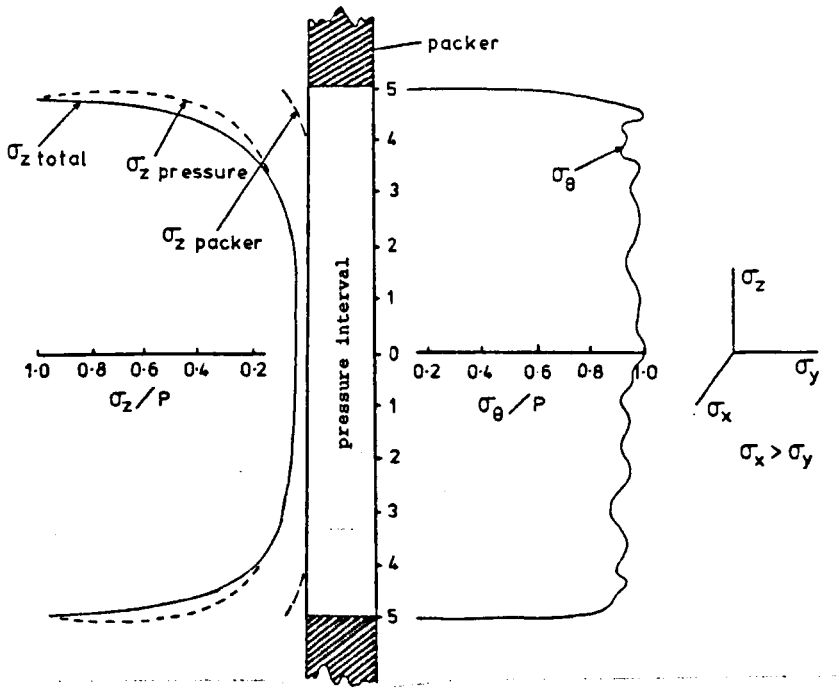

(a) Borehole section cut off by packers and internally pressurised.

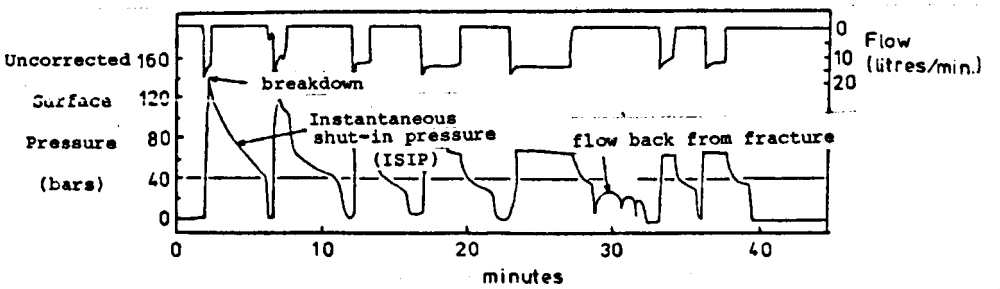

(b) Pressure history of typical hydrofrac experiment (Obert , 1967).

$\sigma_z = \rho.g.z$ $\quad p_c = ISIP$

1) If $0.94(p_c-p_o) < |\sigma_z+p_o| + T_o$ and $p_s < |\sigma_z|$ (vertical fracture)

then $\sigma_y = 3\sigma_x + p_o + p_c - T_o$

and $\sigma_x = -p_s$

2) If $0.94(p_s-p_o) > |\sigma_z+p_o| + T_o$ and $p_s > |\sigma_z|$ (horizontal fracture)

then $3\sigma_y - \sigma_x < T_o - p_c - p_o$

3) If $0.94(p_s-p_o) > |\sigma_z+p_o| + T_o$ and $p_s < |\sigma_z|$ (horizontal fracture becoming vertical)

then $\sigma_y > -3p_s - \sigma_z + 0.94p_o + 0.06p_c$

and $\sigma_x = -p_s$

where p_o is the natural formation pressure , and p_s is the pressure necessary to sustain fracture.

(c) Interpretive stress relationships.

Figure 3.1 Theory of the hydrofracture technique for in situ stress measurement.

(b) one of the principal stresses is vertical and is equal to the weight of the overburden.

Other complications which may arise are due to:

(a) penetration of low-viscosity fluid into pre-existing fractures in the packed-off area, which results in rate-dependent, and thus spurious, estimates of the break-down pressure (Zoback and Pollard, 1978),

(b) fracture occurring in advance of the observed break-down because the propagation has been retarded by high-viscosity fluid, which leads to over-estimates of the breakdown pressure,

(c) shut-in pressure decaying with time, perhaps due to an unknown amount of rotation of the fracture plane while propagating. This leads to uncertain values for the horizontal stresses (e.g. Zoback et. al., 1977),

(d) fracture being due to shear, rather than tensile, stresses, if the fluid injection rate is too slow, in areas of high tectonic shear stress (Lockner and Byerlee, 1977).

There is still much debate about the exact interpretation of the pressures recorded, but usually estimates of the minimum horizontal stress and the directions of both horizontal principal stresses can be relied upon. Indeed, there have been several cases where hydrofracture results have been in concordance with other observations (e.g. Raleigh et al., 1972).

This technique measures the average of the total stresses in the rock over the vertical interval concerned, and due to its nature it should provide data useful for the consideration of failure on pre-existing fault planes. The method is potentially of great use for the total in-situ stress state.

(iv) X-Ray Diffraction

Although some studies were carried out by Paterson (1959), Friedman (1966) first showed how the total strain in a rock mineral crystal can be calculated by obtaining a set of measurements of the d-spacing for, say , $\{32\bar{5}4\}$ in quartz, by observing the broadening of X-ray lines. It is important that the stresses are calculated using 'X-ray elastic constants' (Donachie

and Norton, 1962), but the correct selection of these is a matter subject to discussion (Albritton, 1964), and large errors can be introduced.

The technique is unique in the small scale (a few millimetres) on which the measurements are made, and hence suffers from not taking sufficient account of the heterogeneity of the in situ stress field. This also means that displacements across discontinuities cannot be recorded. In general, strains calculated from the observed diffraction profile will be biased by the strain in the most voluminous rock elements in the diffracting orientation. This, for instance, might occur as a bias towards the 'locked-in' strains in the grains of a quartzite, as opposed to the 'locking-in' strains of the cement crystals (Friedman, 1972). The reliability of the method can be seen from the consistency of the strains measured over several areas of irradiation, which is often good, even where profiles are broad and flat. Also, the degree of homogeneity of the strains can be determined by the amount of agreement among corresponding principal axes calculated from different sets of measurements.

As the rock subject to measurement has to be removed from its in situ position, the technique is essentially one for the determination of residual stresses. The usual method of cutting thin bars of rock means that those residual stresses acting over more than a centimetre or two would mostly be relieved before measurement, and hence not be detected. Nichols (1971) has demonstrated this effect. Sometimes, however, there is good agreement between the principal axis directions found, and those observed in the field (Friedman and Logan, 1970).

3.3 Results of In-Situ Stress Measurements

(i) Vertical Stresses

Brown and Hoek (1978) gathered a large amount of data and selected 120 measurements that fulfilled their criteria of reliability (Fig. 3.2). Their values for the vertical stress fell almost entirely within the limits set by:

$$\sigma_v = 0.27z(m) \pm 170 \text{ bars} \qquad \text{(to depth 3 km)}$$

where z is the depth in metres.

Data presented by McGarr and Gay (1978) are all within the range:

$$\sigma_v = 0.265z(m) \pm 200 \text{ bars} \qquad (3.3.1)$$

Herget (1973) has found the best linear fit to a large set of disparately derived data to be:

$$\sigma_v = (18.8 \pm 12.3)\text{bars} + (0.26 \pm 0.3)z(m) \qquad (3.3.2)$$

Thus it seems that the assumption that the vertical stresses increase at the same rate as that of the overburden (= ρgz) holds true in many cases. However, the wide limits to the measured values warn against total reliance on this simple formula, especially where near-surface estimates are required; for example Worotnicki and Denham (1976) report vertical stresses of up to 140 bars at depths of only 90 m in Tasmania. Large deviations can also occur at depth, under special circumstances. Herget (op.cit.) took a measurement at 1700 m near an extensive sheared zone and obtained a value for the vertical stress more than twice that which would be expected theoretically. All these large deviations from the theoretical stress due to the weight of the overburden must be due to the presence of residual tectonic stresses. Smaller deviations might be produced by the additional vertical shear stresses resulting from geological or topographical inhomogeneities.

(ii) Horizontal Stress

The following values have been published recently for the average horizontal stress (depth, z, in metres):

$\sigma H_{av} = 0.5z + 93.2$ bars - Hast (1969), Fennoscandia (3.3.3)

$\sigma H_{av} = 0.13z + 25.0$ bars - Bulin (1971) (3.3.4)

$\sigma H_{av} = 0.42z + 81.6$ bars - Herget (1972), various localities (3.3.5)

$\sigma H_{av} = 0.2z + 72.6$ bars - Worotnicki and Denham (1976) Australia (3.3.6)

$\sigma H_{av} = 0.2z + 49.0$ bars - Haimson (1978), U.S.A.hydrofrac (3.3.7)

$\sigma H_{av} = 0.11z + 80.0$ bars - McGarr and Gay (1978), S.Africa (3.3.8)

Kropotkin (1972) found that 3.3.3 also fitted the data he had obtained in the USSR. All the variations above have been shown in Fig. 3.3. There is obviously a large scatter present. It seems that no horizontal stresses have been discovered which are less than the elastically estimated value, indicating that present-day compressional tectonic forces and the effects of creep have had more influence than the tensional residual stresses frequently measured. An attempt to combine the above relationships into one general equation would be unwise, as each probably represents the state of stress pertaining to the region where the measurements were made, and is dependent on the particular geology and tectonic history of the rocks involved.

Similar variations occur when dealing with the maximum horizontal stress. Three sets of data presented in the literature can be described by (Fig. 3.3):

$$\sigma H_{max} = 0.67z + 100 \text{ bars} \quad - \text{ Hast (1973), Fennoscandia} \qquad (3.3.9)$$

$$\sigma H_{max} = 0.12z + 130 \text{ bars} \quad - \text{ McGarr and Gay (1978), S.Africa} \qquad (3.3.10)$$

$$\sigma H_{max} = 0.46z + 90 \text{ bars} \quad - \text{ McGarr and Gay (1978), Canada} \qquad (3.3.11)$$

Unfortunately, it is difficult to see what are the relevant factors determining the relationship in each case, and when attempting to estimate what the stress state might be, it is at present still necessary to be guided by previous measurements taken in the area in question.

However, some general guidelines are available. McGarr and Gay (op.cit.) studied their selections of measurements of horizontal stress, both in South Africa and Canada, and they found a significant difference between the two regions, the Canadian stresses being typically double or more those of Witwatersrand. The Canadian measurements were taken near the margin of the Canadian Shield where thrusting and folding are predominant, whereas in the Witwatersrand Basin normal faulting and subsidence are the main mechanisms of deformation.

These authors also used hydrofrac data from U.S. basins to compare values of the minimum horizontal stress in hard and soft rocks. The

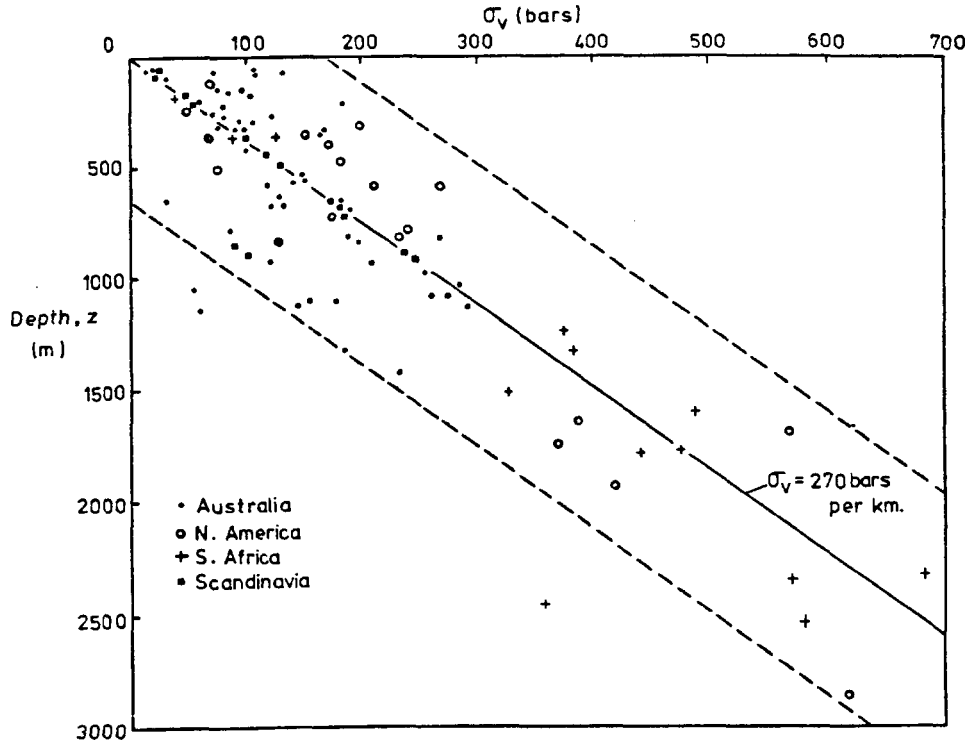

Figure 3.2 (after Brown and Hoek ,1978) Variations of vertical stress with depth.

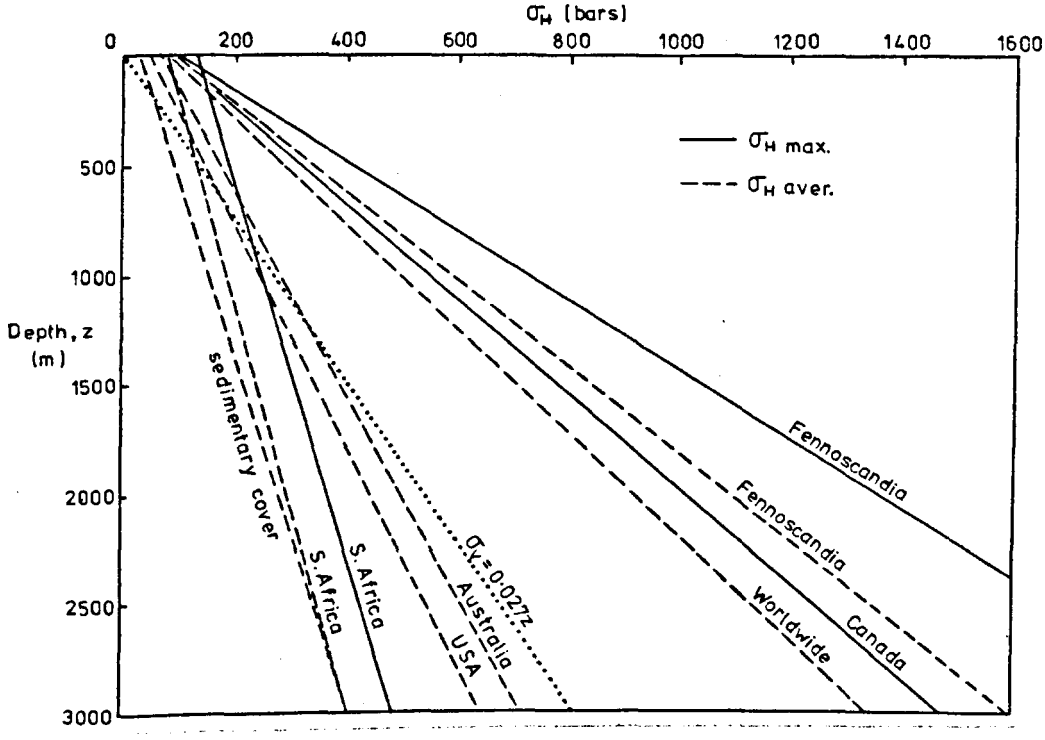

Figure 3.3 Variation of horizontal stress with depth.

measurements in shales and sandstones showed much less scatter than those in the granites and quartzites, both in the U.S. and also in S.Africa and Canada. The U.S. data also suggested that the stresses in the soft rocks are affected by their inability to sustain shear stresses much above 400 bars, at any depth.

Brown and Hoek (1978) (Fig. 3.4) and Jamieson and Cook (1979) have plotted values for the ratio of σH_{av} to σ_v, using a wide variety of data. This ratio in both cases varies between 0.5 and 3.5 at 500 m depth, but this range decreases to between 0.35 and 1.25 when 2 km is reached. However there is much more consistency when only data from a particular area are considered.

(iii) Shear Stress

McGarr and Gay (1978) plotted the values of all their shear stress data against depth, and found a large scatter of points. These fall into the range:

$$\tau_{max} = (30 \pm 50) + (0.076 \pm 0.058)z \text{ bars} \quad \text{(down to 4 km)} \qquad (3.3.12)$$

However, the shear stress does show a general increase in depth which, for the softer rocks at least, is apparently more rapid in the upper one or two kilometres. Hast (1973) claims that his data indicate that there is no shear stress increase with depth, but they can more readily be interpreted as representing a linear increase which is approximately given by

$$\tau_{max} = 15 + 0.12z \text{ bars} \quad \text{(down to 1 km)} \qquad (3.3.13)$$

- Fennoscandia

Jamieson and Cook (1979) went further, and showed the extent of the linear relationship between the shear and average normal stresses at their points of measurement. Jaeger and Cook (1979) claim that this suggests strongly that the state of stress down to about 1 km is determined largely by the frictional resistance to slippage along pre-existing planes, and hence probably indicates prevalent incipient failure in the upper crust. However, this reasoning also necessitates that one accepts that the value of the

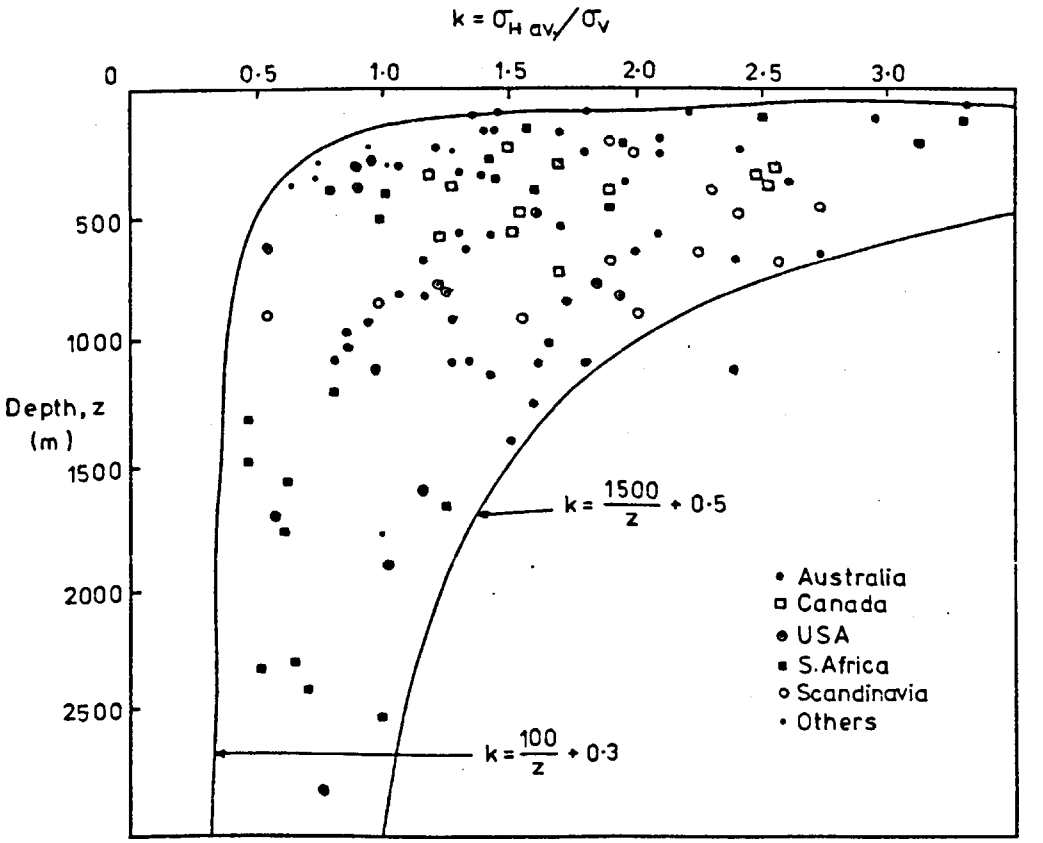

Figure 3.4 Relationship between horizontal and vertical stresses with depth (after Brown and Hoek ,1978).

coefficient of sliding friction is a function of the nature of the faulting (i.e. normal, strike-slip, etc.) almost to the exclusion of the properties of the rock. This is hard to reconcile with our present state of knowledge concerning rock friction, and perhaps suggests a flaw in the presentation of the data.

3.4 Estimation of the Initial Stress State and Stability of the Upper Crust

In deciding the likely state of stress in an area which has not been investigated by stress measurements, the only data available for use are those which, for the most part, would result from mechanical, structural and tectonic surveys. It must be decided how the area compares in these respects with other regions of similar character where the stress state is known. Ranalli and Chandler (1975) have tried to establish a connection between the stress magnitudes in an area and its tectonic and/or petrologic setting. When considering the average horizontal stress, they found a broad division into three main groups. A first group, where there are high stresses corresponding to Hast's (1969) relationship (eqn. 3.3.13)are typically shield areas and competent Palaeozoic fold belts, whereas a second group of regions, where the horizontal stresses are lower than the expected vertical stress, are mainly those of slightly deformed sedimentary rocks, rift zones or fissured Palaeozoic fold belts. Other regions, such as more recent fold belts, which comprise a third group, produce widely scattered results.

It will be assumed in the following analyses both that the vertical stress is in fact principal, and also that it is equal to the overburden. The generalised nature of the discussion is such that the quite large deviations from the first assumption that do occur in places are not significant. The second assumption has been made in order to simplify dealing with the more complex situation of the horizontal stresses, and is justifiable by the usually good agreement in the field. Fig. 3.5 will be used as the basic guideline for all the limiting values on the stresses to be discussed, as it

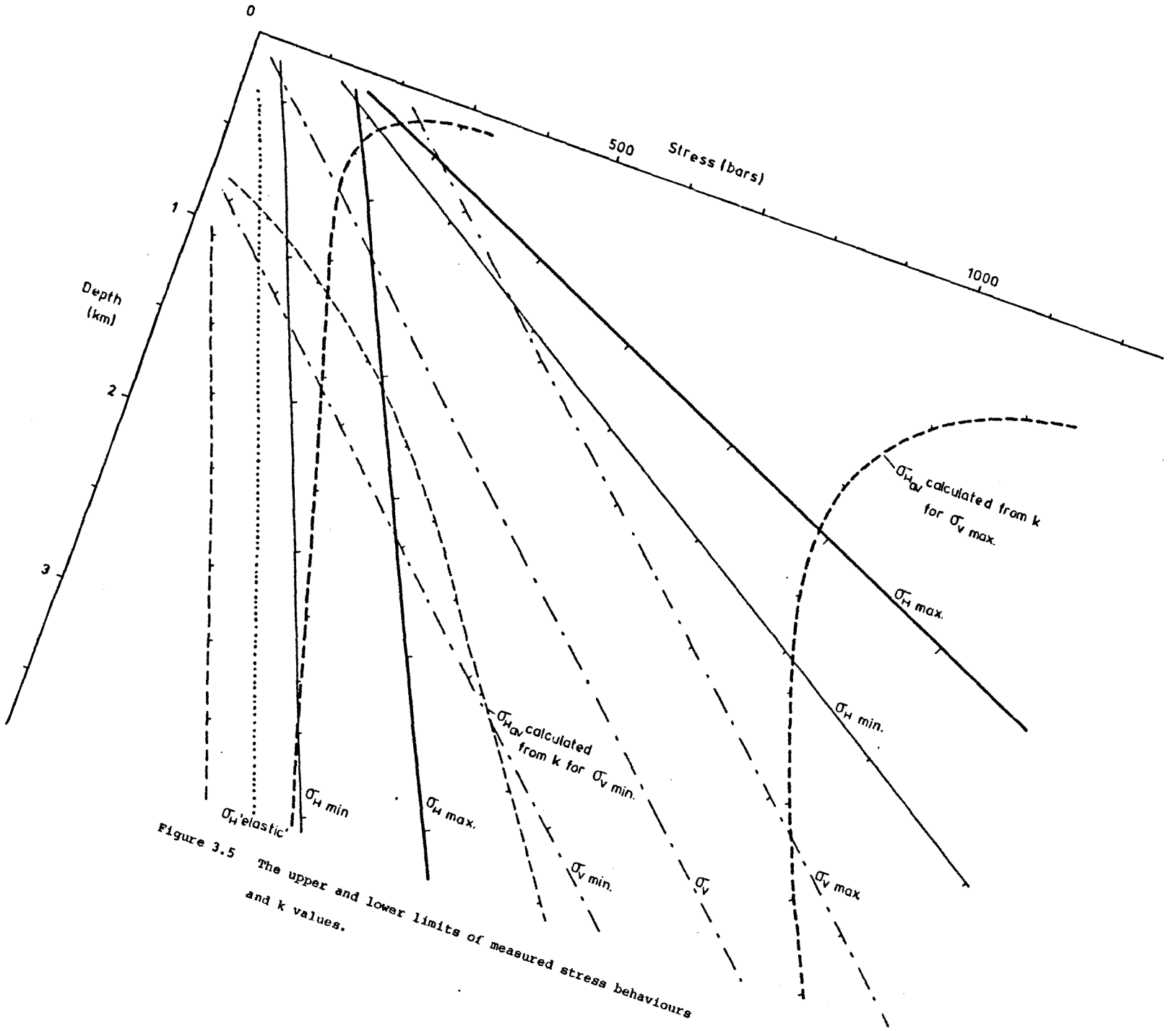

Figure 3.5 The upper and lower limits of measured stress behaviours and k values.

is constructed from the maximum and minimum values so far measured in the field. It also shows the elastic minimum ($\nu = 0.25$) for the horizontal stress (which is never brought in to use as a restriction), and the limiting values of the average horizontal stress [σH_{av}] corresponding to both the maximum and minimum values of the vertical stress, as derived from the empirical relationships between these two variables by Brown and Hoek (1978):

$$k_{max} = \frac{1500}{z} + 0.5, \qquad k_{min} = \frac{100}{z} + 0.3 \qquad \text{(Fig. 3.4)}$$

where z is the depth in metres and $k = \sigma H_{av}/\sigma_v$. These limits are very rarely exceeded and have been found to apply equally well to the data of Jamieson and Cook (1979) by Jaeger and Cook (1979). These authors conjecture that their existence may be a consequence of the finite strength of crustal rock. The wide nature of all the limits in Fig. 3.5 means that no information can be deduced concerning the orientation of the stress ellipsoid, for a particular location, at any depth above 3 km, without imposing further restrictions. It is the interaction between these restrictions and the empirical limits in Fig. 3.5 that produces the new relationships presented in the remainder of this section.

(i) The Implications of Possible Principal Stress Behaviours

In the following it is of importance to bear in mind that use of terms such as 'increasing', when referring to the behaviour of stress with depth, does not necessarily infer that this physically occurs in a particular region but that the subject of discussion has moved to another (theoretical) part of the crust where the relative values of the stresses are as described. The method of investigation prevents the adoption of unrealistic stress behaviours in specific areas where little direct evidence is available for the estimation of stress at depth. The conclusions are based on the assumption that the field stresses measured to date and their ratios include the extreme values that exist in regions of the upper crust where reservoirs are likely to be founded.

Figs. 3.6, 3.7 and 3.8 represent different configurations of the rate of stress increase with depth corresponding to various stress behaviours imposed upon two individual stress components. In each of these cases the maximum depth of 3 km has been chosen to coincide with the approximate limit of actual stress measurements, and the maximum stresses shown in, or implied by, Fig. 3.5 are never exceeded. One general point immediately noticeable is that $\sigma H_{min\ av}$ and σv_{av} are very similar, and thus the depth of conversion from a thrust to a strike-slip regime will be highly dependent on their exact behaviours, and in practice may well form a hazily defined boundary.

Fig. 3.6 shows that it is impossible for both the principal horizontal stresses to have their values equal to the average of their limits below 2 km because there the average horizontal stress would become much greater than that allowed by the k_{max} formula (k_{max} and k_{min} for σ_v equal to the overburden are both indicated in the figure). To prevent this occurring, σH_{max} and/or σH_{min} must increase at a slower rate. The stresses below 2 km plotted in Fig. 3.6 have been arbitrarily chosen to keep the shear stress increasing at the same rate. It seems likely that when σH_{max} takes on average values, σH_{min} is likely to take on below-average values for most depths since this would avoid the unrealistic abrupt change of slope. This will also mean that the shear stress will be closer to some of the actual field measurements, (eqns. 3.3.12 and 3.3.13) which are also shown in Fig. 3.6. The conversion from thrusting to strike-slip is shown to take place at around 2 km, although this figure cannot be very reliable because of the similar gradients involved. Where the horizontal stresses do stay close to their average values below 2 km, it can be assumed that the vertical stress must be increasing faster than the theoretical lithostatic stress, resulting in a higher transition from thrust to strike-slip to normal faulting. In fact the thrust region may not exist at all, and strike-slip surface faulting may be an indication that σH_{min} as well as σH_{max} is of average proportions down to at least 3 km. In Fig. 3.6 however, the shear stress is on the low

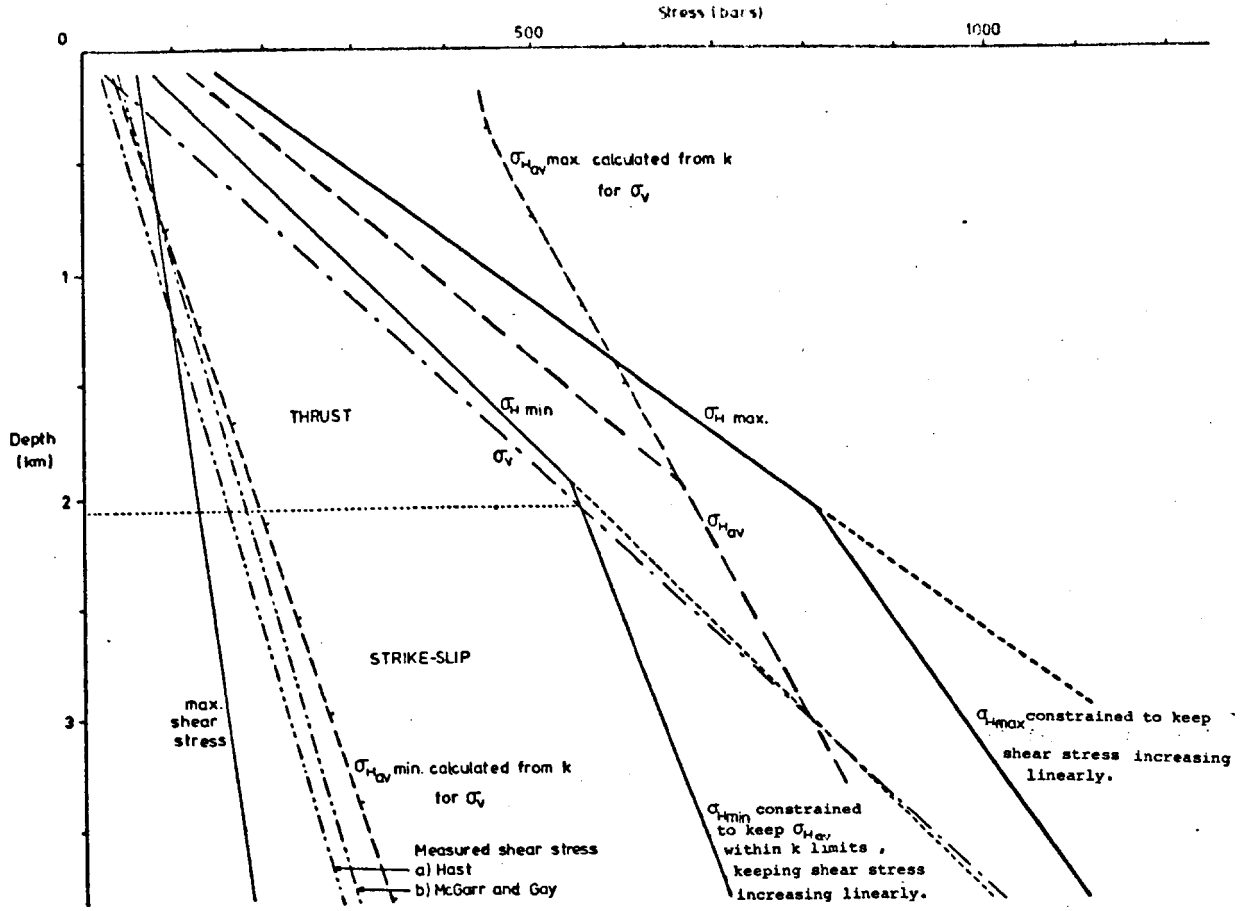

Figure 3.6 Effect of k restraints upon $\sigma_{H_{av}}$ in attempt to keep $\sigma_{H_{max}}$ and $\sigma_{H_{min}}$ to their average measured values.

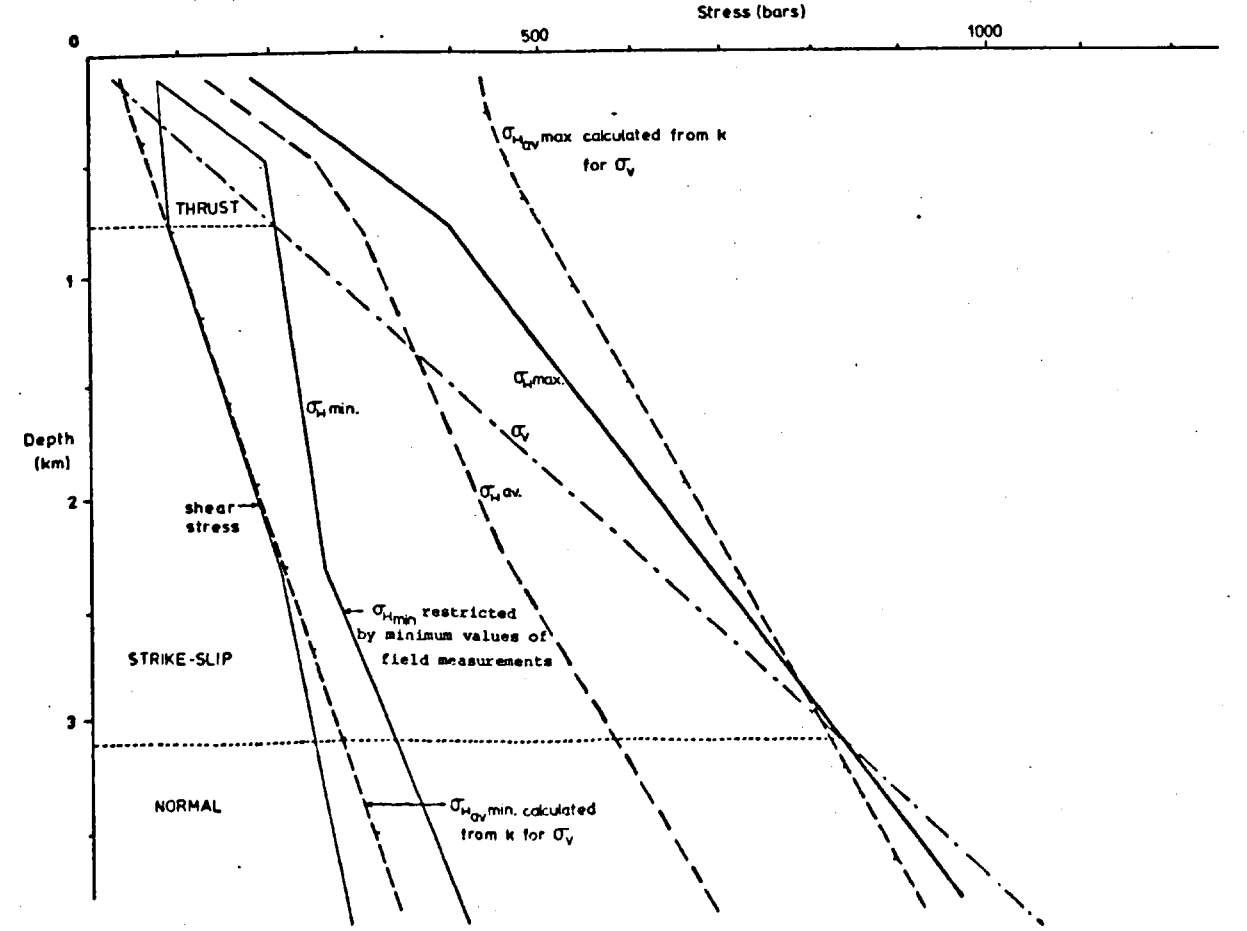

Figure 3.7 Effects of restraints upon attempt to keep $\sigma_{H_{av}}$ to the average indicated by k values, and also shear stress to average values.

side, and σ_{Hav} is largely divergent from the average of those indicated by the k values.

In Fig. 3.7 the normal stresses have been constrained to keep σ_{Hav} as close as possible to the average value indicated by the k ratio, and at the same time the shear stress has been kept as close as possible to the average value determined from the data of McGarr and Gay (1978). The horizontal stresses are now much lower, beneath about 750 m, and the transitions between faulting regimes occur quite high in the crust. The shear stress is mostly of realistic values, but it is not possible in these circumstances to keep it to the average value in the thrusting region near the surface. It is thought however that such near-surface predictions are unlikely to be of much value, as the field stresses are so diverse in this region.

Fig. 3.8 shows the results of keeping $\sigma_{H\ max}$ to its maximum limit in an attempt to maximise the shear stress. Above about 1800 m the shear stress is determined simply by the limiting horizontal stresses, but below this it becomes further restricted by the k_{max} ratio. At all depths the shear stress reaches large values - almost 500 bars by 3 km, and this will cause failure on faults of all friction coefficients less than 0.9 (Fig. 3.9), provided they have zero shear strength, but the friction can be reduced considerably (to around 0.45) for failure when the shear strength takes on average values ($\sim$200 bars; Handin, 1966). Fig. 3.8 shows that failure will always be in terms of strike-slip faulting except perhaps near the surface. Linear extrapolation gives conversion to normal faulting at depths of around 8 km. The maximum ratio of the horizontal stresses in Fig. 3.8, however, of just less than 6:1, is rare in field measurements, and 4:1 is a much more realistic limit (Ranalli and Chandler, 1975). However, keeping to this latter figure results only in a decrease from 0.9 to 0.8 in the maximum coefficient of friction of susceptible cohesionless faults (Fig. 3.9).

The three stress behaviours so far examined are shown in terms of Mohr diagrams in Fig. 3.9, by means of which the friction angles corresponding to

failure in each of the above cases can be ascertained. It is considered unlikely that any of the stress-depth relationships shown here or in Figs. 3.6 - 3.8 actually occur in the field as they are so artificially extreme as to necessitate the sudden onset of the empirical limits. As such they represent unrealistic conditions, and it is only their relative properties that are of interest. The upper line in Fig. 3.9 represents the least stable stress state that it is possible to conceive of if all the known limits are kept to (see Fig. 3.8). No field stresses measured to date have exceeded this, unless the vertical stress had below-normal values near the surface (i.e. probably a vertical tensional residual stress is present), which would slightly increase the shear stress there. It would also increase the likelyhood of thrust faulting in that region, whereas normally these large shear stresses correspond to a prevalent strike-slip regime for the upper few kilometres.

The central line in Fig. 3.9 shows an increase in the regions of both thrust and normal faulting. This, and the decreased shear stress, is the result of near-average shear and horizontal stresses (Fig. 3.7). The depths of the transitions are closely dependent on the behaviour of the vertical stress, rising if this is abnormally low, and vice versa. The lowest line, which represents a very stable upper crust, is the result of an attempt to keep both the horizontal stresses close to their averages, which are only about 250 bars apart (Fig. 3.6). In this case both transitions have been lowered considerably, the thrust/strike-slip boundary depth decreasing by well over a kilometre.

In summary, one of the underlying principles that causes the effects described above is the fact that the average horizontal stresses as calculated by the k ratio and by the maximum and minimum field stresses do not coincide, and hence no horizontal stress pair can satisfy them both. For example, as the k ratio is dependent on σ_v, this means that for σ_H to have average values at all depths, σ_v must be high compared to the overburden pressure,

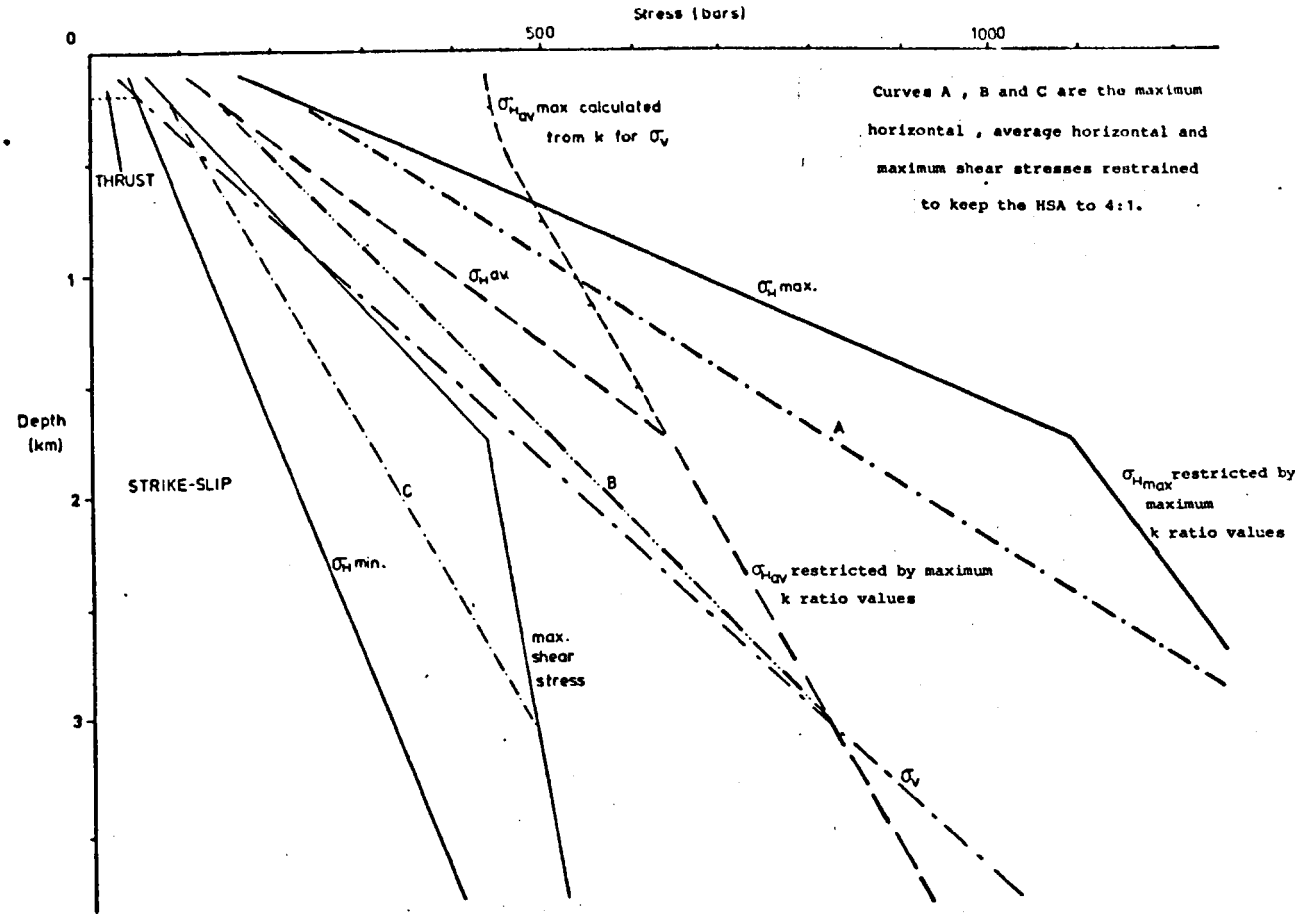

Figure 3.8 Effects of k and HSA restraints upon attempt to maximise shear stress.

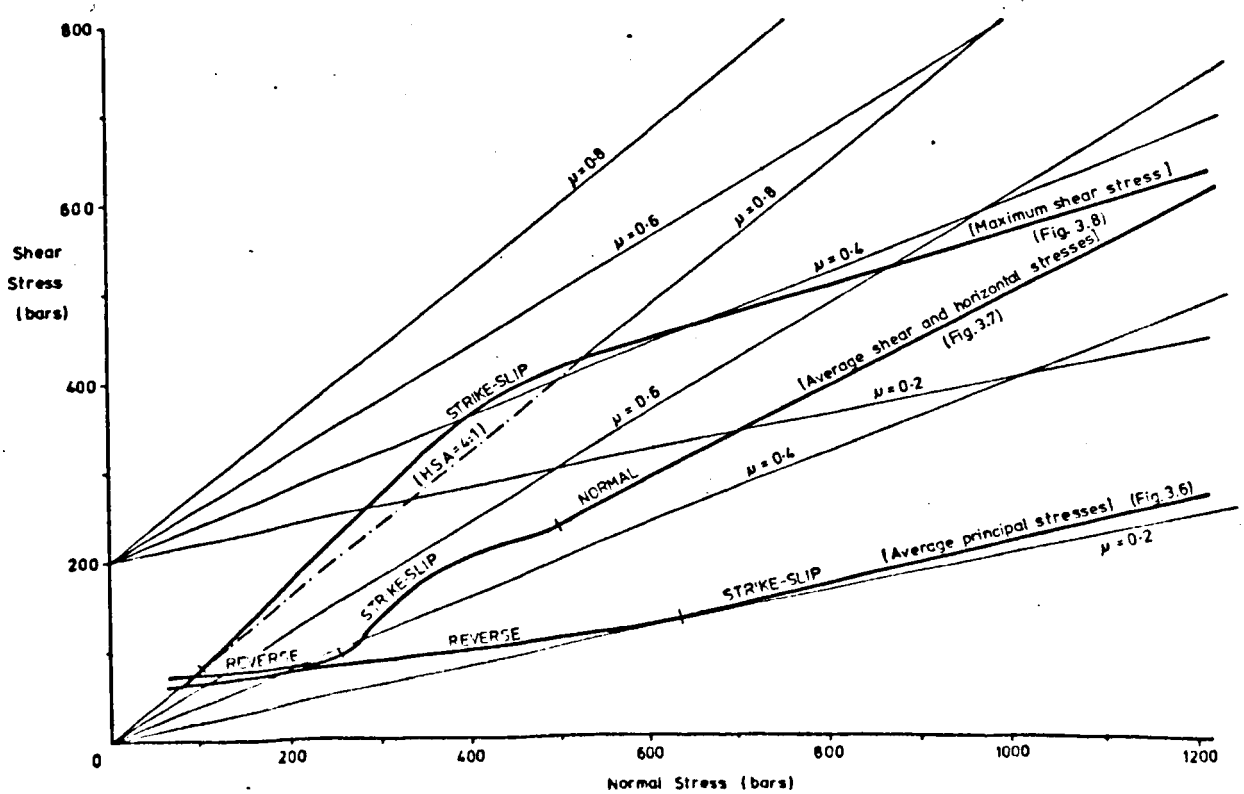

Figure 3.9 Approach to Coulomb-Mohr failure of the stress behaviours of Figs. 3.6 , 3.7 and 3.8.

presuming shear stresses to be of average size. The various combinations in the figures show how the shear stress behaves in different circumstances as a result of this. According to this method of analysis, in order for the shear stress to achieve magnitudes capable of triggering slippage on most faults it must be at least partially due to $\sigma_{H\ min}$ being less than $\sigma_{v\ av}$, i.e. probable strike-slip movement. This tendency may provide one reason why thrust-faulting, even at the surface, is relatively uncommon in the field.

(ii) Fault Stability and the Stress Regime

In order to facilitate the examination of the approach to failure of a particular stress situation and the importance of the individual components when dealing with faults of varying strengths, Figs. 3.10 - 3.14 have been constructed. Fig. 3.10a shows the areas which, if occupied by $\sigma_{H\ min}$ would result in Coulomb-Mohr failure on a fault of the indicated strengths, given that $\sigma_{H\ max}$ behaves according to the line shown (the average of the limits in field measurements). These areas are bounded by 'failure criteria' for $\sigma_{H\ min}$, the lengths of which are limited by the constraints on the maximum values of k, on the horizontal stress anisotropy (HSA, equal to $\sigma_{H\ max}/\sigma_{H\ min}$) and on $\sigma_{H\ min\ min}$ itself. These failure areas are shown to change considerably, depending on the friction coefficient, μ (only shown above 0.2). The shear strengths of the faults are taken to be zero. Fig. 3.10b shows the alternative situation where $\sigma_{H\ min}$ is specified and the values of $\sigma_{H\ max}$ for failure are shown. In both these figures the values for $\sigma_{H\ max}$ and $\sigma_{H\ min}$ respectively have been chosen to be equal to their average field values. One distinction between the two situations is the much greater likelihood of failure when $\sigma_{H\ max}$ is kept to an average value, especially beneath 2 km where Fig. 3.10b shows no failure.

Fig. 3.11 shows the effect of increasing the HSA and displays the criteria for failure when either of the horizontal stresses is at its limit for the depth. It can be seen that an increase in the maximum horizontal stress results in a slight increase in the already quite large susceptibility

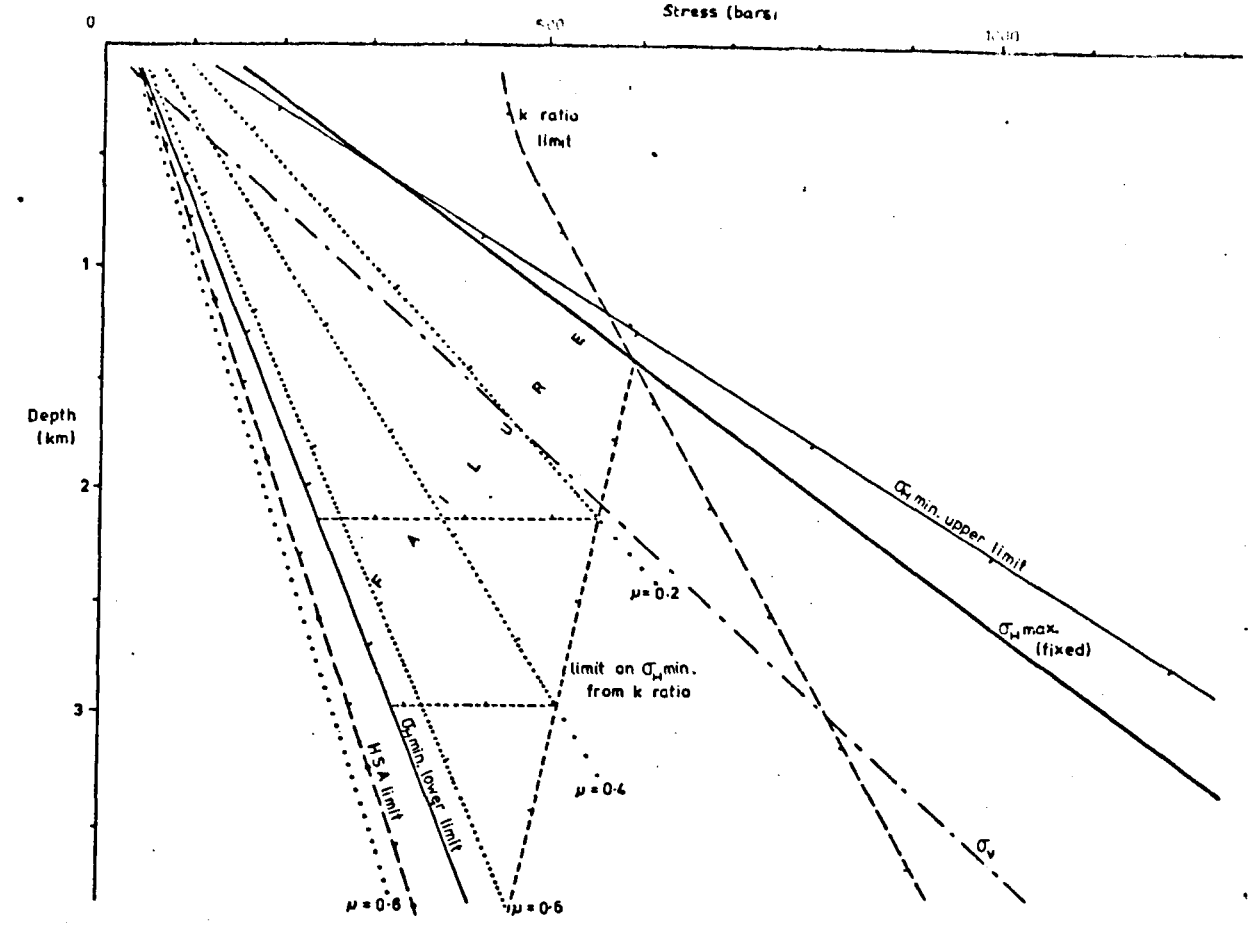

Figure 3.10a Failure zone for σ_{Hmin} when σ_{Hmax} is kept fixed to the average of the field limits. (Zero shear strength on faults.)

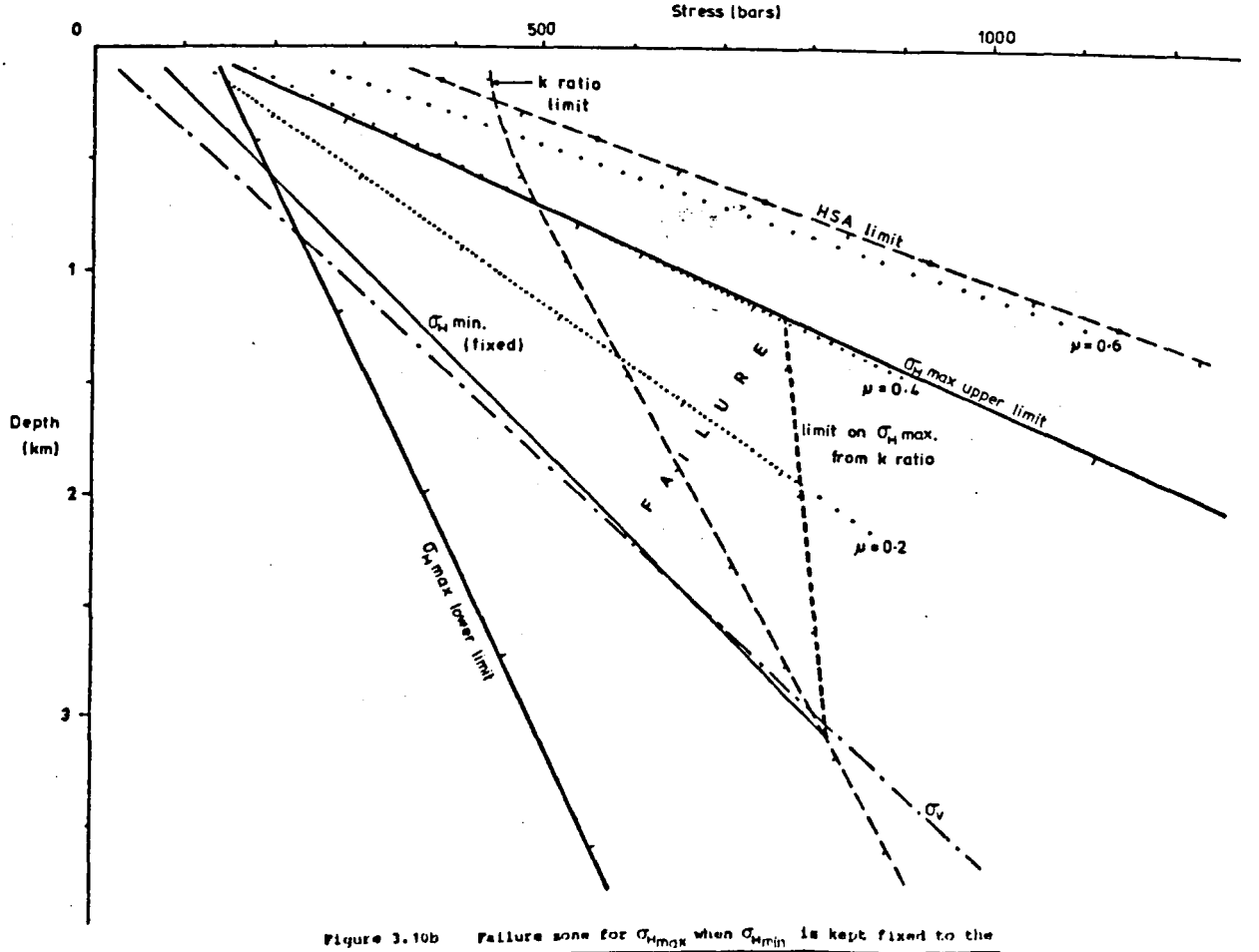

Figure 3.10b Failure zone for σ_{Hmax} when σ_{Hmin} is kept fixed to the average of the field limits. (Zero shear strength on faults.)

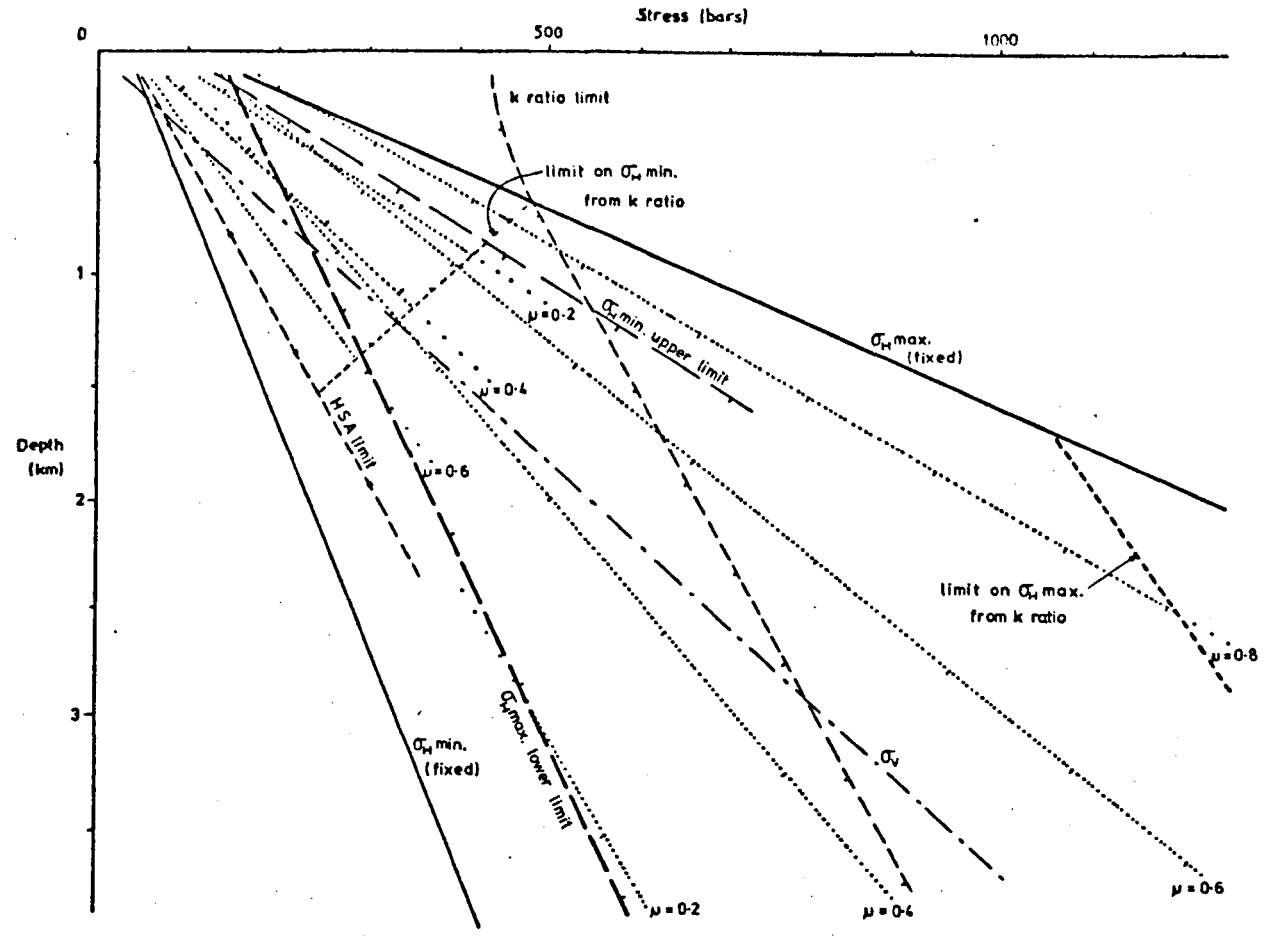

Figure 3.11 Delineation of failure zones for either fixed maximum $\sigma_{H_{max}}$ or for fixed minimum $\sigma_{H_{min}}$. (Zero shear strength on faults.)

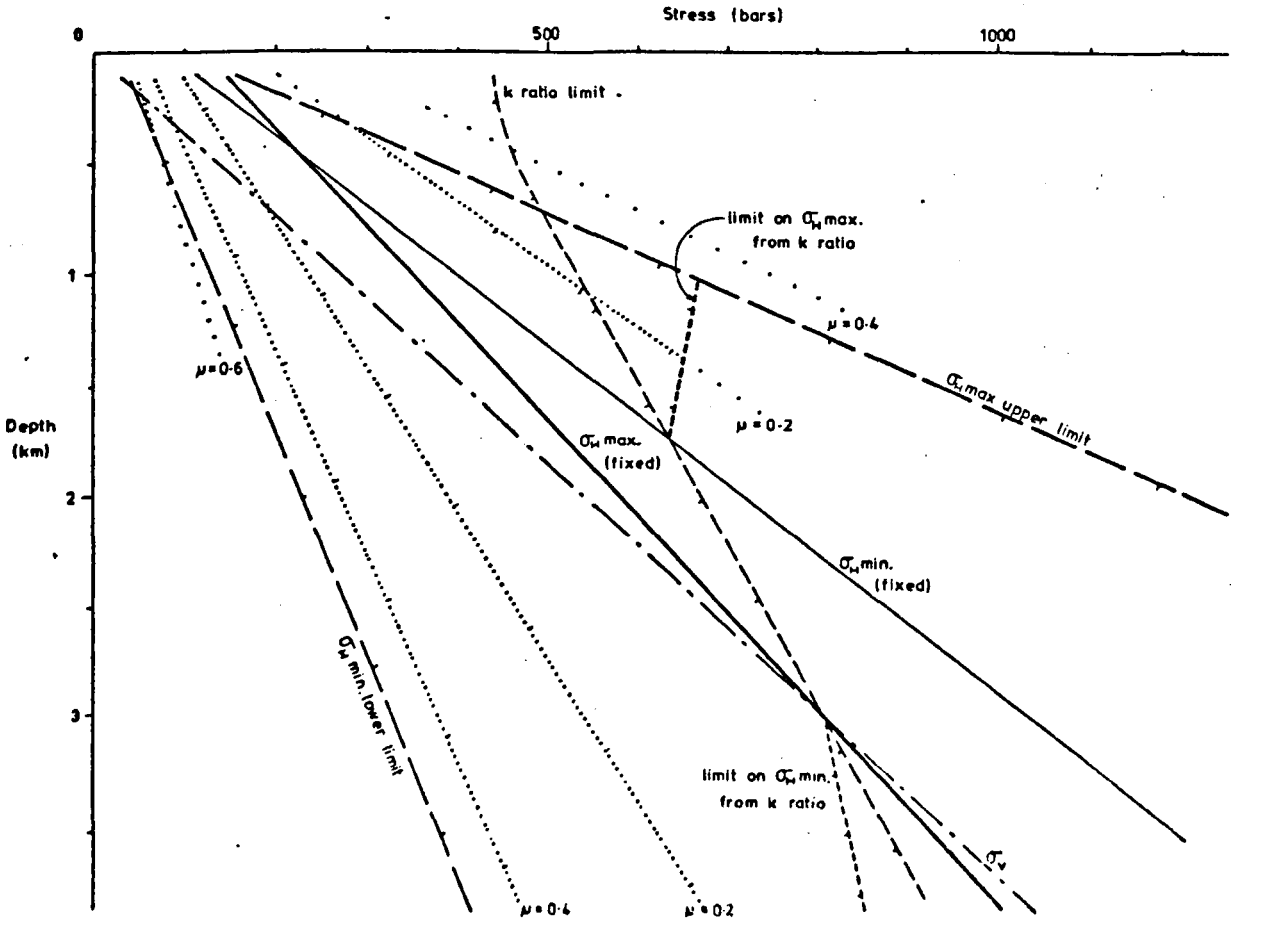

Figure 3.12 Delineation of failure zones for either fixed low $\sigma_{H_{min}}$ or for fixed high $\sigma_{H_{max}}$. (Zero shear strength on faults.)

to failure of faults, as would be expected. However, the restrictions imposed by the k ratio result in a marked raising of the depth below which the corresponding maximum horizontal stresses can exist to produce this failure state (from 4000 m to 1400 m). Also noticeable from the diagrams is a small increase in the thrust faulting areawith increasing $\sigma_{H\ max}$ for a given coefficient of friction. An increase of $\sigma_{H\ min}$, as can be seen, also results in a rapid increase in fault stability; when $\sigma_{H\ min}$ is at its minimum field values, faults up to friction coefficient 0.75 are vulnerable, whereas when it takes on average values, faults much above 0.4 are safe. Again, in a similar fashion to $\sigma_{H\ max}$, the boundary of the region susceptible to failure rises closer to the surface when $\sigma_{H\ min}$ is increased.

Fig. 3.12 shows how the increase in stability continues with increasing $\sigma_{H\ min}$, as is intuitively obvious, and how a thrust regime exists deep into the crust in this situation. The failure region produced by the low $\sigma_{H\ max}$ is no longer limited by the k ratio, and hence instability reaches much greater depths, with strike-slip and normal faulting being prevalent. The stronger faults are no longer susceptible however, and the weaker ones will become stronger as $\sigma_{H\ max}$ decreases further. In general, not only do the magnitudes of the stresses control whether failure occurs, but they also have considerable effect on the depths at which it may take place.

Fig. 3.13 shows the effects of a non-zero shear strength, and should be compared with Fig. 3.11 as the horizontal stresses are at their greatest deviation in both. It is clearly seen that increasing the shear strength up to average values results in a marked increase in fault stability in that the stronger faults become safe, and that this increase is at least as important as that produced by manipulation of the principal stresses throughout their entire range. It does not, however, have any effect on the type of faulting or the extent of the susceptible area over a range of depths, both of which are controlled by the stresses themselves, as has been shown above.

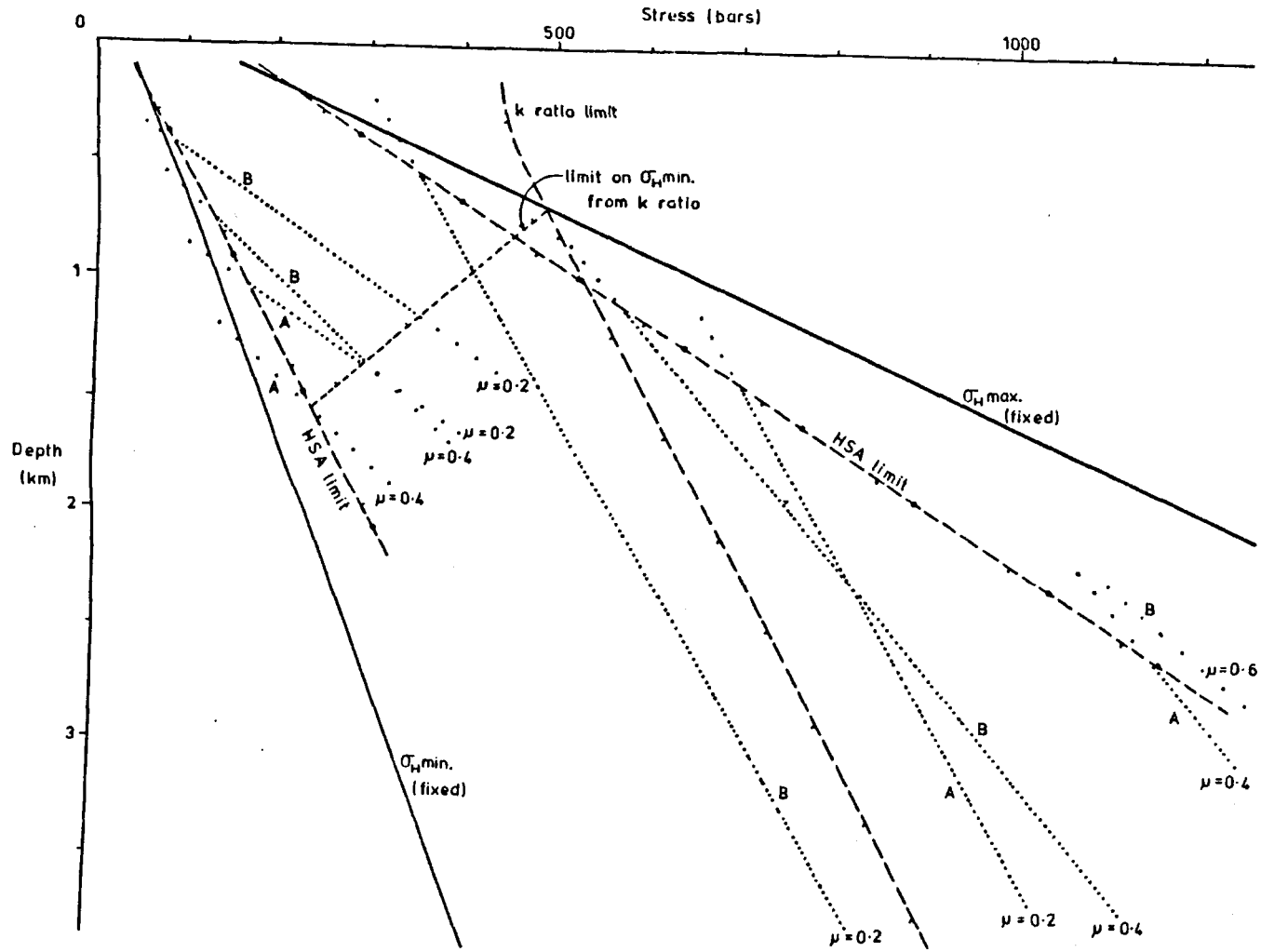

Figure 3.13 Delineation of failure zones for either fixed maximum $\sigma_{H_{max}}$ or fixed minimum $\sigma_{H_{min}}$. Finite shear strengths on faults.

A : shear strengths 177 bars

B : shear strengths 88.5 bars

It should be noted that with the artificial raising of pore pressure none of the k ratio, HSA ratio or stress maxima and minima limits remain applicable when effective stresses are used, since the limits were derived from natural stress states in rock.

(iii) Concluding Remarks

The discussion in this section has shown that further information about the possible behaviours of $\sigma_{H\ max}$ and $\sigma_{H\ min}$ with depth can be derived from the simultaneous consideration of the empirical limits of both their depth-behaviours measured to date, and of their relationship to the vertical stress. It has been shown, for example, that seemingly plausible representative stress behaviours for the principal horizontal stresses are not in fact compatible with average vertical stresses, below a certain depth. Although several hundred stress measurements have been included in the determination of these limits, they are still too wide to be of great significance in the practical estimation of probable stress behaviour in a particular area, especially as they are obtained by the various methods outlined at the beginning of the chapter. This situation will be much improved when further measurements allow a better grouping of stress states according to the geologic environment: the analyses in this chapter can then be carried out for each group. In this way, the limits imposable upon the critical stress state beneath future reservoir sites may be significantly reduced, and realistic estimates of its magnitude may be then made by consideration of the individual stress sources.

CHAPTER 4

THEORETICAL STUDY OF THE STRESSES ASSOCIATED WITH RESERVOIR IMPOSITION

In this chapter the finite element method is used to model theoretical situations of simple geometry in order to study the reservoir-induced stress field and its interaction with any previously existing stresses due to topography and/or tectonic activity. References to the 'strength' of rocks in the discussion are concerned only with the approach of the stress state within the rock to the failure criterion, and are not intended to imply a change in the properties of the rock material itself.

4.1 The Effects of Topography

Most previous treatments of reservoir-induced stresses have ignored the possible effects of initial stress fields caused by the topography of the reservoir region, in particular the reservoir valley itself. The position of the stresses near the surface, and their relatively recent formation suggest that they will not have had sufficient time to totally equilibrate before reservoir imposition, and substantial vestiges of the initial elastic stress field probably remain. Finite element models have been used in this section to study the possible variations in the pre-loading stress field that are due to the depths and the cross-sectional shapes of the reservoir valleys. The valleys have been modelled as a V-notch, and advantage has been taken of the symmetry by only modelling the valley to one side of its long axis. An initial lithostatic pre-erosional stress state was assumed, and the valley was then modelled using elements of zero density and low Young's Modulus ($E = 10^6$ dynes/cm^2), corresponding to air. A Poisson's Ratio of 0.45, not 0.5, was used in order to avoid numerical instability during the matrix operations. The rock itself was given a density, $\rho = 2.7$ g cm^{-3}, Young's Modulus, $E = 10^{11}$ dynes/cm^2, and a Poisson's Ratio, $\nu = 0.25$.

The first model was of a steep valley, of slope 45° ($\tan^{-1}$ 1.0), and depth 500 m. Fig. 4.1 shows the resulting stress pattern. The arms of the crosses represent the in-plane principal stresses, and the radius of the circle represents the stress into the paper. Fig. 4.1a shows how small the induced stress pattern is, compared to the lithostatic stresses. Small tensional horizontal stresses are seen to occur near the top of the valley. It should be noted that the non-reducable size of the 'arrow-head' symbol means that the size of small tensional stresses tends to be exaggerated in the diagrams. Fig. 4.1b shows the deviatoric stresses caused by the valley. Beneath its base there has developed a reverse faulting regime caused by the pressure of the rocks forming the valley side, and over the whole model the deviatoric stresses are tensional towards the valley. The shear stress pattern, contoured in Fig. 4.1c, shows a maximum value of over 50 bars, and all the stresses correspond to a significant reduction in strength, particularly at the valley bottom. This must be so because whenever there is any reduction of one principal stress from a lithostatic state there must result an approach towards the failure criterion. Because of the erosion of the valley, points beneath it are now closer to the surface than other points on the same datum. In the case of Fig. 4.1 for example, the overburden stress for the depth at which the finite-element solution gives the greatest shear stress, is 121 bars for rock of density 2.7 g cm^{-3}, whereas directly underneath the valley the maximum and minimum principal stresses become 154 and 30 bars respectively. The effective valley load in this case is thus vertically tensile and horizontally compressive. For erosion of a valley slope of 45°, and depth 500 m, therefore, the ratio $d\sigma_3/d\sigma_1$ at this point is -2.76. The effects of the valley become less than 5 bars at a distance of approximately 5 valley-depths (2.5 km) away.

Fig. 4.2 shows the shear stress field produced by a valley only one half the depth of the previous model (i.e. 250 m), but with the same slope, which is equivalent to the valley 'volume' being one quarter of the previous

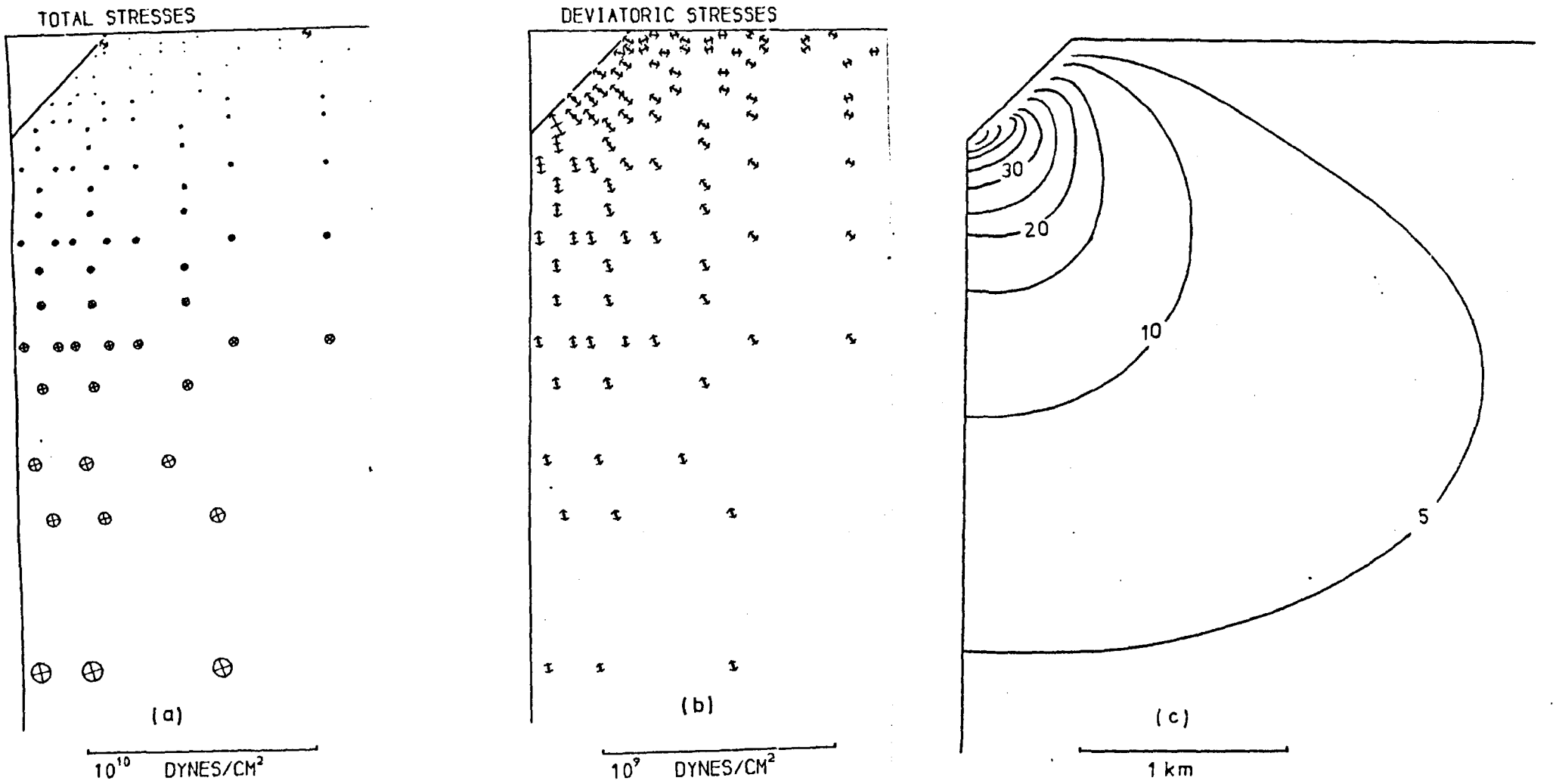

Figure 4.1 Elastic stresses due to a valley 500m deep of slope 45°.

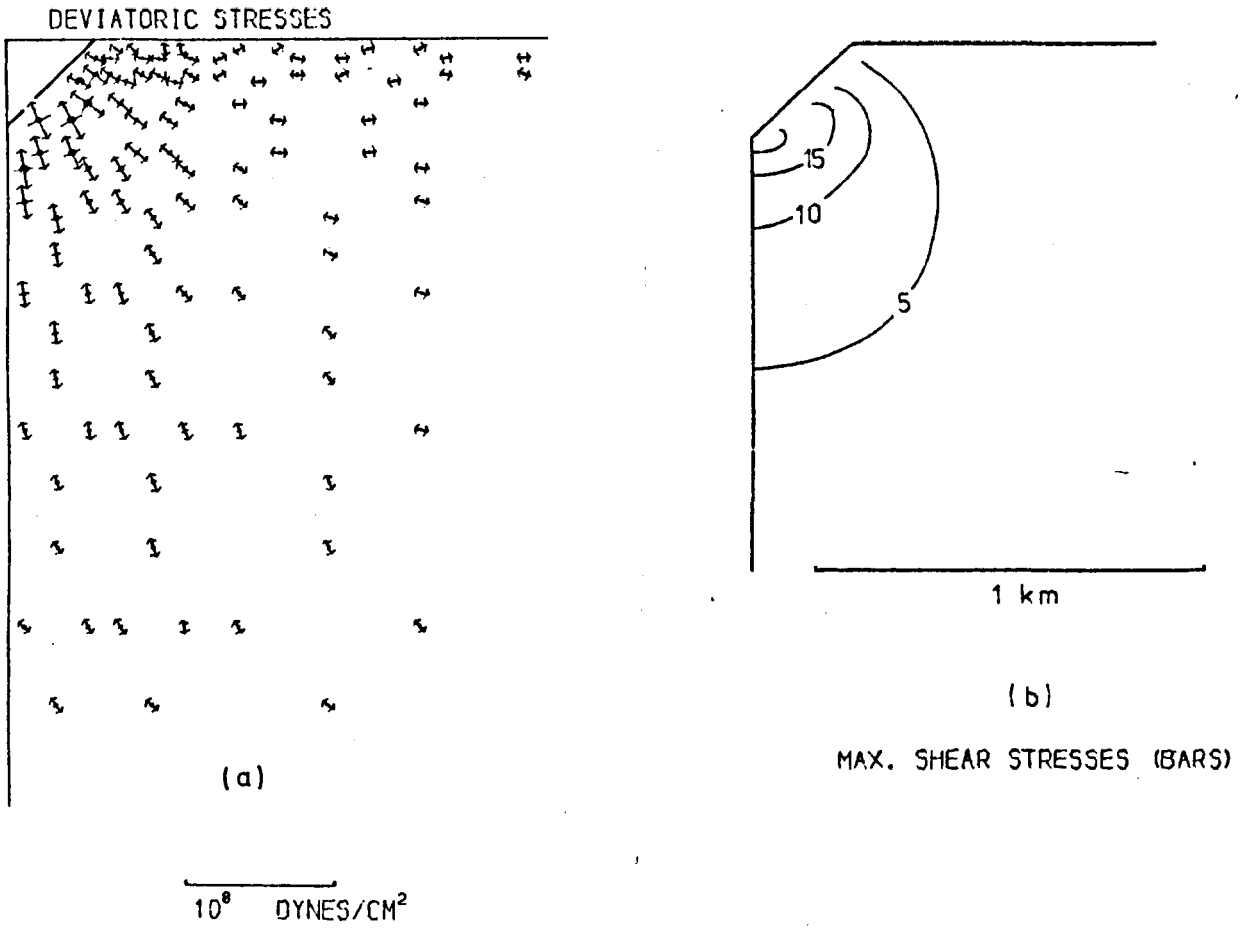

Figure 4.2 Elastic stresses due to a valley 250m deep of slope 45°.

model. The 5 bar shear stress contour is now only at a distance corresponding to two valley-depths (0.5 km) away, and the maximum shear stress is around 20 bars (approximately one half that of the previous model). The qualitative aspects are the same however, and the tensional stresses above the valley are still present, and are found in fact in all the remaining models shown in this section.

Further models have been made to examine the effects of a less steeply sloping valley side. Fig. 4.3 shows the case when the slope has been halved (i.e. $\tan^{-1} 0.5$), while the depth remains at 500 m. The area enclosed by the 5 bar shear stress contour is of much greater extent, and now reaches a depth of over 9 km, as opposed to 2.5 km for the steeper valley. The maximum shear stress however is shown as being slightly less than that for the steeper valley, although this may well be due to lack of resolution in the finite element grid at this point. Fig. 4.4b shows a valley with the same slope but only 250 m deep. Again the extent of the 5 bar contour has more than doubled that of Fig. 4.2 where the slope is twice as great, but the maximum shear stress at the base of the valley is not much different. Fig. 4.5 shows an even shallower valley (depth 500 m), and the extent of the field is now 18 km. The principal stress-change ratio at the base of the valley in this case is 4.46 corresponding to a reduction in both principal stresses. Whether the maximum principal stress is increased or not thus depends on the valley slope, and size as well. In either case, a weakening results. The equivalent half-depth valley is shown in Fig. 4.4a, and this displays the same qualitative features as Figs. 4.2 and 4.4b.

Figs. 4.1 to 4.5 demonstrate the considerable effect on the topography-induced stress field that valley depth and slopes have. The deeper valleys produce greater thrusting stresses at the valley base approximately in proportion to the depth. The shallower valleys produce stress fields, the extents of which increase in an exponential fashion with decrease in valley steepness. All models display small tensional sub-horizontal stresses above

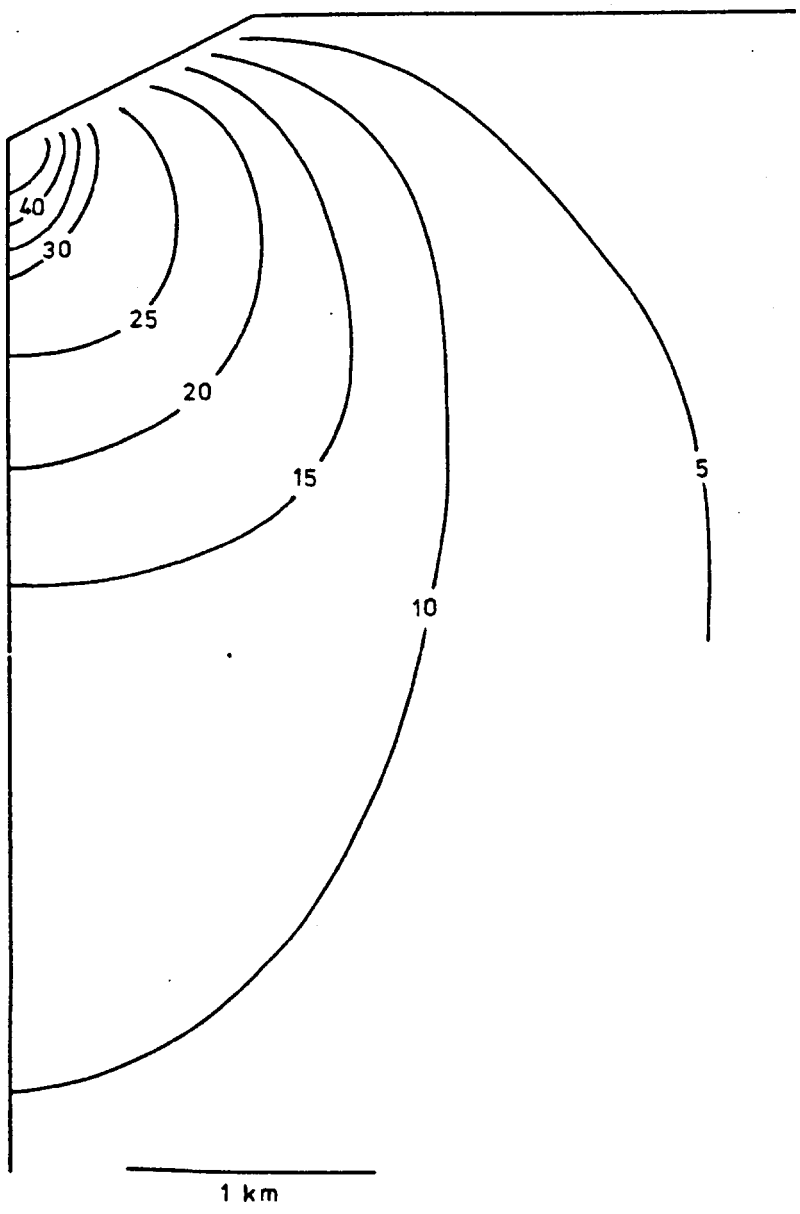

Figure 4.3 Maximum shear stresses due to a valley 500m deep of slope 27°.

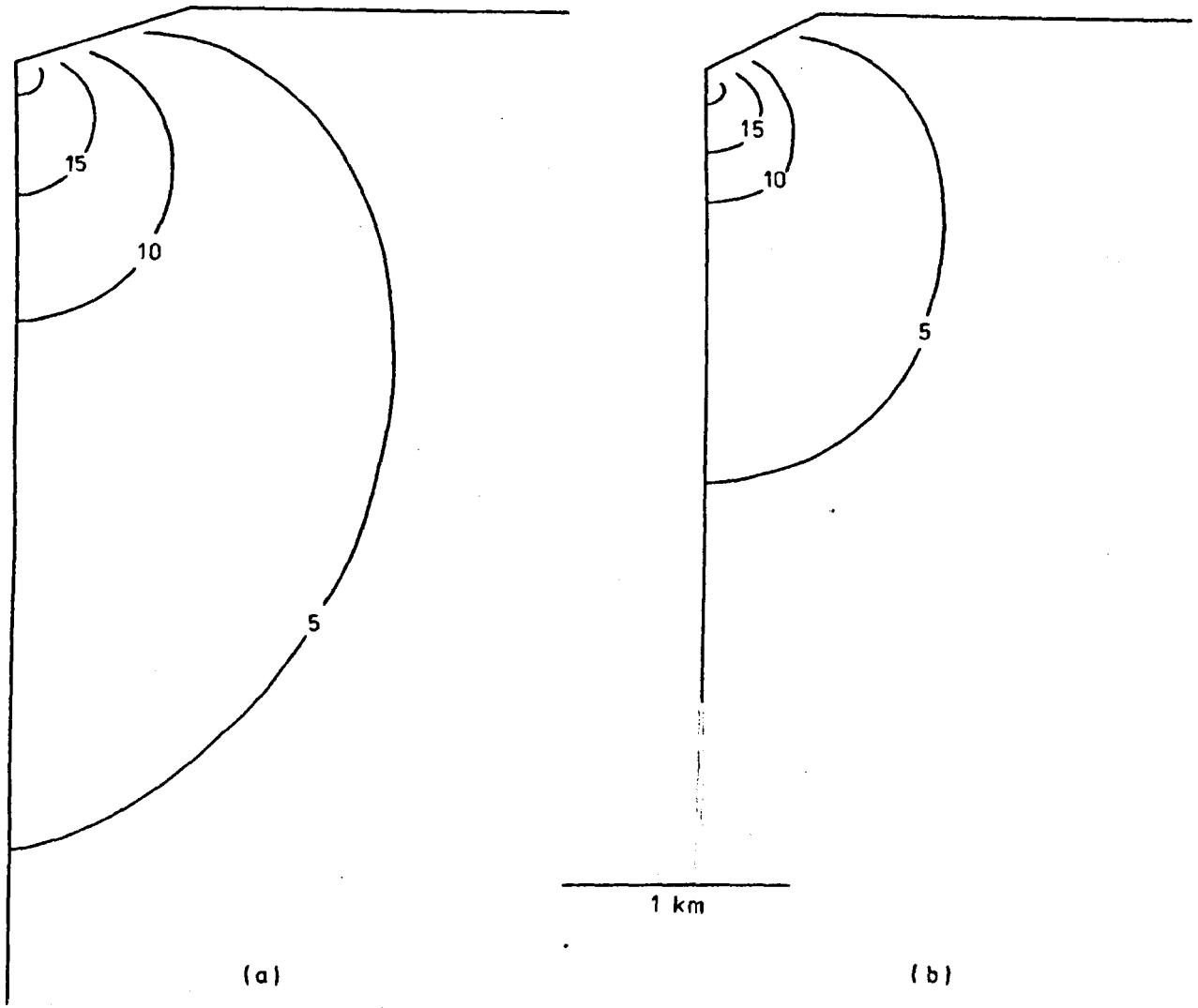

Figure 4.4 Maximum shear stresses due to valleys 250m deep , of slopes (a) 18° , and (b) 27°.

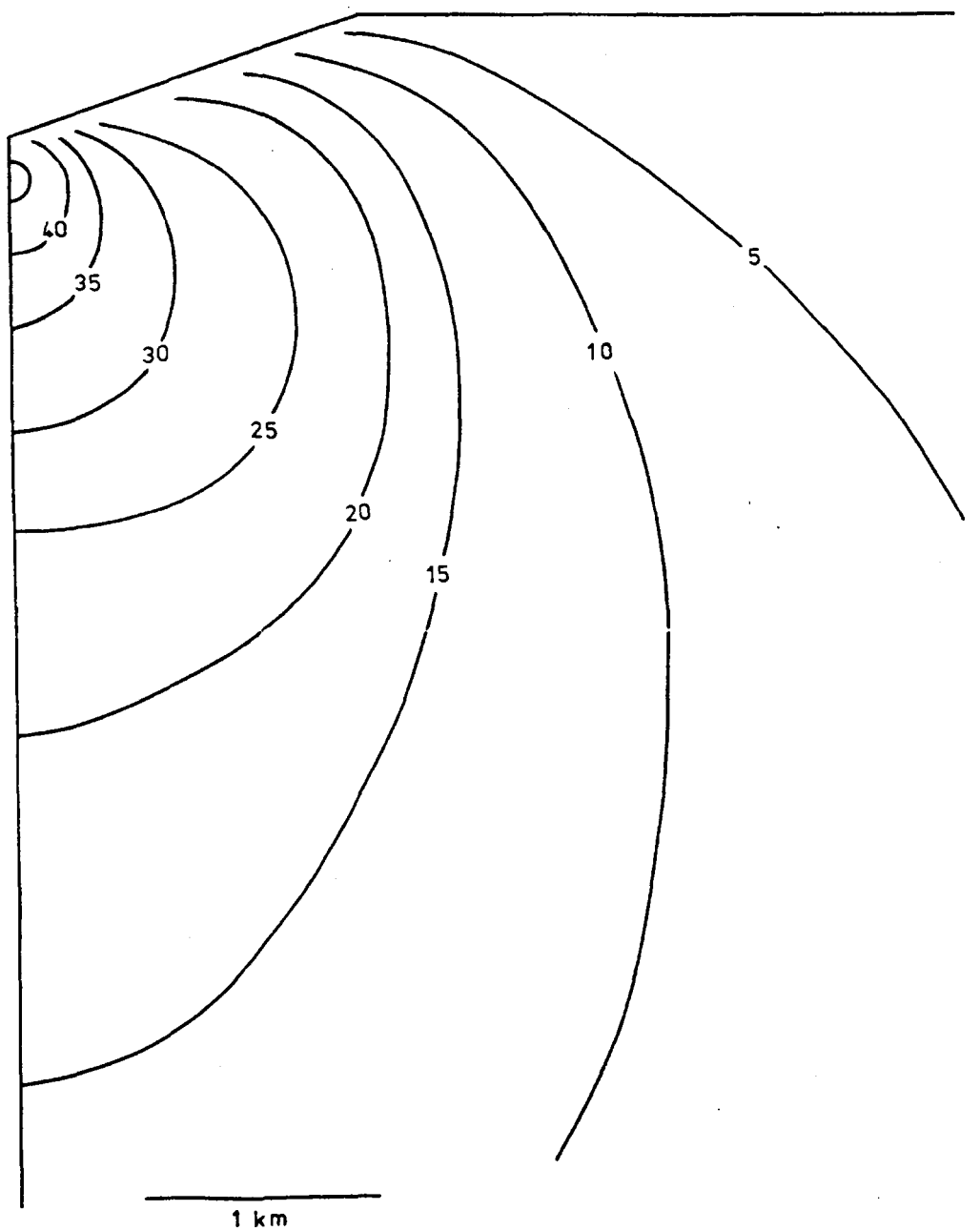

Figure 4.5 Maximum shear stresses due to a valley 500m deep of slope 18°.

the valley sides. The effect of the single valley 'load' is represented in the top left-hand portion of Fig. 4.16.

The figures suggest that an extensive area of rugged topography might well have an associated shear stress field even at middle crustal depths. Fig. 4.6 shows the case where three steep symmetrical V-notch valleys 250 m deep form a region of high topographic relief. The high deviatoric stresses now reach much greater depths, although maximum stresses have not increased greatly. The directions of the principal stresses indicate that the conclusions reached concerning reservoir loading in the next section will remain qualitatively true, even when the effects of neighbouring valleys etc. are not considered.

4.2 The Effects of Reservoir Imposition

The filling of a reservoir is easily accomplished in an elastic finite-element run by assigning a density of 1.0 g cm^{-3} to those elements originally occupied by air with zero density. Fig. 4.7 shows the case where the valley modelled in Fig. 4.1 has been half-filled with 250 m of water. This represents a large depth compared to that of most seismic reservoirs. The differences between the two stress fields are small, and do not show up well on plots of total and deviatoric stresses. They represent a slight diminution of the stress field, and hence a slight increase in strength. The 5 bar shear stress contour extends approximately 400 m less far into the bedrock, and the maximum shear stress has been reduced by an amount less than 10 bars at the valley base. This result is not surprising since the presence of the water load is effectively a partial reduction of the valley, and the elastic normal faulting regime that it imposes on the rocks just beneath it partially negates the thrusting stresses due to the valley topography. This situation is represented in the lower left-hand portion of Fig. 4.16.

With a much shallower valley (slope = $\tan^{-1}$ 0.33) the effect is much the same. Fig. 4.8, which should be compared with Fig. 4.5, shows a small

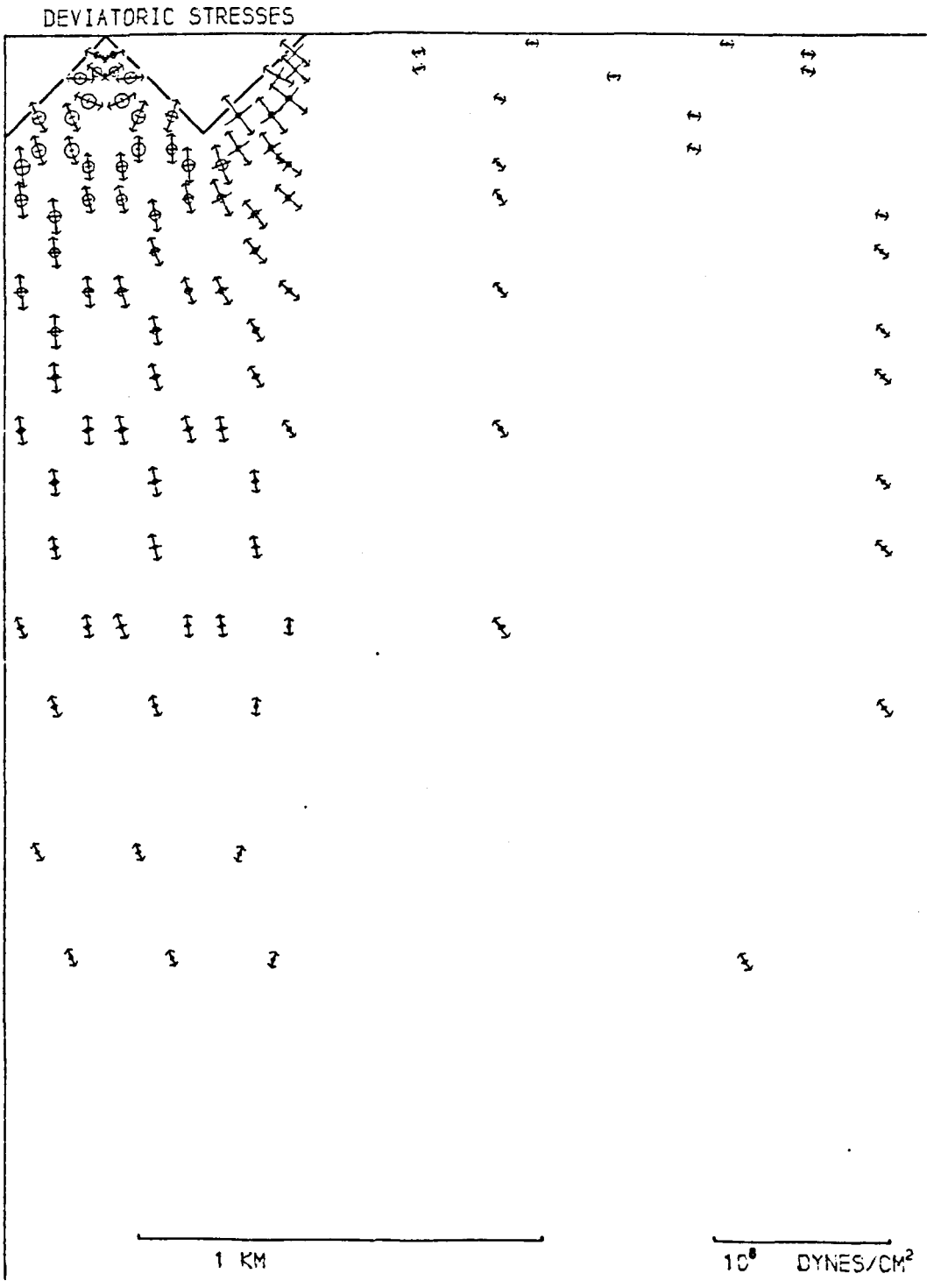

Figure 4.6 Deviatoric stresses resulting from three adjacent valleys of depths 250m and slopes 45°.

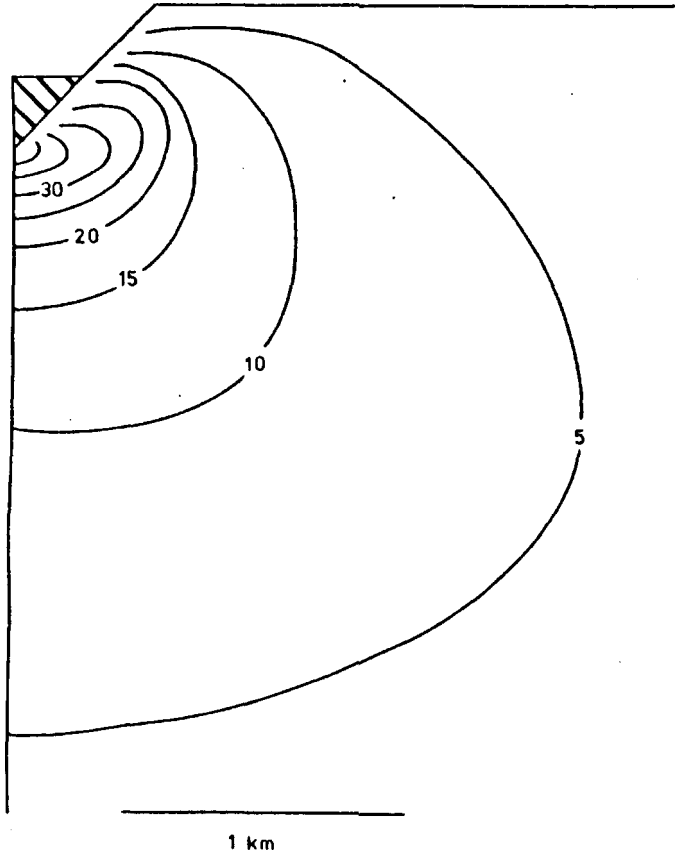

Figure 4.7 Maximum shear stresses due to the imposition of 250m of water in valley of slope 45°.

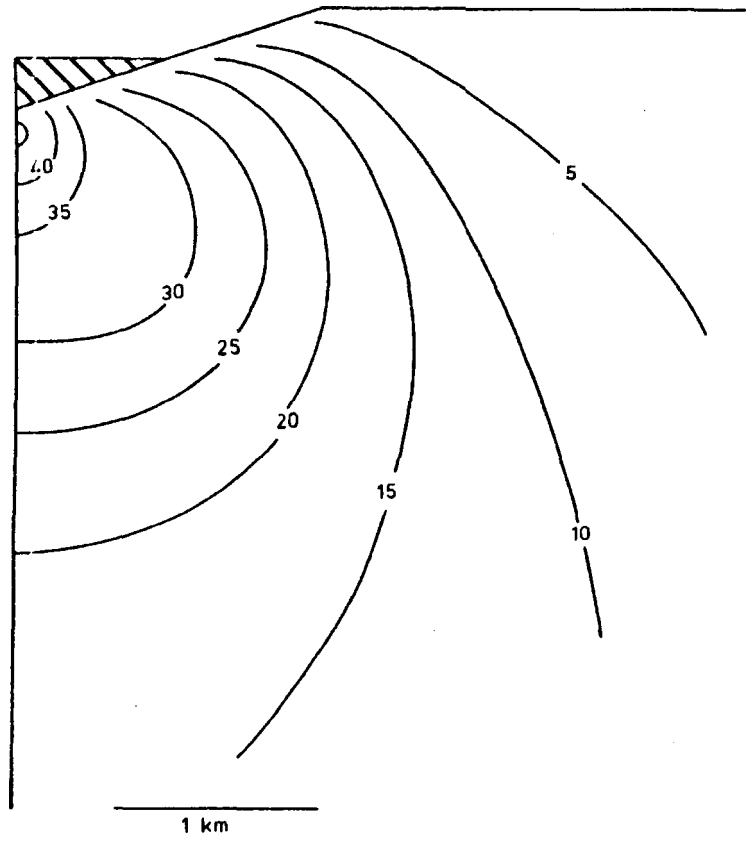

Figure 4.8 Maximum shear stresses due to the imposition of 250m of water in valley 500m deep of slope 18°.

reduction in the stress field, and in this case the maximum shear stress has been reduced by not much more than 2 bars.

The above models show of course the combined effects of the reservoir and the valley. Although this combination occurs in practice, several models were made to examine the stress field induced solely by the weight of water. Greater accuracy regarding the effect of the water was achieved in this way, since the maximum stresses in the model were reduced. This 'water only' model was effected by putting all densities to zero, except those for the water elements which were kept at 1.0 g cm^{-3}. Three of the solutions are shown in Figs. 4.9, 4.10 and 4.11. Figs. 4.9 and 4.10 show the stresses induced by a 250 m deep reservoir in a 500 m valley (although this latter figure is not relevant in this case). In the first diagram, the slope of the valley side is 45^{o}, and hence the situation is comparable with Fig. 4.7. Fig. 4.9a shows a vertical compression beneath the lake, which rapidly dies away, with horizontal stresses which are small and have an average value close to zero. Above the reservoir, the valley-side stresses become distinctly tensile, and hence would increase the topographic stresses in this region. Fig. 4.9b shows that a maximum shear stress of over 5 bars was created, although this in fact would be counteracted by the topographic stresses in practice. A shear stress of 1 bar reaches over 1300 m beneath the base of the reservoir.

Fig. 4.10 shows a similar example, but the valley here has a slope of $\tan^{-1}$ 1/3, and is thus comparable with Fig. 4.8. The necessarily larger body of water now creates a maximum shear stress of over 8 bars, at a depth 100 m - 200 m beneath the water. Shear stresses decrease downwards from here, until they fall below 1 bar, at approximately 6 km depth. It thus appears that stresses caused by such large bodies of water are well capable of penetrating potential hypocentral depths.

Fig. 4.11 shows a much more typical size of seismic reservoir, and is 125 m deep in a valley of slope $\tan^{-1}$ 1/3. The maximum shear stress reached is only 3 bars, and the 1 bar isobar is limited to a depth of 1400 m.

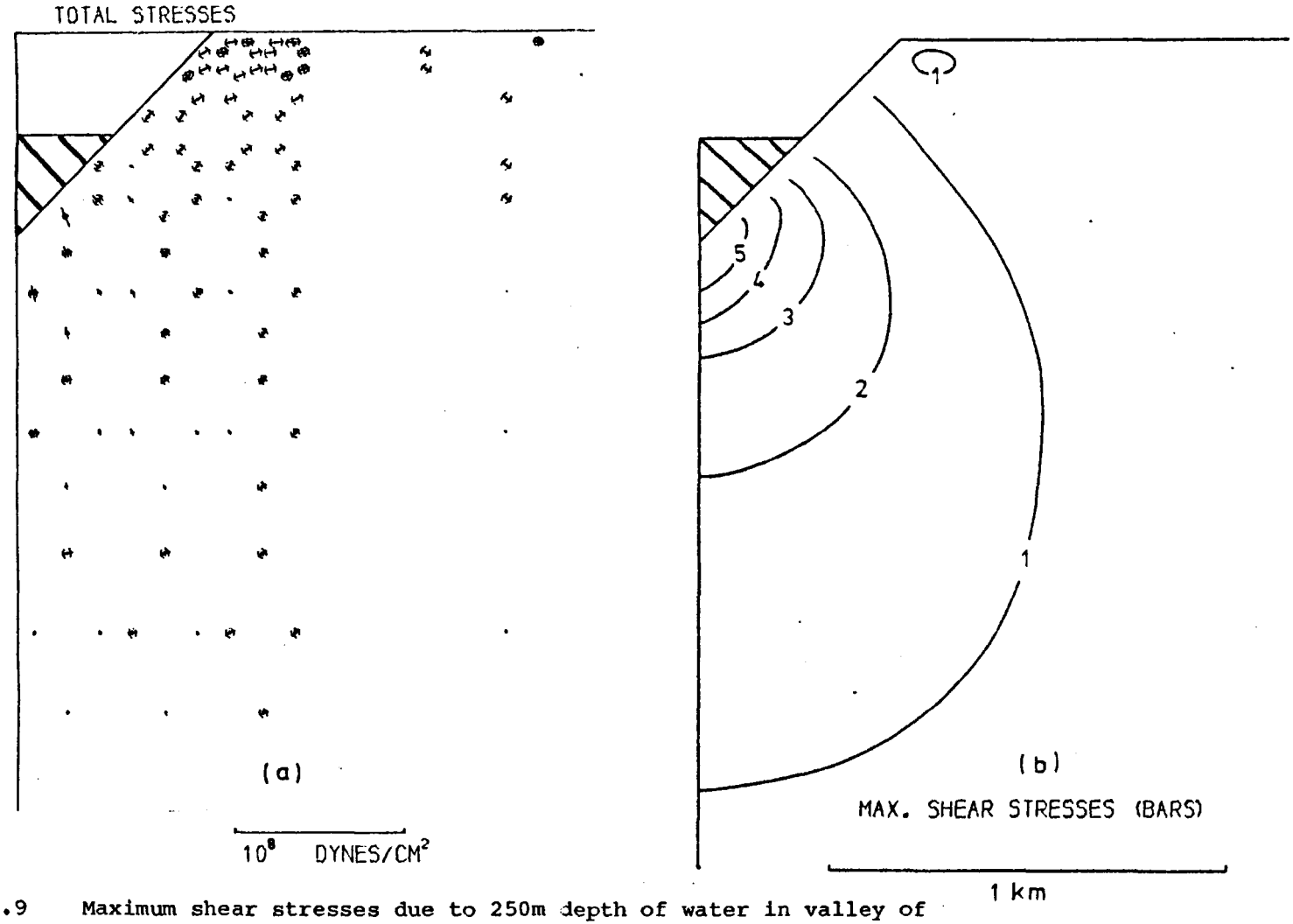

Figure 4.9 Maximum shear stresses due to 250m depth of water in valley of slope 45°.

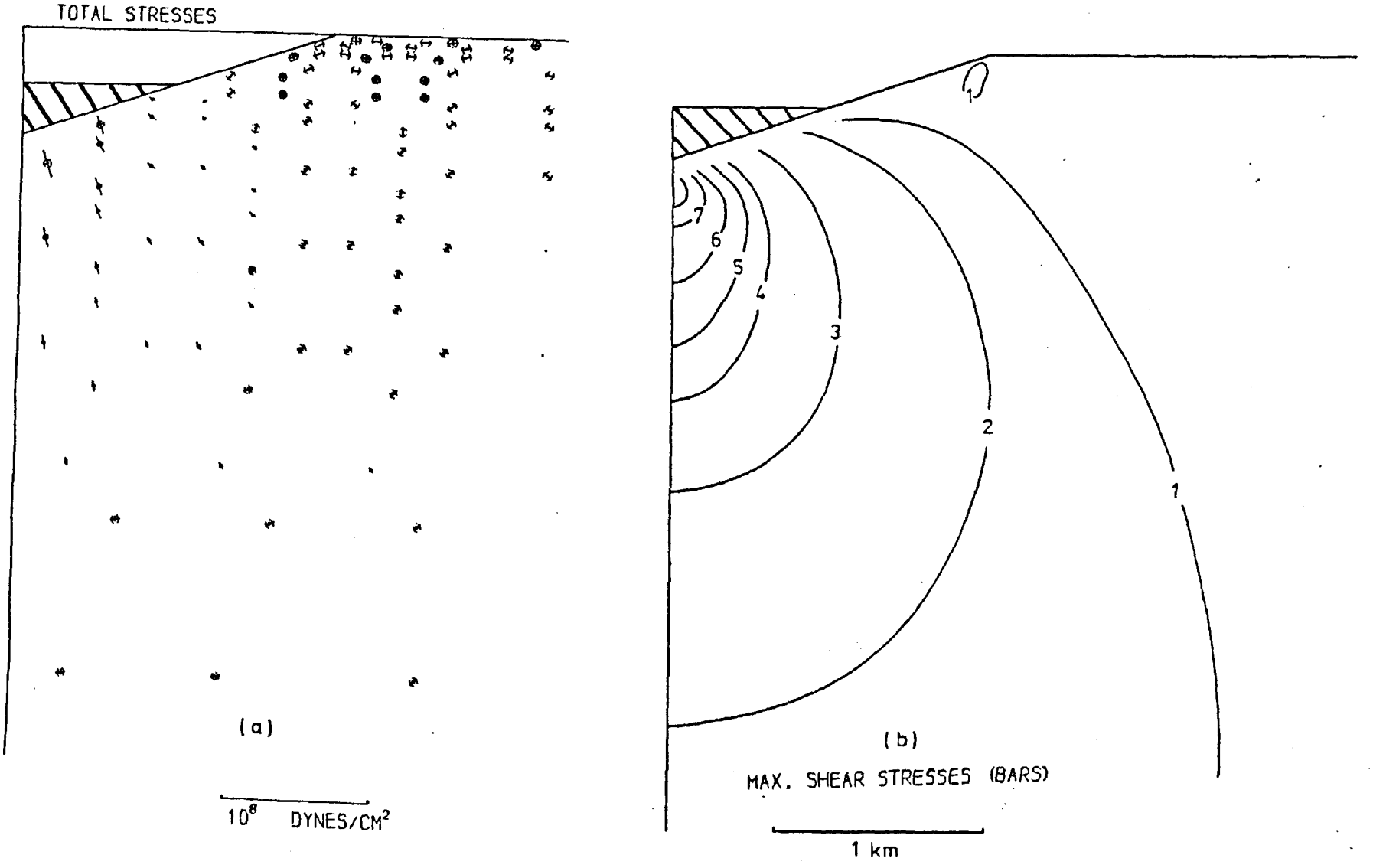

Figure 4.10 Maximum shear stresses due to 250m depth of water in valley of slope 18°.

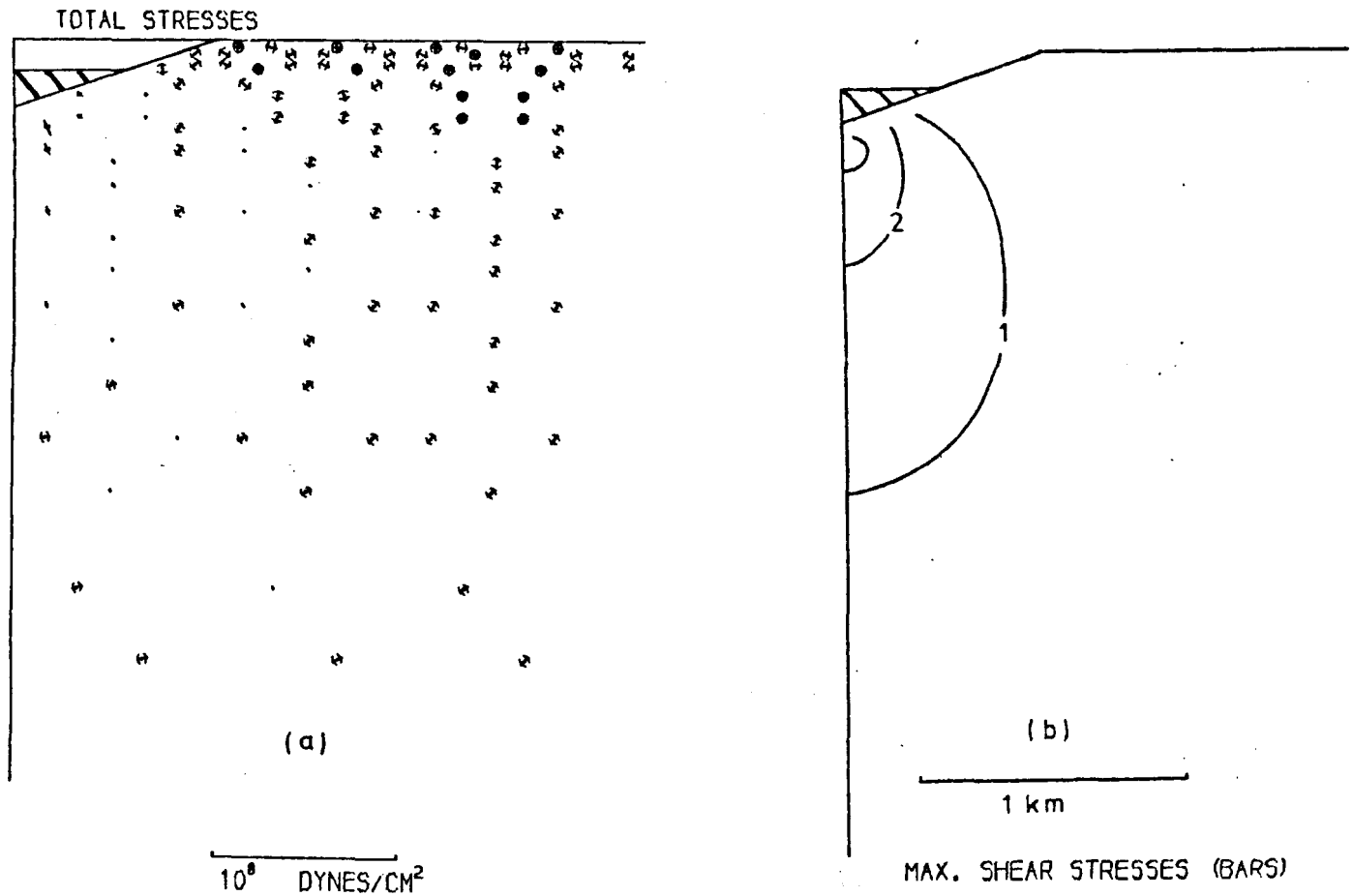

Figure 4.11 Maximum shear stresses due to 125m depth of water in valley of slope 18°.

It appears that these small stress measurements are an unlikely source for the triggering of an earthquake. The large volume that they effect, however, means that if the triggering occurs, the potentially additional available strain energy may well be sufficiently large for the earthquake to make its presence felt at the surface. This aspect will be considered further in Chapter Six.

The analysis of this section differs from previous attempts to study the effects of a reservoir in that the water is considered to accumulate in a pre-formed valley which has already established a stress field. The importance of this is discussed in the following section.

4.3 Tectonic Stress and Reservoir Imposition

The effect of a reservoir load upon a tectonically stressed region, as usually described, is summarised in Fig. 4.12. The situation is shown both in terms of total and deviatoric stresses, and by Mohr circle notation. The left-hand column shows the case when no tectonic stress field is present beforehand. The increased deviatoric stresses due to the normal faulting environment imposed by the water load do not necessarily mean that the rock is weaker. The concomitant increase in normal stress may actually prove more significant and achieve a net strengthening. Whether this is so or not can be determined by comparing the relative changes in the maximum and minimum stress with the internal friction angle. In this case the elastic increase means $d\sigma_3/d\sigma_1 = 0.33$ (for a Poisson's Ratio of 0.25), and the corresponding internal friction angle must be less than 30° if the rock is to be made weaker. Where a tensional tectonic and/or residual stress field exists previously, exactly the same arguments hold, but the rock is initially weaker. On the other hand, an initial compressive stress regime is in an opposite sense to that of the artificial load. This means that the water must strengthen the rock, regardless of the failure parameters. The picture painted by Fig. 4.12 thus implies that in many instances, the positioning

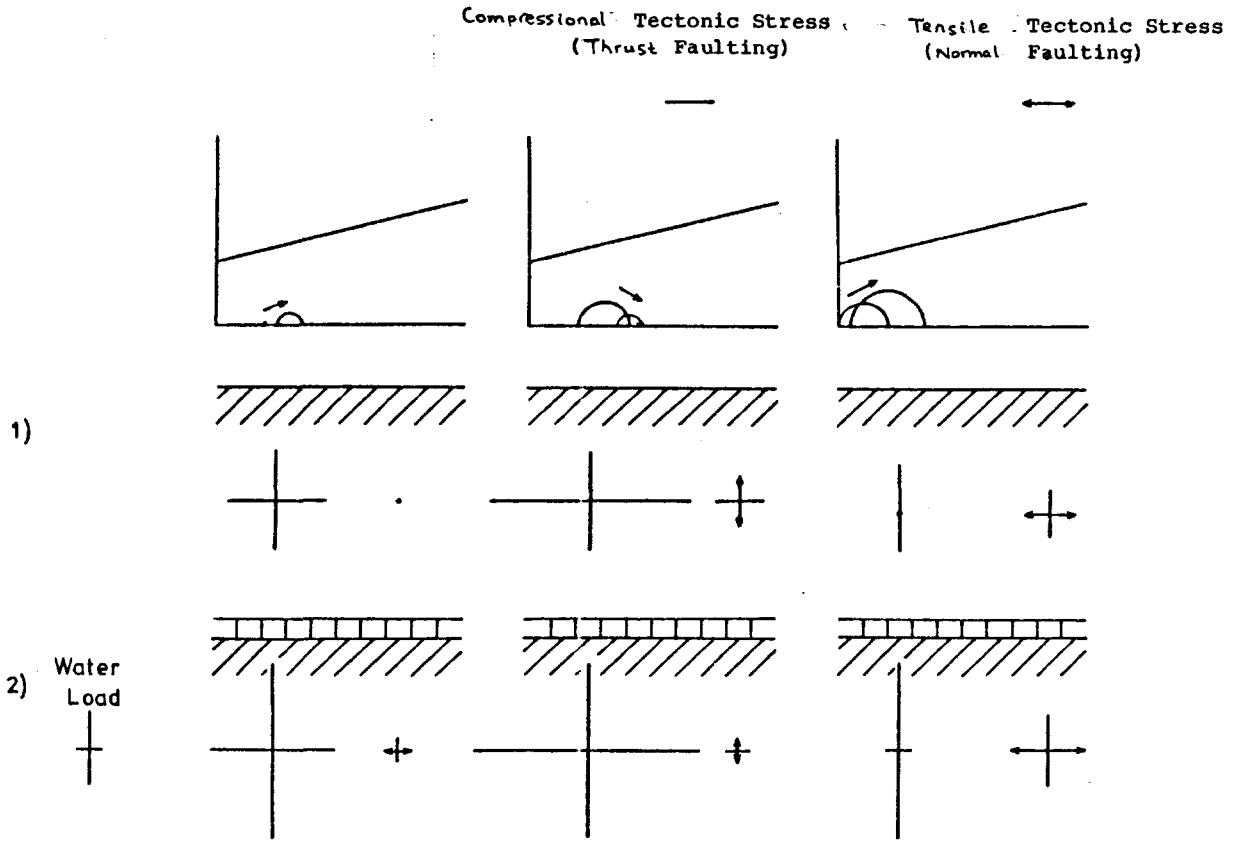

Figure 4.12 Stresses Induced by a Water Load upon a Tectonically Stressed Elastic Half-Space.

Note: Total stresses to the left , deviatoric stresses to the right in each case.

of a reservoir upon a homogeneous, non-porous medium, will provide extra stability.

This view is even stronger if the valley stresses are considered also. In the previous section it has already been shown that the filling of a reservoir in an unstressed valley results in a reduction of the shear stress field. Firstly we examine, using finite element, the combined effects of a valley and a horizontally compressive tectonic stress field. Fig. 4.13 shows an empty valley of slope 45° and depth 500 m, with a thrusting stress field of 100 bars applied. Fig. 4.13d shows the valley without tectonic stress for comparison. The background level of maximum shear stress is thus 50 bars, but due to the changing orientations of the principal stresses that result from the valley, this shear stress field is not simply added arithmetically to the valley shear stress field. In fact, as reference to Fig. 4.1b will show, those valley stresses to the side of the valley constitute a normal faulting regime, and will counteract the tectonic component. This results in the difference in shape of the upper parts of the stress fields in Fig. 4.13. In Fig. 4.13c the shear stress above the valley is several bars lower in comparison with the background field. At the point of greatest shear stress, an increase of 50 bars is of course observed, as this was originally of purely reverse faulting type after formation of the valley. This point is where the greatest weakening takes place; the decreased stresses to the side of the valley are not so effective at achieving this. This situation is represented in the upper central portion of Fig. 4.16.

The effect of subsequently filling the valley partially with water (to a depth of 250 m) is shown in Fig. 4.14. Beneath the valley the effect is identical to that when no tectonic field was present (Fig. 4.6), i.e. a reduction in shear stress of just less than 5 bars on average. The effect directly at the lower valley sides is more complicated due to geometrical effects of the water and valley slope, but is not greatly different. To the sides and above the water, no effect is apparent. This situation is represented in the lower central portion of Fig. 4.16.

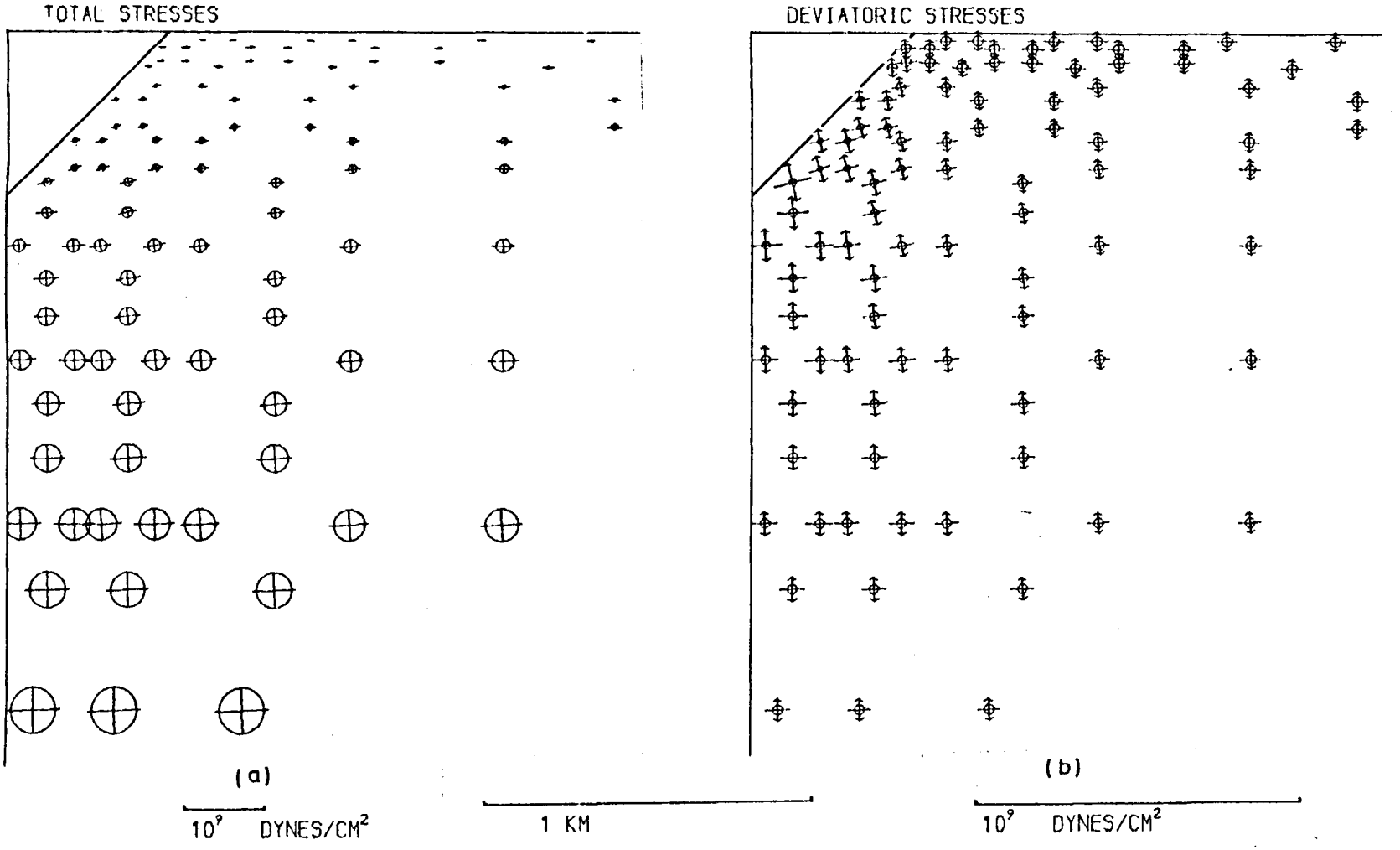

Figure 4.13 (a) Total stresses and (b) deviatoric stresses due to a valley 500m deep of slope 45° formed in rock with a horizontal tectonic compressive stress of 100 bars.

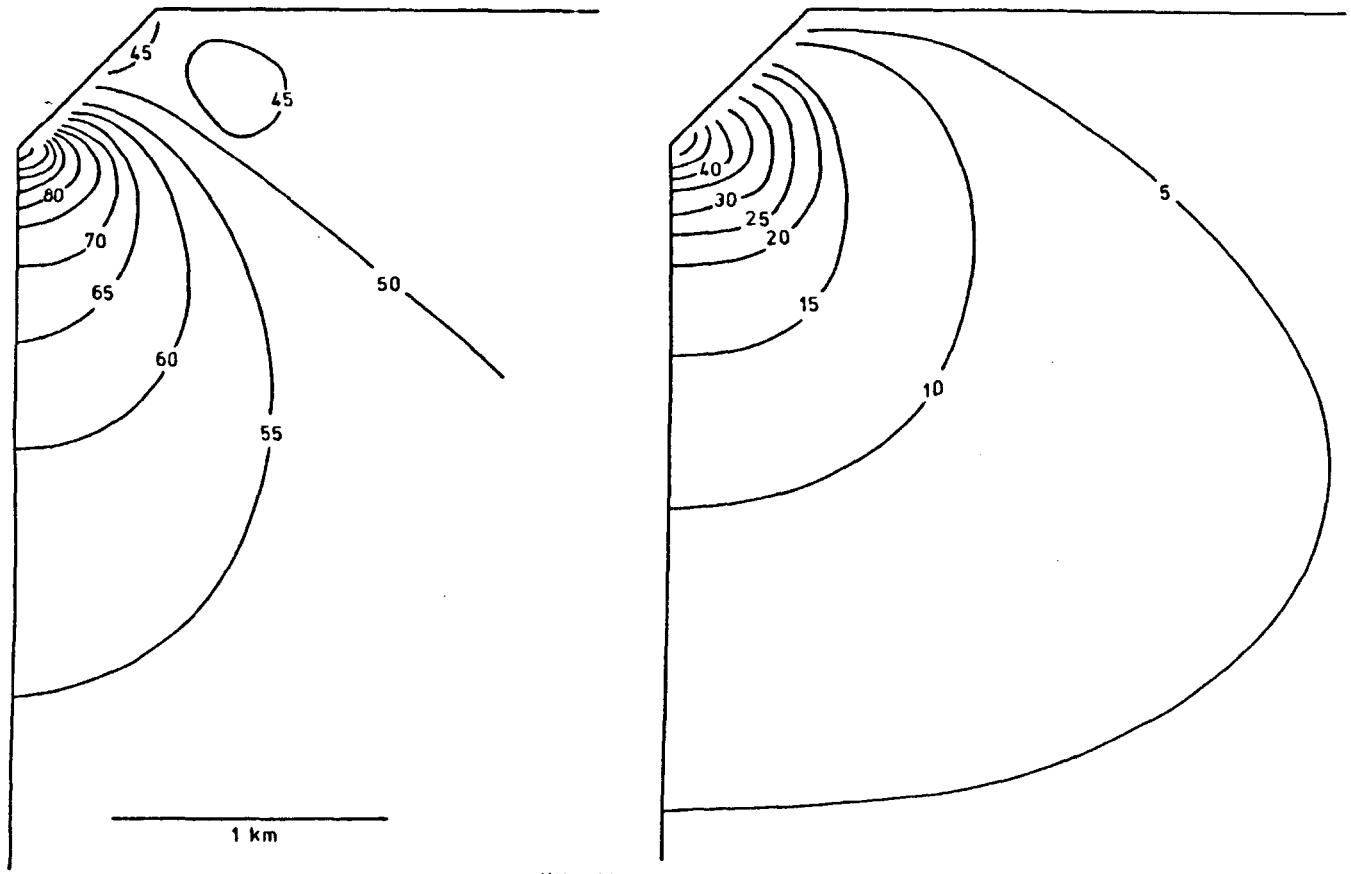

Figure 4.13 (cont.) (c) Maximum shear stresses due to a valley 500m deep of slope 45° formed in rock with a horizontal tectonic compressive stress field of 100 bars. (d) Without tectonic stress.

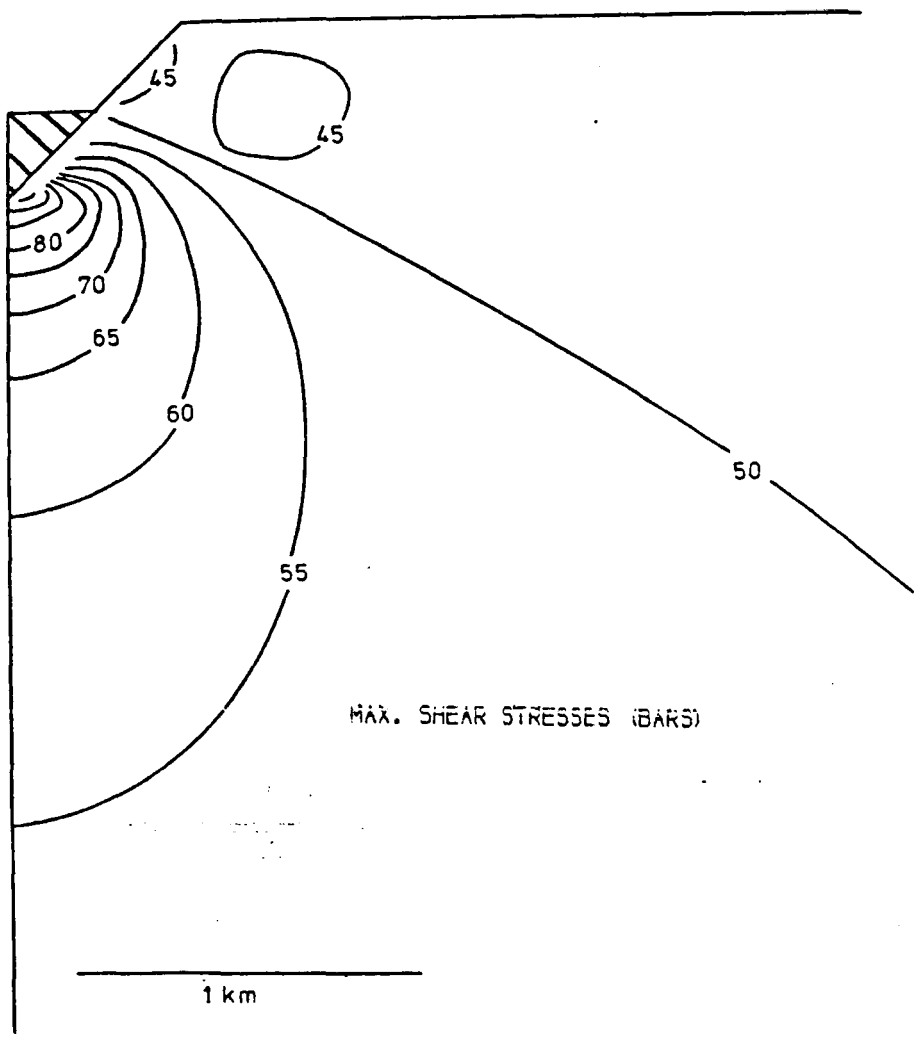

Figure 4.14 Maximum shear stresses due to the imposition of a 250m depth of water in a valley of depth 500m and of slope 45° in a horizontal compressive tectonic stress field of 100 bars.

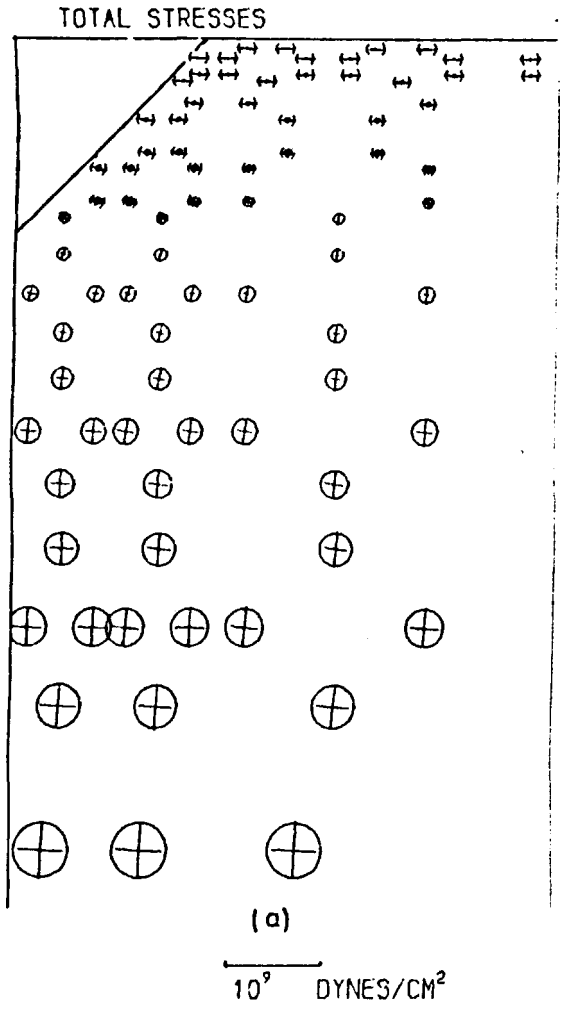

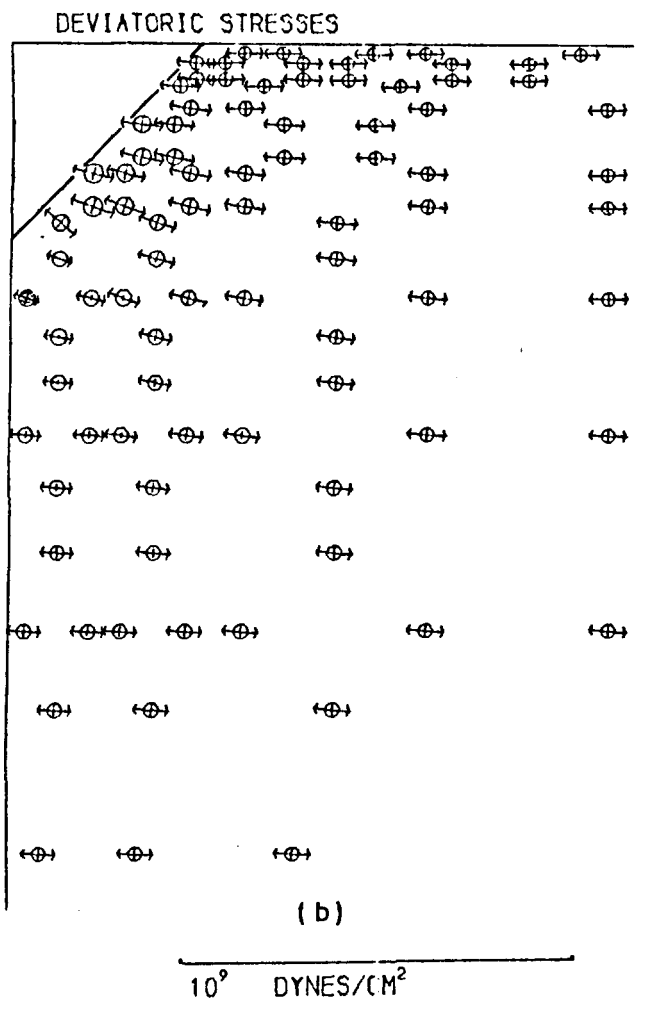

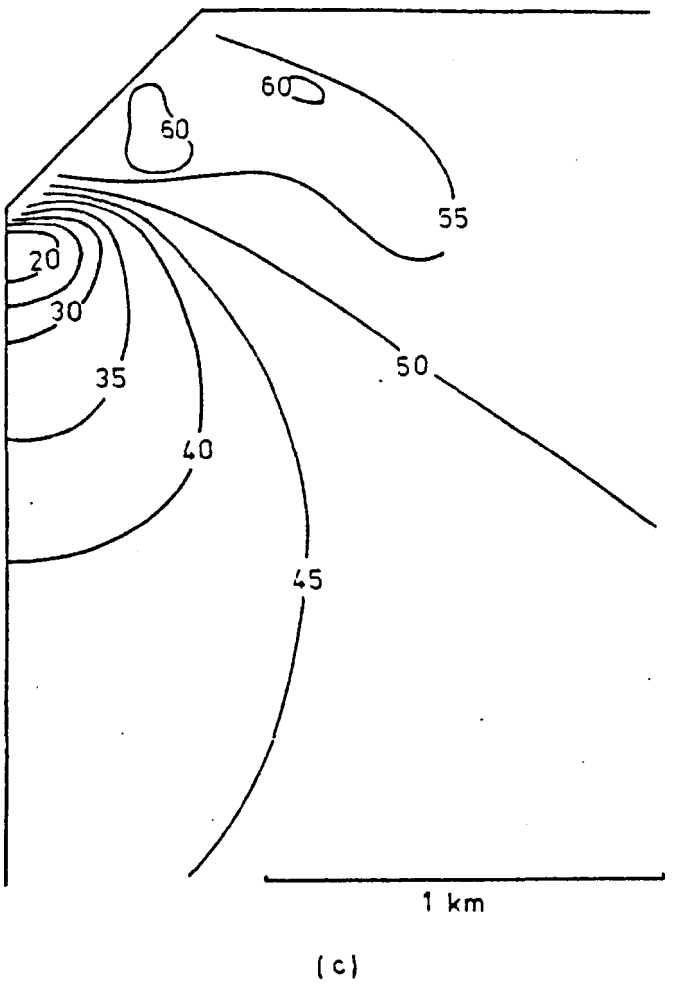

Figure 4.15 (a) Total stresses and (b) deviatoric stresses due to a valley 500 m deep of slope 45° formed rock with a horizontal tectonic tensile stress of 100 bars).

The effects of a tensional regime were also modelled. Fig. 4.15 shows the same valley as in the previous examples, with a tensile horizontal stress of 100 bars applied. In this rather artificial case where the tectonic stress field is uniform right up to the surface, there will always be a surface layer of tensile horizontal stresses, down to a depth dependent on the magnitude of that stress. This is clearly shown in Fig. 4.15a. Fig. 4.15b shows a reduction in deviatoric stress at the base of the valley relative to the background stress. This is to be expected as the valley-formed thrusting stresses now counteract the tectonic regime. A vertical traverse from here downwards to regions of higher shear stress does however represent an increase in strength, due to the increasing lithostatic stresses. The greatest shear stresses are now to be found at the sides of the valley (Fig. 4.15c). In these areas, which contain tensional horizontal stresses, the rock is closest to failure. The subsequent imposition of water results in a small increase in shear stress beneath the valley, giving slightly greater stability.

Fig. 4.16 summarises the above discussion and shows all the possible qualitative effects that the water-loading of a valley may have on a pre-stressed medium. It is generally of the same format as Fig. 4.12, except that three stress sources are now considered. The three columns contain the situations of zero tectonic stress, compressional horizontal tectonic stress, and tensional horizontal tectonic stress respectively. The middle row shows the principal stress magnitudes away from, and beneath, the valley, for each stress regime. Deviatoric stresses are shown beneath the total stresses. The bottom row shows the situation after the water load has been imposed. The stresses away from the valley are not shown here as they do not change perceptibly (see previously given finite-element solutions). The upper row pictures the lower two situations in the form of Mohr circles, with an arbitrary Coulomb-Mohr failure envelope included. The valley 'load' is taken to be a vertical tensional stress, as the finite-element solutions

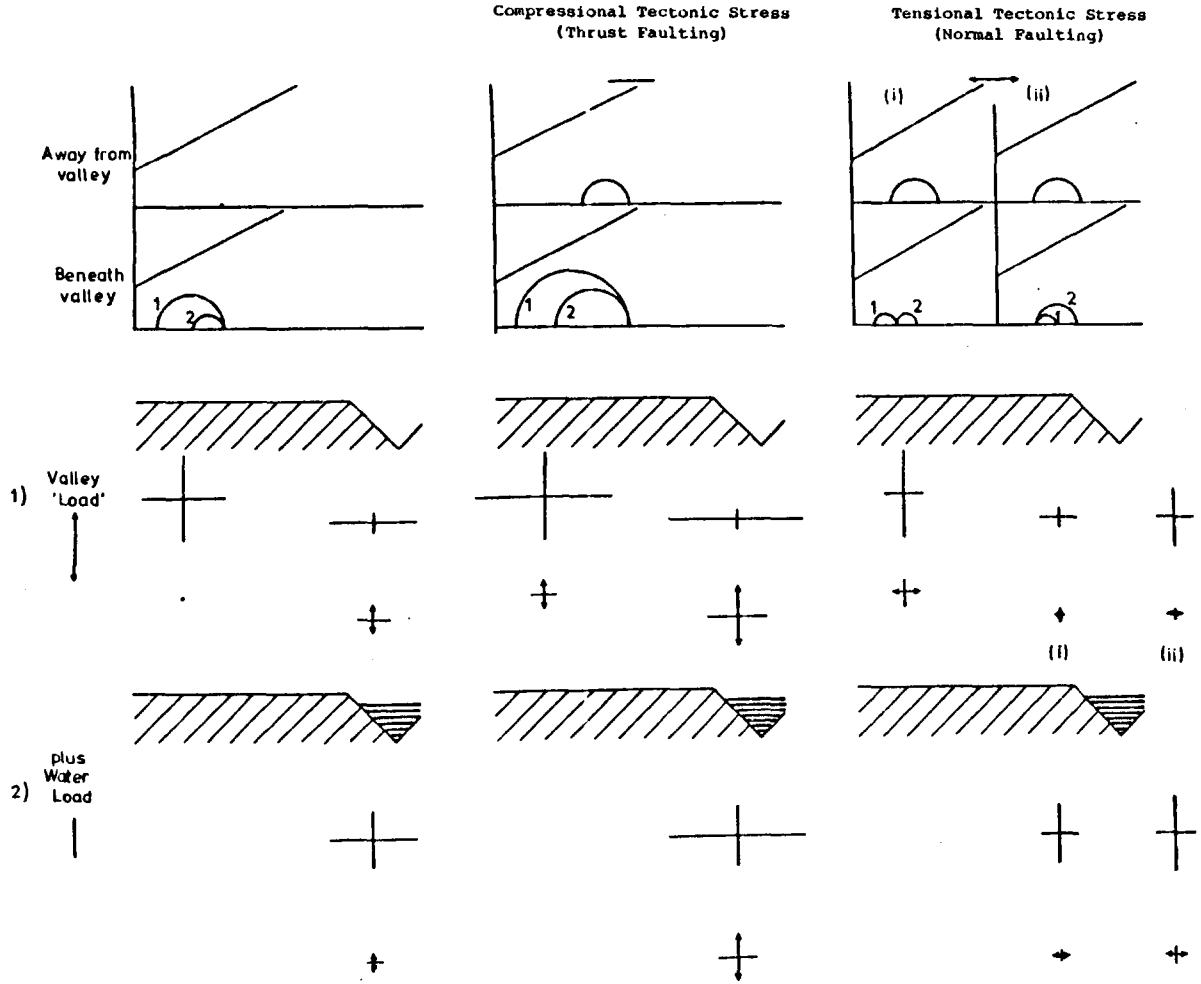

Figure 4.16 Effect on Stability of Water Load in Valley in Elastic Half-Space. (For explanation see text.)

Note: 'Away from valley' stresses to the left , 'Beneath valley' to the right. 'Total stresses' above , and 'Deviatoric stresses' beneath , in each case.

indicate that on average this is the case. The water load is not elastic, in the sense that the principal stresses are not in the ratio 3:1, as might be expected: this is because of the geometrical effects of the valley which mean that the imposed water is effectively wedging apart the valley sides. The true nature of the water load directly beneath the valley is simply one of increasing vertical component, as indicated by the finite-element solutions.

The first column simply shows how the valley stresses decrease the strength of the immediate area (circle 1), and how this is then partly compensated for by addition of water in the valley (circle 2). The lithostatic state is never re-achieved near the valley however, and this area is hence always weaker than the surrounding rocks. Thus, this situation contrasts with that of Fig. 4.12 as now the water strengthens the rock, regardless of the failure parameters. Note that this initial stress state is also equivalent to that of a strike-slip regime. When there is an initial tectonic thrusting regime, as in the second column of Fig. 4.16, the same conclusions can be drawn as from Fig. 4.12 and strengthening must occur in all cases of water imposition. Areas away from the valley still remain stronger though.

When the regional stress is horizontally tensile however, the situation becomes more complex. The erosion of the valley may or may not reduce the vertical stress sufficiently to convert the valley bottom stress regime from normal faulting to thrust faulting. The Mohr diagrams in the right-hand column in Fig. 4.16 have thus been split into two, one diagram for each case. Where the maximum principal stress remains everywhere vertical (a smaller value for the valley load has to be assumed in Fig. 4.16 for this case), the water load then aggravates the stress state, enlarging the Mohr circle and weakening the valley-influenced rocks, regardless of the failure parameters. The state of weakness here cannot however become as great as that in the surrounding rocks, and hence it must be concluded that no failure can take place, as it would have done so already in the neighbouring

regions (e.g. the high-stressed areas of Fig. 4.15c), assuming constant internal friction and shear strengths.

A slightly more complicated case arises when the valley bottom stress state has become thrusting. When the water is first begun to be impounded, the vertical minimum principal stresses will become greater, until eventually a strong lithostatic state is achieved. Further filling will correct the stress regime to normal faulting again, and the situation becomes that when the original stresses were normal. No failure can occur in either case, despite weakening by the water load.

4.4 Effects of Geological Layering

It was considered that the rather small shear stresses resulting from the previous models might be magnified by certain configurations of geological inhomogeneity. In particular it was thought that where there exists a (sub-) horizontal layer of high Young's Modulus, stresses might accumulate, as the layer would be surrounded by a medium providing little support to resist the bending moment provided by the reservoir load. Simple beam theory for three point loading (Jaeger and Cook, 1979, p.130), which approximates to this situation, suggests that the maximum stress induced in the beam is tensile, and proportional to the applied load and the inverse of the square of the beam thickness. There are, however, major differences between the assumptions made in the derivation of this theory and the reservoir situation. For example, the rock layer beneath the reservoir is supported only at infinity, and is in fact subjected to a distributed load which includes traction. It is also of course to some extent supported by the surrounding rock. The theory is used here, however, to compare with the finite element models of reservoir loading above a hard rock lamina.

Three different models were considered, each with a layer of Young's Modulus ($E = 10^{12}$ dynes/cm^2) one order of magnitude greater than the remaining rock. The valley in each case is 500 m deep, has sides of slope

$\tan^{-1}$ 1/3 and is filled with 250 m of water. The figures in this Section can thus be compared with Figs. 4.8 and 4.10. The effects of topography have not been modelled separately here, but can be deduced from the Figures. The first model includes a layer 400 m thick, the top of which is 300 m below the valley bottom. The deviatoric stresses are shown in Fig. 4.17a. Beneath the reservoir, in the hard layer, the shear stresses now reach values of at least 60 bars - double those of Fig. 4.8. Above and beneath the hard layer, however, the shear stress is in fact slightly reduced, by 5-10%. The layer appears to 'concentrate' the available strain energy: in it the deviatoric stresses decrease away from the reservoir, but 5 km away are still 20 bars and are still increasing in comparison with the surrounding stresses. This horizontal geological layering thus provides a marked increase in maximum shear stress, and also propagates this stress horizontally to distances where reservoir loading would normally be negligible. The increased shear stress in the layer has been achieved with little alteration of the average stress value, and the rock layer has therefore been substantially weakened by the combined effects of the valley erosion and the water load. The stresses in the layer in general show a relative horizontal tension due to its being stretched by the load, except directly beneath the reservoir, where the stresses in the lower parts of the layer show compression caused by the concave bending.

To examine the actual loading effects in this situation more accurately, however, the model was run without the action of any rock body forces at all - only the load of the water. These results are shown in Figs. 4.17b and 4.17c, and they show that the maximum shear stress developed is 14 bars, i.e. double that of Fig. 4.10. The deviatoric stresses in the hard layer are in opposition to those shown in Fig. 4.17a. This indicates that despite the increased shear stresses, the effect of the reservoir load is still an increase in stability. This will be seen to be the case in Figs. 4.18 and 4.19 as well.

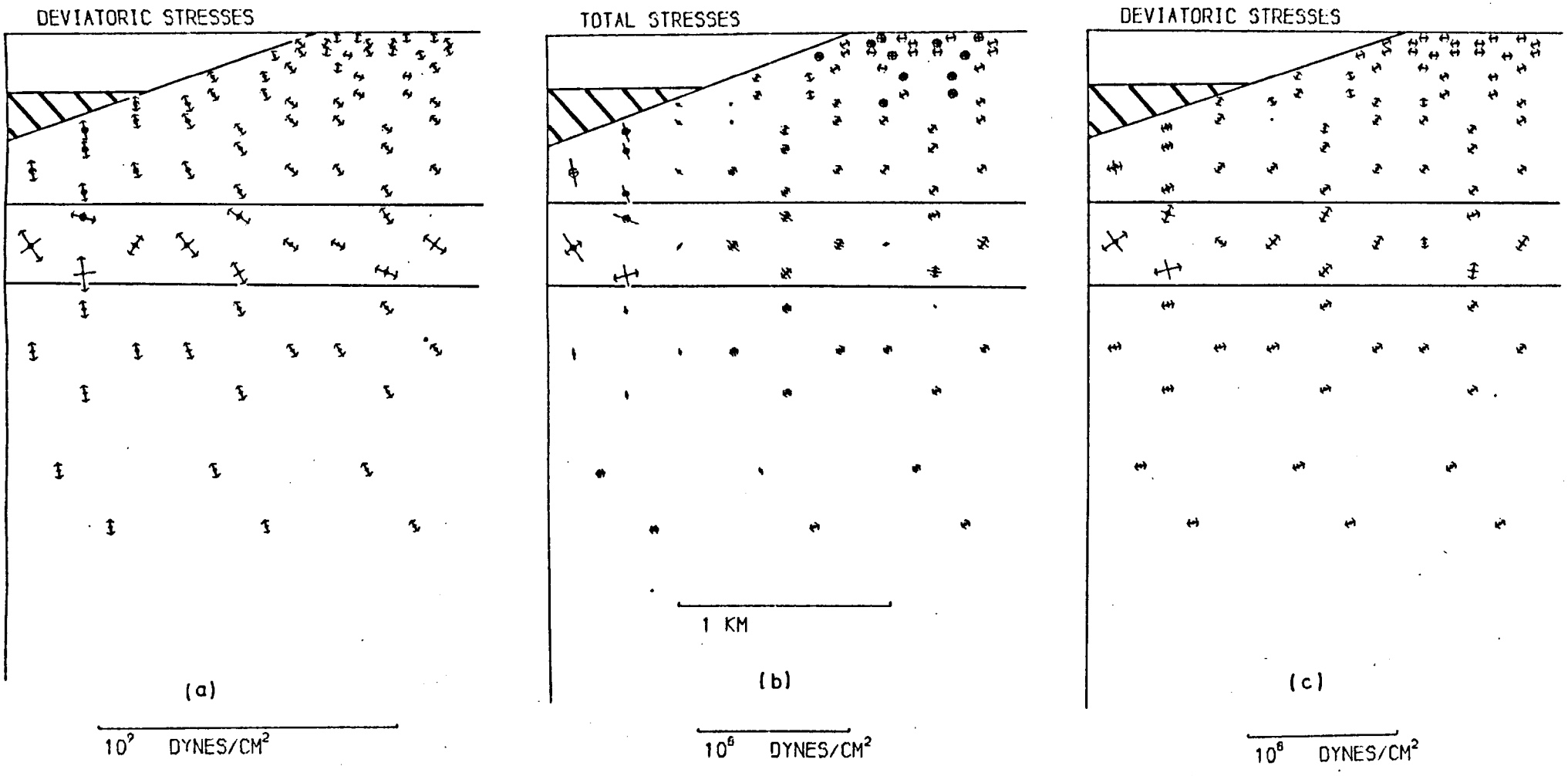

Figure 4.17 Stresses due to the imposition of 250m of water in 500m deep valley of slope 18°. (a) Deviatoric stresses , (b) total stresses due to water load only , and (c) deviatoric stresses due to water load only.

The second model was of a similar layer, but at a depth of 2100 m. As the load of the reservoir is effectively less at this depth, beam theory indicates that the stress changes should also be less in this case. This is shown to be so in Fig. 4.18, where the stresses again approximate to twice those of Fig. 4.8, but at this depth reach only 40 bars. Figs. 4.18b and 4.18c are for the case of water load only, and again show that they have a stabilizing effect.

The third model was of a layer one eighththe thickness (50 m), but at the same average depth (~400 m) as the first model. A maximum shear stress of the order of 100 bars is indicated by Fig. 4.19a, and 20 bars in Fig. 4.19b (water load only). The increase in the total stresses compared to Fig. 4.17 is only of the order of 50%, and thus does not correspond at all with the predictions of beam theory. This large deviation is most likely due to the effects of the supporting rock. The stresses are, however, well into the failure region for cohesionless faults, even for some internal frictions greater than 1.0. This means that the erosional stresses in these cases will cause rock fracture and failure, and the stresses in the hard layer are likely to be at critical magnitudes before reservoir imposition. Thinner layers were not modelled since aspect ratios would have become too large, but the results shown in Figs. 4.17 and 4.19 suggest that stress changes in a layer of thickness 5 m could reach 35 bars. The qualitative aspects of Figs. 4.18 and 4.19 are the same as those for Fig. 4.17 - apart from the stress 'guidance' along the harder layer, the total area of stressed rock is decreased by a few percent in each case. The differentiation between stresses in the top and bottom of the layer becomes much less easy to see in the case of the thin layer, however.

Although not relevant in simple beam theory, the effect of the relative strengths of the beam and the supporting rock must be significant in this case. When there is a small strength difference the situation approaches the homogeneous case, and the induced layer stresses will be correspondingly

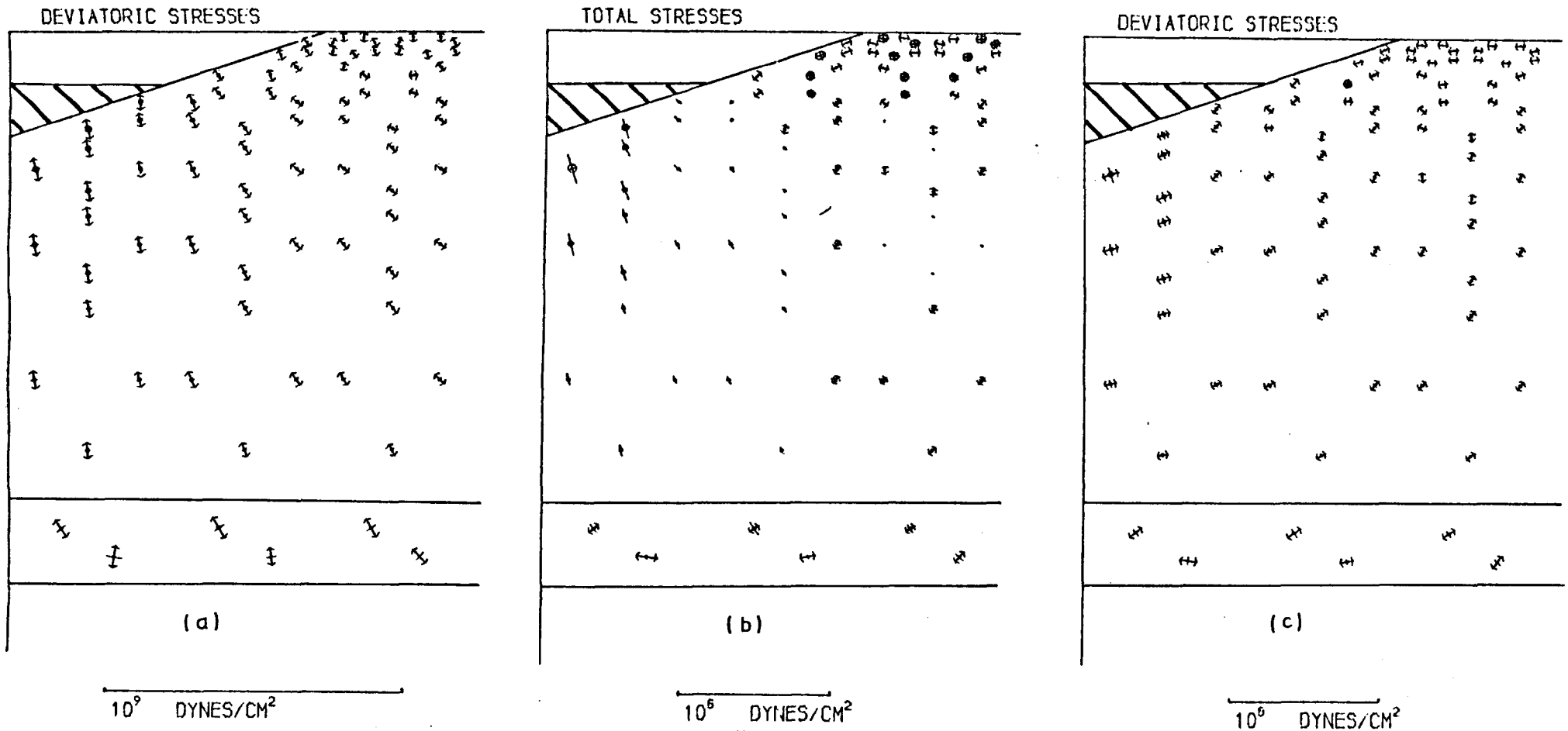

Figure 4.18 Stresses due to imposition of 250m of water in a 500m deep valley of slope 18°. (a) Deviatoric stresses , (b) total stresses due to water load only , and (c) deviatoric stresses due to water load only.

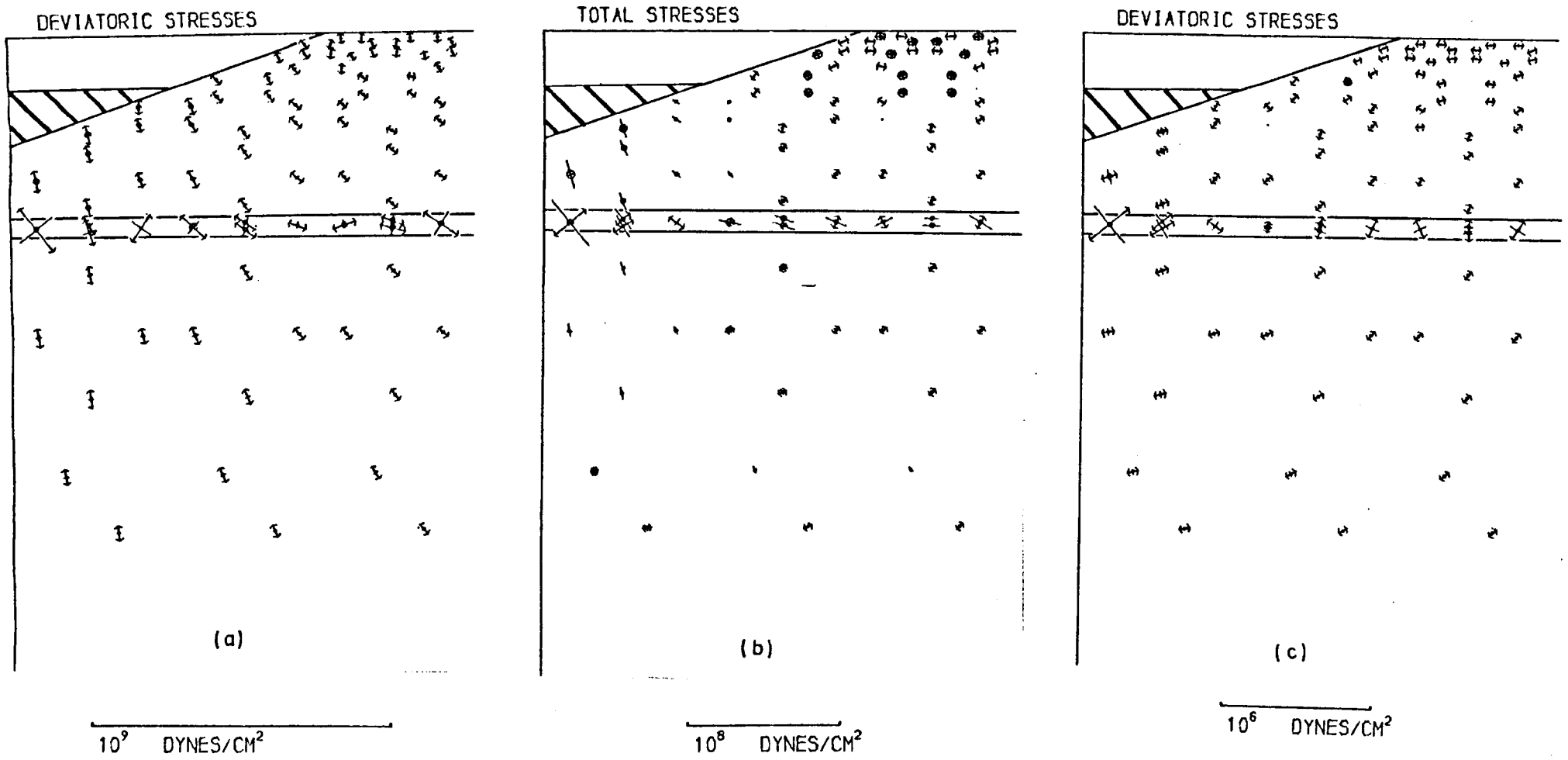

Figure 4.19 Stresses due to the imposition of 250m of water in 500m deep valley of slope 18°.

(a) Deviatoric stresses , (b) total stresses due to water load only , and

(c) deviatoric stresses due to water load only.

small. Models were run to investigate this effect, using different values for the Young's Modulus of the supporting rock. Using the same hard layer as in Fig. 4.17, it was found that the maximum shear stress in the hard layer did not increase proportionately with the ratio of the strengths, but began to level off when the ratio reached 100:1. This latter ratio resulted in maximum shear stresses of around 300 bars. When ratios were low (in the region of 10:1), an almost linear behaviour was observed.

4.5 Conclusions

The theoretical finite element models have shown that maximum shear stress of a few bars, corresponding to an approach to failure,results from the elastic response to the erosion of the valley. These stresses have not before been taken into account when considering the effects of reservoir loads. Their small magnitude means that they are unlikely to be relieved to any significant degree by creep effects or brittle fracture. The models then demonstrated how a water load provides a stabilising effect, under any tectonic conditions, by partially counteracting the stresses created by the valley; a conclusion which is not in total agreement with the classical approach.

Geological inhomogeneities are thought to be of possible great significance in the creation of much larger stress concentrations than those found in the above homogeneous models. In particular the presence of one or, presumably, more hard rock layers can result in large bending and stretching forces. Strain energy is preferentially stored in the harder rock, and significant approaches to the failure state can be the result. The shear stress increases are greater for thinner layers, but become less important with depth. It appears that in this way water load-induced stress changes can reach magnitudes equivalent to the stress drops associated with the largest induced earthquakes and estimates of fault strength at depth, and hence in this way it may be possible for the reservoir load to be

directly and wholly responsible for their release. It is important to note, however, that even in these situations the reservoir still provides an extra stability if elastic valley stresses are present beforehand.

However, considering the magnitudes of shear stress generated in the hard layers by the topography, it seems likely, depending on the strength of the rock, that fractures will have already been formed during the erosional process, with the result that much of the stress will have been relieved before reservoir imposition. Thus, in the same way as when creep relaxation decreases the original topographic stress, the reservoir load, although initially stabilising the rock layer, may now in fact result in stresses which not only counteract the topographic stresses, but also are sufficient to create a different instability by reversing the principal stress orientations. As the layer stresses are, beneath the valley at least, of differing orientations, the sign of any tectonic stress would not effect this conclusion, but would control which parts of the layer became more unstable in this way. A tensile tectonic stress, however, would be the most effective in this as the water load stresses over the greatest portion of the layer correspond to normal faulting.

CHAPTER 5

CONSIDERATION OF THE EFFECTS OF SUBTERRANEAN FLUIDS

5.1 The Effects of Pore Pressure on Rock Material

A further refinement in the modelling of rock material is achieved by the consideration of the mechanical effects of fluids occupying the pore spaces that the rock contains. The two most important effects are the amendments to the stress-strain behaviour and to the failure criteria. There are two aspects to each of these: the distribution of the fluid pressure, and the effect that this pressure has on the mechanical behaviour. Calculation of the pressure distribution and its variation with time will be discussed in Section 5.3.

(i) Modifications of Elastic Behaviour

The way in which the compressive stress-strain behaviour is modified has, since the initial papers of Terzaghi (1923) and Hubbert and Rubey (1959), been implicitly assumed to be identical to that in which the failure criteria are modified: that is to say the stress state in the rock material is to be added to a certain factor to produce effective stress values which can then be used in calculations. This means that deformation can still be described in a similar way to a linear elastic problem in a non-porous material (Biot & Willis, 1957). Terzaghi (op.cit.) proposed that this factor, α, be equal to $(1-n)p$ where 'n' is the porosity and 'p' the pore pressure, but Hubbert and Rubey (op.cit.) later asserted that $\alpha = p$. They supported this proposition with the experimental results of Handin (1958) and McHenry (1948), although these concerned stresses at failure only. Other proposals have been that $\alpha = [\sigma\text{-}1\text{-}(1-\nu)K/K_s]p$ (Suklje, 1969) where ν is the Poisson ratio, K the bulk modulus of porous rock and K_s that of the rock grain, and that $\alpha = (1-K/K_s)p$, (Skempton, 1960; Geertsma, 1957). This latter expression, firstly suggested on empirical grounds, has since been proven by Nur and Byerlee (1971)

to be theoretically exact. These authors demonstrated its much better physical agreement than the conventional effective stress law by means of experiments on rocks with differing porosities, and showed how this relationship almost reduces to the formula of Hubbert and Rubey in the case of natural aggregates, where the presence of a pore network increases the compressibility considerably. K unfortunately is dependent on the pressure, and is usually multiplied by the empirical factor (p_c-p), where p_c is the confining pressure. However, the expression still remains in slight disagreement with experimental evidence, underestimating the pore pressure effect. This is possibly due to its time-dependent nature (Garg and Nur, 1973).

(ii) Modifications to Failure Criteria

Nur and Byerlee (1971) pointed out that their derivation of the effective stress law was not applicable to inelastic processes such as failure. Haimson (1968) had already made use of a dual system of effective stress, and employed the conventional law when dealing with rock strength. This law has been experimentally verified on numerous occasions under all naturally occurring temperature and pressure conditions where the rock remains elastic, whatever mode of failure eventually occurs (e.g. Byerlee, 1971; Cornet and Fairhurst, 1972). At high strain rates, however, an apparent increase in strength may be observed due to excessive dilatancy (Rummel and Gowd, 1973). Bishop (1974) states that it is difficult to find convincing evidence that α is other than p for failure. Thus the Coulomb-Mohr criterion (see Section 2.3) can be satisfactorily used in the form:

$$S = \tau + (\sigma_c - p)\mu$$

where S is the strength, τ the cohesive strength, σ_c the confining pressure, μ the coefficient of static friction, and effective stresses can be inserted directly into Griffith's conditions for fracture (Murrell, 1962).

Rock frequently contains a system of fissures, which are of various scales, down to at least 5 km depth, and in places twice this (Howells, 1974b; Bell and Nur, 1978). The Kola borehole has revealed cracking and considerable quantities of aqueous solutions at 10 km depth (Rich, 1980). These fissures generally have an important influence on the overall deformation of the rock since they have low stiffnesses. Noorishad et al. (1972) found from simple models that the presence of water reduced the fracture deformation by about 30 per cent. Snow (1972) discusses the effect of fluid pressures in these fissures upon the value of the effective stresses, using ($\alpha = p$), and he also considers that the change in effective stresses might be unequal in different directions due to lack of constrictions at the surface boundary. In his 1968 paper he had already introduced the mechanics of fractures, by assuming them to be parallel and propped open jointly by elastic particles and fluid pressure. He derived an expression for the vertical strain in terms of the pore pressure:

$$\varepsilon_v = \frac{1}{CD} \Delta p$$

where 'D' is the average distance between horizontal fractures and 'C' is their stiffness. This is a result of the total vertical strain remaining constant on increase of subterranean pressure ($\Delta\sigma_v = 0$), a phenomenon that would not occur naturally due to the restraint of the surrounding unpressured rocks. This would in fact reduce the total vertical strain to:

$$\varepsilon_v = \frac{1-\chi}{CD} \Delta p$$

where $\chi = \Delta\sigma_v/\Delta p$ (a measure of the restraint).

Unfortunately, Snow's expressions for strain in the rock blocks are only derived one-dimensionally. Nonetheless his general conclusions, namely that almost all horizontal strain is taken up by deformation of the rock blocks, and that the rate of loading is an important strength consideration, probably still hold true.

In his 1972 paper Snow treated the problem three-dimensionally, and considered loading an orthogonally fractured rock mass with an infinitely wide reservoir. Again the horizontal and vertical stress conditions are different, due to plain horizontal stress and constant vertical stress being assumed. The effective stresses then become, after a long period:

$$\Delta\sigma_{H\ eff} = \frac{2\nu - 1}{E/CD + 1 - \nu}\Delta p, \qquad \Delta\sigma_{v\ eff} = 0 \qquad (5.1.1)$$

as opposed to the slightly larger classical value:

$$\Delta\sigma_{H\ eff} = \frac{2\nu - 1}{1 - \nu}\Delta p$$

to which it reduces when E << CD, i.e. for hard, largely intact rock. In weathered, fractured rock Snow says E/CD can reach 300, so that $\Delta\sigma_{H\ eff}$ is virtually zero. On initial loading, the pore pressure will not have affected points beneath the surface, and so here:

$$\Delta\sigma_{H\ eff} = \frac{\nu}{E/CD + 1 - \nu}\Delta p, \qquad \Delta\sigma_{v\ eff} = \Delta p \qquad (5.1.2)$$

which is identical to classical elasticity theory for non-porous material when E << CD. The effective stresses will then change gradually towards those of 5.1.1 as the pressure front diffuses downwards. Where the reservoir is not infinite, there will be adjacent areas affected only by a rise in the water table. Snow gives for this case:

$$\Delta\sigma_{H\ eff} = \frac{\nu - 1}{E/CD + 1 - \nu}\Delta p', \qquad \Delta\sigma_{v\ eff} = -\Delta p' \qquad (5.1.3)$$

where $\Delta p'$ is the excess head thus created, but he assumes that this head has no loading effect on the rock. This is unlikely to be quite true, especially where the rock is mostly intact, so a more generally applicable description would be:

$$\Delta\sigma_{H\ eff} = \frac{(1+\gamma)\nu - 1}{E/CD + 1 - \nu}\Delta p', \qquad \Delta\sigma_{v\ eff} = (\gamma - 1)\Delta p' \qquad (5.1.4)$$

after a long period, where γ varies between 0 and 1 and is a function of the fracture geometry. The initial state beneath the surface then becomes:

$$\Delta\sigma_{H\ eff} = \frac{\gamma\nu}{E/CD + 1 - \nu}\Delta p', \qquad \Delta\sigma_{v\ eff} = \gamma\Delta p' \qquad (5.1.5)$$

Unfortunately, Snow's assumption that the initial pore pressure increase is zero at depth is not tenable since the pores will be compressed,unless points totally unaffected by the reservoir are being considered. Rice and Cleary (1976) give an expression for this initial increase:

$$\Delta p_{init.} = -\ 2/3B(1+\nu_u)\Delta\sigma_c \quad \text{(for plane strain)} \qquad (5.1.6)$$

where $\Delta\sigma_c$ is the change in confining pressure, ν_u is the undrained Poisson's ratio, and B has an empirically determined value $\simeq 0.7$. $\Delta p_{init.}$ thus $\simeq 0.6\times$ $\Delta\sigma_c$ instead of zero. If we represent $-\ 2/3B(1+\nu_u)\Delta\sigma_c$ by λ, λ' can then be used as a parameter which is determined both by λ and by the time passed since impounding relative to the diffusion rates and the distance of the point concerned from the reservoir. Snow's expressions 5.1.1, 5.1.2 and 5.1.3 can then be combined into one more general expression by using both λ' and γ:

$$\Delta\sigma_{H\ eff} = \frac{\nu(\gamma+\lambda') - \lambda'}{E/CD + 1 - \nu}\Delta p, \qquad \Delta\sigma_{v\ eff} = (\gamma-\lambda')\Delta p \qquad (5.1.7)$$

where Δp depends on the location in question and is equal to the change in head directly above it,

λ' lies between 0 and 1 (probably between 0.6 and 1), where 1 represents the situation after a long time or directly beneath the reservoir, and lesser values reflect earlier situations and greater distances away, and

γ also lies between 0 and 1, and is larger for a location beneath the reservoir and/or good coupling of pore pressure with vertical rock stress, and vice versa.

Thus for regions directly beneath the full head increase ($\gamma = 1$) in mostly intact rock ($E \ll CD$), the initial change in effective stress will be ($\lambda \simeq 0.6$):

$$\Delta\sigma_{H\ eff} = \frac{1.6\nu - 0.6}{1 - \nu}\Delta p, \qquad \Delta\sigma_{v\ eff} = 0.4\Delta p$$

which will with time ($\lambda = 1$) become:

$$\Delta\sigma_{H\ eff} = \frac{2\nu - 1}{1 - \nu}\Delta p, \qquad \Delta\sigma_{v\ eff} = 0$$

i.e. if $\nu = 0.25$, $\sigma_{H\ eff}$ will at first decrease by an amount $0.27\Delta p$ and then decrease by a further $0.4\Delta p$, whereas $\sigma_{v\ eff}$ will suddenly increase by 0.4 and then decrease to its original value as the pore pressure front advances. Obviously, for more weathered rocks, where E/CD is not so small, these changes in effective stress will be less marked, and may be effectively zero.

Following Snow (1972) it is possible to calculate whether the changes bring the rock closer to Coulomb-Mohr failure or not. He shows that this will be the case if:

$$\frac{\Delta\sigma_3}{\Delta\sigma_1} < \frac{1 - \sin\phi}{1 + \sin\phi} \qquad (5.1.8)$$

where ϕ is the angle of internal friction and σ_1 and σ_3 are the maximum and minimum principal stresses respectively. From 5.1.7:

$$\frac{\Delta\sigma_3}{\Delta\sigma_1} = \frac{\nu(\gamma+\lambda') - \lambda'}{(E/CD + 1-\nu)(\gamma-\lambda')} \qquad \text{for normal faulting} \qquad (5.1.9)$$

and

$$\frac{\Delta\sigma_3}{\Delta\sigma_1} = \frac{(E/CD + 1-\nu)(\gamma-\lambda')}{\nu(\gamma+\lambda') - \lambda'} \qquad \text{for thrust faulting} \qquad (5.1.10)$$

For strike-slip faulting $\Delta\sigma_3 = \Delta\sigma_1$, and $\phi = 0$ so that positive Δp will weaken the region, and a reduction in pressure will tend to stabilise it.

5.2 Pore Fluid in the Field and its Relation to Induced Seismicity

(i) Natural Pore Pressure Fields

Before discussing the effects of an artificial source of pore pressure, it is pertinent to envisage what the initial state might be. The ground water will, in homogeneous rock beneath a flat ground surface, form a level water table below which all the pores are saturated, and above which they are only partially so. The pore pressures beneath the water table will rise hydrostatically with depth, assuming all are interconnected by highly permeable paths, and above the water table they will be approximately zero. Over short time periods rainfall variations will produce fluctuations in the water table height, and this will be paralleled by increases of pressure in the pore water. Regional erosion will have a similar effect, over a longer period of time (Snow, 1972).

The table might be close to the ground level, or be at a depth of several tens or hundreds of metres below it. This will depend on the relative values of rainfall and permeability, and will also be affected by local topography. Highly porous and fractured rocks, like karstic limestones, will form a level table whatever the irregularity in the ground surface, but shales, for example, will have a table which tends to lie parallel to any topography, and hence might lie at a substantial height above surface water in topographic depressions: in limestone this will only happen in particular local circumstances. The relative height of the water table and a valley in which a reservoir is built has a significant bearing on the change in subterranean pore pressure (Lane, 1971), as can be seen in Fig. 5.1. Figs. 5.1a and 5.1b show two extremes of water table level associated with a river valley. Fig. 5.1a is the result of a relatively high rainfall upon low permeability rock. The pressure contours will parallel the water table to begin with, but at greater depths they will become more planar. The effect of partly filling the valley with a reservoir does not have a great effect on the water table or the pressure contours. Fig. 5.1b however represents

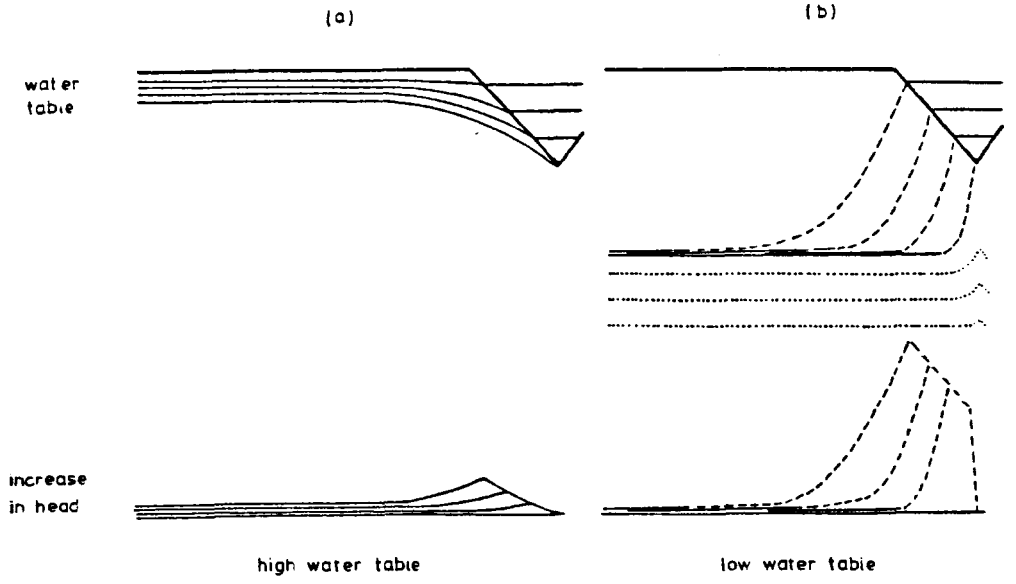

Figure 5.1

Increase in water head associated with reservoir filling

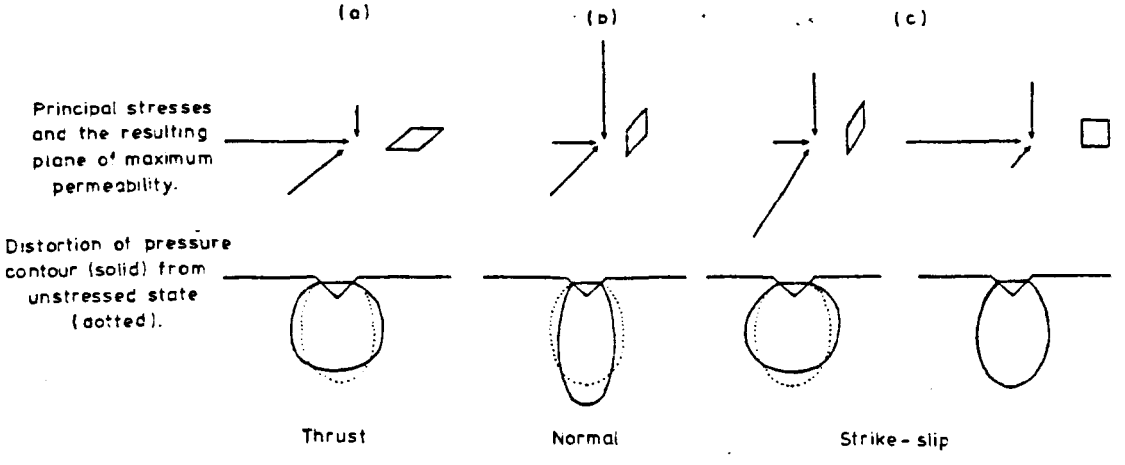

Figure 5.2

The effect of tectonic stress orientation upon pore pressure diffusion

the effects of a low table, which is presumably connected to the surface water by a poorly defined column of water. This column does provide though, very locally, a high water pressure, but this dies out relatively rapidly with depth. On imposition of the reservoir there arises a good hydraulic contact between the surface and underlying water (providing the latter is not excessively deep), and a large head (equal to the sum of the water height and the water table depth) is created beneath it, just as if an extremely deep lake had been impounded (Lane, 1971). A low water table will also tend to increase the delay between impounding and the realisation of maximum water pressure beneath the water table. Areas lubricated by any rise in the water table, although probably not subject to large decreases in effective stress, may well be brought closer to failure by their having the coefficient of friction considerably reduced.

Unfortunately, the sparse data available concerning the magnitude of fluid pressures at depth indicate rather diverse conditions in the field. Handin and Raleigh (1972) report that the natural formation pressure at 3700 m in the Denver disposal well was at least 60 bars less than the theoretical hydrostatic head. On the other hand, Hubbert and Rubey (1959) cite values of ω (where $p = \omega\sigma_c$, σ_c being the confining pressure) to be commonly as high as 0.9 in thick sedimentary sequences and tectonically active regions, which means of course that the effective stresses are especially low in these regions. Pressure gradients arising from the juxtaposition of hydrocarbons and water have sometimes been responsible for aggravating the pressures to these values. They indicate very poor hydraulic contact with the surface (where $p = 0$), and this suggests that the pore pressure has been built up over geological lengths of time since the relatively impermeable layer(s) were formed and overlain. Presumably, where subsurface waters have good hydraulic contact with the surface, e.g. in a highly fractured region, ω will be nearer to 0.35 ($\sim \rho water/\rho rock$). Where high horizontal compressive stresses exist, this contact will be much reduced,

and higher values for ω might obtain. In this case however, a general erosion will reduce ω (eqn. 5.1.6). Alternative relationships to 5.1.6, in terms of other parameters, are given by Biot (1941), Snow (1972), Bishop (1973), but always $\omega < 1$.

(ii) Induced Pore Pressures

Introduction of a high pressure source which achieves hydraulic continuity with the natural pore fluid will usually result in flow by diffusion, under the influence of gravity, away from the source, and there will result temporary fluctuations in the underground pressures. A mathematical approach to determine the nature of these changes is presented in the next section. Here we discuss the factors that will influence it.

The effect of erosion has been mentioned above. In the opposite case, i.e. when an additional load is applied to the surface, ω will increase, decreasing the effective stresses. The impounding of a reservoir upon an impervious bedrock thus tends to weaken the underlying saturated strata (Bell and Nur, 1978), if tectonic forces are neglected. This will in fact apply immediately after the initial stages of all impoundments as long as these are carried out sufficiently quickly to prevent diffusion away from the high pressure region. As the transient pore pressures in each case are quite different, note must be made of the nature of the reservoir foundation.

Obviously, spatial variations in permeability will have an important effect, with shales, volcanics and the like slowing down the spread of the pressure front in their direction, whereas a fracture zone could promote a rapid translation of pressure in either horizontal or vertical directions. This will be discussed quantitatively in the next section.

Even if we assume that the rock mass is intrinsically isotropic with regard to permeability (a degree of layered anisotropy is a more realistic assumption), we fail to allow for the anisotropy induced by both the regional tectonic stress and the stress field due to the water load. Weertman (1974) considered this when dealing with the pore fluid migration about the ends of

an earthquake fault. If we take the natural state of the rock as containing randomly orientated microcracks, then a directed stress will preferentially tend to close those in a plane normal to the maximum stress, σ_1. If we take this stress to be that imposed by a reservoir load, whose greatest value will be of the order 10^7 dynes/cm^2, this is roughly 1/40 of that stress σ' which is needed to close the cracks (taking a small value for σ' = 4.19 x tensile strength, Murrell, 1965). Then using the relation (Louis, 1969):

$$k = \left(\frac{\rho g}{\mu} \cdot \frac{w}{12}\right)^n \qquad n = 1 \rightarrow 3 \text{ depending on fracture roughness}$$

where ρg is the unit weight of the fluid, μ its viscosity and w the crack width, we can estimate the permeability, k, to be reduced by up to 1/40 in the vertical direction just beneath the reservoir, presuming dilatant effects are not significant. It appears that this is a negligible effect compared to any natural irregular anisotropy. However if there is, say, a thrusting stress regime of tectonic origin of the order of σ' then significant anisotropy might be superimposed upon any that is already present. This stress field will preferentially increase permeability in the horizontal plane (Fig. 5.2a), whereas a normal or strike-slip regime tends to ease the passage of water vertically downwards (Figs. 5.2b, 5.2c). The directions of horizontal anisotropy in the latter two cases will depend on the relative orientations of the reservoir valley and the stress field. Note that in each case the tectonic stress inhibits the flow of water in a particular direction, and will not actually accelerate movement in other directions unless a tensile stress is present.

(iii) The Role of Pore Pressure in Faulting

Several ways in which pore fluids interact with faulting processes are now known to exist. The first direct knowledge of this was probably brought to light by Evans (1966) who described the relationship between earthquake frequency and the amount of waste liquid being pumped down the disposal well

near Denver, Colorado. Several other instances of this effect have arisen since then, for instance at Rangely (Munson, 1968) and Dale, New York State (Sykes et al., 1973) in connection with secondary oil recovery and hydraulic salt mining respectively. Both at Rangely (Raleigh et al., 1976) and Matsushiro (Ohtake, 1974) seismically monitored experiments were conducted to study the effects of varying water input, and the former produced remarkably good confirmation of the theories of Coulomb-Mohr failure, effective stress and hydrofracture. So much so, in fact, that it is tempting to suspect a certain amount of good fortune in the agreement between the field and theoretical results. Both at Denver and Matsushiro, encouragingly realistic estimates of permeability could be obtained by measuring the time lag. Healy et al. (1970) indicate that fluid pressure changes control the distribution of aftershock sequences of nuclear explosions, and suggest that the same holds true for injection and reservoir induced seismicity. Nur and Booker (1972) examined the effects of an edge dislocation in a porous elastic material and obtained rates of pressure decay in agreement with those actually observed. Nur (1973) describes how the water level in a 150 m well drilled near an active branch of the San Andreas fault is approximately proportional to the amount of creep on the fault. Dilatancy theory, as proposed by Nur, is also based upon the effects of varying pore pressure. In this case, it should be noted, care must be taken with the application of the effective stress principle, as constant pore pressure within the rock is not maintained (Brace, 1974).

5.3 Calculation of the Diffusion of Pore Pressure

In two dimensions a simple flow equation can be derived as follows. Firstly we must ensure conservation of fluid mass:

$$\frac{\delta q}{\delta x} + \frac{\delta \rho}{\delta t} = 0 \qquad (5.3.1)$$

where q is the fluid mass flow rate, and t is time.

Darcy's law then provides us with the behaviour of the flow rate in terms of the pressure gradient:

$$q = -\rho_o k \, \delta p/\delta x \qquad (5.3.2)$$

where ρ_o is the reference density of the fluid and k is the flow permeability. Lastly we assume that the pores are not deformable, so that ρ_o is independent of elastic constants and is proportional to p:

$$\rho - \rho_o = \text{const.} \times \rho_o \times p \qquad (5.3.3)$$

Combining 5.3.1, 5.3.2 and 5.3.3 and assuming k is a constant, we have our flow equation:

$$\nabla^2 p = \frac{\text{const.}'}{k} \frac{\delta p}{\delta t} \qquad (5.3.4)$$

Jaeger and Cook (1979) give const. = $1/\lambda$, where λ is the specific storage of the aquifer. Equation 5.3.4 can be solved easily by a finite difference method, where the equation is satisfied at a number of different points on a rectangular grid (Fig. 5.3). In finite difference terms, 5.3.4 becomes:

$$\Delta p(t) = c.\Delta t. \nabla^2 p \qquad (5.3.5)$$

where $\nabla^2 p = \dfrac{\Delta p_1/\Delta y_1 - \Delta p_2/\Delta y_2}{\Delta y_{av}} + \dfrac{\Delta p_3/\Delta x_3 - \Delta p_4/\Delta x_4}{\Delta x_{av}}$

and $c = k\lambda$ (which can vary from point to point). To obtain sufficiently accurate answers for the pore pressure at any time it is necessary to proceed by sufficiently small time steps that increase the pressure only by a fraction, 'f', of the maximum pressure difference to ensure convergence, i.e.:

$$\Delta t_{max} \leq a^2/fc \qquad (5.3.6)$$

where a is the maximum distance between adjacent nodes that occurs in the grid. f may be set to 0.1 as a reasonable balance between accuracy and the number of time steps needed to reach a solution; it may be made smaller if the pressure situation at a relatively early stage is required. Details of

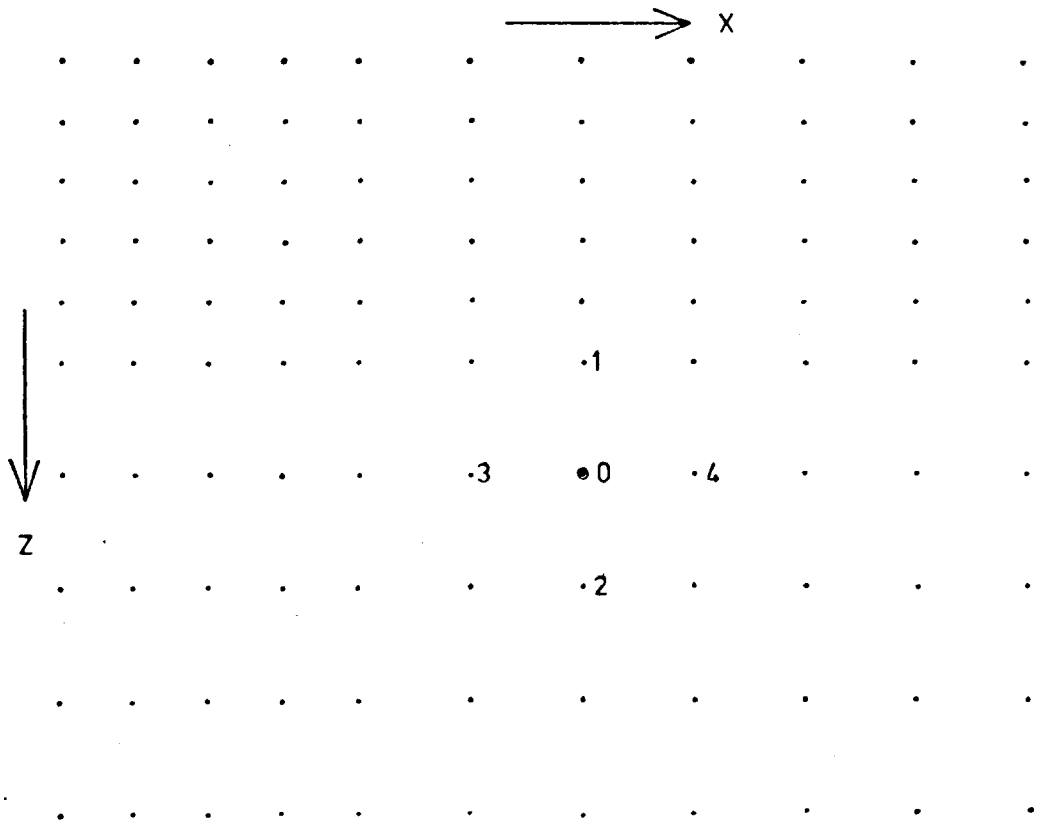

Figure 5.3 Rectangular finite difference grid

the computer program written to calculate the pore pressure are given in Appendix 8, and a one-dimensional test to compare results with an analytical solution is given in Appendix 9.

Howells (1974b) gives a representative value for c of 1.16×10^5 cm^2s^{-1}. Bell and Nur (1978) consider the effects of coupling between the stresses and the pore pressure, and use instead of 5.3.3:

$$\rho - \rho_o = \frac{3\rho_o (\nu_u - \nu)}{2GB (1+\nu)(1+\nu_u)} \left(\sigma_n + \frac{3p}{B} \right) \qquad (5.3.7)$$

where G is the shear modulus, ν_u is the undrained Poisson ratio:

$$\nu_u = \frac{3\nu + \eta}{3-\eta} \qquad \text{(Rice and Cleary, 1976)} \qquad (5.3.8)$$

where $\eta = B(1-2\nu)(1-K/Ks)$,

and $B = -\frac{3\Delta p}{\Delta \sigma n}$

They arrive at a value for $c = \frac{2GB^2(1-\nu)(1+\nu_u)^2}{9k(\nu_u-\nu)(1-\nu_u)}$ (5.3.9)

which, using typical values quoted in Rice and Cleary (1976, Table 1), and k = 1.16 darcy like Howells (op.cit.), gives $c = 2.72 \times 10^5$ cm^2s^{-1}. This means that stress-pore pressure coupling more than doubles the diffusivity. However, considering the probable errors in the values for the constants involved, it does not appear worthwhile to correct for coupling in this simple analysis. Solutions well within an order of magnitude of the correct one are, nevertheless, easily obtained.

Spatial variation in k is easily achieved merely by assigning different values to each node. Simulation of a network of fractures is thus realised by increasing k to appropriate values. Simulation of discrete fractures is not as easy, and some very small internodal distances are required if this is to be carried out realistically, and a fracture zone is usually a better description of the result of attempting to do this. This simple method does

not however allow for the significant deformation of the fractures by the imposed load, and unfortunately fracture permeability is very sensitive to their width. At the same time, the deforming stresses are dependent on the pore pressure, and hence if these effects are to be considered, two coupled analyses, such as those by Noorishad et al. (1972) or Gale et al. (1974), must be formulated. These authors however, neglect the primary porosity when dealing with the fracture flow, and a different set of coupled equations must be used if this is to be taken into account as well (Duguid, 1973).

One major drawback of using finite differences to calculate pore pressure diffusion in large-scale examples such as we have with reservoirs, is that the important influence of potential fields, i.e. in this case gravity, cannot easily be incorporated into the system. To consider the effects of phreatic surfaces, for example, it is necessary to resort to simple analytical calculations concerning the water head in each case. Horizontal transmission of pore pressures however, will be much less affected by this shortcoming. Another effect not taken into account in the finite difference scheme is that of the dynamic forces acting, through the friction of the moving pore fluid, on the fissure sides. The very small velocities involved in this, however, suggest that this is a negligeable effect.

5.4 The Effects of Permeability Variations

A few simple models were made to test the effects on the build-up of pressure that permeability inhomogeneities would have, and to test the portrayal of this process by a diffusional model. Firstly, variations of permeability with depth, as would normally be encountered in horizontally bedded strata, were examined for the case of an infinite reservoir. Fig. 5.4 shows the situation for seven different permeability structures, after periods of 10, 35 and 100 days. Curves A, B and C in each case represent the case where the permeability remains constant with depth, having high, medium and low permeabilities (11.6, 1.16 and 0.116 darcy) respectively.

The specific storage was kept at 10^5 bar for all the examples in this section. Curve D represents the situation where there is low permeability rock lying at depth 2.4 km beneath a medium permeability rock and extending indefinitely downwards. As can be seen, the upper part of the curve does not coincide with that for a constant medium permeability (curve B). This is because of the influence of the low permeability rocks below - their relatively low pore pressures and the diffusional nature of the modelling have effectively resulted in a smaller upwards 'negative diffusion' being superimposed upon the main overall diffusion process downwards away from the source. This is in contrast to what would be intuitively expected when gravity also is acting on the pore fluid. In this case a greater build-up of pressure would probably occur just above the low permeability layer due to the fluid not being able to penetrate the lower layer as easily as it moves through the upper. Secondary diffusion effects would presumably then arise from this new pressure source, and superimpose a radiation of pressure vertically away from this level. Such discrepancies between the pore pressure finite difference model and the probable field situation must be borne in mind when studying case histories. The curves E to H in Fig. 5.4 are also strictly the results of a diffusion process.

All the curves display near linear relationships between the pressure and the depth. Curves E and F show the way that a low permeability layer can cause quite sudden changes in the rate of pressure decay with depth, at least during the first one or two months. The layer for curve F is twice as thick (i.e. 1 km) as that for curve E. After a long time however, both become very similar to that for the completely medium permeability (curve B). Curves G and H represent the cases when the layers in E and F contain rock of a higher (11.6 darcy), rather than lower, permeability. The results are not significantly different to curve B, even for short time periods.

The effect of isolated bodies of lower and higher permeabilities were also investigated, as it was thought that these might provide mechanisms

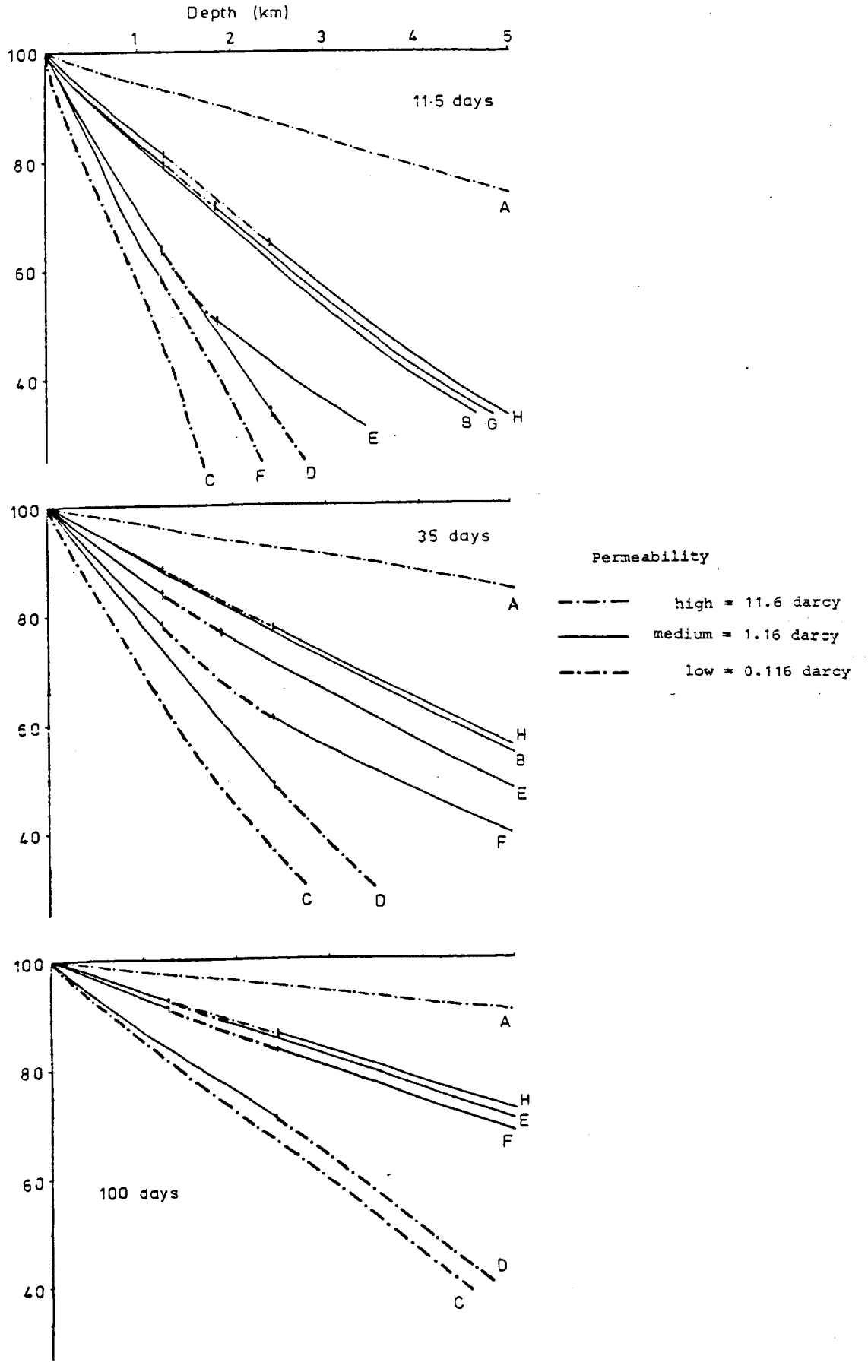

Figure 5.4 Finite difference solutions for pore pressure diffusion down through horizontal layers of differing permeability.

for the 'trapping' of pore pressure, or the formation of substantial pressure gradients. Fig. 5.5 demonstrates how it is the low permeability bodies which have most influence in controlling the pore pressure. Although Figs. 5.5a and 5.5c refer to the same time after imposition, the pore pressure field is noticeably altered only by the low permeability body. Although the high permeability body has the same permeability ratio (10:1) to the matrix, its effects occur for only very short periods of time after reservoir imposition when the pressures are still small; the high permeability results in rapid relaxation of any pressure differences that build up. The same effect is apparent when there is a vertical 'dyke' or fracture with a different permeability to the main rock mass (Fig. 5.6).

Fig. 5.7 shows the situation where the reservoir load is that of a lake of greatest depth 100 m, and width 400 m. Three permeability structures, corresponding to those of curves F, B and H in Fig. 5.4, are considered. There is little variation between the examples, although the horizontal layering does create a slight ellipticity in the radiation pattern. The effect of including a layer with a different permeability in this case approximates closely to a slight overall reduction, or increase, in the model permeability, especially after long time periods and for a higher permeability layer. All the models show how important pressure changes occur at potential hypocentral depths after only a few days, and also how significant changes are still occurring, at higher pore pressures, after several months.

5.5 Conclusions

The effects of pore water pressure have been shown in the past to be of great importance in determining the effective stress state. Although it is established that the effective stresses are able to be used directly in failure criteria and elastic calculations, it is not always clear what the magnitudes of these stresses are. For intact rock the value $\sigma_{eff} = \sigma - P$ is

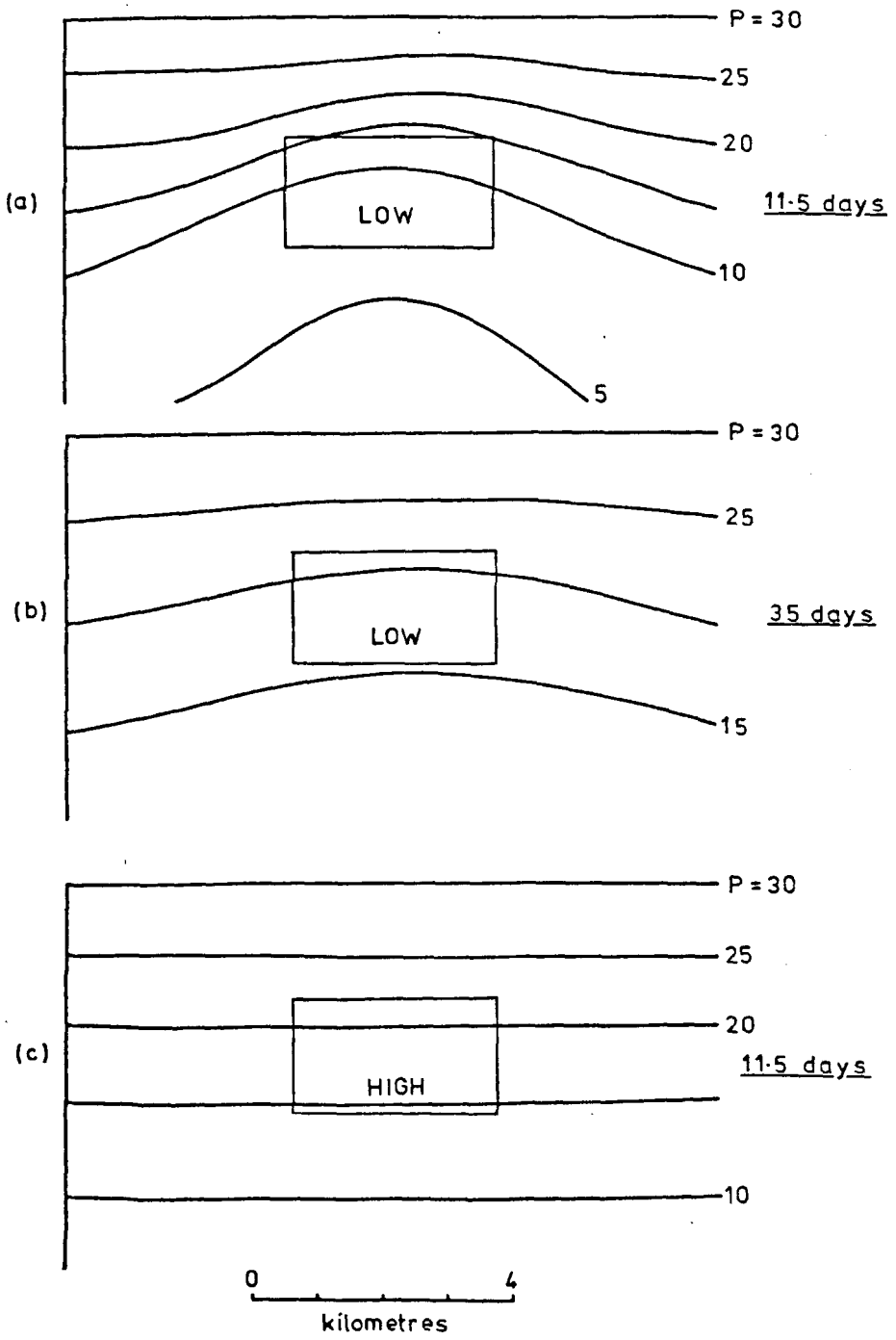

Figure 5.5 Finite difference solutions for pore pressure diffusion downwards from an infinite layer of constant pressure (P = 30 dynes/cm^2)
in the presence of bodies of lower - (a) and (b) - and higher - (c) - permeability.

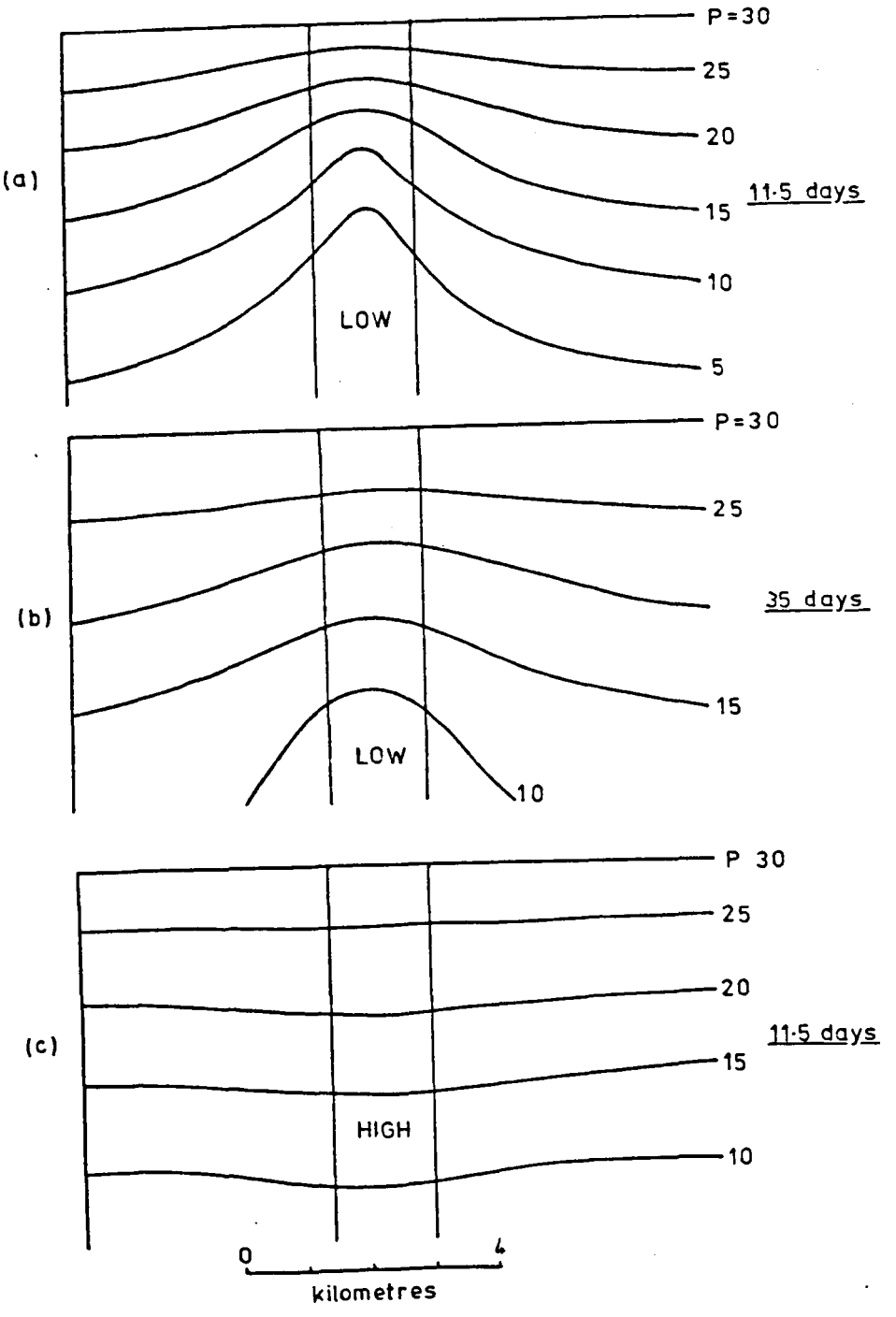

Figure 5.6 Finite difference solutions for pore pressure diffusion downwards from an infinite layer of constant pressure (P = 30 dynes/cm^2) in the presence of vertical pipes of lower - (a) and (b) - and higher - (c) - permeability.

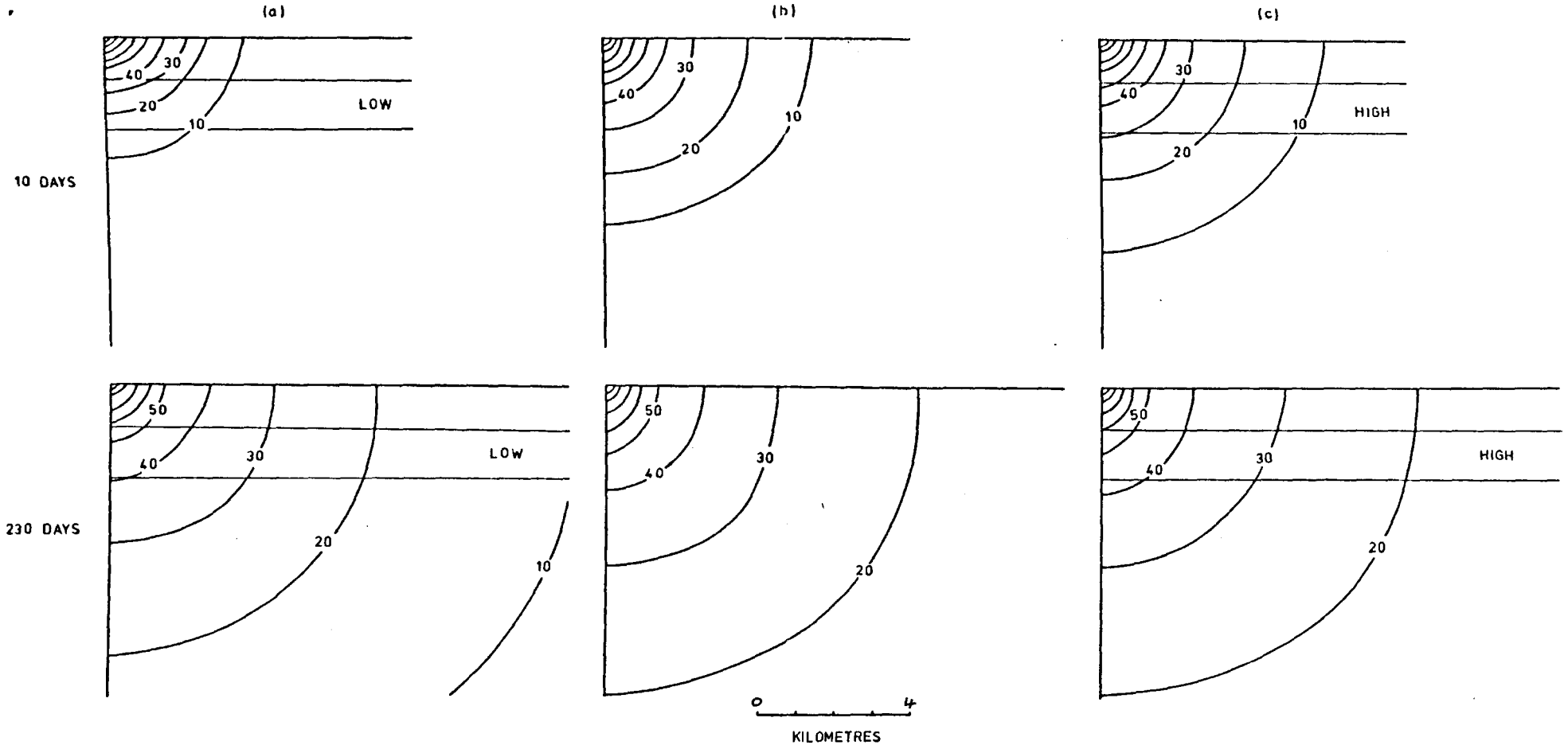

Figure 5.7 Finite difference solutions for pore pressure diffusion away from a reservoir of depth 100m , and the effects of (a) a low permeability layer , and (b) a high permeability layer. Pressure expressed as a percentage of maximum load , P = 10 dynes/cm^2.

a good approximation for the above mentioned purposes, but this expression has been shown not to be applicable when the effects of fractures are accounted for in the mechanics. The effects of the pore pressure are than in fact found to be greatly decreased, and a general expression accounting for these quantitatively has been derived in this chapter. In a very fractured rock, the presence of pore water may not decrease the effective stresses at all.

Little is known about natural formation pressures, but wide variations in the relationships of these with the rock confining pressure have been found in the field. Unfortunately, knowledge of the pre-impounding state is of vital importance in determining the changes in pore pressure, in particular the depth of the water table beneath the surface. Any anisotropy in crack orientation induced by the water load is negligeable in controlling the form of the pore pressure front, but tectonic stress fields may have a strong influence. The calculation of the pressure changes with time using a purely diffusional model has been shown not to be entirely satisfactory, in not considering the influence of gravitational forces, although good approximate solutions may be obtained, especially in horizontal directions. The solutions given in this chapter show agreement in the order of magnitude of the time lags between reservior impounding and the onset of seismicity, indicating a possible connection with pore pressure diffusion.

The model does not originate spontaneously in the human mind, but requires creative activity. Thus senses and intellect both play an active part in our shaping of the model and consequently in our obtaining an insight into the phenomena which have caused us to try and find explanations.

A. Kuipers

CHAPTER 6

PRACTICAL APPLICATION OF NUMERICAL METHODS TO RESERVOIR-INDUCED SEISMICITY

In this chapter the use of numerical methods in predicting and understanding practical examples of reservoir-induced seismicity is examined. The first section attempts to model the situation at one particular reservoir, in order to discover whether or not these techniques could have provided a useful indication of possible seismic induction before impounding. The following section looks at additional problems which arise in this type of modelling, and considers the variety of geometrical and geological properties presented by seismic reservoirs.

6.1 The Induced Seismicity at Koyna Dam, India

The Shivaji Sagar was first impounded behind Koyna Dam (73° 45'E, 17° 23'N) in the late summer of 1962. A detailed account of the case history of this reservoir is given by Gupta and Rastogi (1976). Earth tremors accompanied by sounds became almost immediately prevalent, and two large earthquakes of magnitude 6 occurred in the second half of 1967. A plan of the lake and the epicentres are shown in Fig. 6.1. In this section the factors relevant to the construction of a model of the reservoir, which were known, or could have been known, before construction, are summarised and used. The results are then discussed to see if these help elucidate the question of induced seismicity at Koyna.

(i) The Tectonic Setting

The foundations of the dam comprise a thick series of basaltic lava flows known as the Deccan Traps which errupted in the U.Cretaceous and L.Tertiary. These rocks cover much of West-Central India, and lie unconformably both upon Palaeozoic sediments and the Pre-Cambrian schists and granites which constitute the ancient peninsular shield area. The edge

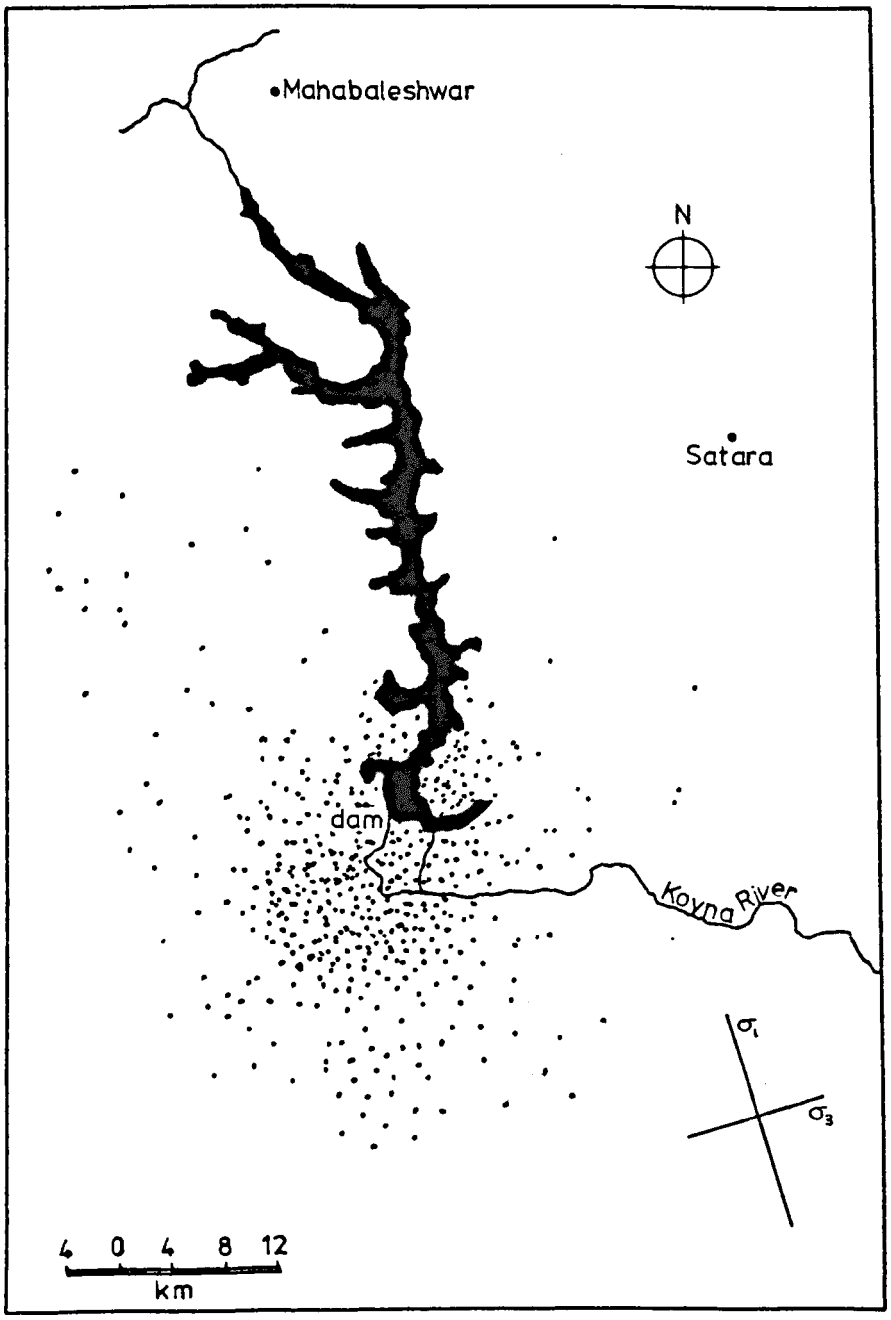

Figure 6.1 Approximate distribution of epicentres, and orientation of tectonic stress at Koyna. (adapted from Gupta and Rastogi, 1976)

of the shield closest to the dam, approximately 110 km to the west, has experienced much tectonic activity during the Tertiary Period. The present coastline is believed to be one of the results of this activity, the transcurrent West Coast Fault being formed in the Eocene and subsequently undergoing a dextral displacement of some 200 km (Balakrishna and Gowd, 1970). Thus although Koyna dam is located upon one of the world's geologically stable Pre-Cambrian shields, it is quite feasible that tectonic activity along the coast has resulted in the development of an extensive stress field in the underlying rocks. The prevailing N-S direction of major fractures and faults in the area indicates the existence of such a field in geologically recent times, although it is possible that these are lineations inherited from the underlying shield rocks. Sykes (1970) and Stonely (1974) give descriptions of the continental collision between Indian and Eurasian plates which would result in a prevalent left-lateral shear stress field in the Koyna region (Balakrishna and Gowd, 1970). The dam area was sufficiently quiet seismically to be included in Zone Ø of the seismic risk map produced by the Indian Standards Institution (1967). Despite several moderately sized tremors in the coastal region, only two important earthquakes occurred in Peninsular India (Gubin, 1969) during the last few centuries before construction of the dam was begun, and local inhabitants have denied experiencing any (Gupta and Rastogi, 1976) in their lifetimes. It is not known whether pre-construction stress measurements were carried out at Koyna, but Guha et al. (1974) reported measurements in the Deccan Traps yielding results of 30-40 bars. These, although taken at shallow depth, conflict with Ranalli and Chandler's (1975) observation, mentioned in Chapter 3, that shield areas contain relatively high horizontal stresses. It seems likely therefore that the Trap lavas and the underlying shield rocks may be in significantly different states of stress. The tectonic considerations above indicate that at least one component of the stress field is a horizontal compression in an approximately NNW-SSE direction,

although of uncertain magnitude. It must be remembered however, that an unknown and complicated system of residual stresses is likely to have developed in the ancient shield rocks prior to the Cretaceous Period, and if the later-developed tectonic stress field is of only a few tens of bars, it is likely to be unrecognisable by measurements in the deeper rocks.

(ii) The Geologic Setting

An account of the geology of the area is given by the Geological Survey of India (1968). The immediate foundation rocks of the reservoir are the horizontally disposed basaltic flows of the Deccan Traps. These flows are individually between 12 m and 40 m thick, but together make up a total thickness of around 1500 m at Koyna and crop out over the entire area likely to be seismically affected by the reservoir. These lavas have a widely varying textural character; usually they contain vescicles or amygdales, but massive flows are also encountered. The flows may be separated by thin layers of red bole clay, which are usually found on top of the non-massive layers or, in the lower Traps, by lacustrine sediments. These freshwater intertrappeans are of small horizontal extent, and rarely exceed 6 m in thickness in the Koyna area. They consist of cherts, impure limestones and pyroclastics, and make up 10% of the total Trap thickness.

Beneath the volcanics lie Dharwarian (Pre-Cambrian), Algonkian (L. Palaeozoic) and Gondwana rocks, all mutually unconformable. The basalts, when errupting, filled in an extremely irregular erosional surface consisting mainly of intensely folded Dharwarian gneisses and schists, but also of Archean granites and Algonkian and freshwater Gondwana sediments. Before deposition of the Gondwana, the region was subjected to intense stressing, resulting in a series of grabens. No major faults are known to exist in the Dharwarian though. Guha et al. (1974) have interpreted a detailed Bouguer anomaly map of the Deccan Trap area (Kailasam et al., 1972) and concluded that a large buried hillock of low density granite or Algonkian sediments is present within 6 km to the west of the lake and reaches up to

within 1000 m of the surface. Within a 25 km radius of the dam this anticlinal hump drops to almost 2500 m beneath the surface in NW and southerly directions, but has a less steeply dipping shoulder to the SW and NE. It is the western profile that is represented in Fig. 6.2.

Major faults are rarely observed in the Deccan Traps. Those that do exist tend to run en echelon with the major N-S fault along the western coast. The Traps are however affected by a series of NNE-WNW fractures along which brecciation and shattering has occurred, although displacement is not evident. Larger fractures with the regional N-S trend are also present. In the Koyna catchment area the fractures are up to 20 km in length and cut through at least 800 m of volcanics. The Koyna valley above the dam is itself believed to be the result of a fault or fracture. Gravity and magnetic profiles (Kailasam et al., 1972) indicate a fault running along the west side of the valley just below the dam. Excavation of the dam foundations revealed a group of fractures with orientations N to NNW. These vary in width between 1 m and 20 m and contain shattered rock in clay gouge. A major shear zone also cuts across the dam, trending NW at an angle of about 60° to the dam axis (Housner, 1970). Fractures in the Traps with an E-W direction are also suspected. A shear zone has been traced crossing the reservoir at Bomnali, and the abrupt turn of the Koyna river itself, just south of the dam, has also been interpreted as being due to a major fault or fracture.

(iii) The Hydrologic Setting

The fluid capacity of the Trap rocks is reduced by their horizontal dips with steeply eroded hill slopes (Gupta and Rastogi, 1976). The upper groundwater seeps out easily through the valley sides, and the basalt flows are drained so rapidly that in the summer wells dry up completely as the water table rapidly lowers. The nature of the flows is important though; the massive lavas with fracture porosities, or the lavas with interconnected vesicles can provide a good water yield, as of course can the intertrappean

sediments. Usually, however, the horizontally disposed massive lavas and intercalated bole clays act to prevent downward seepage (Balakrishna and Gowd, 1970), and deep circulation must depend upon the extensive fractures and fissures which exist in the Koyna area. The deep circulation of water is evidenced by the line of hot springs that runs parallel to the coast west of the reservoir. The temperature of this water suggests a depth reached of about 2000 m, and thus it probably circulates in the underlying Dharwar schists, which have a porosity of 5-10%.

(iv) Finite Element Modelling

(a) The Static Model

Koyna lies at 580 m a.s.l. on a plateau, above which erosional remnants rise to 1650 m (Housner, 1970). The Koyna River used to flow through a 500-600 m deep valley until the Shivaji Sagar was impounded to a depth of about 80 m in 1962. Subsequent annual increments increased the lake level to 85 m and above in the succeeding summers, until the large tremors in 1967. The reservoir has an elongated shape and has been modelled by a cross-section perpendicular to its long axis passing through the deepest portion of the lake by the dam, with plane-strain conditions being assumed. As the valley has a shallow cross-section, the extent of significant topographical and reservoir-induced devatoric stresses is quite large and, by comparison with the modelled examples in Chapter 4, might be expected to be of importance to a depth of 15 km, and to a horizontal distance of 18 km. The outer limits of the finite-element model have thus been placed at much further distances (25 km) to avoid edge effects.

Consideration of the state of knowledge of the subsurface geology at Koyna makes it immediately clear that it is impossible to model in detail the rocks that occur in the potential hypocentral area. Fairly detailed geological information is available about the rocks that crop out in the valley and the dam excavation, but the thickness of the flows and inter-trappeans here are inconveniently small compared to the dimensions of the

model. This interlayering is a possible source of seismogenic stresses, but its detailed modelling in such a grid is precluded when computational factors are taken into account. Certainly, throughout much of the volume of the Traps, a general set of mechanical properties has to be used to represent the average constituents. The use of two models, however, on different scales, does allow part of the Trap structure to be considered in detail. The first model extends to the remote limits discussed above, and uses average properties for the two major rock types present. Several different values are used for the sub-Trappean rocks, as it is not known exactly what these are beneath Koyna. When the regional stresses have been computed with this model, a second, more detailed, sub-grid can then be used to investigate the detailed stress patterns in the lavas. This is now possible because the boundary displacements have been calculated using the primary grid, making remote boundaries no longer necessary. This method is the same as that used by Kidibinski and Babcock (1971) for the investigation of stresses around a longwall coal mine. The two grids are shown in Figs. 6.2 and 6.3. As can be seen, a dense concentration of elements has been used both around the areas modelled in detail and where stress gradients are likely to be high. The density and Young's Modulus for the Traps, shown in the figures, are derived from the average constants given by Birch (1966) for basalts and sandstones. The values used for the basalt were $\rho = 2.85$ g cm^{-3}, $E = 6.8 \times 10^{11}$ dynes/cm^2, and for the sandstone $\rho = 2.35$ g cm^{-3}, $E = 0.5 \times 10^{12}$ dynes/cm^2. These have been combined in the ratio 10:1 in accordance with the field situation. The figures for the underlying metamorphics were derived from a 1:1 ratio of the average values quoted by Birch (op.cit.) for gneiss and schist, i.e. $\rho = 2.75$ gcm^{-3}, $E = 0.3 \times 10^{12}$ dynes/cm^2 in the first case, and $\rho = 2.75$ gcm^{-3}, $E = 0.6 \times 10^{12}$ dynes/cm^2 in the second. The water and air were simulated as described in Chapter 4.

(b) The Initial Stress State

Having selected the static model properties, the original state of

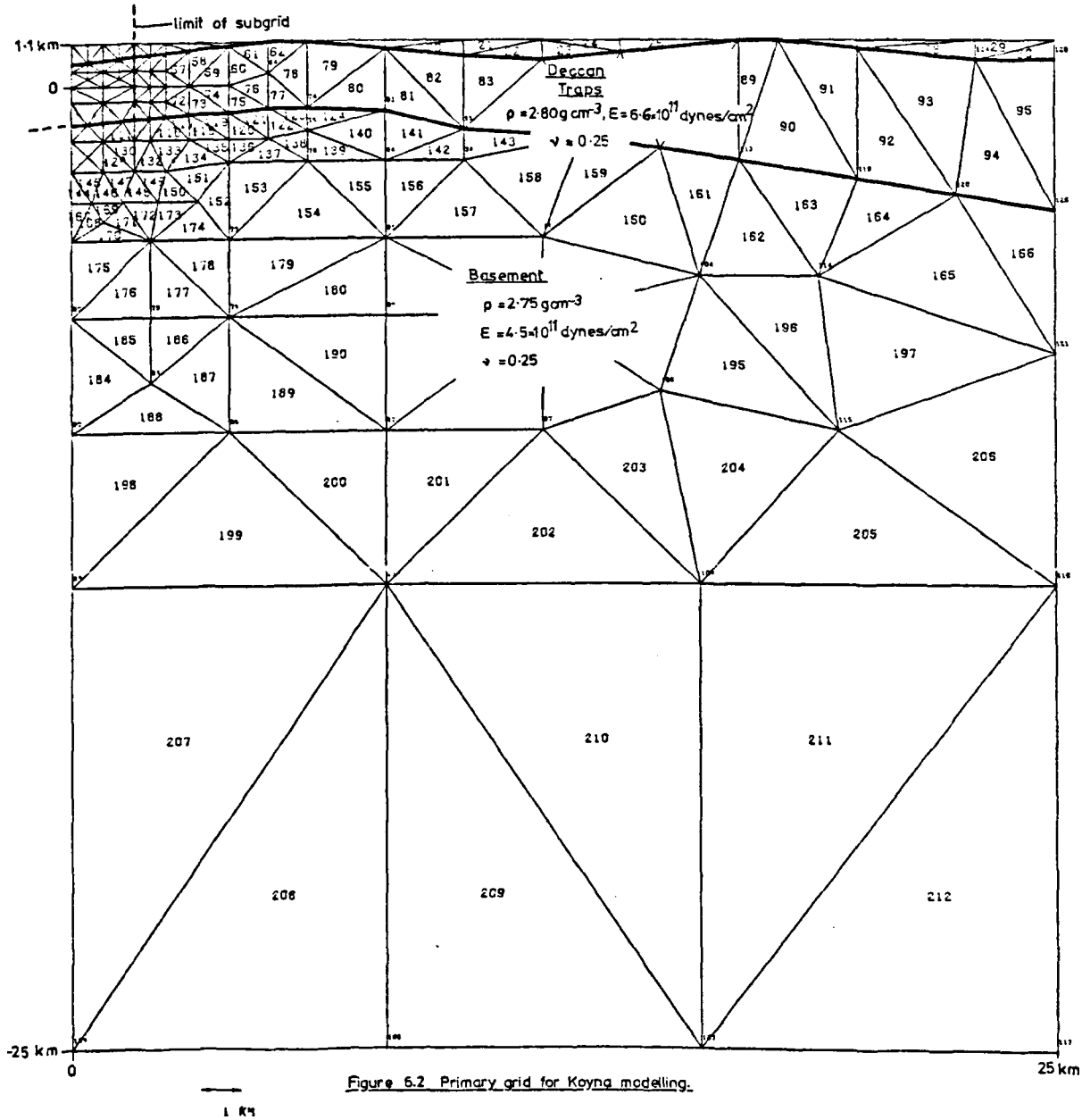

Figure 6.2 Primary grid for Koyna modelling.

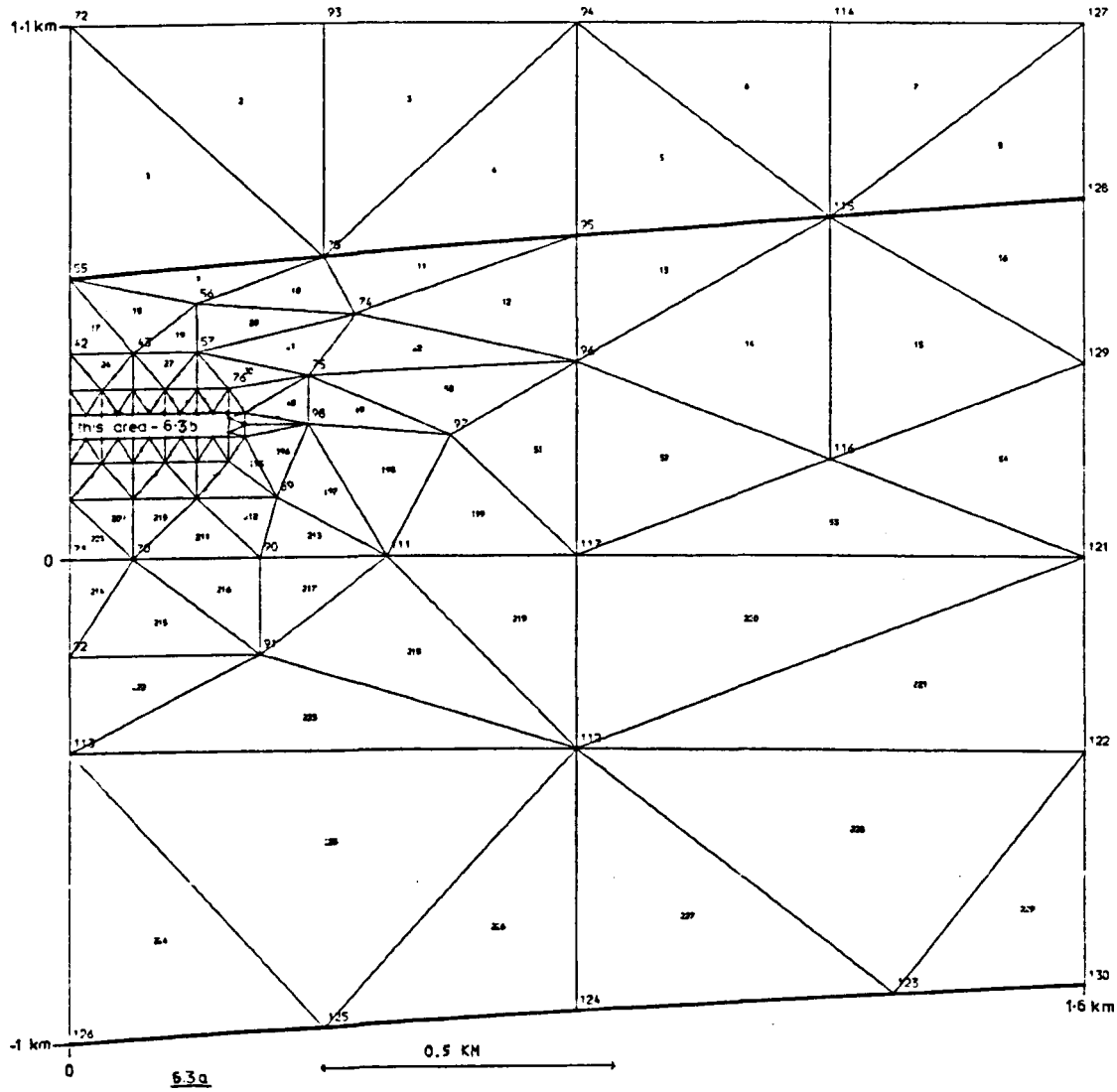

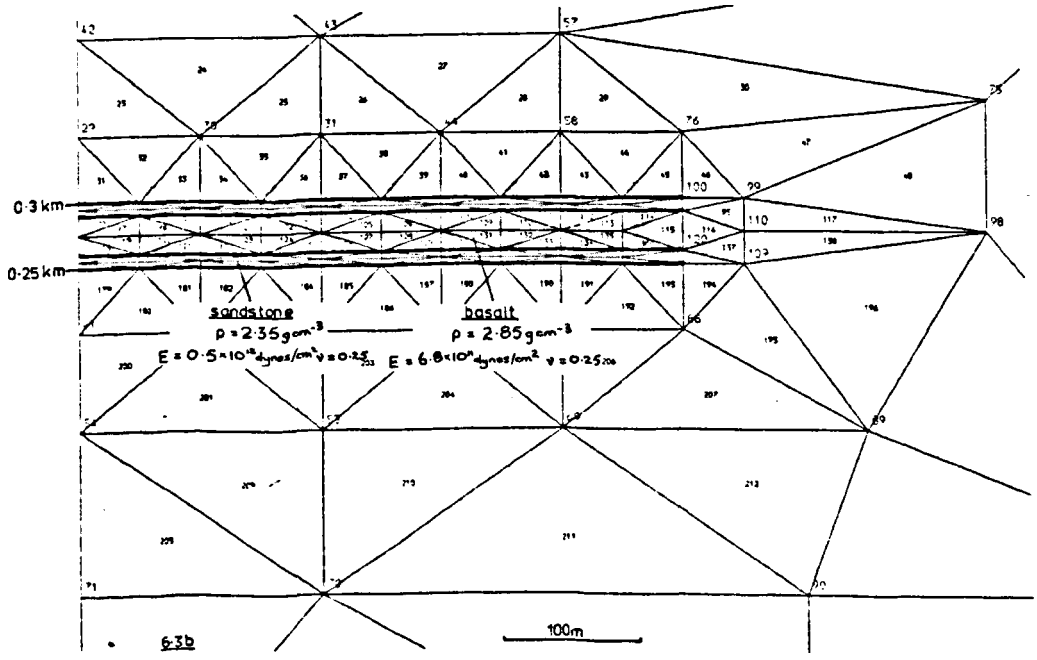

Figure 6.3 Subgrid for Koyna model.

stress must now be determined. When modelling field situations, it is very important to distinguish clearly between current and residual stresses. The distinction between these two types is illustrated by the fact that current stresses will contribute to the strain resulting from a rapid change in, say, topography, whereas residual stresses, being self-equilibrating, may not. However, residual stresses are self-equilibrating on various scales, and it may be that a residual stress will in fact contribute to, say, the stress field induced by a rapidly eroded valley, if it is active and self-equilibrating over a dimension similar to or greater than the valley dimensions. The present state of knowledge concerning residual stress systems in the field does not allow consideration of the larger residual stress domains, but it appears more likely that these will occur where tectonic structures formed by a palaeo-stress field are above a certain size (e.g. measureable in metres or kilometres). Otherwise it is probably a good assumption that residual stresses exist only on a granular scale, or within an order of magnitude of this. Thus no evidence exists to suggest that at Koyna the Traps contain residual stress systems acting over hundreds of metres or more, that could interact with the erosion of the Koyna valley.

The finite-element model therefore will have two clearly differentiated stress systems, which have to be considered separately. Currently-acting forces due to the present tectonic stress field must either be incorporated in the matrix solution process as initial stresses or applied at boundary nodes, since these are the forces that give rise to stress fieldsassociated with the topography. Residual stresses, from all the sources listed in Section 3.1, only have to be considered when discussing the eventuality of rock fracture (which is mostly due to microscopic stress systems), and possibly failure along pre-formed fractures (which is also concerned with larger scale stresses).

Firstly, the initial stress state arising from currently acting sources must be established. It can be taken that, within the Traps at least, the

vertical stresses are equal to the overburden; this means an average value of 490 bars at the base of the lavas in the model. Lack of knowledge concerning the existence of possible vertically acting stress sources at depth beneath Koyna means that the same assumption must be made about the older rocks beneath. Finite element solutions will in any case produce vertical stresses close to the weight of the overburden, at equilibrium, whatever the initial stress, so there is in fact no choice in the matter. Deviations due to shear stresses caused by mechanical irregularities can be to some extent incorporated if the initial vertical stress state is determined by an initial full density run (with no surface topography in the model). Unfortunately, when irregularities in grid dimension and mechanical properties occur, computation time limits the approach to a lithostatic state during the visco-elastic process, and a small, but sufficiently unrealistic, set of tensional horizontal deviatoric stresses still remain even after, say, 2000 iterations. It is better to determine the probable horizontal stresses by analytical means, after the initial run, taking into account knowledge of the current tectonic stress field.

The horizontal stresses in the lavas are likely to be rather greater than that predicted by elasticity theory, as a result of the neighbouring tectonic activity along the coast, but the lack of displacement along the fractures suggests no great magnitudes are reached. This may be partly due to thermal contraction since the formation of the lavas. Faulting that exists is strike-slip, so the maximum and minimum horizontal stresses will be greater and less than the vertical stress respectively. This will be so near the surface at least, assuming that the same tectonic regime is still in operation. The maximum principal stress is thus probably not much different to the vertical stress. The minimum principal stress must have been sufficiently low to create critical shear stress conditions in the not too remote geological past. The stress measurements mentioned in part (i) by no means contradict these assumptions. If the minimum horizontal

stress is taken to be one third that of the vertical then the horizontal stress anisotropy limit of 4:1 (see Chapter 3) restricts the maximum horizontal stress to 4/3 the vertical. If this latter ratio is reduced arbitrarily to 7/6, this creates the suspected relatively high shear stresses while keeping the maximum horizontal stress close to the vertical. The stresses so constructed are shown in Fig. 6.4. It must be borne in mind that these are highly conjectural.

The orientations of fractures in the region, and the dextral displacement along the West Coast Fault suggest that the magnitude of the tectonic stresses in the E-W plane of the model cross-section is closer to the minimum than to the maximum horizontal stress (see Fig. 6.1). This raises an important point concerning the optimum orientation of the model. If a below-average horizontal stress is in fact assumed for the plane in question, this will imply a normal faulting environment, and the action of the valley and reservoir stresses in conjunction with the maximum tectonic stress is not then considered by the finite-element simulation. If, on the other hand, the plane of maximum horizontal stress is chosen for the model, an incorrect thrust-faulting regime now appears to exist, and misleading topographic and water-induced stresses are calculated because the section is not perpendicular to the valley axis. It is perhaps better, if one plane is to be chosen only, to combine a large value for the horizontal stress with the perpendicular X-section, so that stress interactions are not underestimated.

In the underlying rocks the current tectonic stresses are likely to be much the same as in the Traps. The shear stresses resulting from the above assumptions match well with the figures for basement rocks presented in Section 3.1. These measurements are strictly only applicable down to 3 km, but it is assumed here that similar behaviour continues down to 10 km. Beyond this depth the onset of ductile behaviour will reverse the trend of increasing shear stress, and the principal stresses will begin to return

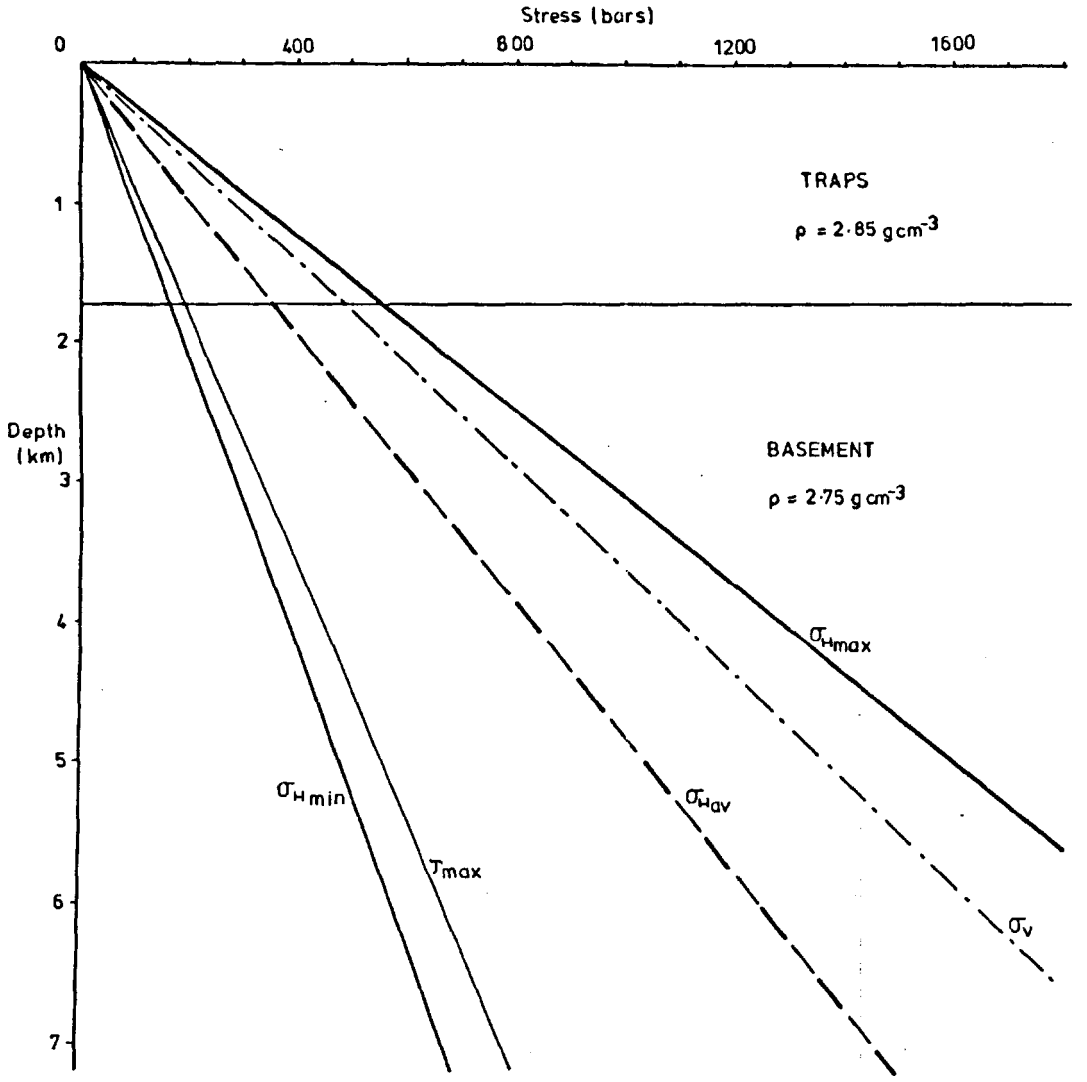

Figure 6.4 Conjectural stress behaviour beneath Koyna.

to a lithostatic state. The k ratio limit (Section 3.4) on average horizontal stress does not restrict either of the principal stresses in this situation. The conversion to normal faulting thus occurs at great depth, if at all.

(c) The Finite Element Strategy

Since the horizontal tectonic stresses are assumed not to be uniform with depth, it is not possible to apply them along the remote boundary, because of St. Venant's Principle (see Section 2.3). They must therefore be incorporated as initial stresses. The finite-element runs can be carried out either with full densities or density contrasts. Unfortunately, the use of density contrasts conflicts with the use of initial horizontal stress, due to boundary condition requirements, so full densities were used in the models. Fig. 6.5 shows the possible approaches to the final stress state, using all the stress sources discussed above. Fig. 6.6 shows how this model was computed using the two grids. It must be noted that if a double grid method is used with density contrast, the same density must be subtracted from both grids. Zero horizontal displacement boundary conditions were used at the remote boundary, since only very small perturbations to the grid would be occurring at these distances.

One further source of error in the modelling so far described, is the assumption that the valley stresses are calculable elastically as in Chapter 4. It is likely that at least part of this stress field has been reduced by a combination of creep effects, crack closure, and small-scale brittle reverse faulting. The situation thus becomes more akin to that of reservoir imposition upon a flat half-space (Fig. 4.12), but the use of a simple elastic approach does not solve the problem properly in this case. The best way is probably to run the model for several visco-elastic iterations, until a time equivalent to whatever amount of relaxation is thought appropriate.

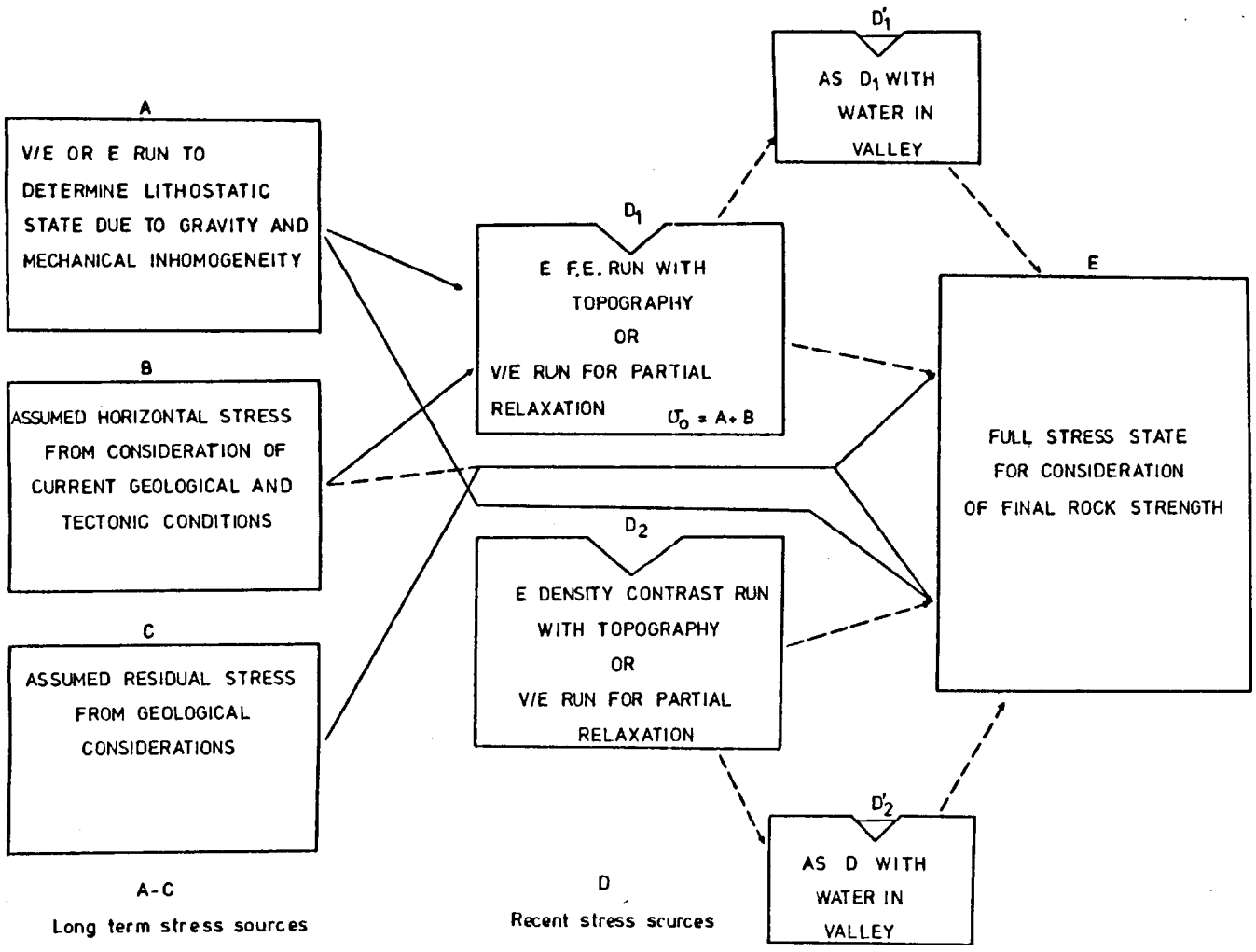

Figure 6.5 Finite element strategy

E = elastic , V/E = visco-elastic.

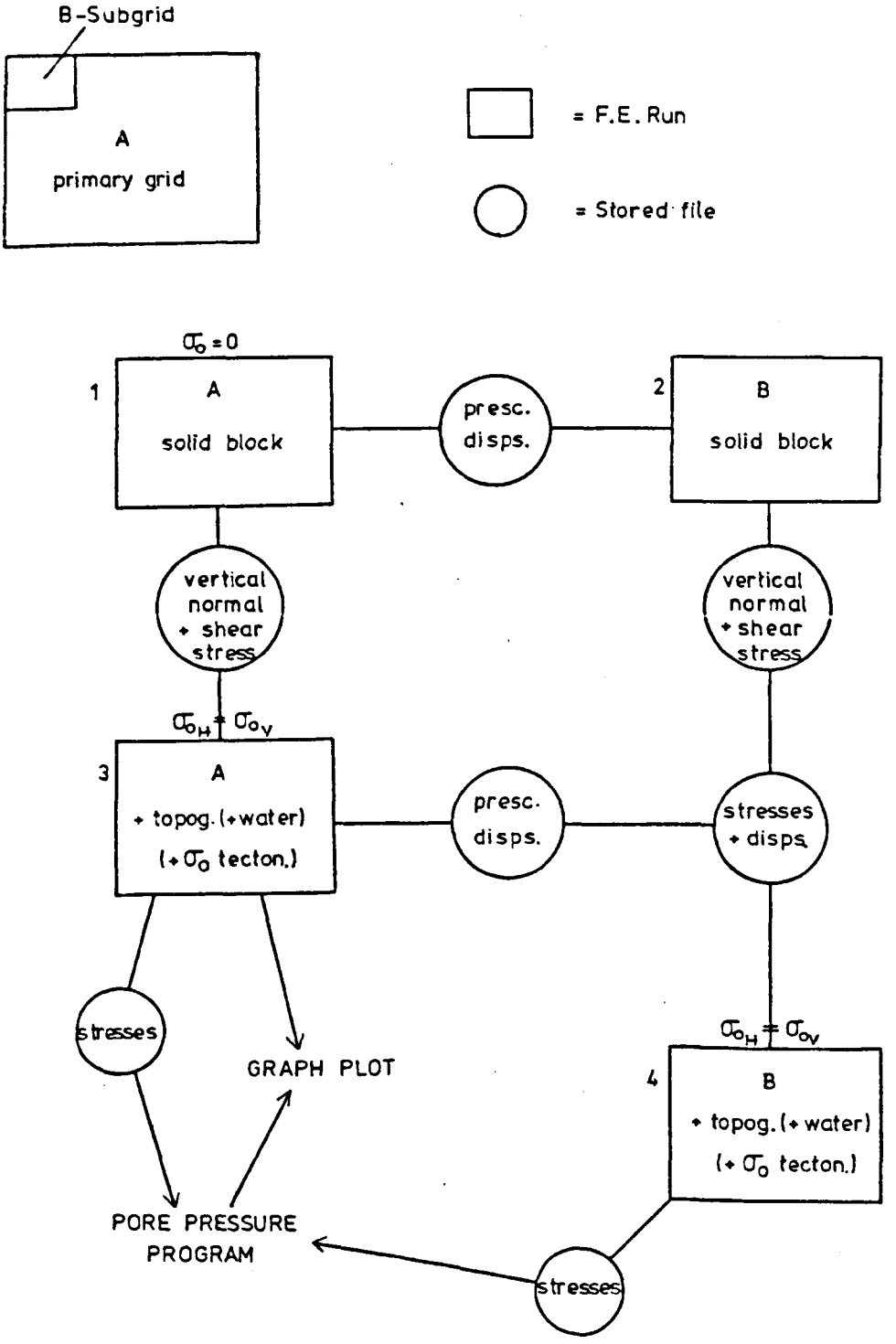

Figure 6.6 Practical double grid computation procedure.

(v) Total and Effective Stresses at Koyna

To examine the changes in stress induced by the reservoir loading at Koyna, a preliminary model was run with the water as the only body of non-zero density. The maximum shear stress generated in this way is 2.7 bars (Fig. 6.7), and the induced stress changes in the region of detailed modelling are very small indeed. Not only do the maximum shear stresses in this region only average about 1 bar, but the strength contrasts in the layering have resulted in only a small ($\sim$0.3 bar) shear stress difference. This part of the grid is only at a depth 300 m beneath the reservoir, which is hardly suitable for the triggering of an event of magnitude 6, but at greater depths the induced stresses are even less.

The elastic topographic shear stresses were found to be of the order of 45 bars, so the presence of the reservoir would have had little effect on the total stress field unless much relaxation had occurred. Fig. 6.8 shows the total and shear stresses resulting from the impounding of the reservoir. When the initial stress state shown in Fig. 6.4 is used, the stresses resulting from impounding are even less significant, and are shown in Fig. 6.9. A close up of the region of detail in the subgrid shows shear stresses of the order of 75 bars, almost all of which is due to the pre-existing tectonic stress(Fig. 6.10).

When the pore pressure program was applied to the final stress solutions, however, failure on faults was indicated by the Edmond-Murrell criterion (eqn. 2.4.21) within approximately 500 m of the reservoir after a time period of 20 days. The expansion of the pore pressure front away from a maximum constant pressure of 9.8 bars created by a reservoir 100 m deep is shown in Fig. 6.11. This failure region did not extend by a very large amount over the ensuing months, although noticeable increases in pore pressure were still occurring within the subgrid after a year. Thus this reduction in effective stress can be invoked to explain directly only some of the earlier, shallower seismicity at Koyna. The mechanism(s) producing the larger shocks need further investigation.

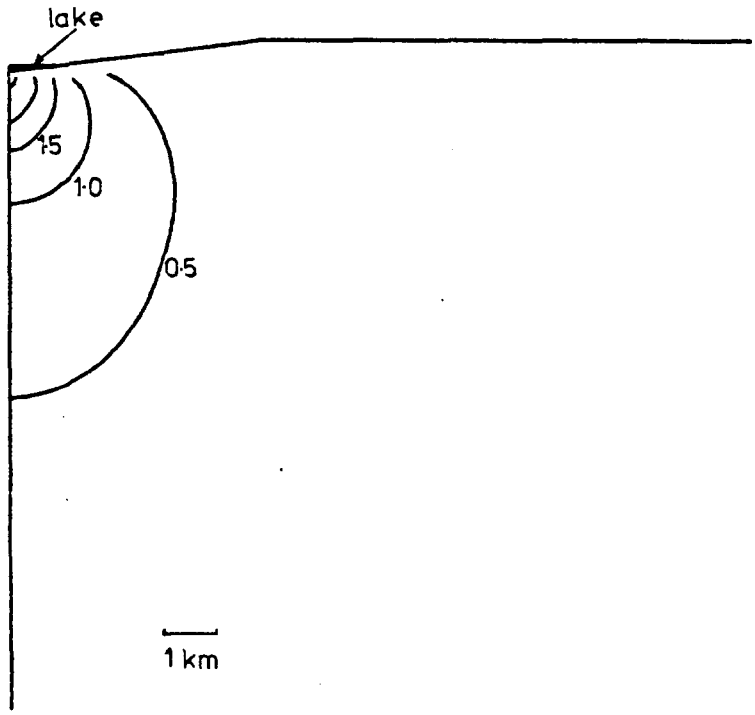

Figure 6.7 Maximum shear stresses due to water load alone at Koyna.(bars).

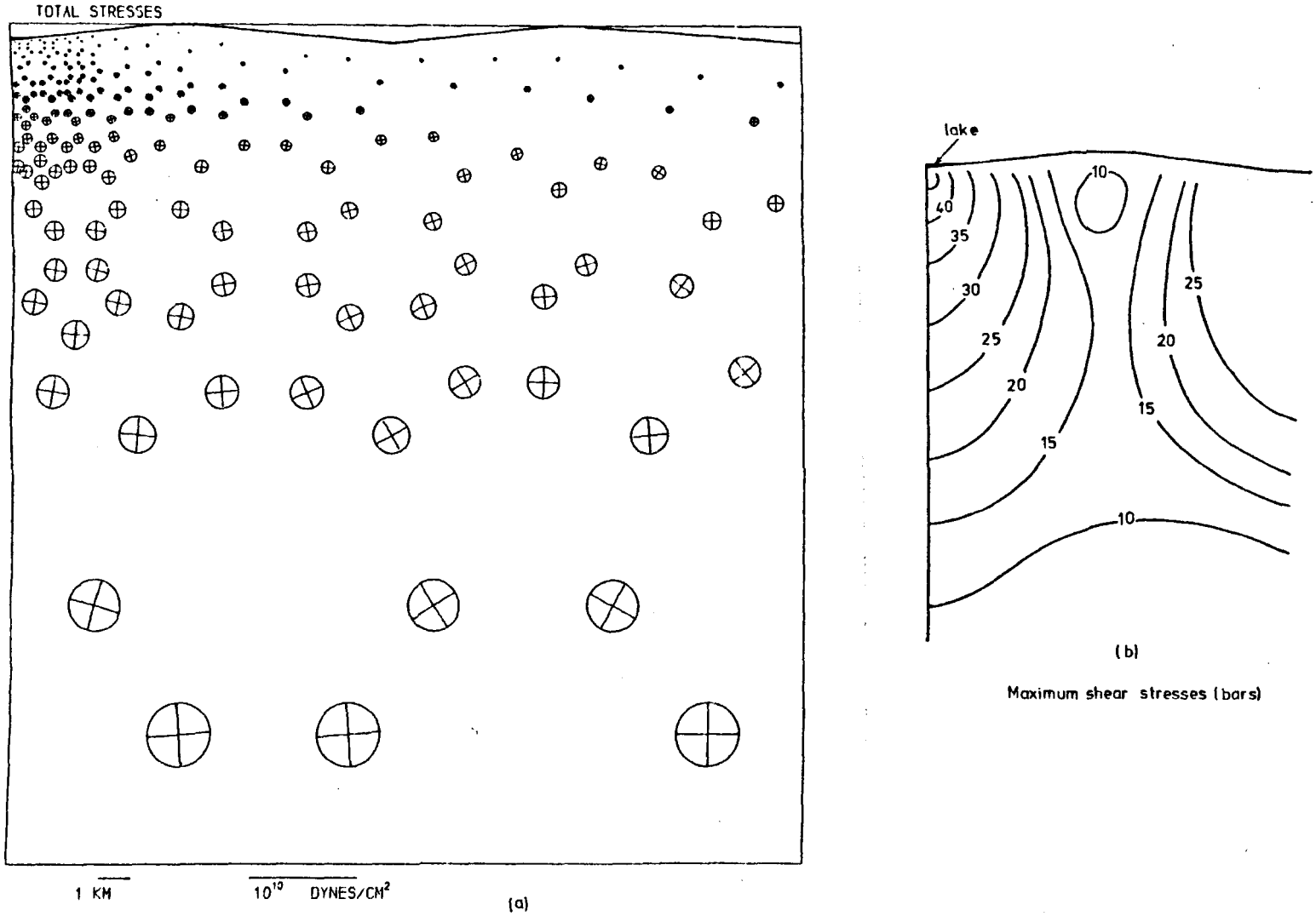

Figure 6.8 Topographic and water load stresses at Koyna.

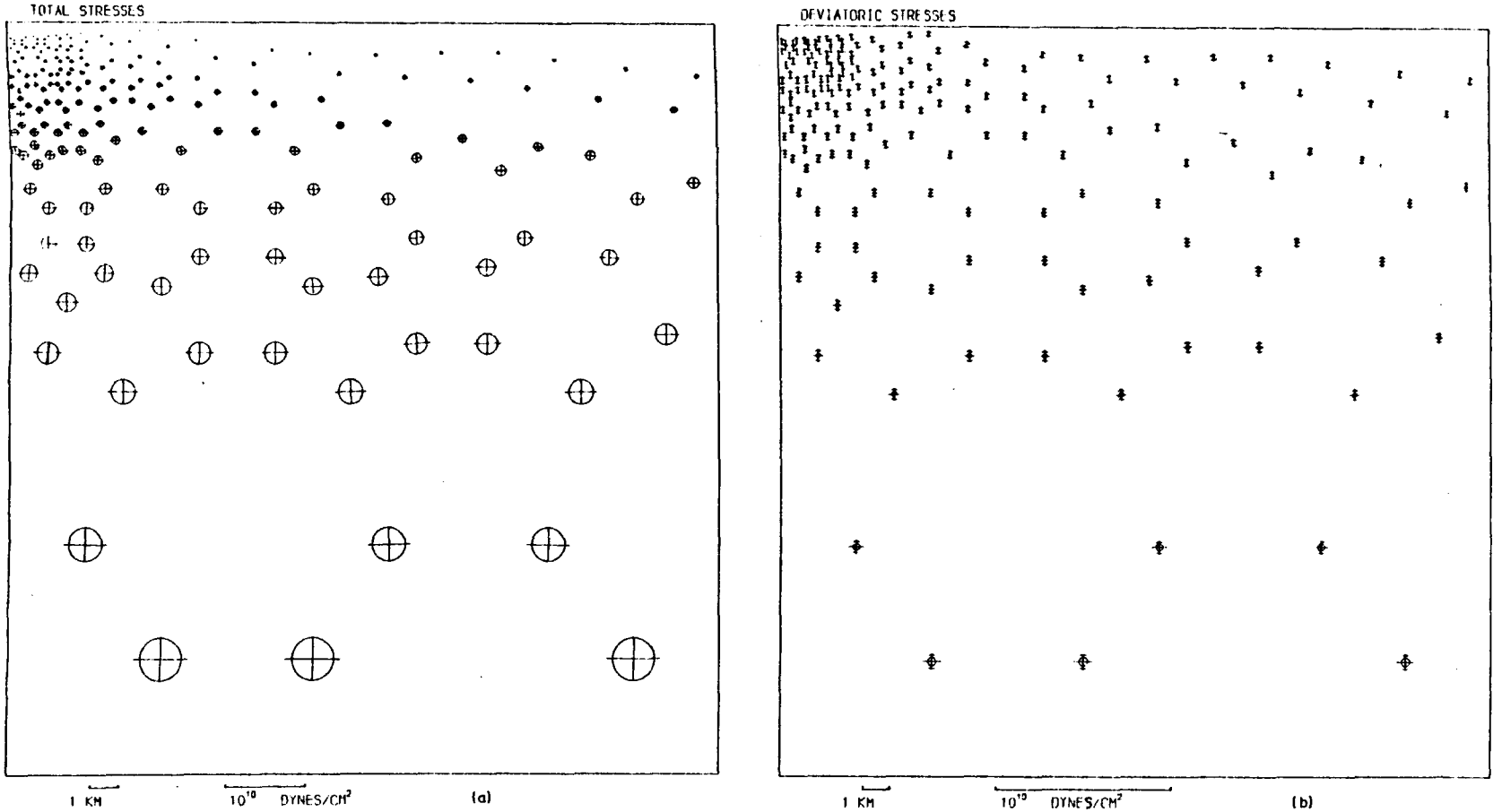

Figure 6.9 Stresses due to topography, water load and tectonic stress at Koyna.

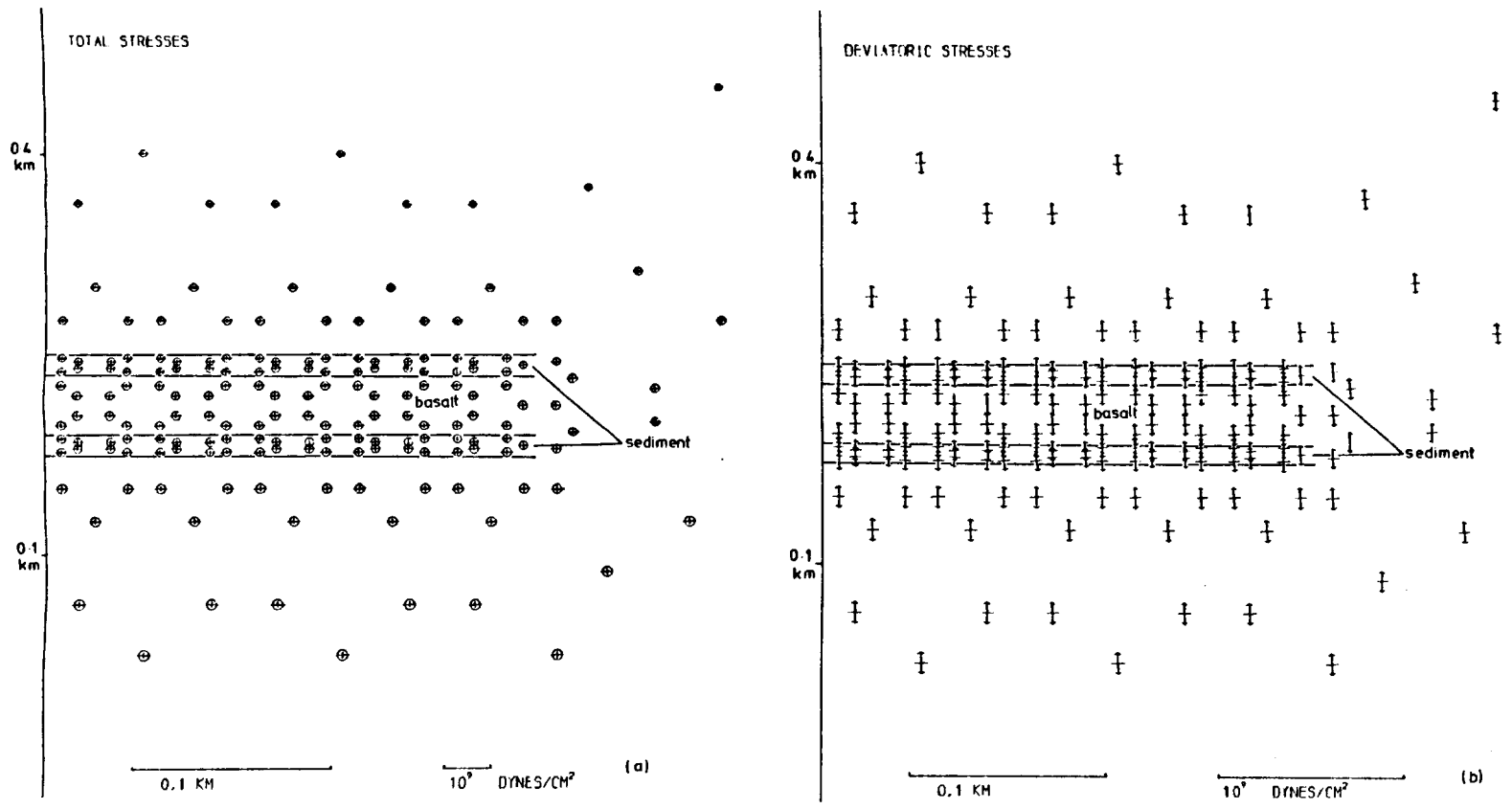

Figure 6.10 Stresses due to topography, water load and tectonic stress at Koyna

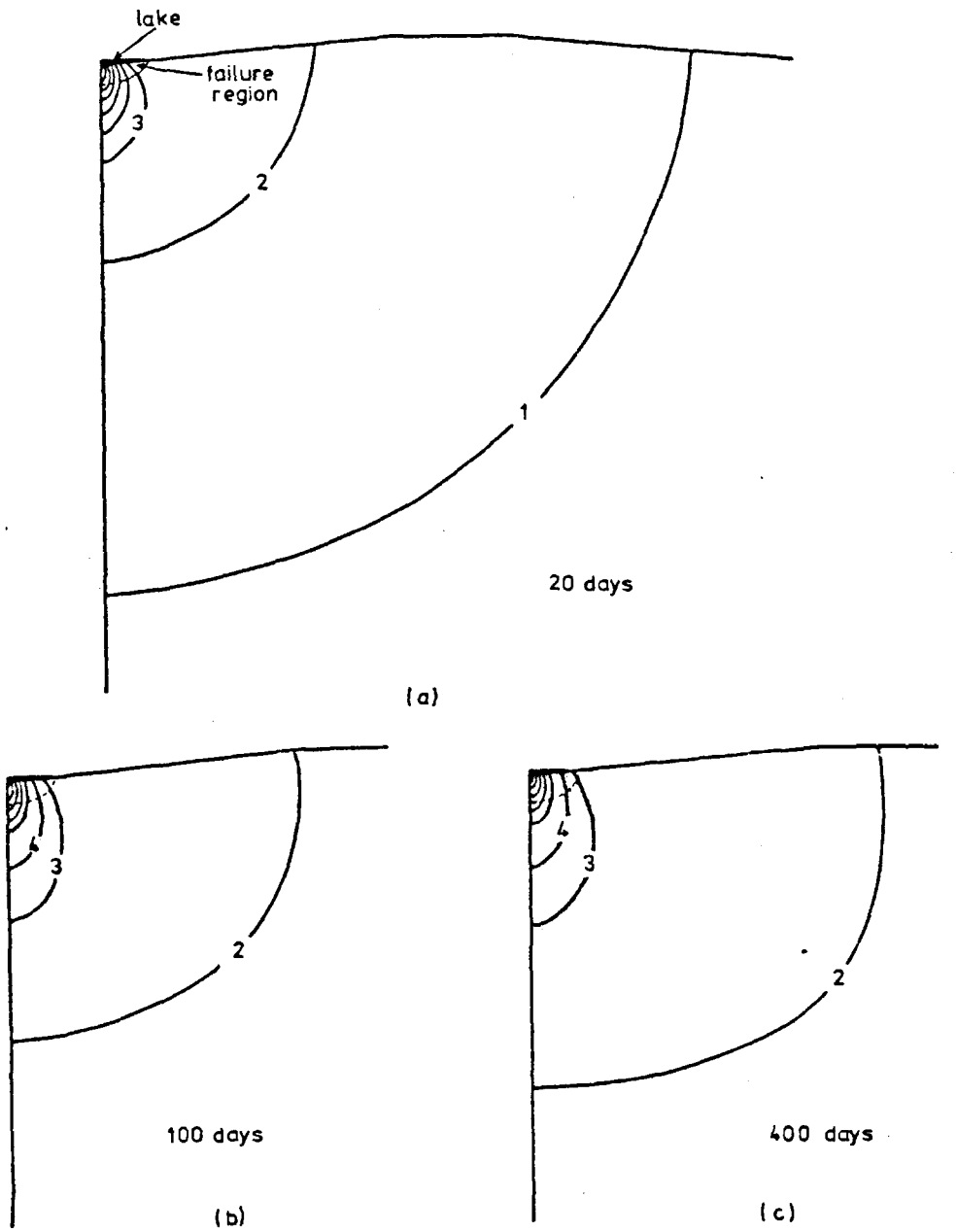

Figure 6.11 Theoretical pore pressure diffusion away from Koyna reservoir and resulting failure region.

The 'water only' models mentioned above were used to calculate the induced strain energy in the Koyna foundation. That for the primary grid cross-section was found to be 4.7×10^{18} ergs/cm. Multiplying this to obtain an estimate for the stored energy within the total strained volume beneath the reservoir, and using the relationship given by Richter (1958, p.366) between energy and earthquake magnitude:

$$\log E = 11.4 + 1.5M$$

it can be concluded that the maximum magnitude of earthquake which used only the induced strain energy is M = 8.9. However, assuming a typical seismic efficiency of only 0.1 - 1.0%, a magnitude of between 6.9 and 7.5 would be a more realistic estimate of the maximum possible, if all the stored energy were available to be released simultaneously.

(vi) Conclusions

The presence of alternating bands of sediments and hard basalts beneath Koyna reservoir does not appear to offer an explanation of the triggering mechanism for the induced seismicity. It is possible however that inappropriate mechanical constants have been assigned to the elements concerned, and that larger shear stresses were in fact produced. The reservoir load stresses are much smaller than those created by the erosion of the Koyna valley, and tend to act in opposition to them. Effective stresses resulting from the pore pressure increases beneath the lake have been shown to be rapidly brought to a failure state, but not at the focal depths ($\sim$1-15 km) associated with most of the Koyna seismicity, including the main shocks. The pattern of seismicity over the years 1963-66 does not show a constant correspondence with water level, although peaks of activity do occur (see Gupta and Rastogi, 1976, p.59). Over this time period the pore pressure may have reached significant values at hypocentral depths, and shear stress changes in the upper 4 km of 0.5 bar or more, caused by the annual filling of the reservoir could then have triggered the main shocks which occurred

in 1967. The first main shock, on September 13th, is believed to be a multiple event (Gupta and Rastogi, 1976) which originated at shallow depths and then propagated into the lower crust. It is thought that many of the deeper smaller shocks must also be the result of triggering by the directly-induced earthquakes whose foci lie within the region effected by the reservoir loading (Fig. 6.7).

The induced strain energy calculated in the previous section is sufficient to account for the two shocks of magnitudes greater than 5 and 6 which occurred in 1967, and also the other smaller tremors which had occurred since impounding. However, much of this energy was not only stored beneath the upper parts of the lake, but was also at relatively shallow depths. It was thus not available for release by most of the tremors (see Fig. 6.1). It can be concluded, particularly for the deeper shocks, that the original tectonic stress provided much of the energy. The energy release for the subsequent seismicity, which culminated in a shock of magnitude 5.1 in 1973, must also have been largely provided by tectonic stress, unless storage of the reservoir load strain energy as residual stress has occurred during the annual fluctuations of water level.

6.2 The Modelling of Other Reservoir Cases

The situation at Koyna reservoir was chosen for special study because of the relative thoroughness of the published data concerning the earthquakes there and their geological background. Despite this, there were grave difficulties in realistically representing the seismogenic processes that took place with the numerical models. When other cases of reservoir-induced seismicity are considered, the necessary assumptions and approximations become even greater. The modelling at Koyna effectively became a summary of the actual situation, with the detailed portion representing only a characteristic generalisation of an area of suspected critical geology. Similar approaches need to be used for other seismic reservoir

case histories: some aspects particular to each are discussed in this section. Firstly the situation at Lake Kariba is discussed in a fashion similar to that of the previous section, and then other reservoir cases are used to point out additional problems that may arise in attempts at practical modelling.

(i) Lake Kariba

Consideration of the results of the previous example, and of the coarse nature of the geological structures of the area (Fig. 6.12), shows that little is to be gained by a detailed attempt at modelling. The resulting stresses would differ to only a small degree from those obtained by extrapolation of the results of the theoretical examples in Chapter 4. Gough and Gough (1970a,b) have in fact already made an adequate analytical calculation of the stresses induced by the load of Lake Kariba assuming a homogeneous foundation, and so no attempt to use numerical modelling techniques has been made here.

(a) The Static Numerical Modelling

Lake Kariba differs from other seismic reservoirs by virtue of its large size. Although the lake has a conveniently elongated shape for the construction of a (N-S) plane-strain cross-section across the deepest part of the lake, the section would have to be well over 150 km wide for the application of zero displacement boundary conditions. This is not a great problem however, as the geological information available (e.g. Gupta and Rastogi, 1976) indicates structures on a similarly large scale, and it would not be necessary to resort to the use of a double grid to incorporate them, as it was with Koyna.

The geological structure of the area is essentially a series of sedimentary layers (the Karoo sequence) resting in a downwarped trough, faulted into the underlying Pre-Cambrian metamorphics (Fig. 6.12). Lake Kariba lies at the centre of this trough, the Middle Zambezi Basin, and the basement rocks directly underneath lie at a depth of around 1000 m. Gough and

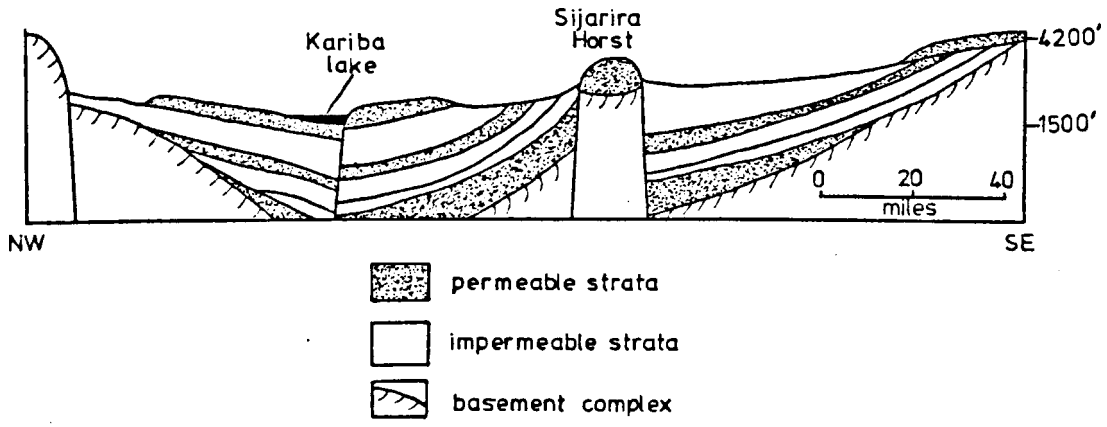

Figure 6.12 Section across the Middle Zambezi Basin showing major faulting and artesian structure (adapted from Gupta and Rastogi, 1976)

Gough (1970a) calculated that maximum shear stresses of over 2 bars reach depths of over 3 km beneath the deepest part of the lake, i.e. well beneath the Karoo rocks. It thus seems possible that a 'beam' mechanism might be applicable in this case also. The considerable thicknesses of these layers and their depths, however, means that great magnification of stresses is unlikely. Although the depth of the model would also have to be large - at least 40 km - Gough and Gough (Op.cit.) have shown that the induced stress in the mantle is insufficient for problems of isostacy to arise.

The direction and nature of tectonic activity in the region appear not to have changed greatly since Palaeozoic times. All the major faults and fractures in the region are oriented NE-SW, as is the Zambezi valley itself, and are the result of a normal faulting regime. This is confirmed by fault-plane solutions from local earthquakes. Thus the cross-section perpendicular to the strike of the valley conveniently contains the maximum horizontal shear stress, the maximum principal stress being vertical. A vertical displacement of 300 m occurs on the main Deka fault, although stresses there have not been great enough to produce mylonite or even much breccia. The minimum horizontal stress is therefore, by this reasoning, small, and considering the 'extensional' tectonics of the area, is probably close to the lower limit (see Fig. 3.5). The natural seismicity near the reservoir is, however, almost zero, although a tremor was felt near the SW end of the lake in 1956, and little active rifting occurred in the Middle Zambezi Trough throughout the Pleistocene. It is probable therefore that the minimum horizontal stress is not at an extremely low value, but at one which for most depths is not greatly different to the vertical stress. The latter is 250 bars/km for the sedimentary rocks of density 2.55 gcm^{-3}, and 270 bars/km for the underlying metamorphics of density 2.75 gcm^{-3}. The minimum horizontal stress might then be expected to increase at around 180 bars/km which would result in a maximum shear stress of about 100 bars at 3 km depth. The maximum horizontal stress must increase at an intermediate rate, and an

appropriate value for this would be 220 bars/km. The use of a plane-strain cross-section across the valley makes the value of this stress irrelevant however.

Residual stresses may well exist in the Karoo Series. These rocks, of up to Permian age, have since been subject to almost continual folding and faulting. The Sijarira Horst (Fig. 6.12) and surrounding related structures, for example, have been formed out of an original monoclinal flexure, and complicated residual stress patterns must have resulted. In the basement rocks, a constant foliation indicates the possible presence of large magnitude and large-scale residual stresses. As always though, these factors cannot be considered in the computation, and would have to be simply made allowance for qualitatively.

The sedimentary rocks of the Karoo Series are for the most part permeable, but to a varying degree. The normal faults allow additional movement of pore water, both upwards and downwards. The structure of the basin suggests the possible development of high water pressures at depth compared to overburden pressures (high ω, see Chapter 5) due to artesian mechanisms, and these might be incremented to critical values by the induced pressure field. The water table in the area is thought to be low, and hence locally pore pressures might be induced to rise by values significantly greater than the head created by the reservoir body.

(b) Relevance of the Model to the Induced Seismicity

Gough and Gough (1970b) have presented strong arguments that the seismicity occurring after impoundment in 1959 and until mid-1966, was a direct result of water loading, and hence predictable, ideally, by the finite-element model of load stresses using the information above. The epicentres of the main shock in 1963 ($M = 5.0$) and its foreshocks were indeed beneath the deepest part of the lake and thus fell in the plane of the model. It is unfortunate though that no focal depths were able to be determined, so that the foci cannot be related to the geology. This means it cannot be

determined which are the particular structures that a worthwhile numerical model would have had to simulate accurately in this case. The crudity of the model described above, although making use of most of the available data, will produce results little better than Gough and Gough's (1970a) homogeneous Boussinesq approach. The 'rift' valley in which the reservoir is placed is in fact extremely flat. The immediate south-east shore of the lake is a little steeper, but this, and other features within the valley, are more a result of tectonics than erosion. The pre-impounding topographic stress systems is thus complicated, and hardly estimable, but extrapolation from the theoretical models in Chapter 4 gives an approximate value of 30 bars for the maximum shear stress. It can thus be assumed that the small reservoir shear stresses mentioned above will act to counter these, even if a large part of the topographic stress has been relieved in some way. Thus if the assumption of purely elastic behaviour is made the load stresses will act as a stabilising influence, contrary to Gough and Gough's (1970a,b) assumptions, and pore pressure reduction of effective stress must be invoked to explain the associated seismicity. However, this is not in agreement with the correlation of seismicity with water level during the first few years of impoundment. It can thus be concluded that the valley stresses are significantly more complicated than those assumed above, either because of the topographic irregularities or non-elastic processes.

(ii) Further Cases

The two cases at Koyna and Kariba were characterised by the ease with which a relevant plane-strain cross-section could be made of the reservoir and underlying geology, and the fact that the induced seismicity occurred within this plane. Had this approach to modelling been applied to all seismic reservoirs before impounding, not only would several difficulties have been encountered, but the final solutions would not always have been relevant to the stresses actually involved in generating the tremors. Many reservoirs are not of a simple elongate shape. Many consist of two

(e.g. Marathon) or more (e.g. Kremasta) elongate arms. If these are relatively narrow and conveniently oriented with respect to each other, it may be possible to assume plane-strain. However, it is more likely that no suitable planes are available - cases such as Hsinfengkiang and Mangla are examples of this. Another reservoir shape which would cause difficulty in this respect is that approximating to a circle, e.g. Hendrik Verwoerd. Lake Mead would provide a particularly difficult problem in that although the induced seismicity occurs on faults closely associated with the roughly circular Boulder Basin, much of the induced stress beneath the Basin is that due to the nearby Virgin-Detrital Basin, subject to the same changes in water level, and which also has a distinctly non-linear shape.

Even if theoretically suitable planes can be chosen, there is no certainty that the stresses studied will be those responsible for seismicity. There are many examples where the seismicity did not occur in the 'best plane' for modelling, even if this plane coincides with the deepest water level. This is often true in cases where the seismicity occurs ten or more kilometres away from the dam, e.g. at Marathon, or Benmore. These cases could be investigated using the pore pressure program, but hydrological data is even less reliable than the geological. Although it would be sensible to attempt to include local faults and important geological inhomogeneities, this still does not improve the model greatly, since usually the seismicity appears unrelated to known geology, and the case of Oroville demonstrates how the eventual major seismic fault might only be discovered by the planar distribution of the induced events themselves.

Geological peculiarities, such as halite bodies, buried karst, or the local argillisation of fault planes are not only unpredictable in many cases, but may not be able to be rendered in numerical code in sufficient detail, particularly in the finite difference pore pressure model. Cases such as Kremasta, which contain complex three-dimensional structures, not only for the mechanical model, but for the hydrology as well, are almost

impossible to model, even crudely, simply because of the lack of computer space. Three-dimensional modelling would have to be applied in this case, and would certainly be beneficial to the representation of the other difficult reservoirs mentioned above. Computer storage prohibits this at present however.

(iii) Conclusions

It should not be thought, however, that numerical modelling techniques are totally inappropriate for studying case histories. There are cases where these would have been appropriate to the eventual seismogenic stresses, providing sufficient detail of the geology, particularly its structure in a vertical direction, was available. As well as Koyna and Kariba, these include Talbingo, Manic 3, Vaiont, Kurobe and Nurek, although the latter has a difficult 180° turn near the dam, and a complex geology.

CHAPTER 7

FINITE ELEMENT ANALYSIS APPLIED TO ASPECTS OF MINING-INDUCED SEISMICITY

7.1 Introduction

In this chapter finite-element modelling is used to investigate certain aspects of the mechanisms responsible for generating mining-induced seismicity, particularly that of the Trent Vale area of the N.Staffordshire coal field. A large amount of literature has been produced concerning mining-induced stress. Much of this introduction is derived from a summary by Al-Saigh (1981).

When an underground opening is constructed, the overlying rock mass is deprived of its natural support, and the original equilibrium is destroyed. Considerable redistribution of stress will therefore take place, and usually the rock will deform towards the opening: elastic bending accompanied by creep flowage and brittle fracturing result in its gradual closure. If the new stresses are not able to be dissipated non-violently, as is usually the case, and they become greater than the strength of the rock at the depth concerned, fracture and/or slippage will occur. Both fracture-generated and implosion-type mechanisms are likely to be produced by the stress-sources involved here, as has been observed in practice (Kusznir et al., 1980). If the fracture is very near to the working, rock bursts can occur, resulting in further severe distortion of the excavation, along with the separation of blocks of rock from the roof, face and walls.

Obviously the mode of mining is an important factor controlling the form of this newly-generated stress field. Two main groups of mining methods exist:

(a) partial extraction, where pillars are left behind, separating rooms, and

(b) longwall extraction, where the roof is allowed to cave in behind the working face.

(i) Stresses in Partial Extraction

This technique is characterised by the excavation being carried out so that the rock left behind remains, ideally, intact. However, in the pillars the vertical stresses may be up to four times the overburden stress (Wilson and Ashwin, 1972), with the stresses increasing outwards from the core until the yield point of the coal is attained 3 - 10 m from the edge. Past this high abutment pressure region, the stress drops considerably in the outer sheath containing the weakened, fractured coal, and eventually falls well below the overburden stress (Fig. 7.1). The depth of this weakened zone can be found directly by drilling, or seismo-acoustically by measuring amplitudes (Petrosyants and Gorbachenko, 1969). In the core the rock remains elastic, and may in fact be strengthened by the increased load.

Wilson and Ashwin (op.cit.) in a study of the effects of pillar size, gave the distance, x, of the peak abutment pressure from the ribside as:

$$x = 0.0049\ hH \quad \text{(metres)} \qquad (7.1.1)$$

where h is the height of the adjacent roadway, and H the depth beneath the surface, which can be up to 1500 m or more in practice. Thus if the pillar width is reduced to less than 2x it will collapse. Differing shapes of pillar will of course have differing safety widths. By equating formulae for the load imposed and the strength of a long pillar surrounded by a 10 foot high roadway, Wilson and Ashwin (1972) arrived at the industrially accepted minimum width of 0.12H. Local mining conditions must be taken into consideration though, and both creep processes and undermining of the seam can promote eventual failure. When mining below an already worked seam, it is usual practice to avoid placing gate roadways beneath pillars, as it is found that the high stresses they transmit lead to high convergence and deterioration of the strata.

(ii) Stresses in Longwall Mining

This method accounts for at least 80% of British extraction. The

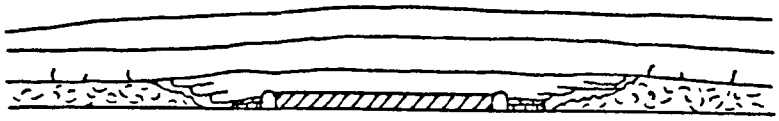

(a) Cross-Section

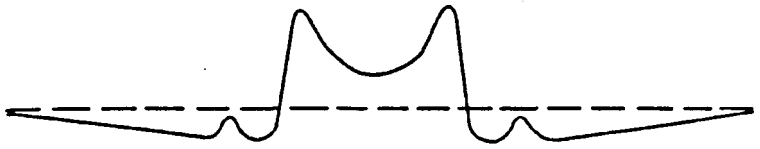

(b) Probable Stress Distribution

Figure 7.1 Pillar Stresses (after Wilson and Ashin, 1972)

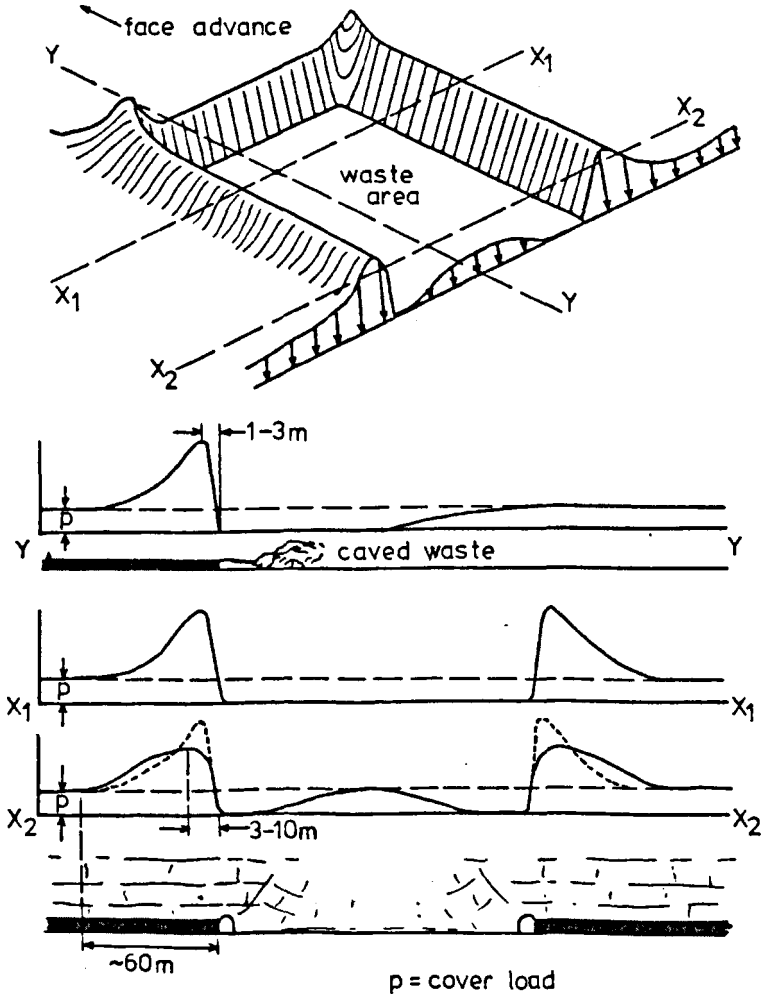

Figure 7.2 Stresses in longwall mining
(after Whittaker, 1974)

longwall face is commonly between 50 m and 300 m long, and the panel stretches back between 300 m and 1000 m maximum, most of which is allowed to cave in. Abutment zones are found just as in partial extraction, with especially high concentrations at the corners (Fig. 7.2, Whittaker, 1974). Some of the cover load is taken up again by the waste zone behind the face as the roof closes in on the caved-in goaf. As the face moves forward, so does the stress field, except that there is a certain time lag while the waste is attracting stresses from the abutments during the closure of the roof and floor.

Additional stresses can be caused by the presence of particular geological conditions, for example, a strong sandstone roof, which does not break down until a large area of coal has been extracted. This sort of roof will act as a cantilever, bending in the centre and applying upward forces ahead of the face. Whittaker and Pye (1975) also suggested some control of the abutment stress pattern by geological conditions. Where the coal seam is weak and friable, and is contained in strong sandstones, as in the Ruhr coalfield, the abutment pressure is relatively low, and occurs between 5 m and 10 m in front of the face. In conditions more typical of British mining, where the coal is relatively strong compared to the mudstone roof and seatearth, the abutment pressure is greater, and is reached much closer to the face, within 1 - 3 m. Boiko (1966) showed how the position of maximum stress can vary with respect to the face, in the Donbass mines in Russia. He also discovered that the seismicity there is much higher when this position is closer (1 - 2 m as opposed to 3 - 6 m), and the stress maximum is also more marked. A way to combat dangerous stress concentrations ahead of the face is to drill destressing boreholes into it. Baule and Rao (1979) drilled 25 m into the face and examined the stress by means of P-wave velocity. They found the velocity rose 5% during stress accumulation, and dropped 10% after destressing.

In a way similar to the partial extraction method, it is usual to position roadways beneath the destressed goaf area to avoid large stress

interactions with any superposed or underlying previously-worked seams. Kusznir et al. (1980) present a clear example of the seismicity which can result from neglecting to do this. The size of the excavations and the interaction between neighbouring excavations or rooms has thus been seen in practice to play an important role in the formation of the critically stressed areas by mining activity.

(iii) Failure of the Mining Medium

The types of seismogenic failure produced by failure in mining areas are of several different forms, of which any combination may occur in a particular region. In general, however, the rate of energy release, $\dot{E}$, can be calculated as a function of the overburden pressure, p, and the half-length of the span of the excavation, s, using the relation:

$$\dot{E} = 4p^2s^2/3G \quad \text{(Cook et al., 1966)} \qquad (7.1.2)$$

where G is the rigidity modulus. Cook et al. also showed that there exists a critical span below which no rockbursts occur, and that this span decreases with increasing depth. In actual mining situations this size is almost invariably exceeded. Also, as the span enlarges, complete closure will occur at the centre of the slope, levelling off the energy release to a constant value.

The seismic sources can usually be classified as one of the following:

(a) The large reduction in horizontal stress in the coal ahead of the face, and the concomitant increases in vertical stress and strain there, lead to the development of high shear stresses. Fractures parallel to and heading towards the face (Shepherd, 1973) may form in these abutments, especially if insufficient time is left for the rock to deform non-violently before further excavation is carried out.

(b) The sandstone cantilever mechanism described in the preceding section may also result in failure. When this occurs there will be a sudden transfer of the load to the face regions, resulting in almost immediate

secondary bumping. There may, depending on the position of the fracture, also be a sudden reversal of the upward forces ahead of the face, which will also then contribute to the sudden stress change there (Sinclair, 1936).

(c) The present working often takes place within the stress field induced by previous workings. Interaction between the two often promotes failure in the highly-stressed pillars of the older excavations, either above or below the present level (e.g. Kusznir et al., 1980).

(d) The presence of pre-formed fault or joint planes in the vicinity of the present working can allow the seismic release of some of the induced stresses (Davison, 1924). Any natural pre-existing stresses may also be partly relieved along these planes of weakness, by the triggering effect of the mining stresses.

(e) Other seismic events, not related to the present mining activity, probably result from the collapse of old pillars or faces (e.g. Gane, 1939). This comes about through the action of long-term anelastic processes which have eventually come to produce a critical stress state resulting in brittle failure.

7.2 Finite Element Applications

(i) Introduction

Analytical studies and solutions abound for the stress fields around geometrically simple underground openings (e.g. Savin, 1961). Almost always though, they make the same assumption, along with many elastic finite-element solutions (e.g. Barla, 1972a), that gravity is 'switched on' instantaneously for both the rock mass and the opening. Photoelastic methods (e.g. Barla and Boshkov, 1969) and elastic-plastic finite-element approaches (Reyes and Deere, 1966) are equally inappropriate in this situation. However, these studies do provide useful indications of general behaviour. Barla (op.cit.) investigated the interaction of an opening with a traction-free surface, and demonstrated how an increase in ellipticity can

create large solid-rock abutment minimum stress even before stress-relieving fracture occurs. He also found that lithostatic stresses are attained, in a horizontal direction away from the opening, at an approximate distance of four times the radius of a (circular) hole. Barla (1972b) also did some preliminary studies on the effects of layering in the medium around an underground opening. He found that situating the opening in a layer harder than the surrounding rock increases the rib stresses greatly, and in the opposite case there is a relief of stress from around the opening, into the harder layers.

Finite element has also been used to examine the detailed stress patterns immediately surrounding a working excavation. Kidibinski and Babcock (1973) produced a detailed elastic analysis of a longwall mine (Fig. 7.3) including the effects of goaf and prop support, and obtained agreement with the following field observations: high abutment pressure, broken zone in coal ahead of the face, tensile stress in fractured roof causing rock to fall into the goaf, and vertical fractures in the roof over the face. An interesting use of effective (much lower) Young's Moduli for the coal was involved in this study. The values were based on direct measurements by Borecki and Kidibinski (1970), and were then adjusted so that the finite-element solution gave displacements compatible with field observations.

(ii) The Nature of the Modelling

In this chapter finite element has mainly been used to examine the results of the interaction between adjacent workings, particularly to examine the possible causes of failure described in parts (iii)(c) and (d) of the preceding section. This analysis requires a model of slightly smaller scale than that used by Kidibinski and Babcock (1973), and hence the exact nature of high stress concentrations such as those at the abutments will not be adequately represented by use of the necessarily coarser grid. The seismicity resulting from the interaction between longwall excavations in the N.Staffordshire coal field has been studied by Kusznir et al. (1980),

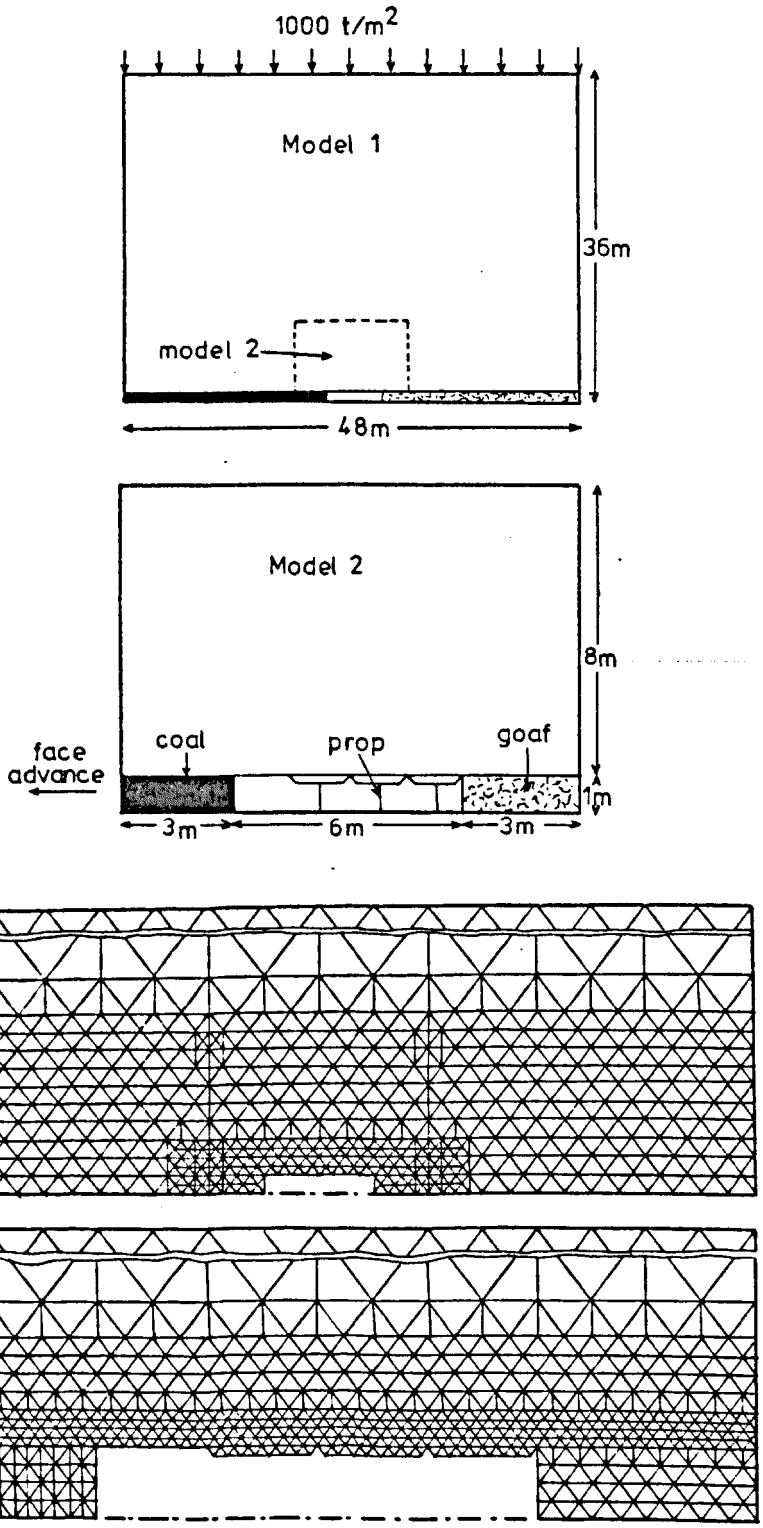

Figure 7.3 Finite element representation of a longwall panel (after Kidibinski and Babcock (1971)

who noted a marked increase in tremor frequency when present workings passed over or beneath pillars left from previous excavations (Fig. 7.4). The models used in this chapter have been designed to investigate the N. Staffordshire situation, and thus have a depth of close to 1000 m. All models have been given a Young's Modulus of 10^{10} dynes/cm^2 and a Poisson's Ratio of 0.35, which represent typical values used in mining engineering.

Unfortunately the mining medium does not lend itself readily to a straightforward elastic treatment, although Ryder and Officer (1964) managed to simulate displacements measured during mining in this way. The problems are due mainly to the fractured nature of much of the rock, but there are other factors as well, which are discussed below. The nature of the failure is most often not governed by large-scale stress systems, but is dependent on localised stresses resulting from geology, fracture patterns, and the previous failure history. It is thus unrealistic to simply apply failure criteria to stresses which are averaged over the area of an element in the mining region. Creep processes are also common, even over the short life-spans of a typical excavation. Vertical closure of the mine is a common occurrence, and is in fact encouraged during longwall mining. This, combined with the fracture processes, results in the relief of much of the stress field which would otherwise be expected around an underground opening. The finite-element method used here does not attempt to compensate for these effects, and thus the solutions will represent a maximum value for the induced stresses. It is believed that the unknown variables which need to be assigned values when compensating for closure and fracture mean that the resulting solutions would not be significant improvements on those shown here. Thus, although stress magnitudes have been used in the diagrams and descriptions, these are mainly for purposes of comparison, and the results should be treated principally as being qualitative.

A further difficulty in the modelling of longwall mining is the assumption of plane-strain conditions. The stresses ahead of the face were

those associated with most of the seismicity in Trent Vale,and yet when the mine has reached the seismically critical length it is usually longer than it is wide, rendering invalid an assumption of plane-strain on a section along the working. Unfortunately there is no completely satisfactory solution to this problem, unless a three-dimensional analysis is used. Models of the stresses associated with the side abutments of the excavations can however be assumed to be in plane-strain if the mining has been carried out for a sufficient time. Most of the models of longwall panels presented in the following sections have a length of 200 m, corresponding to a common width for longwall excavations, particularly in N.Staffordshire. This model, however, may also be taken to represent qualitatively a lengthwise section through the mine if the unsuitability of the plane-strain assumption is borne in mind.

The following sections consider the effects of a single mine, the lateral approach of two mines, and the effects of over- and under-mining previous workings and pillars. Initial tectonic stresses will also be considered, although this is not considered applicable to the N.Staffordshire stress fields.

It is noted here that the mechanical situation in modelling mining-induced stresses is fundamentally different to that when dealing with reservoir stresses. Mining stress fields result primarily from the contrasts in strength (i.e. Young's Moduli) that exist between the rock and the artificial void. The buoyancy effects are relatively small, but will provide some vertical assymmetry to the situations, as will the presence of the traction-free surface above.

7.3 Mining-Induced Seismicity in N.Staffordshire

A case history of the seismicity associated with mining in the Trent Vale/Hanford area of the N.Staffordshire coalfield has been described by Kusznir et al. (1980). The seismicity occurred in 1975/76 and was directly

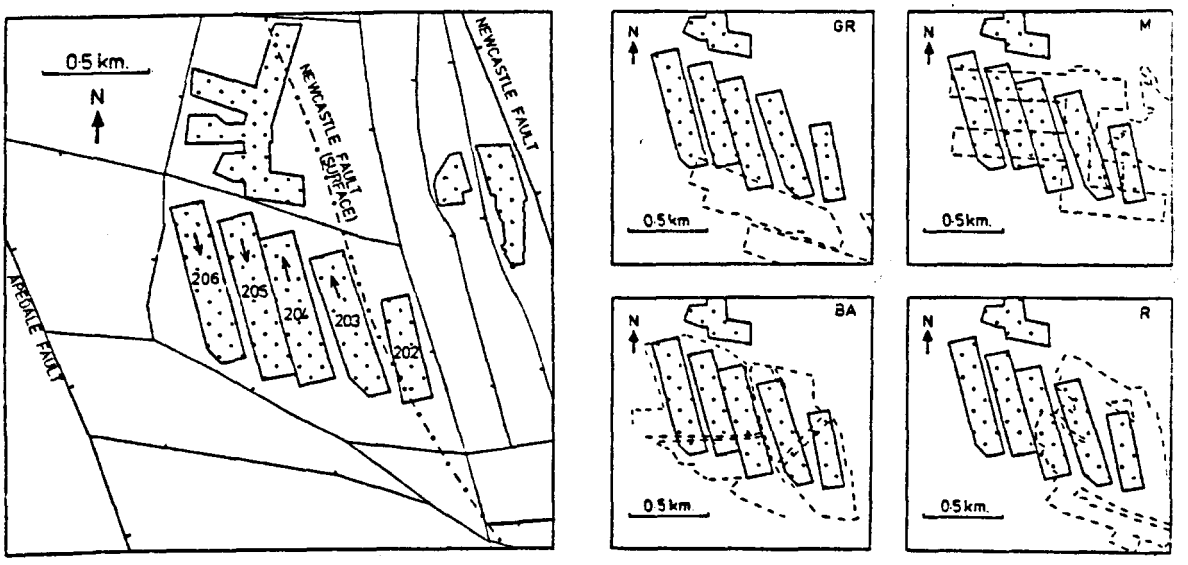

(a)

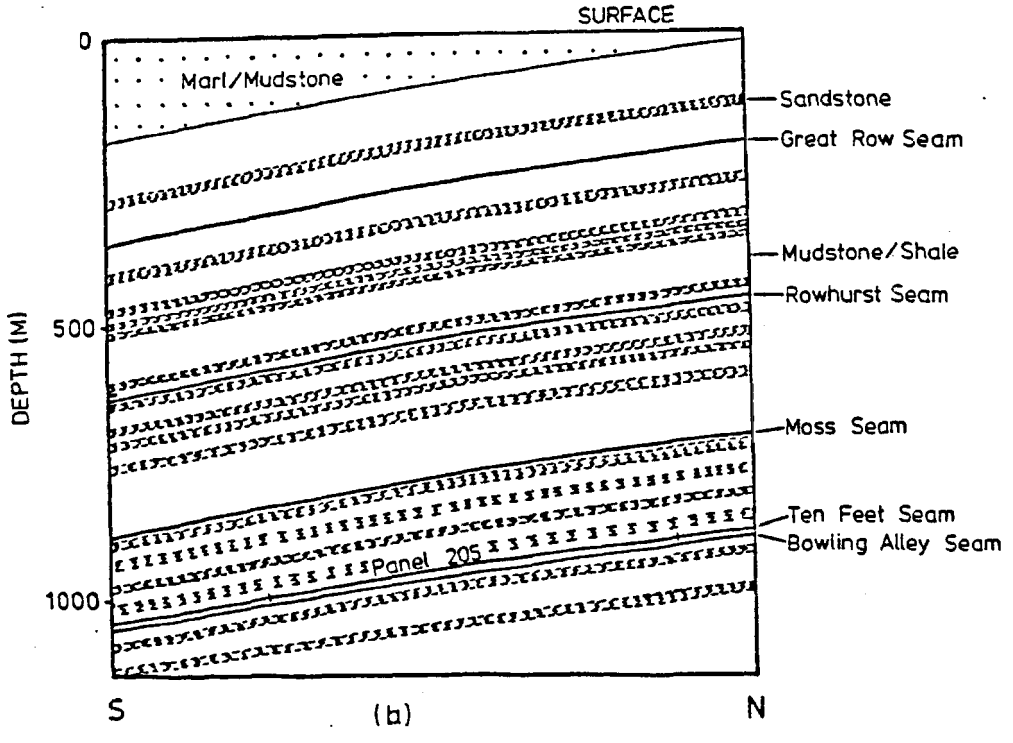

(b)

Figure 7.4a Plan of Ten Feet seam panels, and 7.4b geological section beneath Trent Vale, N Staffs. (after Kusznir et al., 1980)

a result of the contemporary working in the Ten Feet seam, which used longwall extraction with total caving. A geological section and a plan of the workings is shown in Fig. 7.4. The panels are 150 m - 200 m wide, and numbers 204, 205 and 206 were being mined when the bulk of the tremors occurred. As can be seen, this work involved passing above pillars in the Bowling Alley seam, which is only 15 m from the Ten Feet seam, and below pillars in the overlying Moss seam which is at a distance of 170 m. The two main pillars in the Bowling Alley seam are 25 m and 40 m wide, whilst the main pillar in the Moss seam is 200 m wide.

The following relationships between the mining and the seismicity have been established:

1. The tremors were not associated with any of the major faults in the area.
2. The tremor hypocentres lay adjacent to, and moved in unison with the face.
3. The large magnitude events occurred where the Ten Feet seam passed under or above pillars of adjacent previous workings.
4. These larger events possessed a shear-source mechanism and were situated in the pillars of the previous workings.
5. The smaller events, lying usually within 150 m height of the level of the active panel, have a collapse source mechanism.

The models presented in the following sections were set up particularly to gain further insight into mechanisms '3', '4' and '5' above, but information was also obtained concerning mechanism '1', which is a factor more relevant to other case histories, e.g. in Utah (Smith et al., 1974).

7.4 The Single Mine

(i) Excavation Size and the Extent of Stressed Rock

In order to assess the results obtained from models of two or more excavations, some models of a single mine were first made. Approximate

estimates for the magnitudes of the maximum induced stresses, the behaviour of the stresses around the mine, and the extent of their effect are obtained, and can be compared with the later results. These single mines were assigned a depth of 1050 m, which is that of the Ten Feet seam in the Trent Vale case history (Fig. 7.4). The slight slope of the seam has been ignored. All mines have been modelled with a height of 10 m - this is unrealistically large, but was imposed by the necessity of reducing the aspect ratios in the computer-drawn grid to reasonable values. The mine was simulated in the same way as the valley in Chapter 4, by using elements of zero density and weak mechanical properties. Use was made of the symmetry of the situation by dividing the model vertically down the centre with a zero horizontal displacement boundary. The fact that all the models in this and the following sections are mechanically homogeneous, meant that it was a straightforward matter to calculate the lithostatic stress state before running the elastic model of the mine(s).

Three models have been used in this section, with differing lengths. Fig. 7.5 shows a mine of length 100 m. The nature of the resulting stress field is not very well defined in this case because of the coarseness of the grid compared to the extent of the field. However, it can be seen that behind the side abutment large normal stresses have developed, particularly the vertical, which reaches well above 500 bars. Shear stresses all around the face are of the order of 100 bars, and are associated with low normal stresses perpendicular to the mine. Contours of shear stress were plotted for all the examples in this Chapter. Although they helped provide useful information concerning maximum values, and an approximation to the shape and areal extent of the stress field, the effects of the lack of grid resolution meant that most were not of sufficient quality to be included here. The 25 bar shear stress contour in this case, extended vertically to a distance just greater than the lateral dimension of the mine (100 m), although horizontally there is a large shear stress gradient, and beyond 50 m the shear stresses become much less than 25 bars.

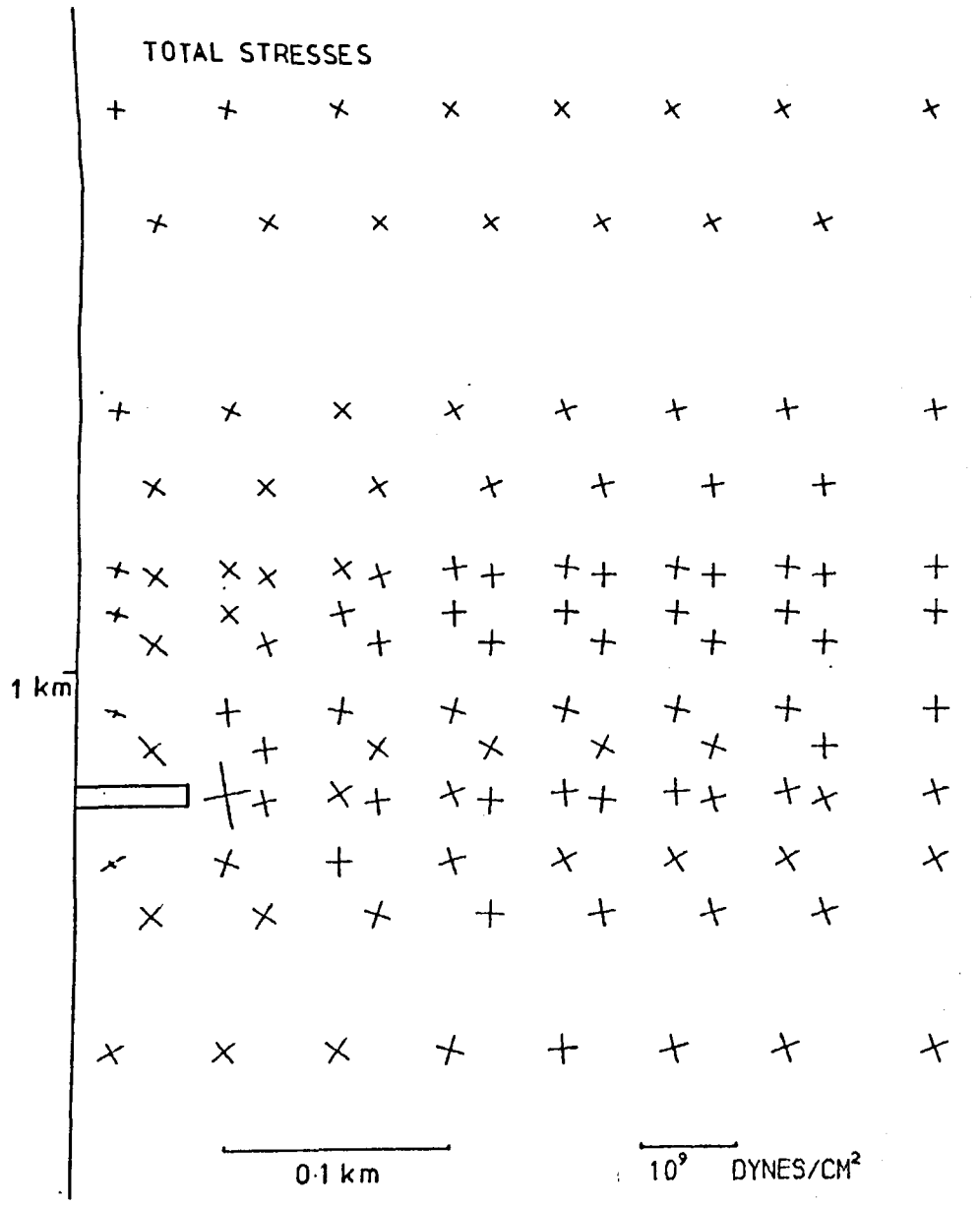

Figure 7.5 Stresses induced by a mine 100m in length.

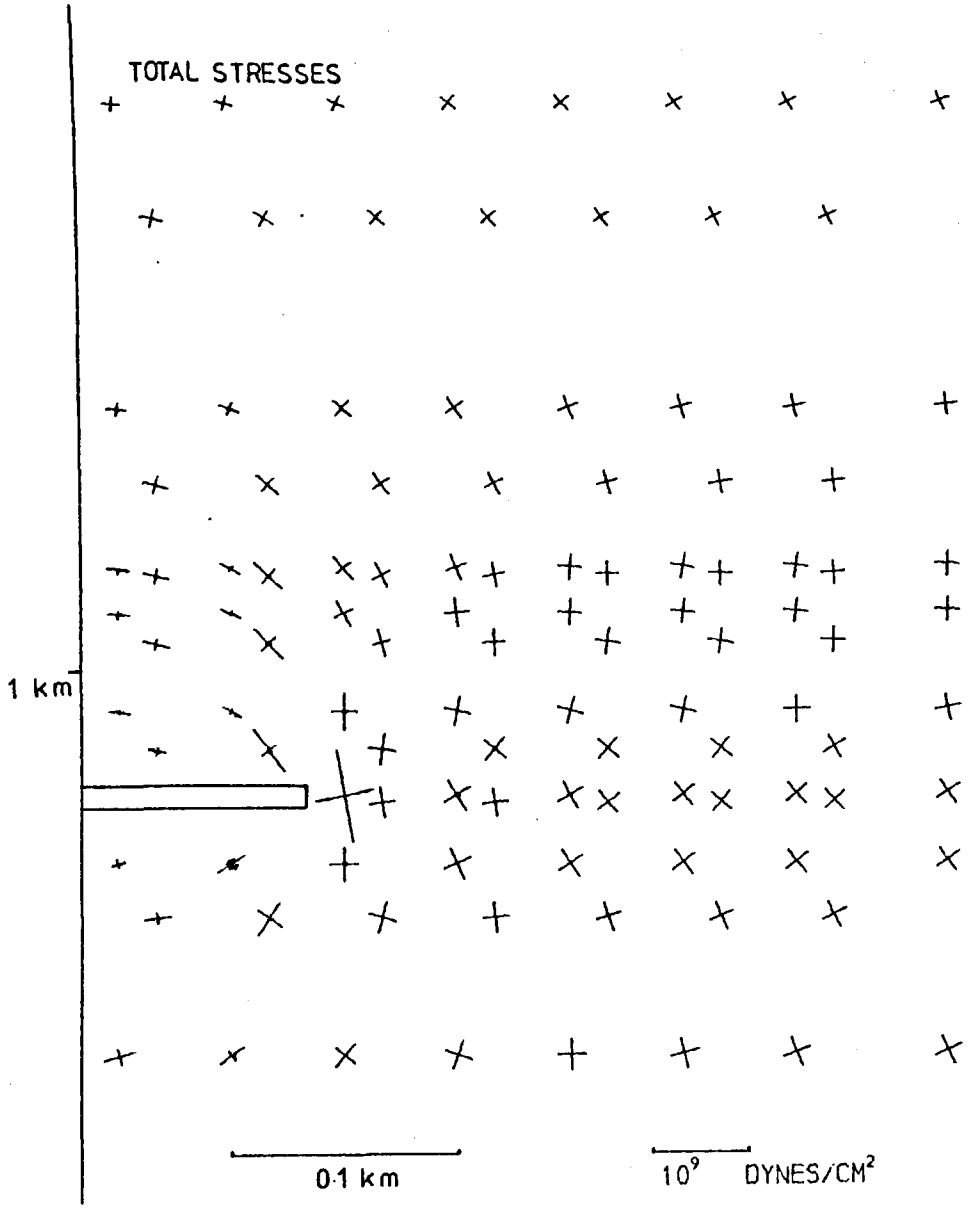

Figure 7.6 Stresses induced by a mine 200m in length.

The second model, shown in Fig. 7.6, is of a mine of length 200 m, and this has a much greater stress field. The qualitative aspects are now clearer, and large stresses are seen to develop around the end of the mine, with a less extensive region of low shear stress around the centre of the mine. The maximum shear stresses have increased by about 25%, and the 25 bar isobar now extends vertically 250 m, although the horizontal limit does not seem to have increased significantly.

Fig. 7.7 shows the situation for a mine of length 300 m. The same qualitative features as in the previous figure are shown, but now the vertical extent of the 25 bar contour has reached 400m. The extension of the mine has resulted in a relative concentration of shear stress around its ends compared to the centre, where the shear stress has in fact decreased by a small amount.

(ii) The Effects of Mechanical Properties

Although a realistic set of values for elastic constants has been used, the effects of variations in these are examined here, to determine how much effect variations from those values chosen will have upon the solutions presented later. Different Young's Moduli (for a homogeneous rock mass) will not of course alter the stress magnitudes or pattern, and the effects of different rock densities are entirely predictable by analytical methods once a solution for one particular density has been obtained. This section therefore examines only the effects of a Poisson's Ratio (ν) both higher and lower than the value of 0.35 which has been used in all the other models. A mine of length 200 m has been used, so comparison is possible with Fig. 7.6. The two cases, one for $\nu = 0.45$ and one for $\nu = 0.25$, are shown in Figs. 7.8 and 7.9 respectively. The former value is closer to those usually used in mining engineering, and Fig. 7.8 shows a small reduction in shear stress around the mine, although the extent or shape of the field is little affected. Fig. 7.9 is similar, in that the shear stresses due to the excavation have been increased without a great change in the area of

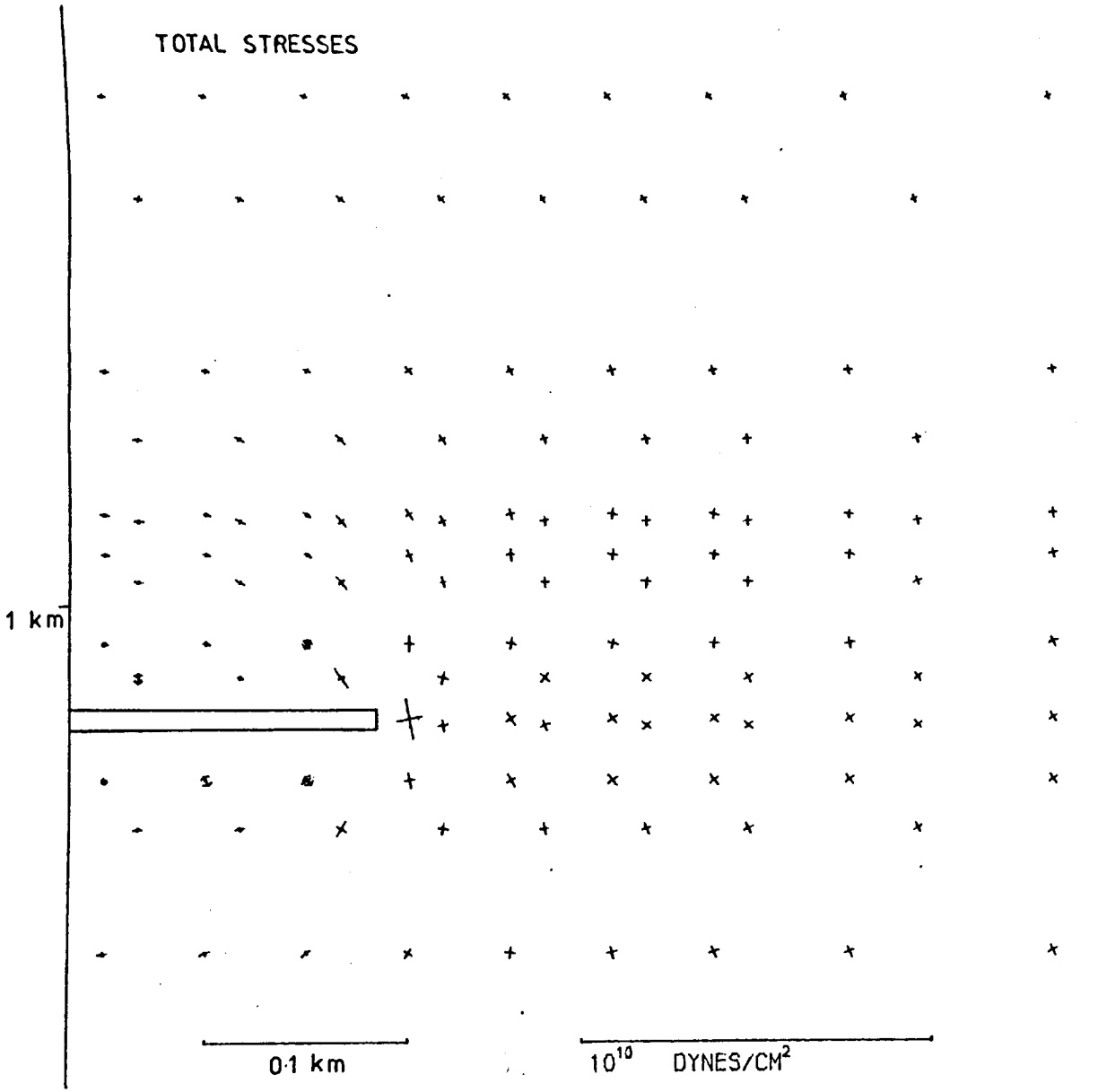

Figure 7.7 Stresses induced by a mine 300m in length.

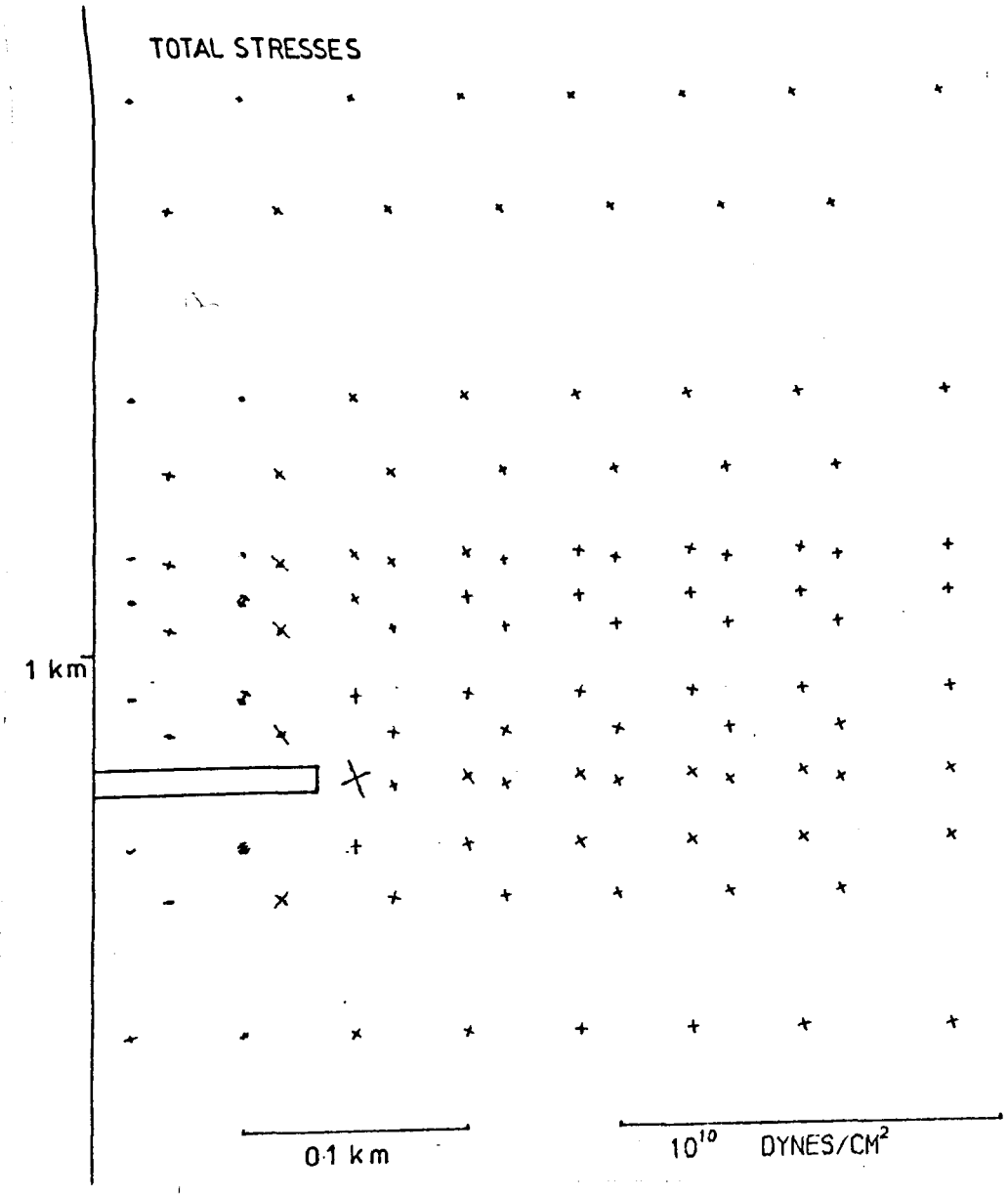

Figure 7.8 Stresses induced by a mine 200m in length (ν = 0.45).

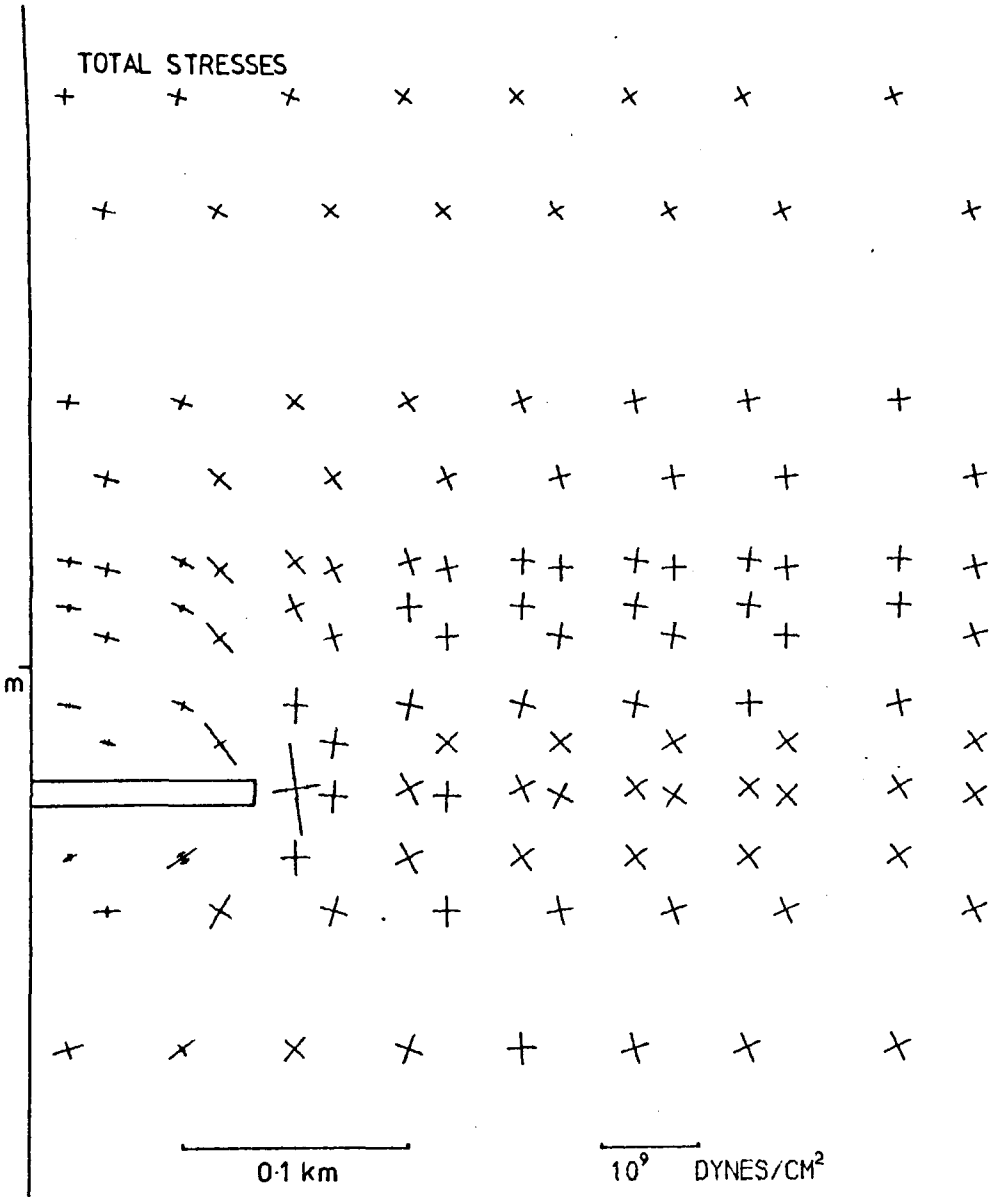

Figure 7.9 Stresses induced by a mine 200m in length (ν = 0.25)

stressed rock. It appears that even these large variations in Poisson's Ratio will not affect the qualitative conclusions to follow.

(iii) Tectonic Stress

Although not thought appropriate for the N.Staffordshire mining, the effects of excavating underground in the presence of a pre-existing stress field were investigated, as this sort of interaction has been thought to be responsible for mining-induced seismicity in some other areas, e.g. in Utah (Smith et al., 1974). As the mines are modelled by a horizontal slit, it is sufficiently accurate to simulate the horizontal stress field by adding it to the induced field after the finite element calculations. Two stress fields were imposed upon the case of the 200 m mine, one of a tensional 100 bars (Fig. 7.10) and the other compressional and of the same magnitude (Fig. 7.11). The background shear stress fields in both cases were thus very close to 50 bars.

To explain the results, it must first be noted that the induced stress field has larger vertical stress to the side of the opening, and larger horizontal stress above and below it. Thus each type of applied field will affect these two areas in opposite ways, with an intermediate area between them where they merge into each other. The tensional tectonic stress field will increase the shear stresses at the ends and to the side of the mine, and reduce those above and below its centre. Thus while the higher shear stresses become even more concentrated around the ends of the opening, there is in fact an increase in stability in other parts, and the area of increased shear stress is only one half that shown in Fig. 7.6.

When there exists a horizontally compressional tectonic stress regime, however, the situation is very different. Fig. 7.11 shows that although the increase in maximum shear stress at the mine ends is still slightly less than that when no tectonic stress field exists, the extent of the field has not been reduced at all. It appears therefore, that in the case of a thrusting tectonic stress field, only stresses immediately around the edges

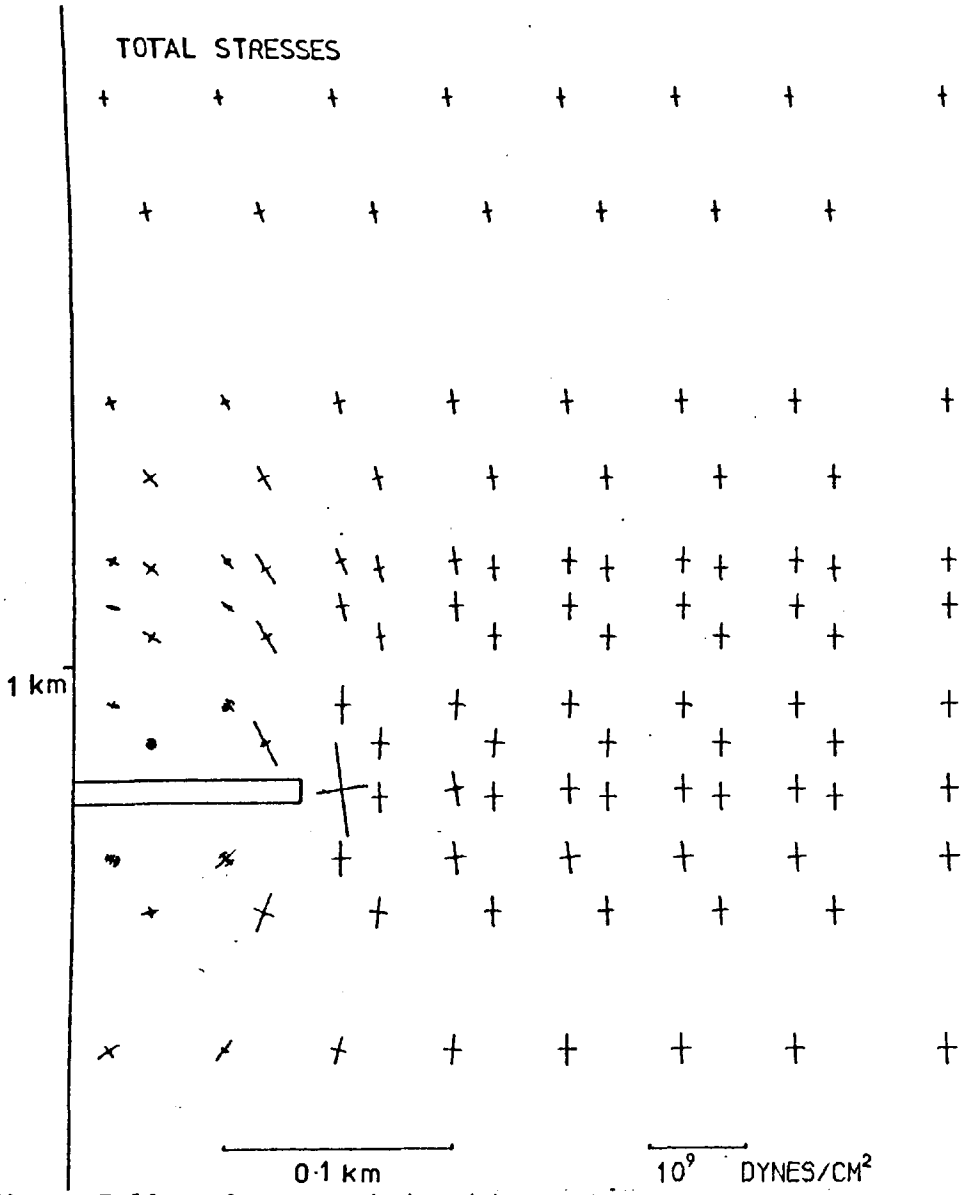

Figure 7.10 Stresses induced by a mine 200m in length in the presence of a horizontal tensional tectonic stress field.

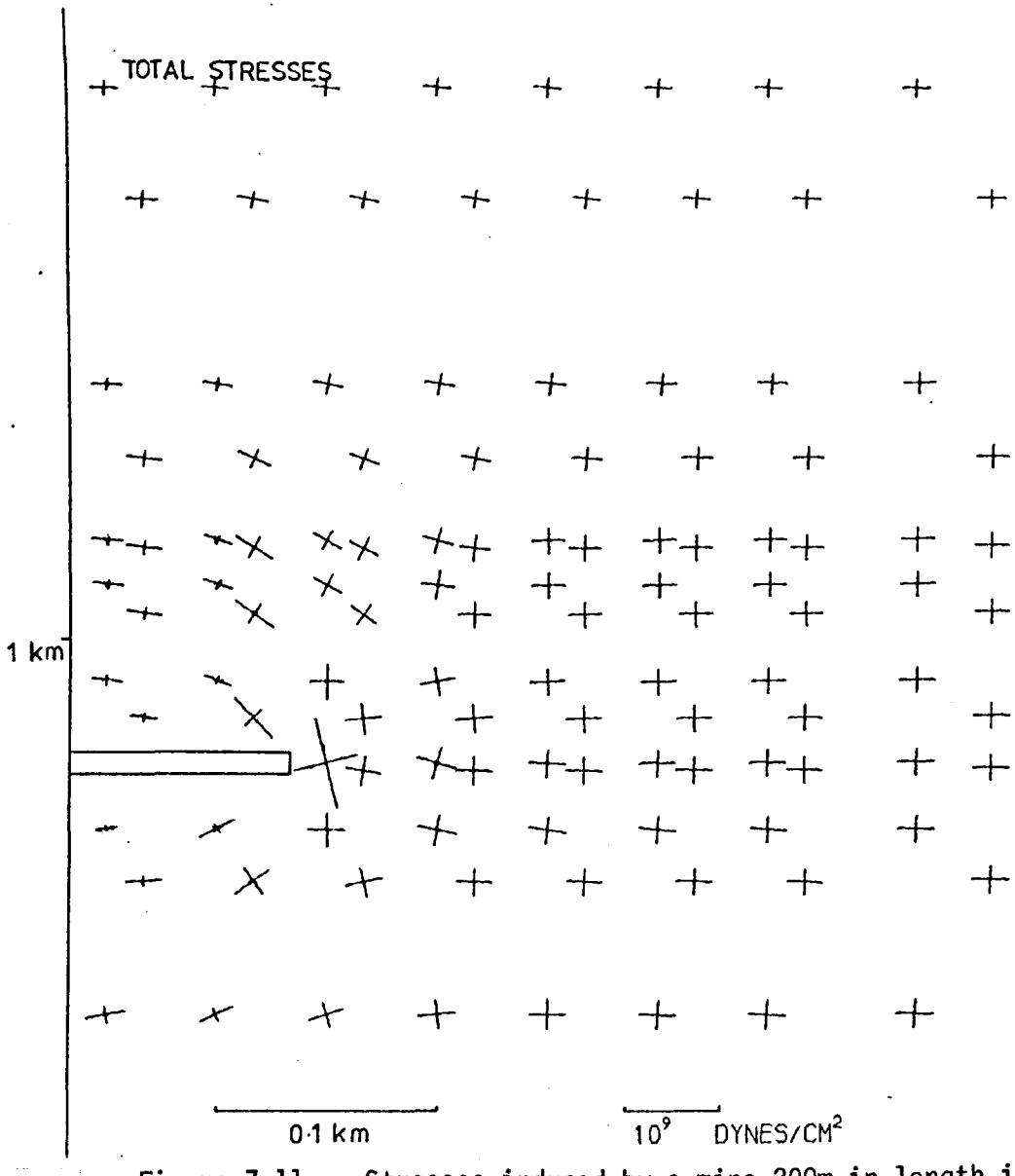

Figure 7.11 Stresses induced by a mine 200m in length in the presence of a horizontal compressional tectonic stress field.

of a mine are greatly affected (the exact nature of this is not distinguishable with these models), and stresses at a distance are not different to those when no original stress exists. In the case of a tensional field, the stress state immediately around the mine is also intensified, but there is a stabilizing effect at further distances away.

7.5 The Interactions of Two Workings

(i) Reduction of Pillar Width

The most common interaction between different workings in the same coal mine is that which occurs when a pillar is left between two excavations in the same seam. It was found that the stress fields generated by two 150 m long model excavations do not interact significantly until they approach within about 80 m of each other. Three examples are shown in this section, representing pillar widths of 50 m, 30 m and 20 m respectively, which are representative of the widths of pillars left in the portion of the Bowling Alley seam involved in the Trent Vale seismicity (Fig. 7.4).

Fig. 7.12 shows a situation where the two stress fields are only partly independent. The fields associated with the far ends of the mines, which have a lateral dimension of 150 m and are positioned 50 m apart at a depth of 1050 m, are similar to the single mine case. Between the mines there is still a region of relatively low shear stress, although the stresses near the abutments are more than double those at the outer edges. This high concentration of stress appears to have attracted the strain energy from the outer part of the stress field above and below the pillar: the 25 bar shear stress contour in Fig. 7.12 is unaffected by the presence of the additional working except in these regions. Fig. 7.13 shows the same features except that the zone of low shear stress between the workings is no longer apparent, although this is due partly to the lack of grid resolution. The approach of the two openings to 30 m has now increased the shear stresses in the pillar to three times those at the opposite ends

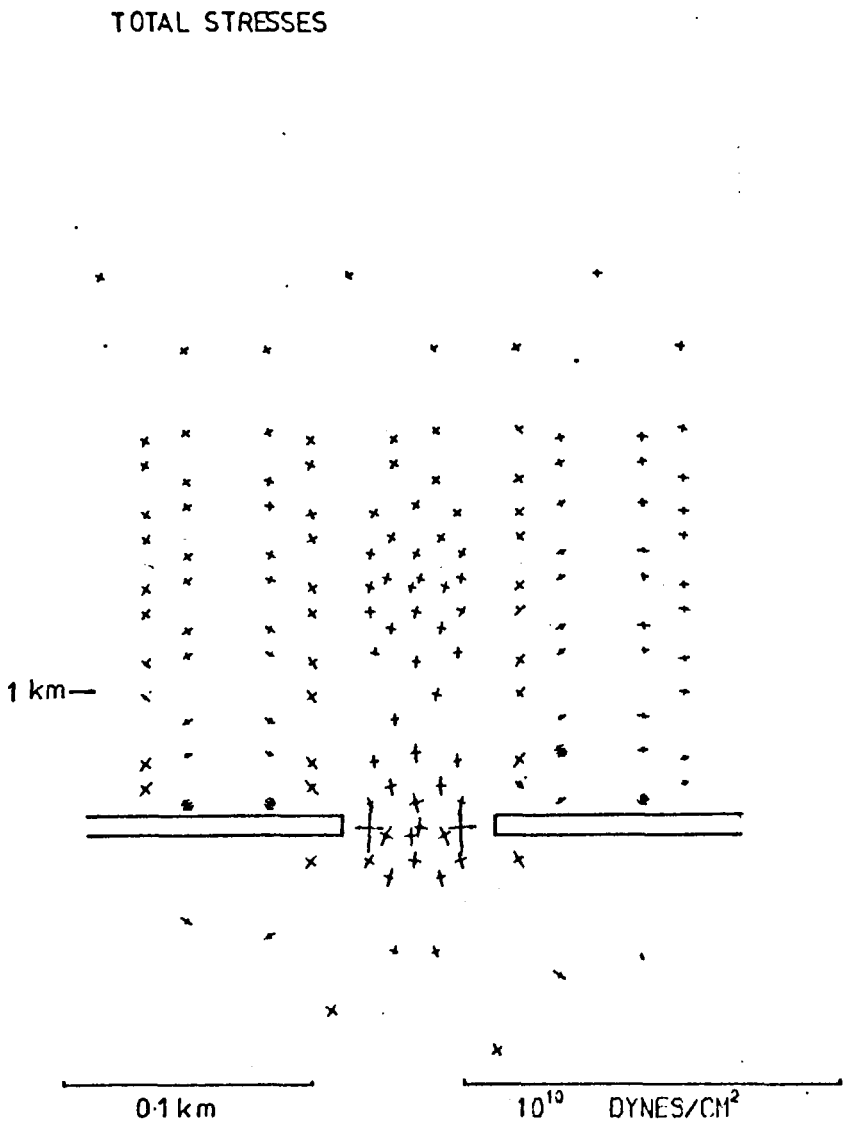

Figure 7.12 Stresses induced around a pillar 50m in width.

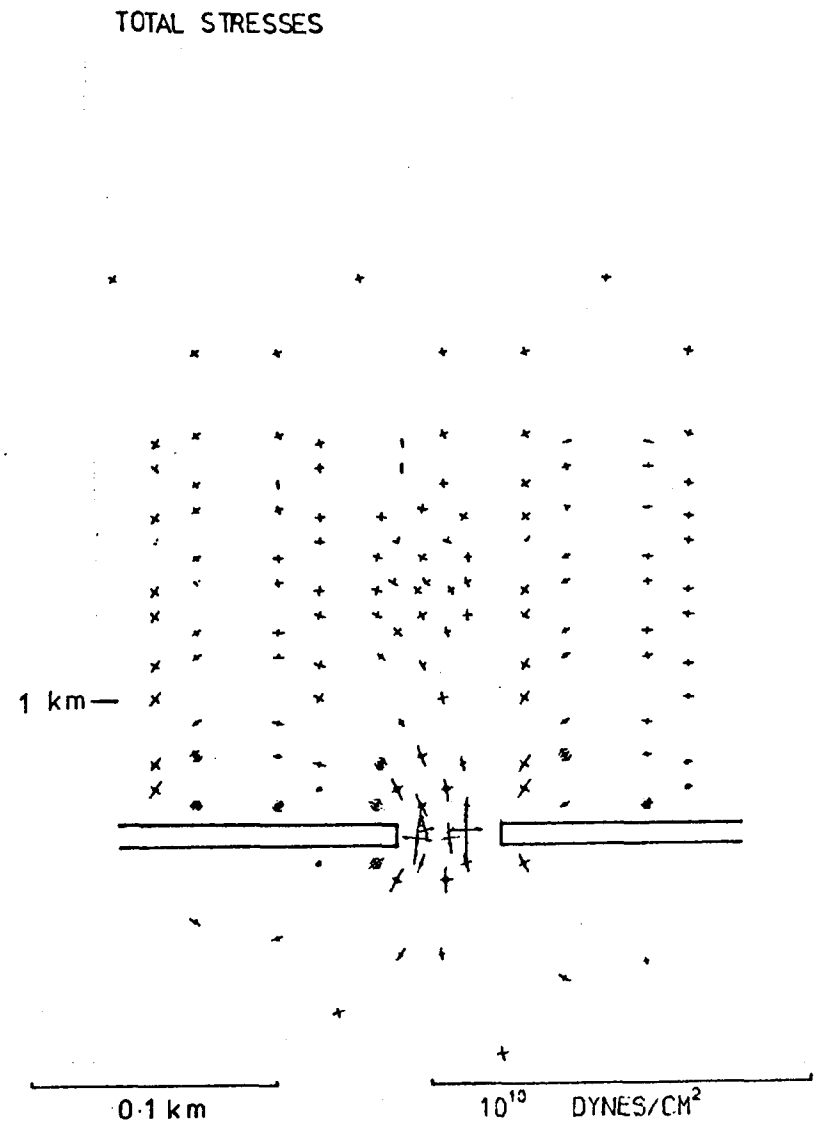

Figure 7.13 Stresses induced around a pillar 30m in width.

of the mines. Fig. 7.14 shows the workings only 20 m apart, and the stresses are now concentrated by a factor of almost four, and the individual stress fields appear to act as one.

Throughout the approach of the workings, as described above, the total extent of the stress field has increased only marginally, in the vertical directions. It does not appear from these results that the positioning of workings above and below the pillar will encounter stress fields any larger than those due to single workings, unless a close approach to a very narrow pillar is made. This is investigated further in a later section, however.

(ii) Mining Under a Previous Excavation

The removal of the optimum amount of coal from a mine frequently results, in practice, in having to mine a seam directly beneath or above previously worked-out panels or rooms. Ideally, the newer workings are planned to coincide laterally with the older ones, as this is found to reduce the problems associated with the resulting high stresses (Whittaker and Pye, 1975). Fig. 7.15 shows the stress field resulting from the interaction of a 100 m wide excavation when it has been situated directly beneath an older 200 m working, before much stress relaxation has occurred. When compared to the individual stress fields (Figs. 7.5 and 7.6), there is little change in the maximum stresses or in the areal extent of the fields. The stresses at the ends of the newer working are perceptibly reduced however, although the 75 bar contour extends further away under the influence of the larger opening above it. Between the excavations the stress field is for the most part shaped by that due to the 200 m working, but there is a relatively large area within the 75 bar contour where the two stress fields interact.

Fig. 7.16 shows the case where the lower working has been extended so that it is now also 200 m in length. The stress fields above the upper and below the lower mines are almost the same as those which would exist without the other working, although there is in fact a reduction of a few bars. Between the workings there is no concentration of the stresses from the two

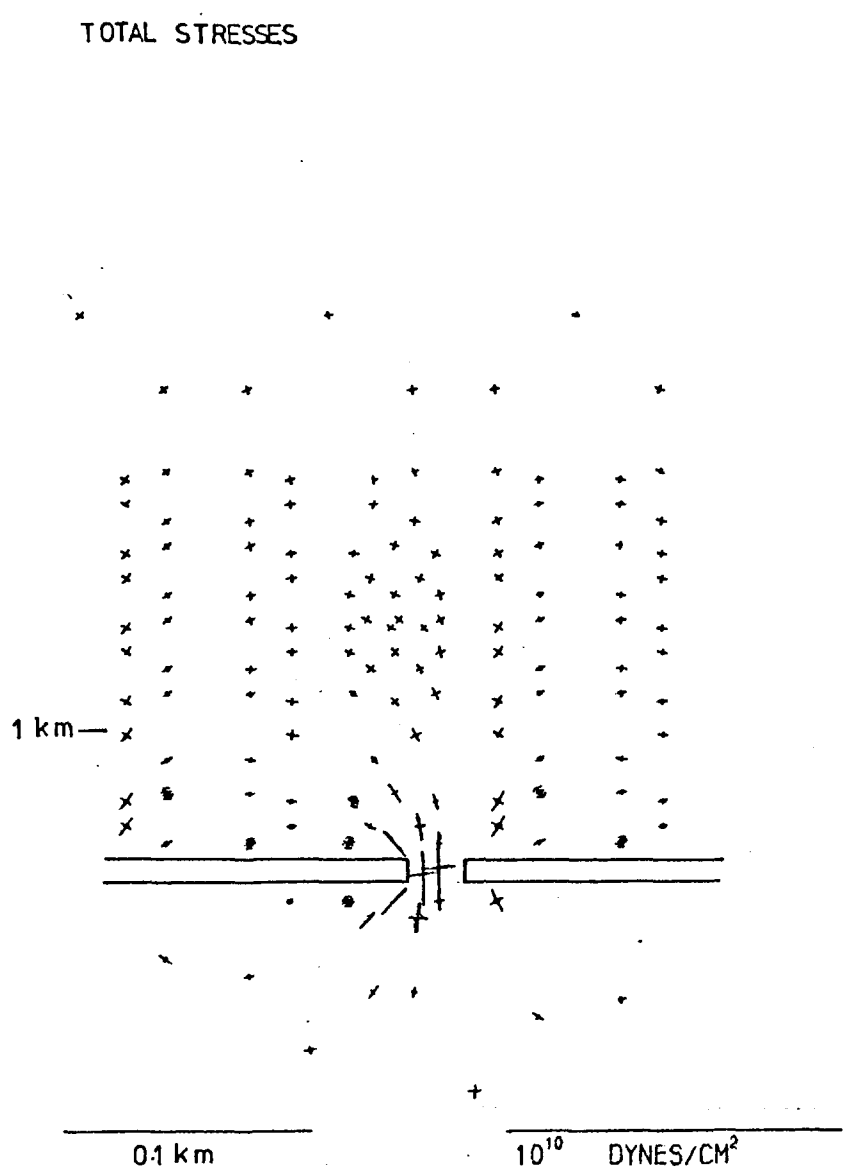

Figure 7.14 Stresses induced around a pillar 20m in width.

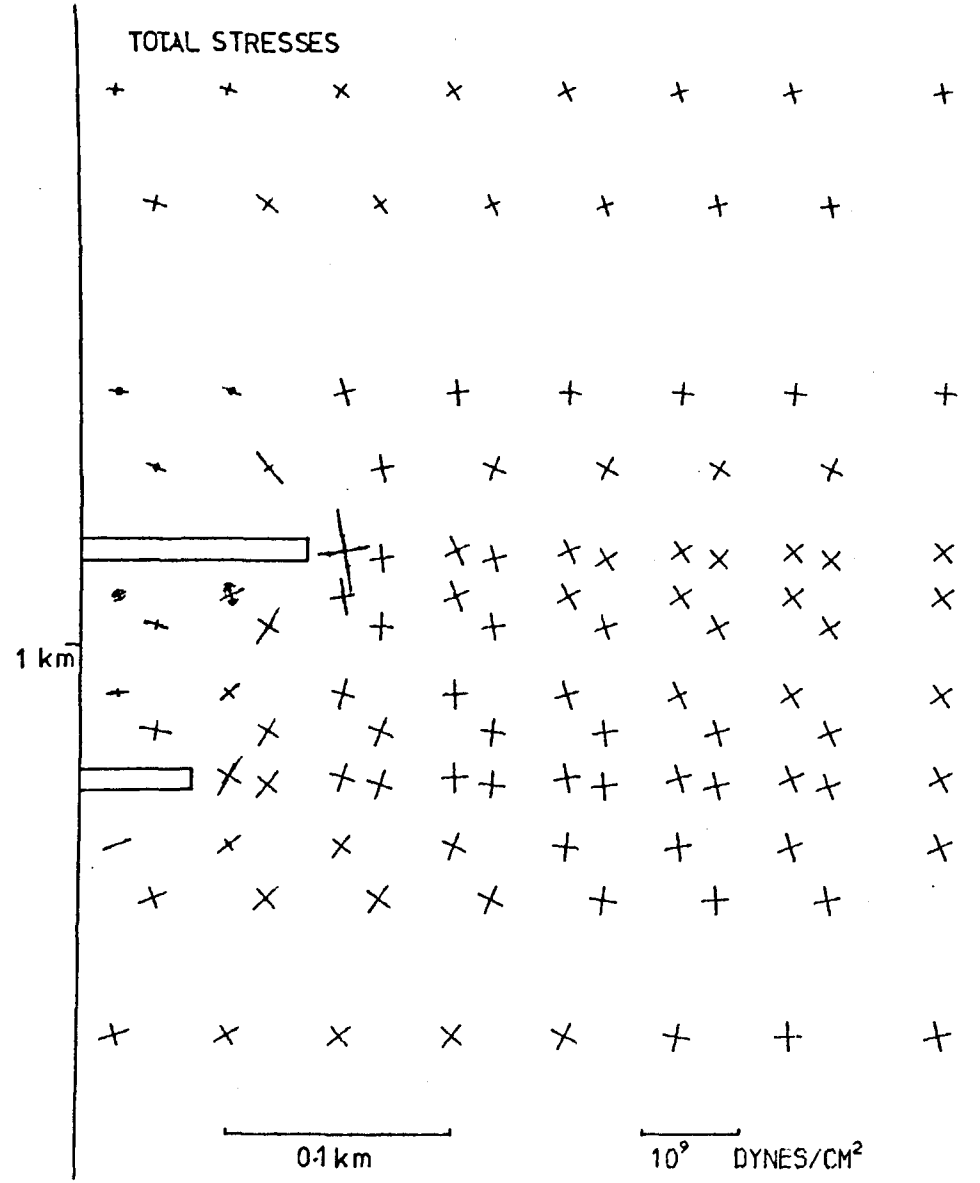

Figure 7.15 Stresses induced by a 100m mine beneath a 200m mine.

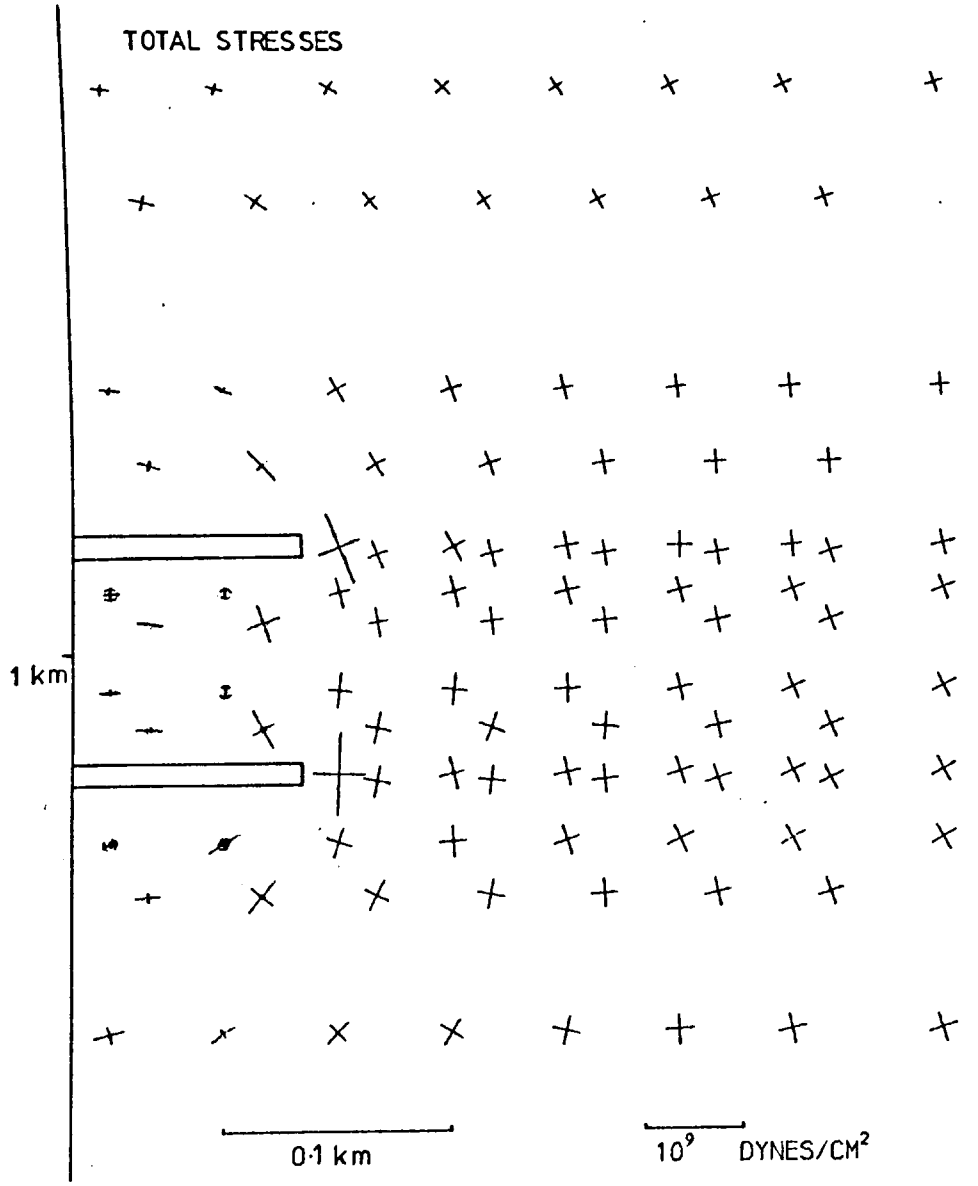

Figure 7.16 Stresses induced by a 200m mine beneath a 200m mine.

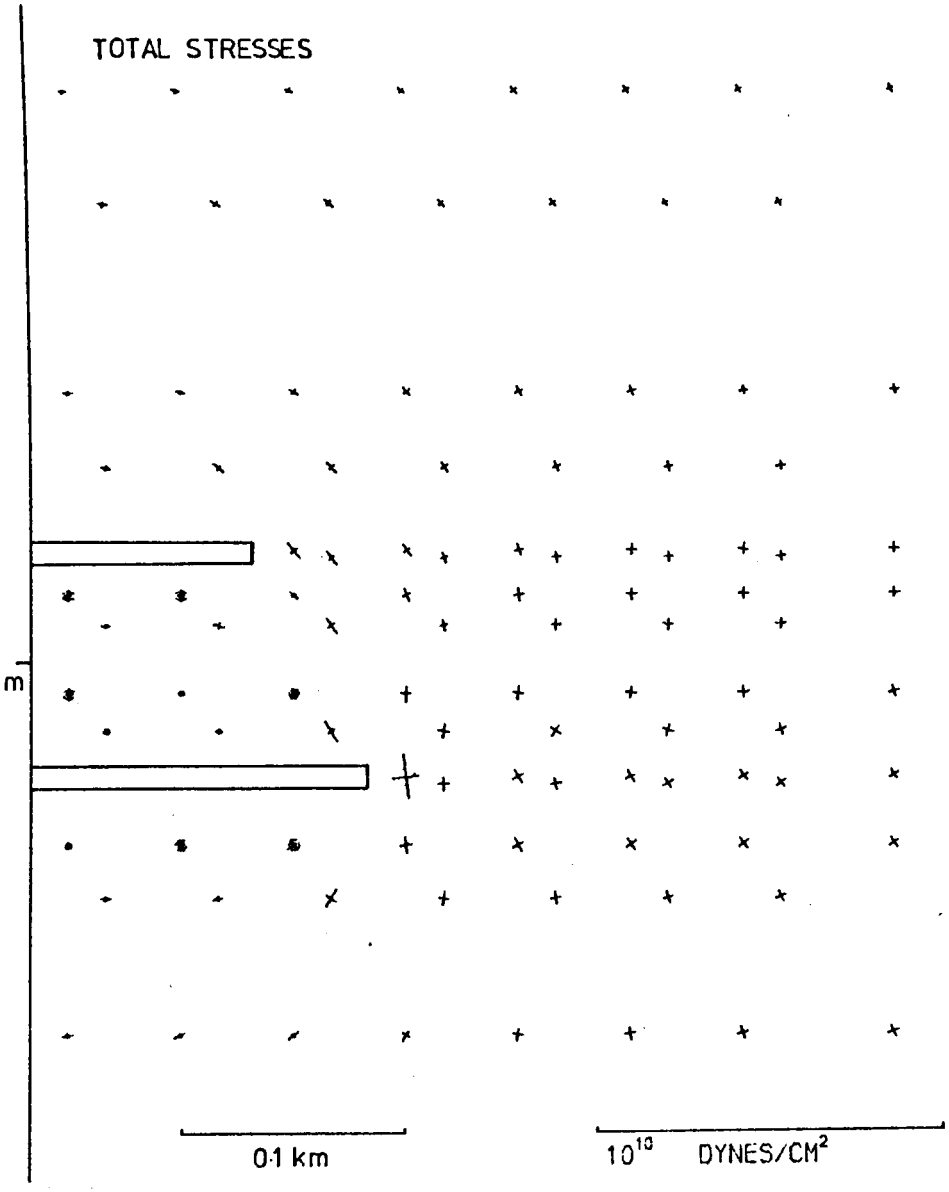

Figure 7.17 Stresses induced by a 300m mine beneath a 200m mine.

stress fields. Instead, there is an area of shear stress averaging around 85 bars, but the vertical principal stresses are very small and are often tensile. This region will therefore be very susceptible to failure. The result of extending the mine further is shown in Fig. 7.17. Again the areal extent of the larger stress field is little altered by the presence of the smaller one.

In general, the stress field surrounding the smaller working is the one which is most altered. Thus in the examples shown, when extending the lower mine, the stress field around it is at first rather larger than that which would be encountered (neglecting the low-stressed inter-mine area). As the working reaches beyond the upper one, its stress field becomes more dominant, and there is little difference between this case and that for the single mine, as far as the lower mine is concerned. The field around the upper mine will have undergone considerable changes, particularly when the newer working becomes larger than it. No large concentrations of stress appear to have been developed, and the weakest rock is shown to be at all times in the region of low-stress. Fig. 7.18 shows that almost the same situation arises when mining above a previous working.

(iii) Offset Mines

Further models were made to look at the stresses caused when a seam is mined not directly beneath a previous working, but to one side of it. Fig. 7.19 shows two 200 m wide mines, whose edges lie in the same vertical plane. This configuration results in a marked increase in shear stresses. At the far ends of the mines shear stresses have increased by approximately 20%, but where the two fields interact most, the maximum stresses have increased by one third. The shear stresses are associated with relatively small normal stresses, and this suggests that the rock here will be prone to failure. These effects are produced as a result of a combination of the two stress sources established in the previous section. The small and/or vertically tensile stresses caused by partial elastic closure of the

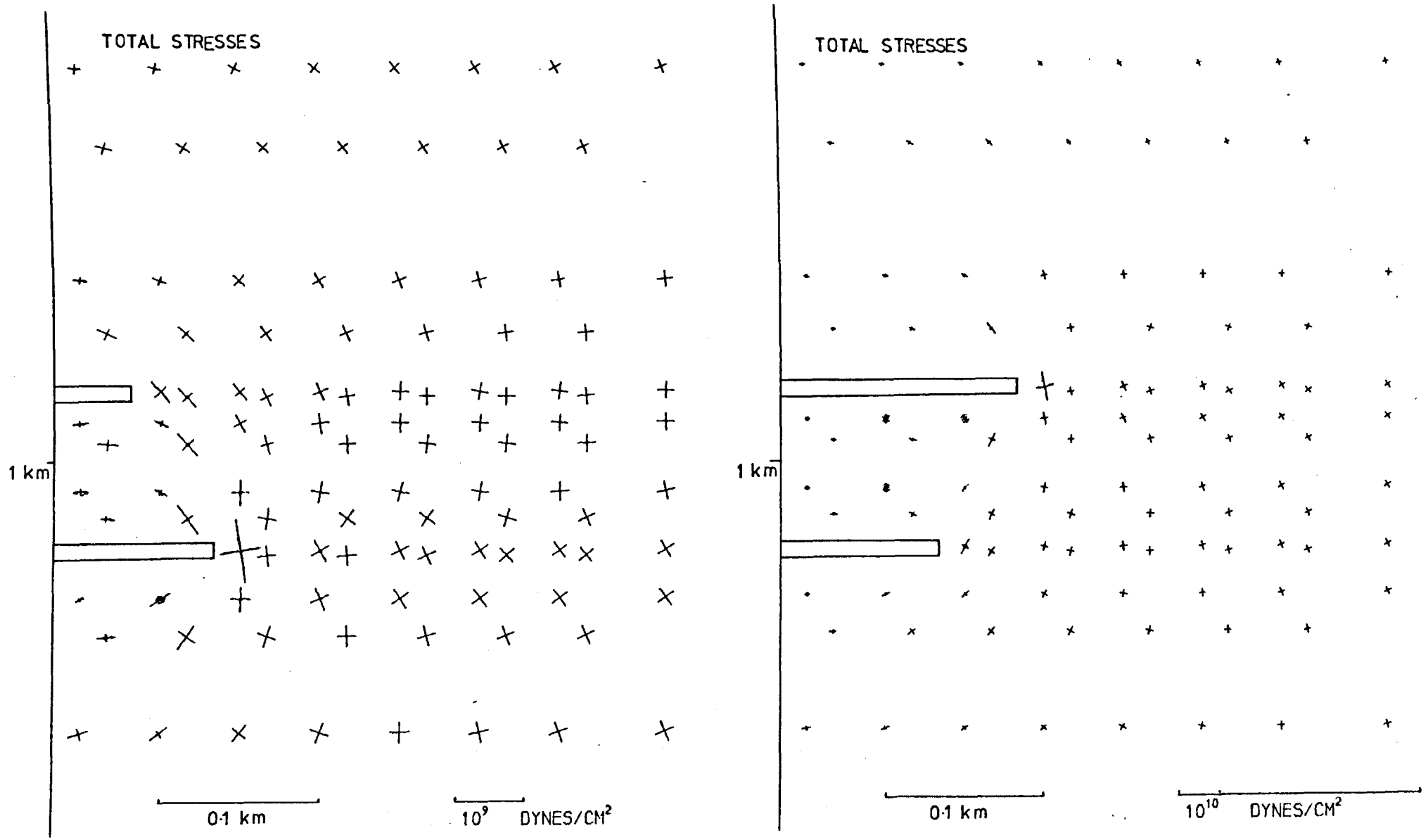

Figure 7.18 Stresses induced by (a) a 100m mine and (b) a 300m mine above a 200m mine.

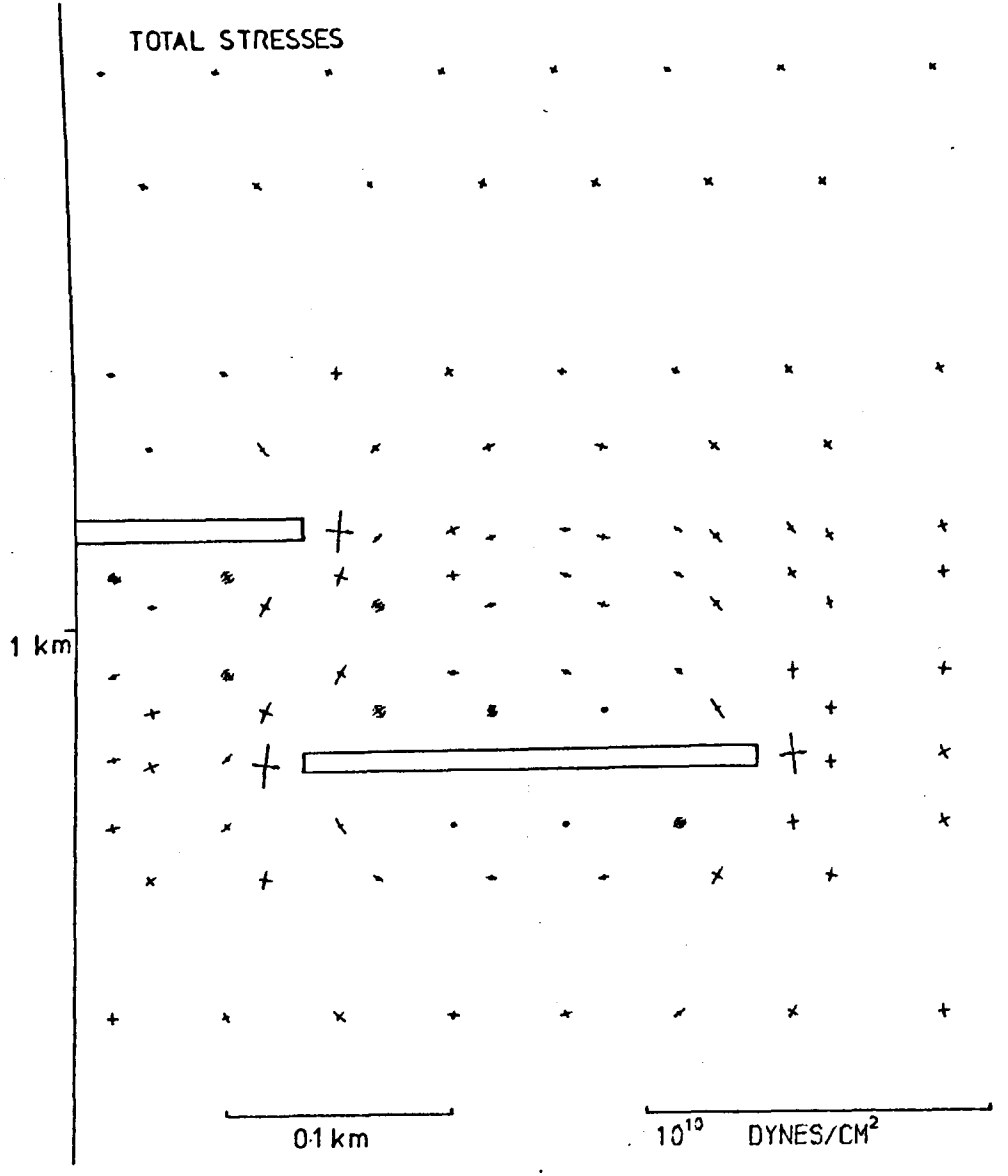

Figure 7.19 Stresses induced by two offset mines.

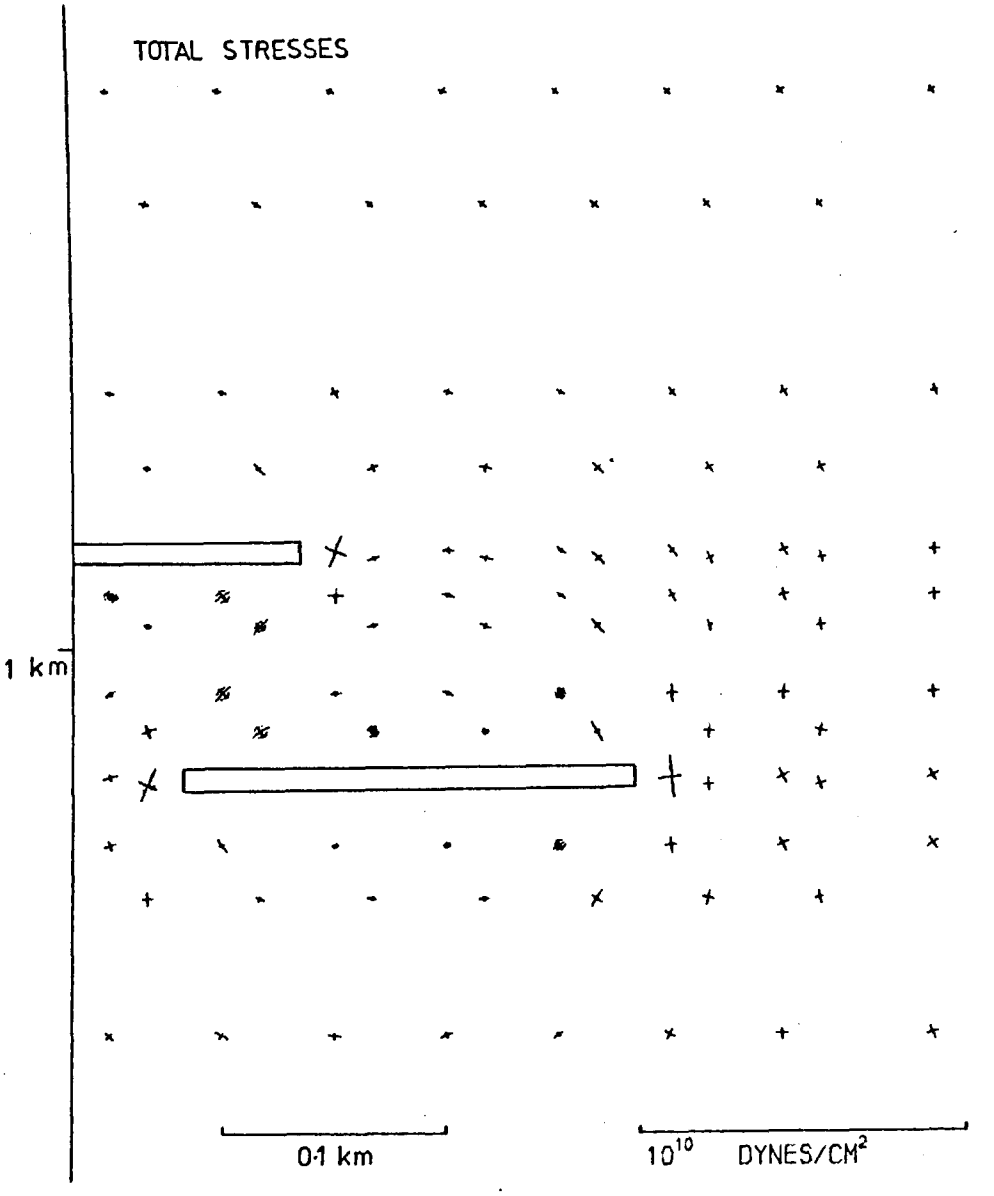

Figure 7.20 Stresses induced by two overlapping mines.

excavations are now situated in the same area as the large stresses derived from the edges of the openings.

When the mines overlap to some extent, as shown in Fig. 7.20, extremely large shear stresses can result (more than double those expected from a single working). Here the two stress effects not only act in the same region, but combine positively to increase the resulting shear stresses. This effect is further enhanced by a positive combination of the two edge stress fields. In practice then, the positioning of mines relative to older workings is thus critical, and especial care should be taken not to encourage the build-up of stresses by using partial overlap configurations such as shown in Fig. 7.20.

The effects of an initial stress field in this situation were examined, to see if this made any significant difference to these large induced shear stresses. The results with a horizontal tensile stress of 100 bars, and a horizontal compressional stress of 100 bars are shown in Figs. 7.21 and 7.22 respectively. As was seen in Figs. 7.10 and 7.11, the tensile stress compacts the stress field, and the compressive stress field tends to disperse it. There is no great change in the magnitude of the largest shear stresses, since neither of the principal stresses, in the region between the mines, is oriented vertically.

7.6 Undermining a Pillar

Figs. 7.23 to 7.25 illustrate the changing stress field whilst a face is being advanced beneath a 50 m pillar between two 200 m excavations in the seam above. This situation is similar to that which was found to coincide with mining-induced seismicity in the Trent Vale case history (Kusznir et al., 1980). The distance here between the seams is 100 m. This value falls between the interseam distances of 150 m and 15 m which occur in the described case history (Fig. 7.4). Fig. 7.23, where the more recent working lies wholly beneath one of the upper workings, is similar to the situation

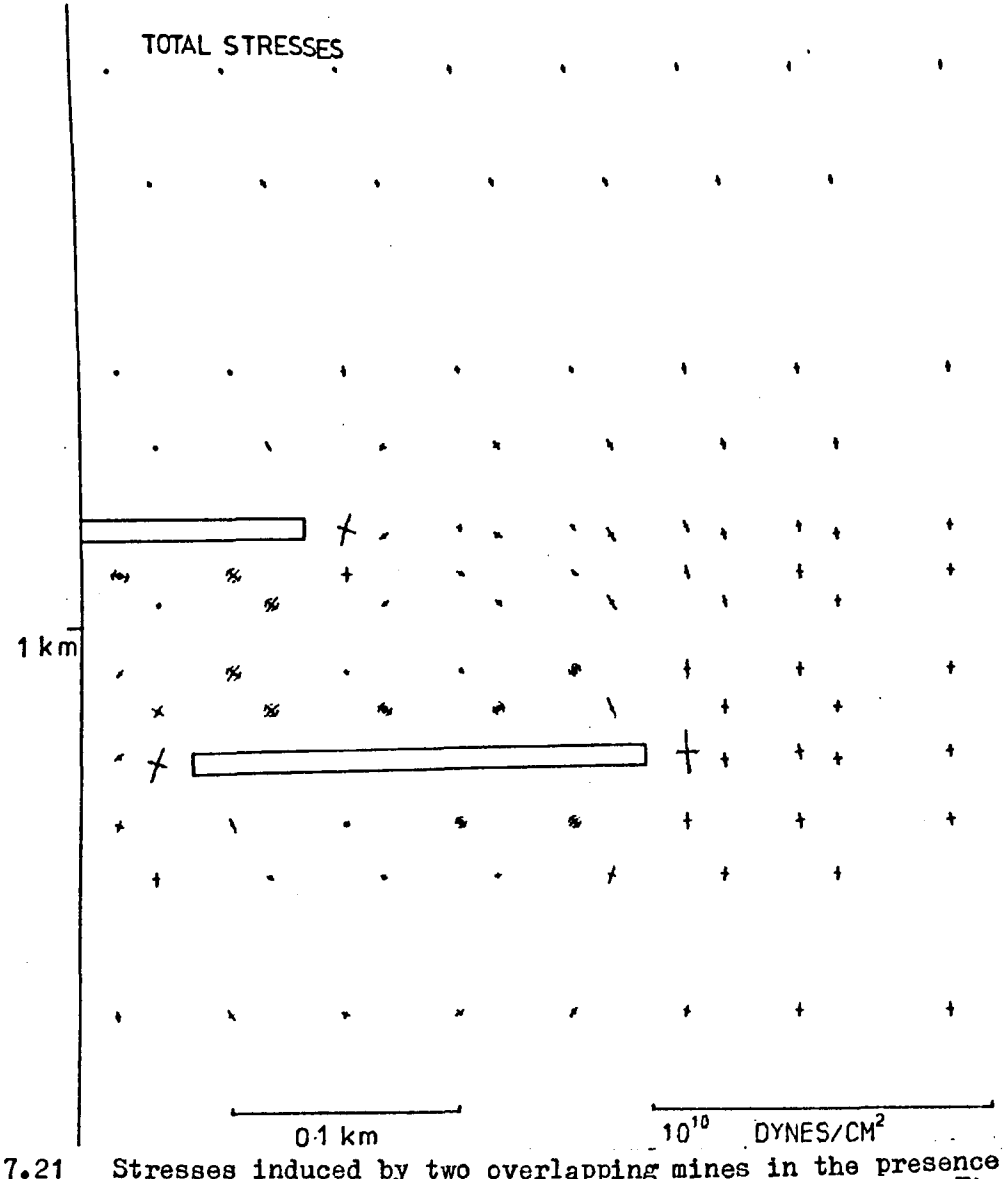

Figure 7.21 Stresses induced by two overlapping mines in the presence of a horizontal tectonic tensile stress of 100 bars.

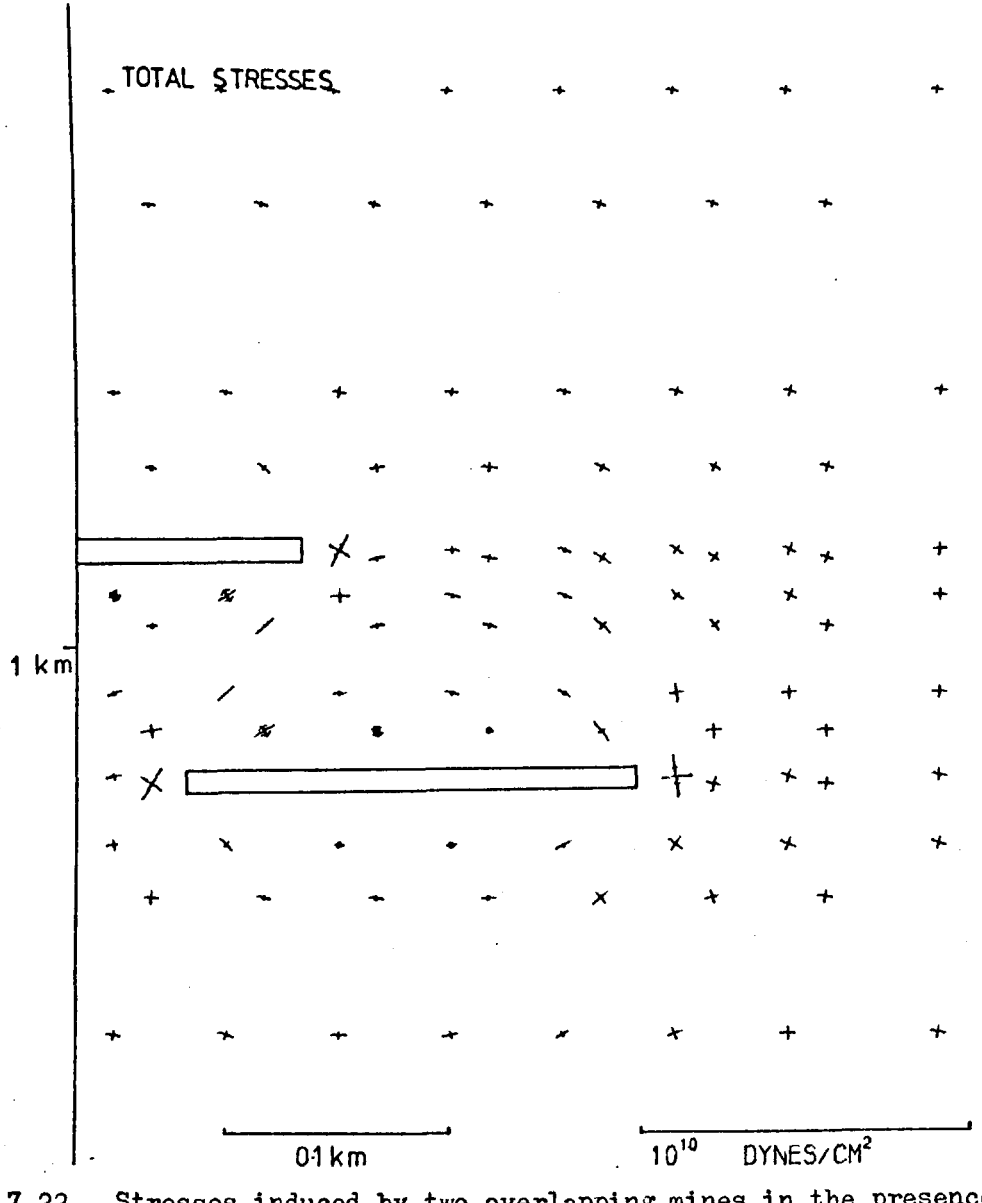

Figure 7.22 Stresses induced by two overlapping mines in the presence of a horizontal tectonic compressive stress of 100 bars.

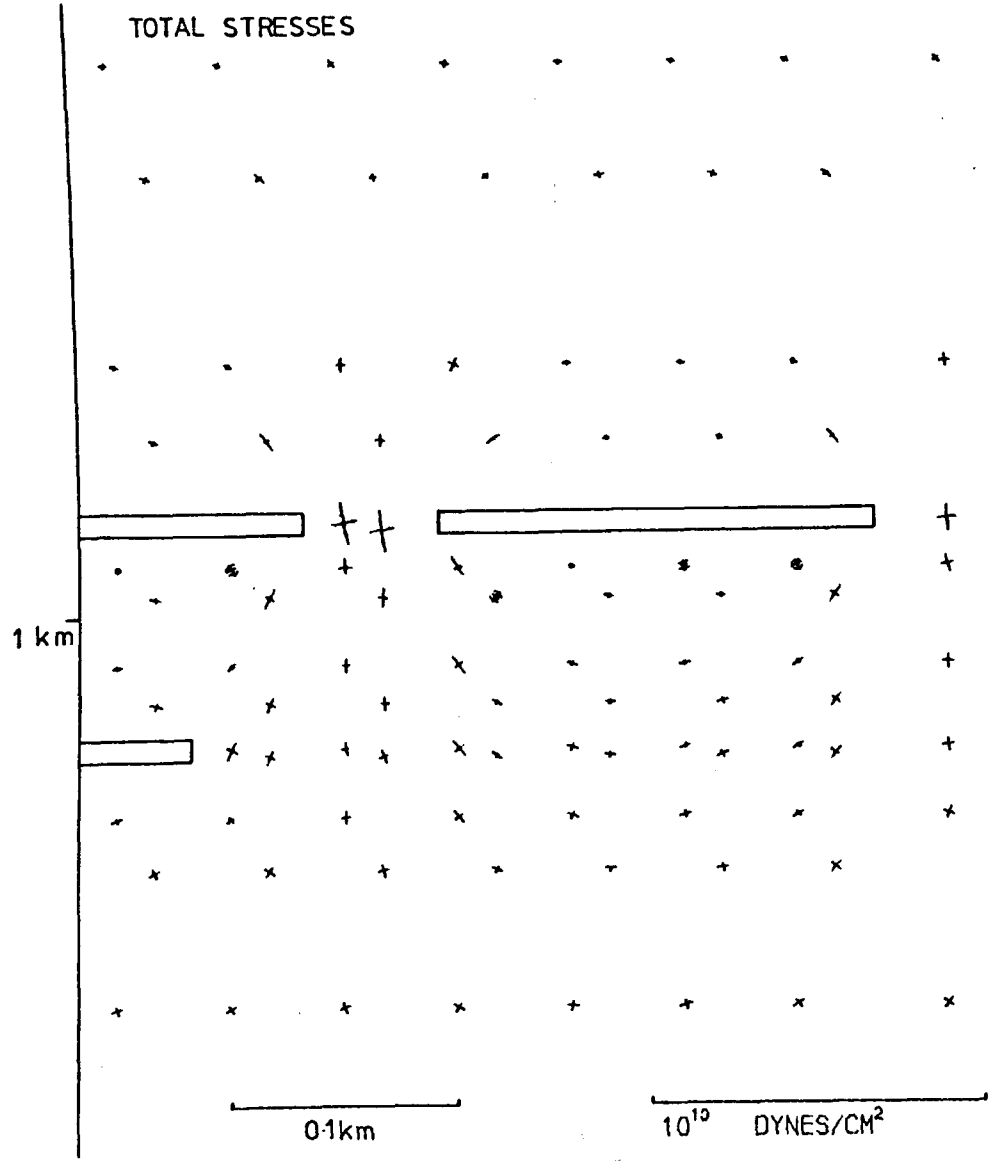

Figure 7.23 Stresses induced by a 100m length mine beneath a 50m pillar.

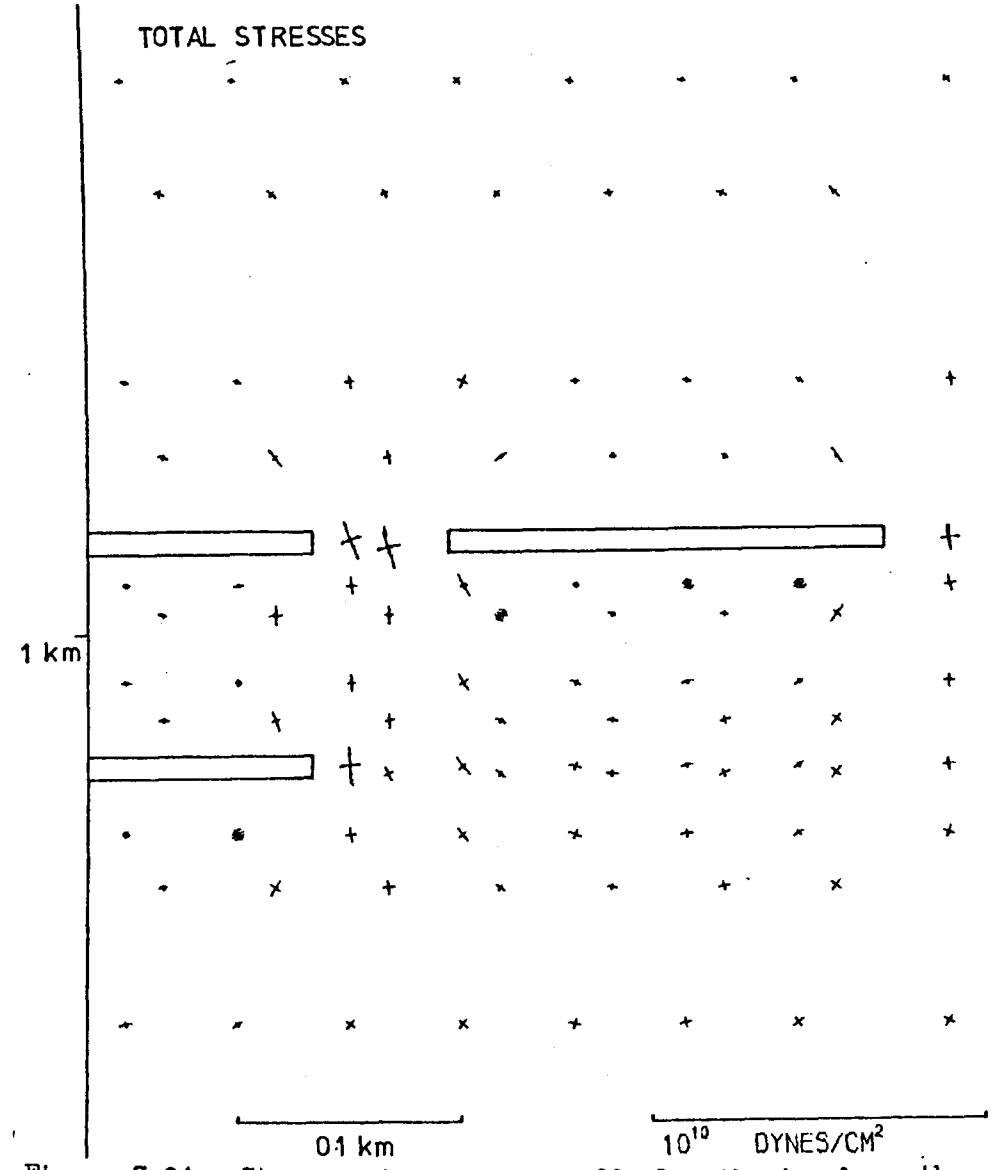

Figure 7.24 Stresses induced by a 200m length mine beneath a 50m pillar.

in Fig. 7.15, as the pillar plays little part in the stress field interaction in this case. When the lower mine is advanced further, so that it is 200 m long, as in Fig. 7.24, the stress field surrounding it is significantly greater than that which would be developed on its own (cf. Fig. 7.6). The shear stress field associated with the pillar area is also distorted greatly, and the maximum stresses have increased by 15%. On extending the mine to beneath the pillar (Fig. 7.25), the maximum shear stresses in the pillar rise by a further 20%. The shear stresses around the working, which is now 300 m in length, are 40% greater than for a single mine. Further extension will result in partial overlap with the working above, and will result in very large stresses similar to those in Fig. 7.20. Fig. 7.26 shows a case where there is partial overlap with both the upper mines. Although the shear stresses in the pillar are reduced, presumably because of the compensatory closure of the lower working, the shear stresses between the openings reach great magnitudes.

The results in this section indicate that high shear stresses encountered when mining beneath or above previous workings, are primarily a result of the stresses deriving from the edge effects of the workings, rather than with high normal stresses transmitted by a 'funnelling' process through the pillars themselves. Partial overlap of one mine with another above or below it, has been shown to be a configuration of high seismic risk. Large changes in stress occurring around the older workings whilst undermining have also been shown to occur, and seismicity with foci near the previous excavations could well be induced in this way.

7.7 The Effects of Geological Layering

The mining medium generally consists of a set of (sub-) horizontal sedimentary layers, usually a combination of shales, sandstones and coal. In N.Staffordshire the coal measures comprise a typical cyclical sequence of pelites and sandstones, with thicknesses in an approximate ratio of 5:1.

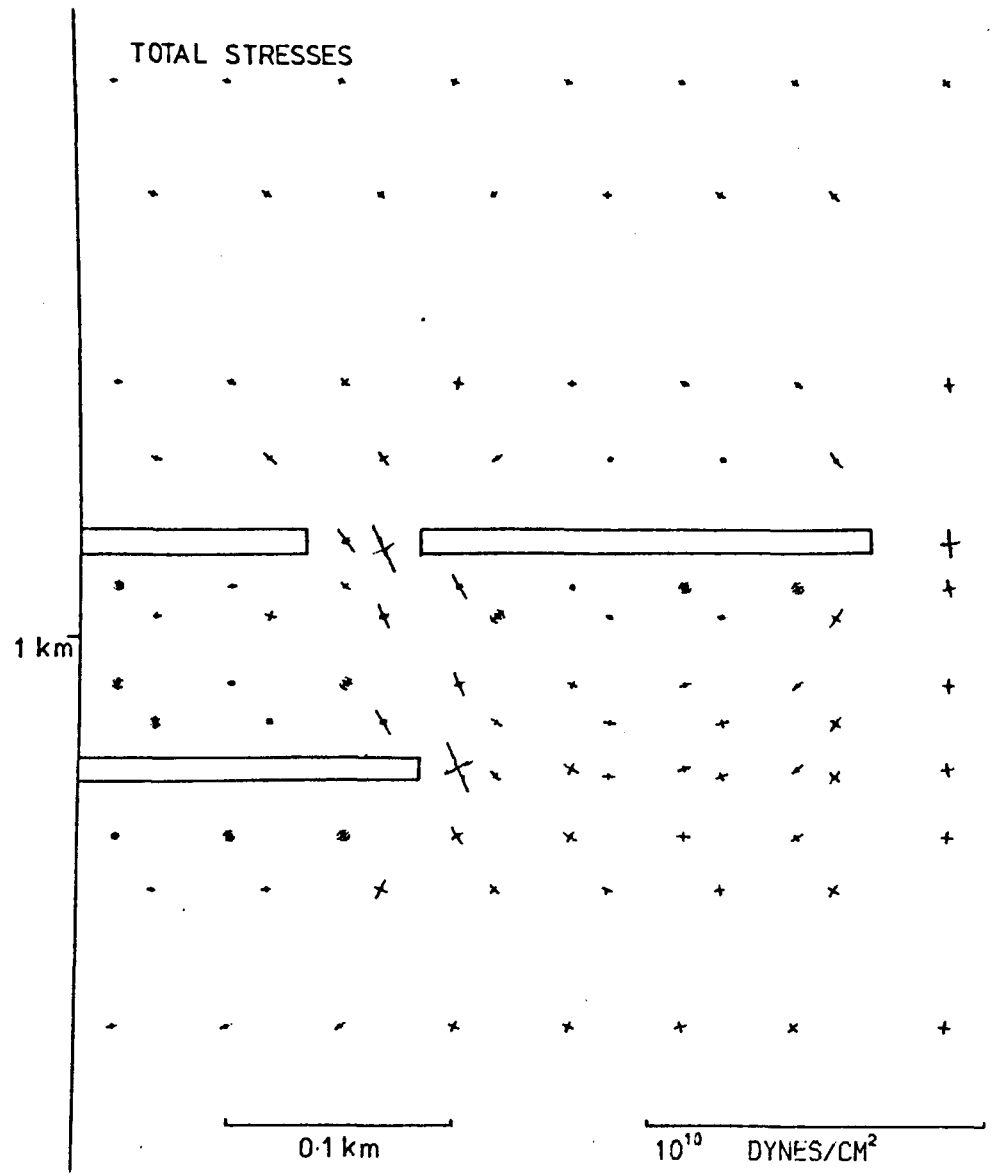

Figure 7.25 Stresses induced by a 390m length mine beneath a 50m pillar.

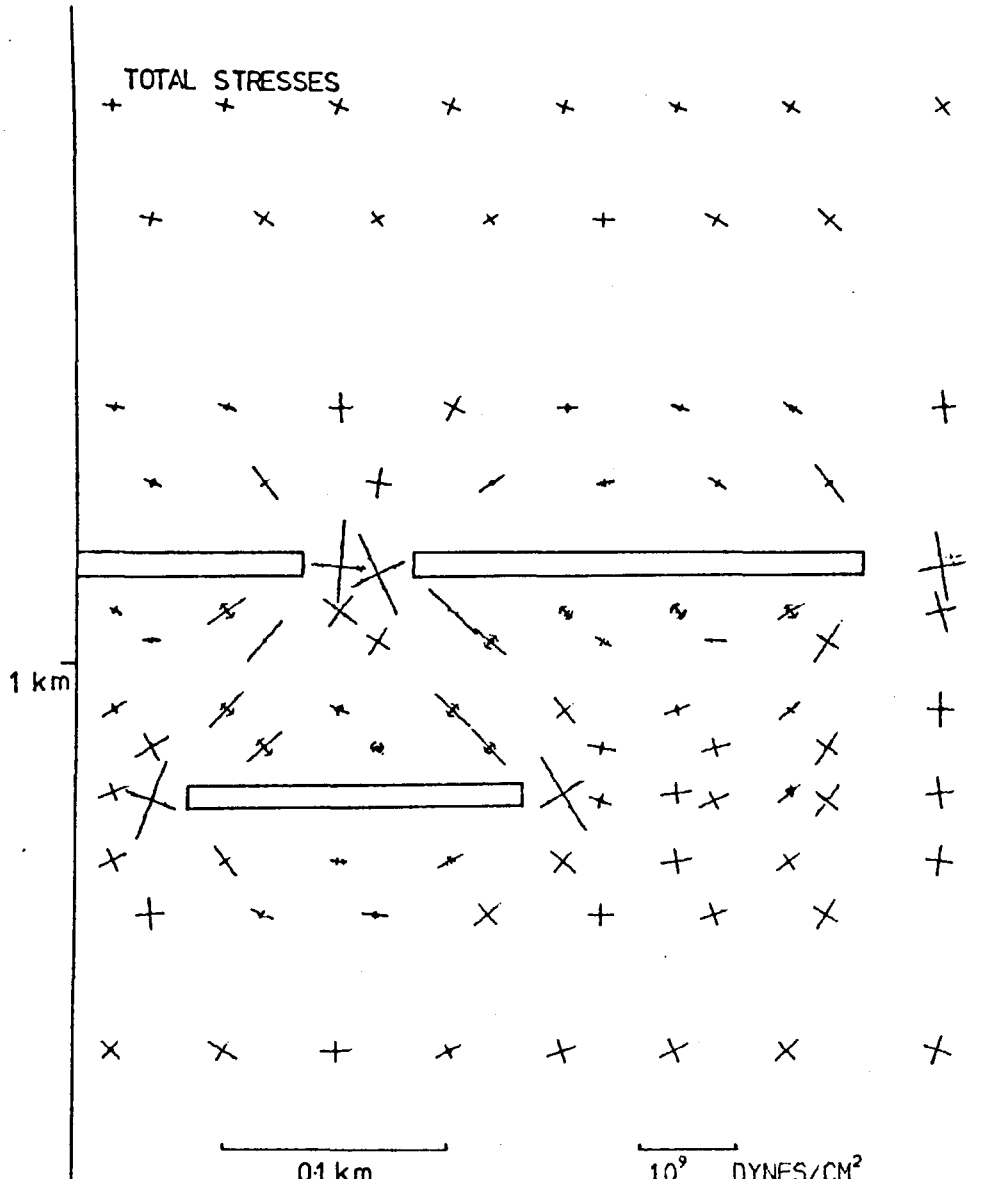

Figure 7.26 Stresses induced by a 150m length mine directly beneath a 50m pillar.

The sandstones are mostly of the order of 10-15 m thick, but tend to be lenticular and have limited lateral continuity (Kusznir et al., 1980).

The effects on the mining-induced stress field of the presence of these harder layers was investigated to see (a) whether this caused the extent of the influence of the stress field to change, and (b) the magnitude of the stress concentrations to be expected in the layers. The mine was modelled in the same way as that in Fig. 7.6, but above this, at intervals of 50 m on average, were positioned horizontal, 10 m thick layers of Young's Modulus 10^{11} dynes/cm^2, i.e. ten times that of the surrounding rock. The resulting finite element solution is shown in Fig. 7.27. Immediately noticeable are the large total and deviatoric stresses in the harder layers. The shear stresses in these layers decrease away from a point directly above the centre of the mine, and reach over 300 bars at their maximum point. The shear stresses in the surrounding rocks, however, when compared to Fig. 7.6, show a marked decrease, both in their areal extent and in the maximum value reached. Beneath the mine, though, where no layering is present, the stress field does closely approximate that of Fig. 7.6. The strain energy has thus been transferred from the supporting rock to the harder layers, causing the build-up of stresses there. It can be concluded, therefore, that although the risk of seismicity when mining in these circumstances is greater because of the large stress concentrations, the influence of the mining stress field is very much reduced as regards other mines, or nearby fault planes, which are in the softer rock.

The sedimentary sequence is also likely to contain layers which are weaker in some way than the surrounding rocks. This weakness may be the result of a low Young's Modulus, in which case the whole rock body will effectively behave as one containing thick hard layers, and the nature of the stresses can be surmised from Fig. 7.27 and Section 4.4. The weakness may take another form however. Soft mudstones, possibly containing much water, are liable to deform non-elastically, and have elastic properties

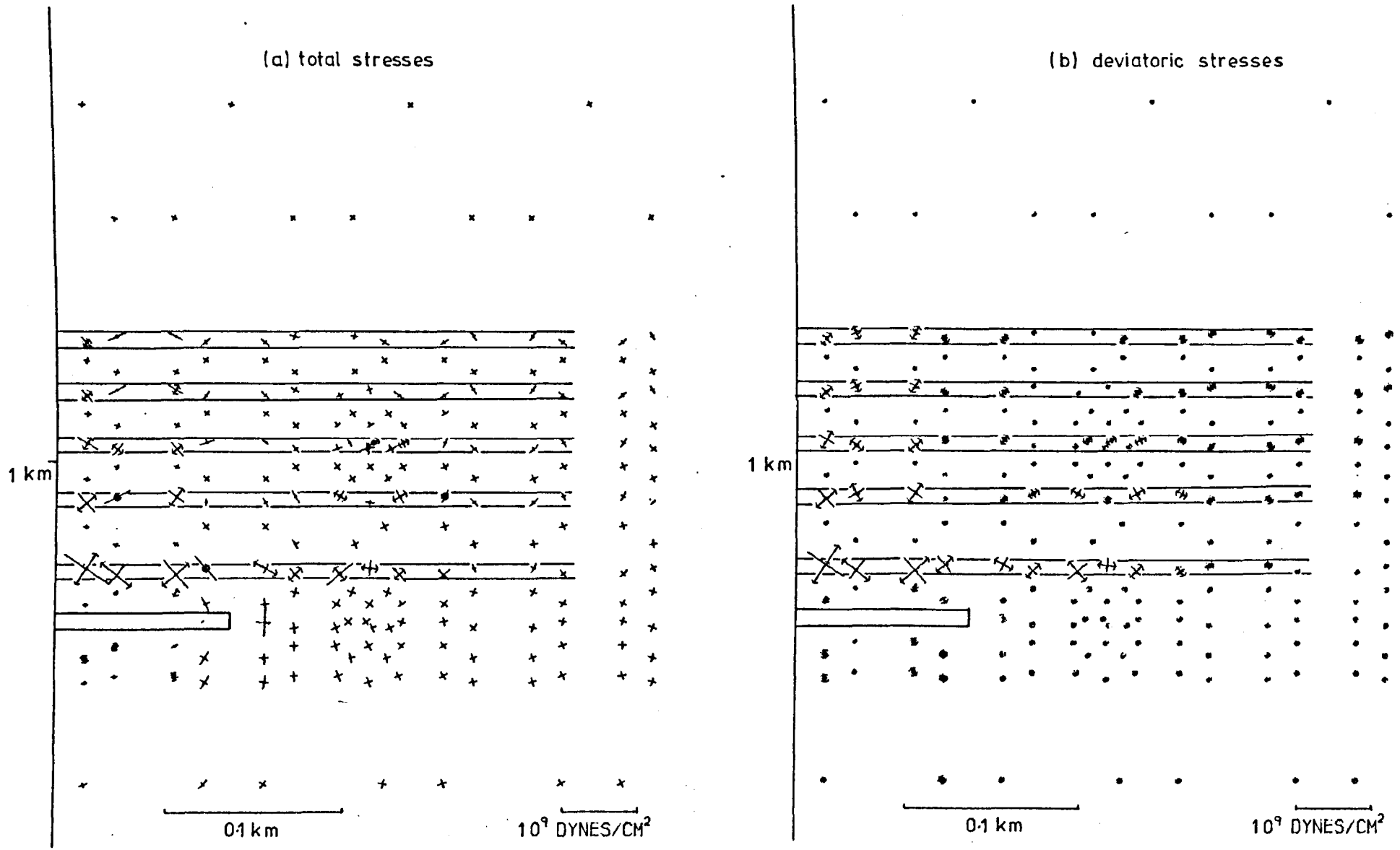

Figure 7.27 Stresses induced by a mine 200m in length beneath a series of high Young's Modulus layers.

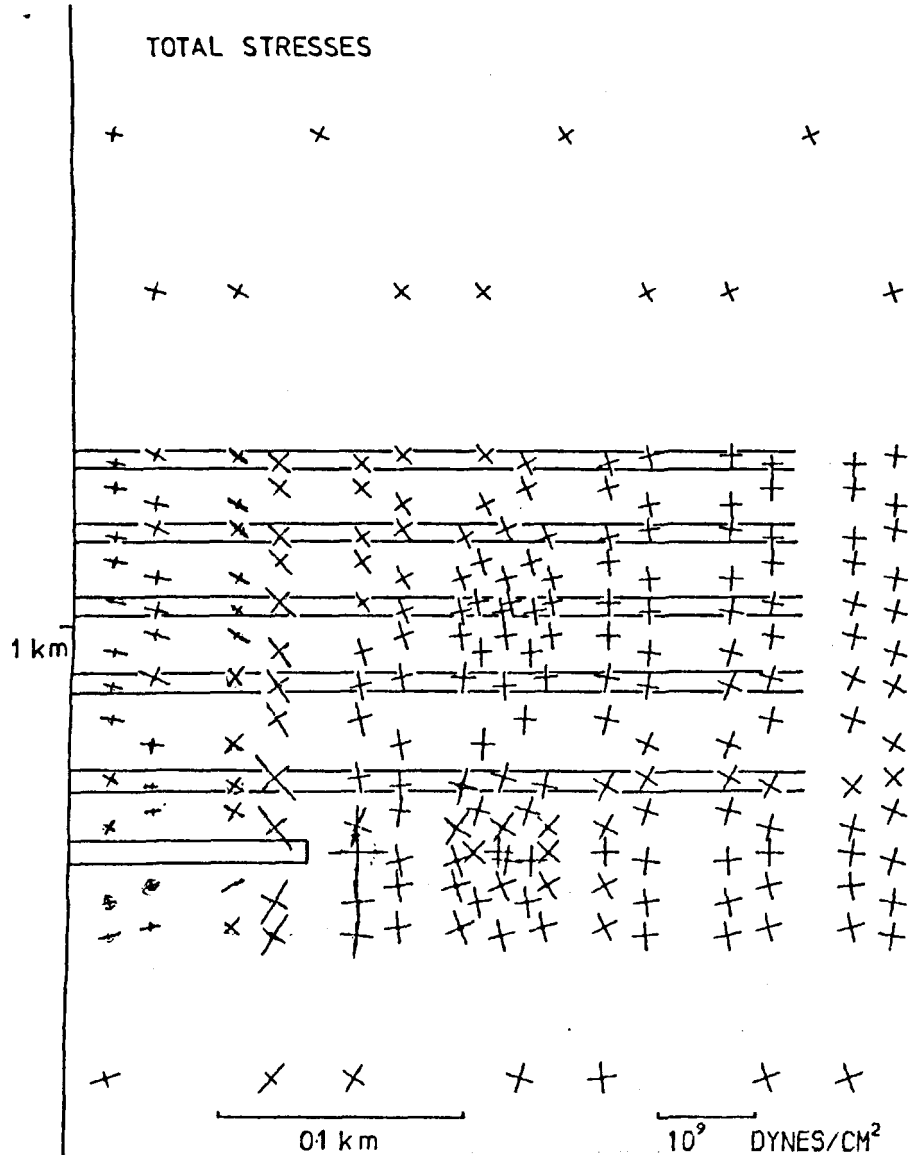

Figure 7.28 Stresses induced by a mine 200m in length beneath a series of high Poisson's Ratio layers.

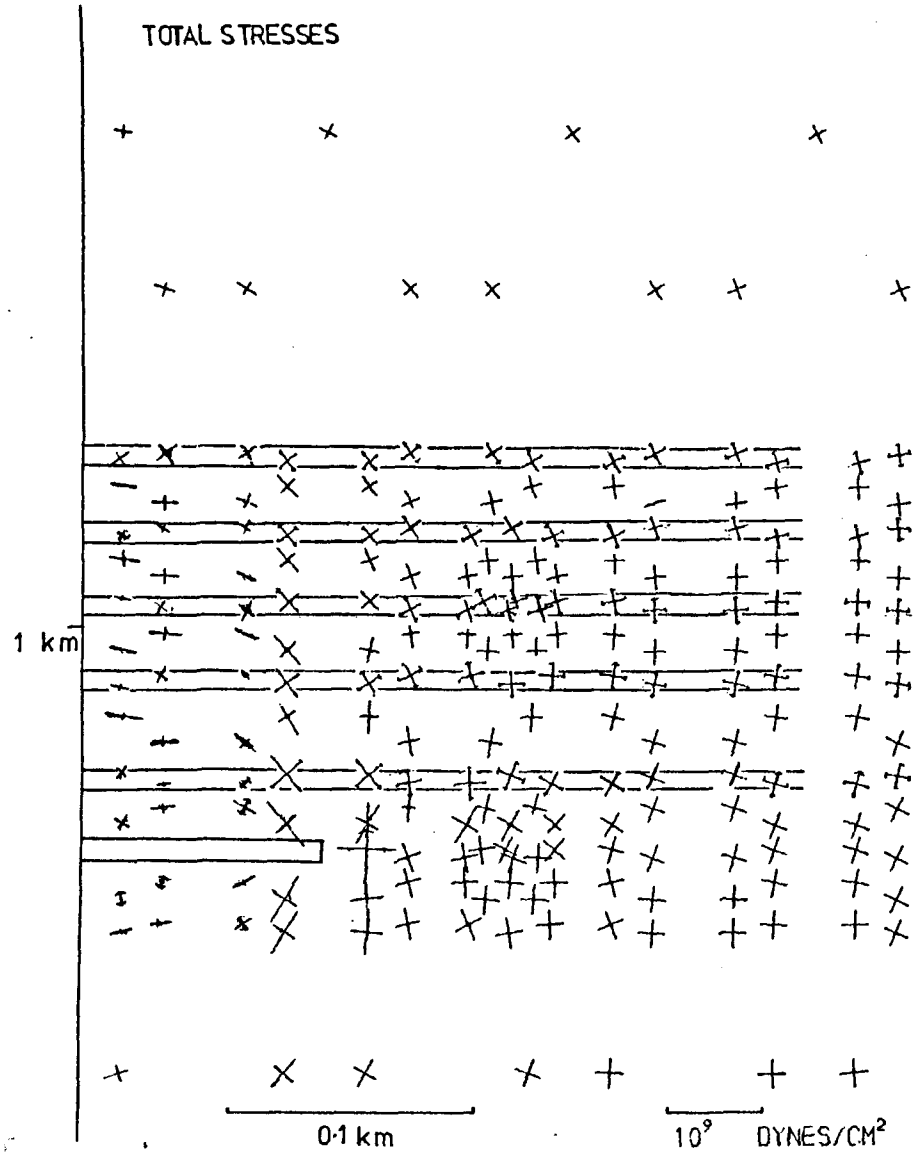

Figure 7.29 Stresses induced by a mine 200m in length beneath a series of viscous layers.

incompatible with large stress accumulation. The surrounding layers, on the other hand, may be subjected to significantly different stress changes. Two approaches were used to model these effects. Both used the same layering pattern as in Fig. 7.27, but assigned different properties to the layer elements. In the first case, the effect simply of assigning a high Poisson's Ratio (0.45) to the layers was looked at: the results are shown in Fig. 7.28. Very little change in either the extent or magnitude of the stress field (compared to Fig. 7.6) can be seen, but it does become slightly wider. In general the stresses in the soft layers are about one third of those in the harder layers.

A second model was tried where the stresses in the layers were allowed to relax visco-elastically to some extent. A viscosity of 10^{17} poise was assigned to them (compared to 10^{60} poise for the surrounding rock), and the model was run for the equivalent of ten time steps. The shear stresses in the layers, as a result of this, became of the order of one quarter the surrounding stresses, although the normal stresses were not greatly different (Fig. 7.29). The maximum shear stresses of the surrounding rock show a large increase around the mine edge, of about 20%. This increase affects greatly only the isobars of 50 bars and above, and the total vertical extent of the field is not changed (compared to Fig. 7.6). There is however a notable increase in the lateral extent of the field above the mine. This type of layering, then, is certainly a mechanism by which interactions between one mine and others in the vicinity could be increased. The main effect, however, only seems to be significant when close approaches to the working are made.

7.8 Conclusions

Numerical modelling of the stresses around an underground excavation is subject to many complications. The most important of these are effects due to creep and the fractured nature of the mining medium, which make

unsuitable the assumption of elastically induced stresses, and the geometry of the longwall mine, which conflicts with the assumption of plane-strain. Despite these drawbacks it is possible, however, using results for the maximum possible stresses, to obtain qualitative information regarding the nature of the outer parts of the induced stress field. By these means the relative interactions of one working with other workings, or with planes of weakness, in the vicinity, can be examined.

The stress field associated with a slit-like excavation extends primarily in the vertical direction, to a distance approximately 1½ times its length, or width. The nature of this stress field is little altered by overall changes in elastic constants, but has a different character when imposed upon an original horizontal tectonic stress field. The curvature of the stress trajectories means that compressional and tensional fields will affect the induced stress field in different ways. A compressional stress hardly changes the outer parts of the stress field, but does cause concentrations around the mine edges. A tensional tectonic stress, however, means that the outer parts of the field do not become as unstable as in other cases, and interaction in these regions will therefore be less marked.

Although the stresses associated with a pillar are very great in the pillar itself, they do not have a very far-reaching effect unless other workings are excavated either above or below. The particular location of these workings in relation to the lateral position of the pillar is however also important in determining the nature of any interaction. In fact, the stresses 'transmitted' by the pillar quickly disperse beneath it, and it is the shear stress fields associated with edges of the workings which interact with other mines. Mining wholly above or beneath another mine does not tend to intensify stresses since these are partly compensated for by convergence of the upper mine. Mining so that a partial overlap of the edge stresses occurs can however result in critically large combinations of the two stress fields.

The conclusions above apply to homogeneous rock masses. The stratified nature of coal measure sequences results in slightly different configurations of induced stress. The presence of harder layers, for instance, such as sandstone beds, can result in high shear stresses. Soft, pliable layers tend to produce significant increases in the supporting rock stress field, both in lateral extent and in the maximum shear stresses around the mine.

Both the presence of thin sandstone beds, and mining activity beneath and above the edges of previous workings are factors common to the N. Staffordshire mining tremors (Kusznir et al., 1980). The results in this chapter indicate that these may well be the mechanisms behind the seismicity there. They do not however explain the distribution of hypocentres ranging from the level of the seam almost up to the surface, i.e. to a distance well beyond the effective length of the workings (noting that the examples in this chapter give maximum stresses). As the effects of geological layering are to reduce the vertical extent of the stress field, it is thought that these must be due to a vertical series of settling movements and 'readjustments' to the tremors occurring at seam level.

Models are undeniably beautiful, and a man may justly proud to be seen in their company. But they may have their hidden vices. The question is, after all, not only whether they are good to look at, but whether we can live happily with them.

A. Kaplan

CHAPTER 8

DISCUSSION AND CONCLUSIONS

8.1 Mechanisms of Reservoir-Induced Seismicity

Previous attempts to calculate reservoir-induced stresses have ignored the probable pre-existing stress state caused by erosion of the topography. This omission is important since, as it has been shown here, the impounding of a reservoir in a valley with an associated elastic stress field invariably results in a partial stabilisation of the underlying stress state. This is so whatever the sign of any initial tectonic stress may be, and whatever stress concentrations have been caused by geological inhomogeneity. However, evidence has been presented that the occurrence of seismicity is sensitive to the depth of the water. This could be considered surprising because, even assuming that destabilisation occurs, the models presented indicate maximum changes in shear stress of no more than 8 bars, and usually less than 3 bars. Moreover, for more than one third of seismic reservoirs, activity was induced when the water level was below 100 m; Camarillas was only 30 m deep when the first tremors were felt. The vertical extent of the induced stress field can also be very limited: a 125 m deep reservoir in a valley of slope 18° produces a shear strength change of 1 bar down to 1400 m only. Wider reservoirs can penetrate the depths associated with the major induced shocks however.

It is most usual for at least a low level of seismicity to commence within a month of impounding, a fact which may often have been missed at many inadequately monitored reservoirs. This type of seismicity, directly linked with the initial loading will have seismic parameters typical of upper crustal earthquakes. Comninakis et al. (1967) have shown that the seismic parameters for shallow seismicity correspond with those for heterogeneous media: 'b' values are usually found to decrease markedly and fairly

consistently with depth. The shallowness of these induced earthquakes is thus most probably the major cause of the high 'b' values and Mogi Type II and III sequences usually recorded. Vibrations, stress redistribution and pore pressure flowage resulting from these minor shocks or swarms could then trigger movement on faults deeper than those directly affected by the load stresses, and the aftershock sequences would then have the lower 'b' values normally associated with deeper, natural earthquakes.

This however begs the question of the original triggering mechanism. The effects of the subsequent expanding of the pore pressure front created by hydraulic continuity between the reservoir and the formation fluids is often invoked to explain the time lags which range from zero (e.g. at Kurobe) up to 12 months (Hsinfengkiang) or more. Simple diffusion of the pore pressure through the foundation rocks would explain this time lag, and account for a reduction in effective stress. However, the amount of fracturing present is very important: although the diffusion process is accelerated considerably by their presence, their deformability results in a marked reduction in the resulting effective stress changes. Another effect, which often reduces the initial load stresses, is that of the initial pore pressure rise due to pore compression. This results in a (partial) negation - maybe of the order of 60% - of the initial load stresses, and hence often a reduction in the initial stabilisation depending on the sign of tectonic stress. In fact, as the load stresses for steep valleys (slope less than $\tan^{-1} \frac{1}{2}$) approximate to a vertical compression only, the horizontal change of effective stresses due to loading may become significantly tensile. Fig. 8.1 compares these effects for a point directly beneath the valley bottom, with the classical description of the imposition of an elastic water load and the subsequent pore pressure radiation, in terms of Mohr diagrams. The changes in effective stress have been calculated here using $\gamma = 1.0$ in eqn. 5.1.10. The consideration of these effects always results in initial load stresses being closer to the failure state than in the

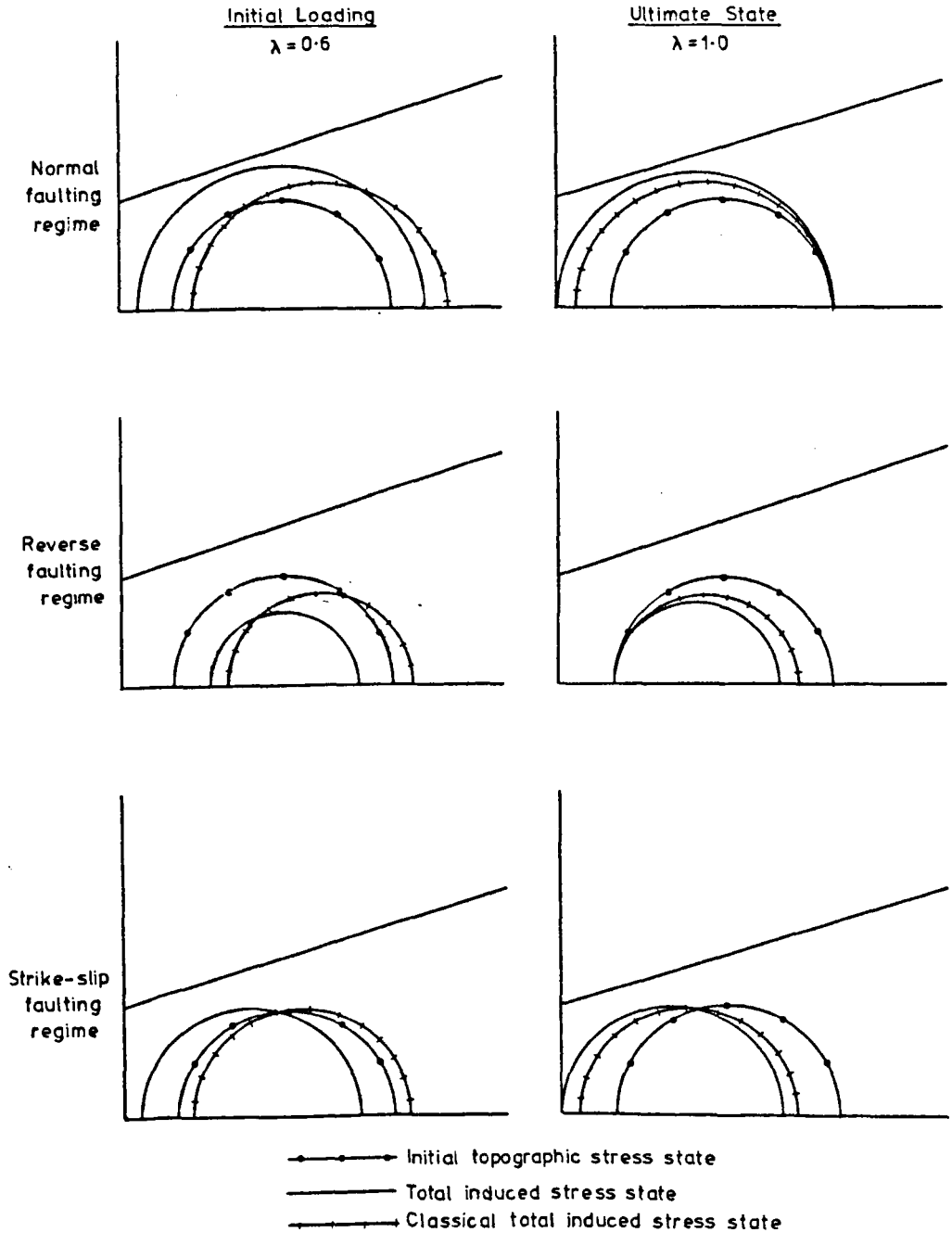

Figure 8.1 Mohr diagrams showing effects of initial and ultimate increases in pore pressure upon effective stresses beneath a reservoir.

classical case (except for reverse faulting regimes). For strike-slip regimes this means that there is now the possibility of failure - which is directly opposed to the classical conclusions. For normal faulting the difference is that now there is destabilisation regardless of the friction coefficients on faults. In this way then, the impounding of a reservoir can induce immediate seismogenic instability. The conclusions for the ultimate (after a long time period) state however, are similar to the classical case, except that now the pore pressure effects are distinctly larger. This effect is dependent on the particular form of the load stress at the point in question, and may be not quite so marked for shallow valleys or points laterally distant from the valley bottom. In most circumstances the consideration of initial induced pore pressure and the particular form of the water load results in a greater destabilisation effect throughout the diffusion time period. Also, it must be noted, points further from the reservoir would not be subject to such a large amount of stabilisation, but might still be affected, after a long while, by the full effective stress reduction.

Other considerations also can explain why instability results. One is the allowance for relaxation of the erosional stresses. Another is to consider the possibility that stresses have already been released by fracturing. Although any geological factors which are relevant in determining the occurrence of reservoir-induced seismicity are neither necessary nor sufficient (i.e. they are of several types), the presence of thin, harder layers of rock might well result in erosional stress-relieving fracture. In this way the potential stress build-up is never realised, and the ensuing reservoir load and pore pressure effects can then produce normal faulting where there was originally a reverse faulting regime.

Different factors are behind the initiation of seismicity (e.g. the closeness of the initial stresses in the rock to rock strength) and the eventual magnitude, which is governed by the initial rock strength and/or

the amount of tectonic stress. However, the three M > 5 earthquakes and many smaller shocks which occurred at Koyna, mean that probably at least some of the energy was derived from the previously existing tectonic stress. The smaller activities, however, e.g. at Clark Hill or Manic 3, may well have used strain energy provided totally by the water load. The relative concentration of seismic reservoirs in the younger orogenic belts, however, indicates that even for many of these smaller activities, tectonic stress is a vital factor, although this is probably equally a result of the relative weakness of faults in these regions of high shear stress.

8.2 Practical Modelling of Reservoir Influence

Modelling of an actual case history is a process beset with pitfalls. Firstly, it is important not to model the body force loads as though they are purely the result of gravity upon a confined elastic body. An initial state of stress, more likely to be lithostatic, or even with a horizontal stress greater than the vertical, must be assumed. The use of a density contrast method is also to be recommended in order to reduce numerical error. There are four major obstacles to the practical modelling of the mechanisms of reservoir-induced seismicity:

1. Insufficient geological knowledge.
2. Insufficient knowledge of the initial state of stress.
3. Insufficient grid resolution available.
4. (In many cases) - Inapplicability of a plane-strain assumption.

Initial stresses are always poorly known, particularly where there are significant residual stress systems, and the situation is not improved by the use of various measurement techniques. Hydrofracture appears the most relevant to the stress state pertaining to fracture on a fault plane, but this unfortunately requires the assumption that one principal stress is vertical and equal to the weight of the overburden. Use of an additional method to render this unnecessary would improve the situation considerably.

Stress behaviour with depth is usually close to linear, but geological influences govern the rate of increase. Geological influence also appears to control the ratio of vertical to average horizontal stress. Combined use of these behaviours can be used at present to avoid the assumption of unnatural initial stress states, but this will probably not be of great practical importance until the relation of geologic environment to the stress behaviours is better understood.

The accuracy of any modelling is limited by computer storage and the need for aspect ratios of less than 5. It is thus not possible to faithfully simulate all the mechanical variations in potential hypocentral regions, even if sufficient information concerning the cross-sectional geology were available. It is possible however, especially if use of a double, or even triple grid system is made, to model a characteristic generalisation of what are suspected to be the salient geological features for a particular case.

The limitations of practical modelling are such that little further information can be gained at present, particularly as the induction mechanisms are still poorly understood. Numerical methods are better suited to the analysis of theoretical situations in order to throw light upon the mechanisms themselves, so that any practical modelling can in future be carried out with greater purposefullness.

8.3 Suggestions for Further Work

Further theoretical work using numerical modelling should ideally be able to simulate:

(a) pore and fracture compressibility and effective stress interaction,

(b) differential pore water flow and storage in the fractures and porous rock matrix,

(c) body force influence on diffusional behaviour (thus including effects of water table depth),

(d) effects of changing water load with time,

(e) anisotropic rock material, and

(f) partial relaxation of elastic stress by creep and brittle fracture.

These could be accomplished by using coupled pore-pressure (e.g. Duguid, 1973) and visco-elastic stress finite element programs, in a way similar to Gale et al. (1974). The results should be expressed in terms of 'strength' changes, where strength is expressed as the distance between the Mohr circle and the failure criterion. This would represent the most adequate way to examine theoretically the effects of reservoir imposition upon a pre-stressed, fractured and porous foundation rock mass. Advances in rock mechanics, especially that part concerned with earthquake initiation, will provide better guides for the exact formulation of these programs. In the meantime, preparatory work for the construction of reservoirs should include detailed surveys of the geology, hydrology and stress-state of the area, with the possibility of induced seismicity in mind. If hydrofracture experiments were carried out, this would not only given an idea of the ambient stress field, but would also provide immediate knowledge concerning the amount of pore pressure needed to create instability. The presence of fault and joint planes in the foundation rock would mean that this latter figure would be strictly a maximum, and large-scale experiments on the fault surfaces would then give a better idea of the in situ rock strength. Also, a low water table should be regarded as a potential mechanism for pore pressure increases greater than the reservoir head. This information, combined with continual seismic observation (especially determination of focal depths) would not only aid the engineers on the site in question, but could be extremely valuable in understanding at least one of the mechanisms responsible for reservoir-induced seismicity.

BIBLIOGRAPHY

ABEL, J. F. and LEE, F. T., 1973. Stress changes ahead of an advancing tunnel. Int. J.Rock.Mech.Sci.Geomech.Abstr., Vol. 10, 673-97.

ADAMS, R. D., 1974. Earthquakes near Mangla dam. Bull.Seis.Soc.Am., 62, (6), 1787.

ALBRITTON, O., 1964. Residual stresses in a weld with one free surface. Welding J.Res.Suppl., Feb. 1964, pp.1-6.

AL-SAIGH, N. H., 1981. Mining-Induced Seismicity in the North Staffordshire Coalfield. Ph.D. Thesis, University of Keele, Staffs.

ANDERSON, R. E., 1973. Late Cenozoic tectonic setting of Lake Mead, Nevada, Arizona, U.S.A. Int. Colloq. on Seismic Effects of Reservoir Impounding, March 1973, The Royal Soc., London, pp.151-152 (summaries).

ANTSYFEROV, M. S., 1966. Seismo-acoustic methods in mining. Inst.Mining., Acad.Sci. USSR, Moscow. Transl. from Russian by S. E. Hall. Trans. editor G. E. KELLER, Colorado School of Mines.

BALAKRISHNA, S. and GOWD, T. N., 1970. Role of Fluid Pressure in the Mechanics of Transcurrent Faulting at Koyna (India), Tecton., 9, 301-321.

BARLA, G., 1972a. A method for the analysis of stress in brittle rock. Int.J.Rock Mech.Min.Sci., 9, 87-102.

BARLA, G., 1972b. Stresses around a single underground opening near a traction-free surface. Int.J.Rock Mech.Min.Sci., 9, 103-126.

BARLA, G. and BOSHKOV, S. H., 1969. Two-dimensional photoelastic analysis of gravity-loaded rock structures using gelatine mixture models. Trans.Am.Inst.Min.Metall.Engrs., 244, 99-115.

BARNES, B. K., DUNRUD, C. R., and HERNANDEZ, J., 1969. Seismic activity in the Sunnyside Mining District, Utah, during 1967. Openfile Report No. R290 (U.S. Geol. Surv., Ed.) pp.26-32.

BATH, M., 1965. Lateral inhomogeneities in the upper mantle. Tecton., 2, 483-514.

BAULE, H. and RAO, M. V. M. S., 1979. Seismoacoustic activity in a coal seam and relevance to destressing. Rock Mechanics, 11, 177-87.

BELL, M. L. and NUR, A., 1978. Strength changes due to reservoir-induced pore pressure and stresses and application to Lake Oroville. J. Geoph.Res., 83, (139),4469-83.

BERG, E., 1968. Relation between earthquake foreshocks, stress and main-shocks. Nature, 219, 1141-1143.

BIOT, M. A., 1941. General theory of three-dimensional consolidation. J.Appl. Phys., 12, 155-164.

BIOT, M. A. and WILLIS, D. G., 1957. The elastic coefficients of the theory of consolidation. J.Appl.Mech., 24, p.594.

BIRCH, F., 1966. In: 'Handbook of Physical Constants', Memoir 97, Geol. Soc.Am. (S. P. Clark, Ed.), Section 7.

BISHOP, A. W., 1973. The influence of an undrained change in stress on the pore pressure in porous media of low compressibility. Geotechnique, 23, 435-442.

BISHOP, A. W., 1974. The strength of crustal materials. Eng.Geol., 8, 139-153.

BOIKO, G. K., 1966. Relation between rock pressure diagrams and the seismo-acoustic conditions in a coal seam. In: 'Seismo-acoustic Methods in Mining'. Transl. from Russian by S. E. Hall. Transl. Ed. G. E. KELLER, Consultants Bureau, New York, 75-78.

BORECKI, M. and KIDIBINSKI, A., 1970. Coal strength and bearing capacity of coal pillars. Proc. 2nd Congr. I.S.R.M., 3-21, Belgrad, Yugoslavia.

BOZOVIC, A., 1974. Review and appraisal of case histories related to seismic effects of reservoir impounding. Eng.Geol., 8, 9-27.

BRACE, W. F., 1961. Dependence of fracture strength of rocks on grain size. Bull.Min.Ind.Exp.Sta., Pennsylvania State Univ., 72, 99-103.

BRACE, W. F., 1974. Experimental Studies of Seismic Behaviour of rocks under crustal conditions. Eng.Geol., 8, 109-127.

BRADY, B. T., 1970. Effect of the intermediate principal stress on the fracture of brittle rock. Proc. 11th Symp. Rock Mech., Univ. California, pp.267-279.

BROWN, E. T. and HOEK, E., 1978. Trends in relationships between measured in-situ stresses and depth. Int.J.Rock Mech.Min.Sci. and Geomech. Abstr., 15, 211-215.

BUCKLE, F., 1965. Rockburst Hazard in the Wright-Hargreaves Mine at Kirkland Lake, Ontario. Can.Min.J., 86, (9), 81-7.

BULIN, N. K., 1971. The present stress field in the upper parts of the crust. Geotectonics, 3, 133-139.

BYERLEE, J. D., 1971. Mechanical behaviour of the Weber sandstone. EOS, Trans.Am.Geophys. Union, 52, p.343 (abstract).

BYERLEE, J. D. and BRACE, W. F., 1968. Stick-slip, stable sliding and earthquakes-effect of rock type, pressure, strain rate and stiffness. J.Geoph.Res., 73, (18), 6031-7.

CARDER, D. S., 1945. Seismic investigations in the Boulder Dam area, 1940-1944, and the influence of reservoir loading on local earthquake activity. Bull.Seis.Soc.Am., 35, 175-192.

CARDER, D. S., 1968. Reservoir loading and local earthquakes. Proc. 6th Ann.Eng.Geol. and Soils Eng. Symp., Boise, Idaho, pp.225-241.

CAZALET, P., 1920. Notes on the study of records of earth tremors on the Central Rand. J.S.A. Inst. Engineers, 18, 211-28.

COMNINAKIS, P., DRAKOPOULOS, J., MOUMOULIDIS, G. and PAPAZACHOS, B. C., 1968. Foreshock sequences of the Kremasta earthquake and their relation to the water loading of the Kremasta artificial lake. Ann.Geofis. (Rome), 21, 39-71.

COOK, N. G. W., 1962. Seismic location of rockbursts. Rock Mechanics, Proc. 5th Symp., May 1962, pp.493-516.

COOK, N. G. W., HOCK, E., PRETORIUS, J. P. E., ORTLEPP, W. D. and SALAMON, M. D. G., 1966. Rock mechanics applied to the study of rockbursts. J.S. African Inst.Min.Metall., July 1966, 695-714.

CORNET, C. and FAIRHURST, C., 1972. Variation of pore volume in disintegrating rock. Proc. Symp. on Percolation Through Fissured Rocks. Deutsche Gesellschaff fur Erd-und Grundbau, Stuttgart, T2-A1, 1-8.

DAVISON, C., 1924. A History of British Earthquakes. Cambridge Univ. Press.

DIAB, B., 1976. Une explication de l'origine de l'energie liberee lors des seismes induits par le remplissage de certains lacs-barrages (in French) Eng.Geol., 10, 283-292.

DONACHIE, M. and NORTON, J., 1962. X-ray studies of lattice strains under elastic loading. Trans.ASM, Vol. 55, 51-57.

DUGUID, J. O., 1973. Flow in fractured porous media. Ph.D. Thesis, Princetown Univ., Civil Eng.

EDMOND, O. and MURRELL, S. A. F., 1971. Experimental observations on rock fracture at pressures up to 7 kbar and the implications for earthquake faulting. Tecton., 16, 71-87.

EVANS, D. M., 1966. The Denver area earthquakes and the Rocky Mountain arsenal disposal well. Mountain Geologist, 3, (1), 23-26.

FRIEDMAN, M., 1966. Measurement of the state of residual elastic strains by X-Ray diffractometry. Trans. AGU, 47, 190.

FRIEDMAN, M., 1972. Residual elastic strain in rocks. Tecton., 15, 297-330.

FRIEDMAN, M. and LOGAN, J. M., 1970. The influence of residual elastic strain on the orientation of experimental fractures in three quartzose sandstones. J.Geoph.Res., 75, 387-405.

GALANOPOULOS, A. G., 1967. The influence of the fluctuation of Marathon Lake elevation on local earthquake activity in the Attica Basin area (in Greek). Annales Geol. Pays Helleniques, 181, 281-306.

GALE, J. E., TAYLOR, R. L., WITHERSPOON, P. A. and AYATOLLAHI, M. S., 1974. Flow in rocks with deformable fractures. In: 'Finite Elements in Flow Problems', pp.583-598.

GANE, P. G., 1939. A statistical study of the Witwatersrand earth tremors. J.Chem., Metall. and Mining Soc. of S.Africa, pp.155-171.

GANE, P. G., HALES, A. L. and OLIVER, H. A., 1946. A seismic investigation of Witwatersrand earth tremors. Bull.Seis.Soc.Am., 36, 49-80.

GANE, P. G., SELIGMAN, P. and STEPHEN, J. H., 1952. Focal depths of Witwatersrand tremors. Bull. Seis.Soc.Am., 42, (3), 239-50.

GARG, S. K. and NUR, A., 1973. Effective stress laws for fluid saturated porous rocks. J.Geoph.Res., 78, (26), 5911-21.

GEERTSMA, J., 1957. The effect of fluid pressure decline on volumetric changes of porous rocks. Trans. AIME, 210, p.331.

GEOLOGICAL SURVEY OF INDIA, 1968. A Geological Report on the Koyna Earthquake of 11th December, 1967. Calcutta, pp.242.

GIBOWICZ, S., 1963. An energy classification of underground tremors in U. Silesia and their frequency of occurrence in relation to energy level. Archiwum Gornictva, 8, (1), 17-41.

GOUGH, D. I., 1969. Incremental stress under a two-dimensional artificial lake. Can.J.Earth Sci., 6, 1067-1075.

GOUGH, D. I., 1976. 'Induced Seismicity'. Unpublished preprint.

GOUGH, D. I. and GOUGH, W. I., 1970a. Stress deflection in the lithosphere near Lake Kariba - I. Geoph.J.Roy.Astro.Soc., 21, 65-78.

GOUGH, D. I. and GOUGH, W. I., 1970b. Load induced earthquakes at Lake Kariba - II. Geoph.J.Roy.Astro.Soc., 21, 79-101.

GOURINARD, Y., 1952. Le barrage de L'Oued Fodda. La geologie et les problemes de l'eau en Algeire. 19th Congr. Geol. Int., C.R., 1, 155-181.

GREEN, R. W. E., 1974. Seismic activity observed at the Hendrik Verwoerd dam. Paper presented at: Int. Colloq. on Seismic Effects of Reservoir Impounding. The Royal Co., London, March 1973. Communicated to J.Eng.Geol.

GRIFFITH, A. A., 1920. The phenomena of rupture and flow in solids. Phil.Trans.Roy.Soc., London, A, 221, 163-198.

GUBIN, I. E., 1969. Koyna Earthquake of 1967. Bull.Inst.Seism. Earthquake Eng., 6, 45-62.

GUHA, S. K., GOSAVI, P. D., AGARWAL, B. N. P., PADALE, J. G. and MARWADI, S. C., 1974. Case histories of some artificial crustal disturbances. Eng.Geol., 8, 59-77.

GUPTA, H. K., MOHAN, I. and NARAIN, H., 1972c. The Broach earthquake of March 23, 1970. Bull.Seis.Soc.Am., 62, 47-61.

GUPTA, H. K., NARAIN, H., RASTOGI, B. K. and MOHAN, I., 1969. A study of the Koyna earthquake of December 10, 1967. Bull.Seis.Soc.Am., 59, 1149-1162.

GUPTA, H. K. and RASTOGI, B. K., 1974. Investigations of the behaviour of reservoir-associated earthquakes. Eng.Geol., 8, 29-38.

GUPTA, H. K. and RASTOGI, B. K., 1976. 'Dams and Earthquakes', Developments in geotechnical engineering, Vol. II. Elsevier Scientific Publishing Co., pp.229.

GUPTA, H. K., RASTOGI, B. K. and NARAIN, H., 1972a. Common features of the reservoir-associated seismic activities. Bull.Seis.Soc.Am., 62, (2), 481-492.

GUPTA, H. K., RASTOGI, B. K. and NARAIN, H., 1972b. Some discriminatory characteristics of earthquakes near Kariba, Kremasta and Koyna artificial lakes. Bull.Seis.Soc.Am., 62, (2), 493-507.

HABIB, P. and MARCHAND, R., 1952. Mesures des pressious de terrain par l'essai de verin plat. Annis.Inst.Tech.Batim. Série sols et fondations x. 5th ann. No. 58, 967-971.

HAGIWARA, T. and OHTAKE, M., 1972. Seismic activity associated with the filling of the reservoir behind the Kurobe Dam, Japan, 1963-70. Tecton., 15, 241-254.

HAIMSON, B. C., 1968. Hydraulic fracturing in porous and non-porous rock and its potential for determining in-situ stresses at great depth. Ph.D. Thesis, Univ. of Minn., Minneapolis - St.Paul.

HAIMSON, B. C., 1978. The hydrofracturing stress measuring method and recent field results. Int.J. Rock Mech.Min.Sci., 15, 167-178.

HANDIN, J., 1958. Effects of pore pressure on the experimental deformation of sedimentary rocks under high pressure: tests at room temperature on dry samples. Am.Assoc.Pet.Geol.Bull., 41, 1-50.

HANDIN, J., 1966. In: 'Handbook of Physical Constants', Memoir 97, Geol. Soc.Am. (S. P. Clark, Ed.), Section 11.

HANDIN, J. and RALEIGH, C., 1972. Man-made earthquakes and earthquake control. Proc.Symp.Int.Soc.Rock Mech., Stuttgart, T2-D, pp.1-10.

HARDY, H. R. and MOWNEY, G. L., 1976. Study of microseismic activity associated with a longwall coal mining operation using a near-surface array. Eng.Geol., 10, 263-281.

HAST, N., 1958. The measurement of rock pressure in mines. Arsb.Sver. Geol.Unders., 52.

HAST, N., 1969. The state of stress in the upper part of the earth's crust. Tecton., 8, 169-211.

HAST, N., 1973. Global measurements of absolute stress. Phil.Trans.Roy. Soc., London, A., 274, 409-419.

HAXBY, W. F. and TURCOTTE, D. L., 1967. Stresses induced by the addition or removal of overburden and associated thermal effects. Geology, 4, 181-184.

HEALY, J. H., HAMILTON, R. M. and RALEIGH, C. B., 1970. Earthquakes induced by fluid injection and explosion. Tecton., 9, 205-214.

HEALY, J. H., RUBEY, W. W., GRIGGS, D. T. and RALEIGH, C. B., 1968. The Denver earthquakes. Science, 161, 1301-1310.

HERGET, G., 1973. Variation of rock stresses with depth at a Canadian iron mine. Int.J.Rock Mech. Min.Sci., 10, 37-51.

HODGSON, E. A., 1958. Rockburst Research 1938-45. Publication of the Dominion Observatory, Ottowa, Dominion Obs., Vol. XX, No. 1.

HOUSNER, G. W., 1970. Seismic Events at Koyna Dam. Proc. 11th Symp. Rock Mechanics, Univ. of Calif., Ch. 27, 541-558.

HOWARD, J. H., 1966. Structural development of the Williams Range Thrust, Colorado. Bull.Geol.Soc.Am., Memoir 97, 1247-1264.

HOWELLS, D. A., 1974. Time for a significant change of pore pressure. Eng.Geol., 8, 135-138.

HUBBERT, M. K. and RUBEY, W. W., 1959. Role of fluid pressure in mechanics of overthrust faulting. Bull.Seis.Soc.Am., 70, 115-166.

INDIAN STANDARDS INSTITUTION, 1967. 'Criteria for Earthquake-Resistant Design of Structures', Indian Standard 1893-1966, New Delhi, Nov. 1967.

ISAACSON, E. Dest.Q., 1957. Research into the rockburst problem on the Kolar Gold field. Mine and Quarry Engineer, Dec. 1957, 520-6.

IVANOV, V. S. and PARKISHOV, N. B., 1966. Seismo-acoustic method for determining the efficiency of measures to combat rockbursts. Openfile Rep. No. R290 (U.S. Geol.Surv., Ed.), pp.87-91.

JAEGER, J. C. and COOK, N. G. W., 1979. 'Fundamentals of Rock Mechanics', 3rd ed. Chapman and Hall, London, pp.593.

JAMIESON, D. B. and COOK, N. G. W., 1979. An analysis of the measured values for the state of stress in the earth's crust. J.Geoph.Res. (submitted).

JANCZEWSKI, E. W., 1950. The problem of underground tremors in the Polish coal basin and methods of studying the phenomena. Biuletin SlasKiej Stacji Geofizycznej w Raciborzu, ROK 1948, 25-55.

KAGAN, Y. Y. and LAVROV, I. M., 1966. Locating the sources of seismo-acoustic pulses in a coal seam. Openfile Rep. No. R290, (U.S. Geol. Surv., Eds.), pp.81-86.

KAILASAM, L. N., MURTHY, B. E. K. and CHAYANULU, A. Y. S. R., 1972. Regional Gravity Studies of the Deccan Trap areas of Peninsular India. Current Science, 41 (11), 403-407.

KIDIBINSKI, A. and BABCOCK, C. O., 1973. Stress distribution and rock fracture zones in the roof of a longwall face in a coal mine. Rock Mechanics, 5, 1-19.

KOTZE, T. J., 1970. Virgin rock stress measurements in the Evander gold field. C.O.M. Res. Rep. 30/70, Chamber of Mines of South Africa, Johannesburg, pp.33.

KROPOTKIN, K. N., 1972. The state of stress in the earth's crust as based on measurements in mines and on geophysical data. Phys.Earth Planet, Interiors, 6, 219-220.

KULPINSKI, J. et al., 1966. A micro-survey of bounces and tremors in the Miechowice mine. Przeglad Gorniczy, 12, 530-534.

KUSZNIR, N. J., 1976. Theoretical studies of the geodynamics of accretion boundaries in plate tectonics. Unpublished Ph.D. Thesis, Univ. of Durham.

KUSZNIR, N. J., ASHWIN, D. P. and BRADLEY, A. G., 1980. Mining Induced Seismicity in the North Staffordshire Coalfield, England. Int.J. Rock Mech.Min.Sci. & Geomech.Abstr., 17, 45-55.

LANE, R. G.T., 1971. Seismic activity at man-made reservoirs. Proc.Inst. Civ.Eng., 50, (9), 15-24.

LEBLANC, G. and ANGLIN, F., 1978. Induced seismicity at the Manic 3 reservoir, Quebec. Bull.Seis.Soc.Am., 68, (5), 1469-1485.

LOCKNER, D. and BYERLEE, J. D., 1977. Hydrofracture in Weber sandstone at high confining pressure and differential stress. J.Geoph.Res., 82, 2018-26.

LOUIS, C., 1969. "A study of Groundwater Flow in Jointed Rock and its Influence on the Stability of Rock Masses", Rock Mechanics Research Rep. No. 10, Imperial College, Univ. of London, Sept. 1969.

McEVILLY, T. V., BAKUN, W. W. H. and CASSADAY, K. B., 1967. The Parkfield, California, earthquakes of 1966. Bull.Seis.Soc.Am., 57, 1221-1224.

McEVILLY, T. V. and CASSADAY, K. B., 1967. The earthquake sequence of September 1965 near Antioch, California. Bull.Seis.Soc.Am., 57, 113-124.

McGARR, A. and GAY, N.C., 1978. State of Stress in the Earth's Crust. Ann.Rev.Earth Planet Sci., 6, 405-36.

McHENRY, D., 1948. The effect of uplift pressure on the shearing strength of concrete. Trans.Int.Congr. large dams, 3rd, Stockholm, Vol. 1.

MICKEY, W. V., 1973. Reservoir seismic effects. In: W. C. Ackermann, G. F. White and E. B. Worthington (eds.) Geophys.Monog. series No. 17. Amer.Geophys.Union, Washington D.C., 472-479.

MOGI, K., 1962. On the time distribution of aftershocks accompanying the recent major earthquakes in and near Japan. Bull.Earthquake Res.Inst., 40, 107-124.

MOGI, K., 1963a. The fracture of a semi-infinite body caused by an inner stress origin and its relation to earthquake phenomena. Bull. Earthquake Res.Inst., 41, 595-614.

MOGI, K., 1963b. Some discussion on aftershocks, foreshocks and earthquake swarms. Bull.Earthquake Res.Inst., 41, 615-658.

MOGI, K., 1967. Effect of the intermediate principal stress on rock failure. J.Geoph.Res., 72, (20), 5117-5131.

MUNSON, R. C., 1968. Relationship of effect of waterflooding of the Rangely oil field on seismicity. Condensation of a thesis: 'An investigation of the seismicity in the vicinity of Rangely, Colorado. Colorado School of Mines.

MURRELL, S. A. F., 1958. Strength of coal under triaxial compression. In: 'Mechanical Properties of Non-Metallic Brittle Materials', W. H. Walton (Ed.), London, Butterworths.

MURRELL, S. A. F., 1962. A criterion for brittle fracture of rocks and concrete under triaxial stress, and the effects of pore pressure on the criterion. 5th Symp. Rock Mech., Univ. Minnesota, pp.563-577. Ed. C. FAIRHURST.

MURRELL, S. A. F., 1964. The theory of the propagation of elliptical Griffith cracks under various conditions of plane strain and plane stress I, II and III. Brit.J.Appl.Phys., 15, 1195-1223.

MURRELL, S. A. F., 1965. The effect of triaxial stress systems on the strength of rocks at atmospheric temperatures. Geol.J.Roy.Astro. Soc., 10, 231-281.

MURRELL, S. A. F. and DIGBY, P. J., 1970a. The theory of brittle fracture initiation under triaxial stress conditions - I. Geol.J.Roy.Astro. Soc., 19, 309-334.

MURRELL, S. A. F. and DIGBY, P. J., 1970b. The theory of brittle fracture initiation under triaxial stress conditions - II. Geol.J.Roy.Astro. Soc., 19, 499-512.

NEYMAN, B., 1955. The location of rockbursts in the coal mines of the Upper Silesian coal basin. Archiwum Gornictwa, 11, (1), 249-265.

NICHOLS, T. C. Jr., 1971. Deformations associated with Relaxation of Residual Stresses in the Barre Granite of Vermont. Thesis, Texas A. and M. Univ., College Station, Texas, pp.92.

NIKOLAEV, N. I., 1974. Tectonic conditions favourable for causing earthquakes occurring in connection with reservoir filling. Eng.Geol., 8, 171-189.

NOORISHAD, J., WITHERSPOON, P. A. and MAINI, Y. N. T., 1972. The influence of fluid injection on the state of stress in the earth's crust. Proc. Symp.Int.Soc.Rock Mech. 'Percolation through fissured rock'. T2-H, 1-11.

NUR, A., 1973. Role of pore fluids in faulting. Phil.Trans.Roy.Soc. London, 274, 297-304.

NUR, A. and BOOKER, J. R., 1972. Aftershocks caused by pore fluid flow? Science, 175, 885-887.

NUR, A. and BYERLEE, J. D., 1971. An exact effective stress law for elastic deformation of rock with fluids. J.Geoph.Res., 76, (26), 6614-6619.

OHTAKE, M., 1974. Seismic activity induced by water injection at Matsushiro, Japan. J.Phys.Earth, 22, 163-176.

OROWAN, E., 1948. Classification and nomenclature of internal stresses. Symp. on Internal Stresses, Ins.Metals, p.47-59.

OSTERWALD, F. W. and DUNRUD, C. R., 1966. Instrumentation study of coal mine bumps, Sunnyside District, Utah. Utah Geol. & Miner. Surv., Central Utah Coals. Bull., 80, Nov. 1966.

PAPAZOCHOS, B. C., 1971. Aftershock activity and aftershock risk in the area of Greece. Ann.Geofis. (Rome), 24, 439-456.

PAPAZACHOS, B. C., 1974. On the relation between certain artificial lakes and the associated seismic sequences. Eng.Geol., 8, 39-48.

PAPAZACHOS, B. C., COMNINAKIS, P., DRAKOPOULOS, J. and MOUMOULIDES, G., 1968. Foreshock and aftershock sequences of the Cremasta earthquake and their relation to the water loading of the Cremasta artificial lake. Seismol.Inst., Nat'l. Observ. of Athens, Athens, 39-71.

PATERSON, M. S., 1959. X-ray line broadening in plastically-deformed calcite. Philos.Mag., 4, 451-466.

PETROSYANT S, E. V. and GORBACHENKO, V. A., 1969. Seismo-acoustic study of the stability of the rocks above a mine working. Soviet Mining Science, 4, 391-394.

PHILLIPS, D. W., 1944-5. Rock bursts or bumps in coal-mines. Trans.Inst. Mining Engineers, Vol. CIV, 55-84.

PRICE, N. J., 1959. Mechanics of jointing in rocks. Geol.Mag., 96, 149.

PRICE, N. J., 1970. Laws of rock behaviour in the Earth's crust. In: 'Rock Mechanics - theory and practice'. Proc. 11th Symp. Rock Mech., Berkeley ,California. (Ed. W. H. Somerton) (Am.Inst.Min.Metall. & Pet.Eng., New York), 1-23.

RALEIGH, C. B., HEALY, J. H. and BREDEHOEFT, J. D., 1976. An experiment in earthquake control at Rangely, Colorado. Science, 191, 1230-1237.

RANALLI, G. and CHANDLER, T. E., 1975. The stress field in the upper crust as determined from in-situ measurements. Geol.Rundsch., 64, 653-74.

REYES, S. F. and DEERE, D. U., 1966. Elastic-plastic analysis of underground openings by the finite-element method. 1st Congr. Int.Soc. Rock Mech., Lisbon, 2, 477-483.

RICE, J. R. and CLEARY, M. P., 1976. Some basic stress diffusion solutions for fluid - saturated elastic porous media with compressible constituents. Rev.Geoph. and Space Phys., 14, 227-241.

RICH, V., 1980. Drilling Deeper. Nature, 287, (5785), 774.

RICHTER, C. F., 1958. 'Elementary Seismology'. W. H. Freeman and Co. Inc., San Francisco, 768 pp.

ROBSON, W. T., 1946. Rockburst incidence, research and control measures. Trans.Can.Inst.Min. & Metall. of the Min.Soc. of Nova Scotia. Vol. XLIX, pp.347-74.

ROTHE, J. P., 1968. Fill a lake, start an earthquake. New Scientist, 39, 75-78.

ROTHE, J. P., 1969. Earthquakes and reservoir loading. Proc. 4th World Conf. on Earthquake Eng., Santiago, Vol. A-1, 28-38.

ROTHE, J. P., 1970. Seismes artificiels (in French). Tecton., 9, 215-238.

ROTHE, J. P., 1973. Summary: Geophysics Report. Geophys. Monog. 'Man-made Lakes', 17, 441-454.

RUMMEL, F. and GOWD, T. N., 1973. Effect of interstitial fluid pressure on faulting in Ruhr Sandstone specimens. Int.Colloq. on Seismic Effects of Reservoir Impounding, March 1973. The Royal Society, London, pp.39 (summaries).

RYDER, J. A. and OFFICER, N. C., 1964. An elastic analysis of strata movement observed in the vicinity of inclined excavations. J.S.A. Inst. Min. and Metallurgy, 64, (6), 219-244.

SAVIN, G. N., 1961. Stress concentration around holes. Translated by E. Gros, Oxford, Pergamon.

SEBOR, G., RUDJEV, V., SIMANE, J. and ROCEK, V., 1976. Rockbursts and possibilities of their prevention. Proc. IXth World Mining Cong., F. D. Germany, May 1976, 11-14.

SERVICE, K. G. and DOUGLAS, A., 1973. Boundaries and fractures in finite element models of geological structures. Geophys.J.Roy.Astro.Soc., 32, 1-14.

SHEPHERD, R. and KELLET, W. H., 1973. Strata behaviour. Colliery Guardian, 221, (3), 93-102.

SIMPSON, D. W., 1976. Seismicity changes associated with reservoir loading. Eng.Geol., 10, 123-150.

SINCLAIR, W. E., 1936. Rockbursts - Their Causes and Prevention. J.Chem., Metall. and Mining Soc. of S.Africa, July 1936, 4-11.

SKEMPTON, A. W., 1960. Effective Stress in soils concrete and rocks. In: Pore pressure and suction in soils. London, Butterworths.

SMITH, R. B., WINKLER, P. L., ANDERSON, J. G. and SCHOLZ, C. H., 1974. Source mechanisms of microearthquakes associated with underground mines in Eastern Utah. Bull.Seis.Soc.Am., 64, (4), 1295-1317.

SNOW, D. T., 1972. Geodynamics of Seismic Reservoirs. Proc.Symp.Perc. Thro.Fiss.Rocks, Stuttgart, T2-J, 1-19.

SOBOLEV, G., SPETZLER, H. and SALOV, B., 1978. Precursors to failure in rocks while undergoing anelastic deformations. J.Geoph.Res., 83, 1775-1784.

SOBOLEVA, O. V. and MAMADALIEV, U. A., 1976. The influence of the Nurek reservoir on local earthquake activity. Eng.Geol., 10, 293-305.

STONELY, R., 1974. Evolution of the continental margins bounding a former southern Tethys. In: 'The Geology of Continental Margins', 889-903. Eds. C. A. Burk and C. L. Drake, Springer-Verlag, New York Inc.

STURGUL, J. R., SCHEIDEGGER, A. E. and GRINSHPAN, Z., 1976. Finite element model of a mountain massif. Geology, 4, 439-442.

SUKLJE, L., 1969. Rheological aspects of Soil Mechanics. Interscience, New York, p.123.

SUSSTRUNK, A., 1968. Erdstosse im Verzascatal beim Aufstau des Speicherbekens, Vagorno (in German). Verh.Schweiz. Naturforsch, Ges., 89-92.

SYKES, L. R., 1970. Seismicity of the Indian Ocean and a possible nascent island arc between Ceylon and Australia. J.Geoph.Res., 75, 5041-5055.

SYKES, L. R., FLETCHER, J. P. and SBAR, M. L., 1973. Contemporary stresses, intraplate earthquakes, and seismic risk associated with high-pressure fluid injection wells in New York State. Int.Colloq. on Seismic Effects of Reservoir Impounding, March 1973. The Royal Society, London, pp.46 (summaries).

TALWANI, P., STEVENSON, D., AMICK, D. and CHIANG, J., 1979. An earthquake swam at Lake Keowee, South Carolina. Bull.Seis.Soc.Am., 69, (3), 825-841.

TAYLOR, J. T. M., 1963. Research on ground control and rockbursts in the Kolar gold field, India. Bull.Inst. Min. and Metallurgy, 72, 317-338.

TERZAGHI, K. VAN., 1923. Die Berechnung der Durchlassigkeitsziffer des Tones aus dem Verlauf der hydrodynamischen Spannungserscheinungen. Sber.Akad.Wrss.Wien, 132, p.105.

TULLIS, T. E., 1977. Reflections on measurement of residual stress in rock. Pageoph., Vol. 115. In: 'Stress in the Earth', C.C.R.G. 3, M.Wyss (Ed.), 57-68.

TURCOTTE, D. L. and OXBURGH, E. R., 1976. Stress accumulation in the lithosphere. Tecton., 35, 183.

TURNER, M. J., CLOUGH, R. W., MARTIN, H. C. and TOPP, L. J., 1956. Stiffness and deflection analysis of complex structures. J.Aeron.Sci., 23, 805-854.

UTSU, T., 1969. Aftershocks and earthquake statistics, I. Some parameters which characterise an aftershock sequence and their interrelations. J.Fac.Sci., Hokkaido Univ., Ser. 7 (Geophysics), 3, 129-195.

VOIGHT, B., 1966. Beziehung zuischen grossen horizontalen spannungen im Gebirge und der Tektonik und der Abstragung. 1st Congr. Int.Soc. Rock Mech., Lisbon, 1966, Proc. 2, 51-56.

VOIGHT, B., 1967. Interpretation of in-situ stress measurements. Proc. 1st Conf.Int.Soc. Rock Mechanics, 3, 332-348.

VOIGHT, B. and SAMUELSON, A. C., 1968. On the application of finite-element techniques to problems concerning potential distribution and stress analysis in the earth sciences. Pageoph., 76, 40-55.

VOIGHT, B. and ST.PIERRE, B. H. P., 1974. Stress history and rock stress. Advances in Rock Mechanics, Part II. Proc. 3rd Congr. Int.Soc. Rock Mech., pp.580-582.

WANG, C. T., 1953. 'Applied Elasticity'. McGraw-Hill Publ. Co. Ltd., London.

WEERTMAN, J., 1974. Water flow paths around a dislocation on an earthquake fault. J.Geoph.Res., 79, (23), 3291-3293.

WHITTAKER, B. N., 1974. An appraisal of Strat Control Practice. Mining Engineer, 166, 9-24.

WHITTAKER, B. N. and PYE, J. H., 1975. Design and layout aspects of long-wall methods of coal mining. Proc. 16th Symp. Rock Mech., Sept. 22-24, 1975, University of Minnesota, Mineapolis, M.N., pp.198-209.

WIERZCHOWSKA, Z., 1962. New views on the origin of earth tremors in U. Silesia. Przeglad Gerniezy Pt (7-8), 18, 417-22.

WILSON, A. H. and ASHWIN, D. P., 1972. Research into the determination of pillar size. The Mining Engineer, 131, (141), 409-427.

WOROTNICKI, G. and DENHAM, D., 1976. The state of stress in the upper part of the Earth's crust in Australia according to measurements in tunnels and mines and from seismic observations. Investigation of Stress in Rock - Advances in Stress Measurement, pp.71-82. Preprints, Int. Soc. Rock Mech., Symp., Sydney.

ZIENKIEWICZ, O. C., 1977. 'The Finite Element Method'. 3rd ed. McGraw-Hill Book Co. (U.K.) Ltd., 787 pp.

ZOBACK, M. D. and POLLARD, D. D., 1978. Hydraulic fracture propagation and the interpretation of pressure-time records for in-situ stress determinations. Submitted to: 19th Symp. Rock Mech., Lake Tahoe, Calif., May 1978.

A P P E N D I C E S

Note

The programs listed in the following Appendices have been run successfully using the CDC FORTRAN Extended compiler on a CDC 7600. Standard FORTRAN compilers may require use of H format in output statements and use of double precision for all arrays involved in matrix operations. Also, all LEVEL 2 statements and the PROGRAM statement will have to be omitted.

The plotting subroutines are written using the GHOST graphical output system and may have to be substantially translated for use with other systems.

References

1. 'CDC FORTRAN Extended Reference Manual', publication no. 60497800.

2. 'GHOST Graphical Output System Manual (NW6)', North West Universities Document.

APPENDIX 1

Computer Generation of a Finite Element Grid

A simple rectangular grid for theoretical models can be easily generated by computer. The listing in this Appendix produces a grid suitable for the study of the effects of horizontal mines at depths of 950 m and 1050 m. A simpler version of the program can be used to prepare hand-drawn grid data.

INPUT DATA: The program does not read input data (unless using a hand-drawn grid), but changes in the grid are effected by altering the parameters indicated by 'Comment' statements in the listing.

INTERNAL PARAMETERS: The following are not specifically explained in the program listing:-

1. IDIM — is put equal to 0 if the plots produced by the main finite element program are to be of the entire grid, or equal to 1 if the plots are to be limited by the XMIN, XMAX, YMIN, YMAX (km) parameters.
2. P, E, DEN, VISC — are the arrays containing the Poisson's Ratios, Young's Moduli, densities and viscosities (all in C.G.S.) of all the elements.

OUTPUT DATA (Stream 6): The output data is specifically formatted to be read either by the finite element program FERBIS on stream 5 (see Appendix 4), by the preparatory program PREPFE on stream 5 (see Appendix 2), or by the pore pressure diffusion program on stream 5 (see Appendix 8).

```
C****** PROGRAM GRDGEN - GENERATES F.E. GRID
      PROGRAM GRDGEN(INFILE,FF6,OUTPUT,TAPE5=INFILE,TAPE6=FF6
     +,TAPE3=OUTPUT)
      DIMENSION X(500),Y(500),NODEL(1000,3),FORS(300),
     1 E(1000),P(1000),VISC(1000),FORST(1000),
     2 NS(50,3),XS(50),YS(50),DEN(1000),PP(500)
C*     TECTONIC STRESS
      TTS=0.0E8
C*     PLOT DIMENSIONS
      IDIM=1
      XMIN=0.0
      XMAX=0.5
      YMIN=-1.2
      YMAX=-0.6
C*     NO. OF VERTICAL NODES
      NN=13
      NE=NN-1
      NE2=NE*2
C*     INITIAL HORIZONTAL INTERNODAL SPACING
      STEP=0.05
C*     NO. OF HORIZONTAL NODES
      NREP=14
C*     SUBTRACTED DENSITY
      DENSUB=0.0
C*     CONSTRUCT FIRST COLUMN OF ELEMENTS
      K=1
      L=2
      N1=1
      N2=NN+1
      N3=2
      N4=NN+2
      DO 5 I=1,NE
      NS(K,1)=N1+I-1
      NS(K,2)=N2+I-1
      NS(K,3)=N3+I-1
      NS(L,1)=N2+I-1
      NS(L,2)=N3+I-1
      NS(L,3)=N4+I-1
      K=K+2
      L=L+2
    5 CONTINUE
      DO 10 I=1,NN
   10 XS(I)=0.0
C*     COORDINATES OF VERTICAL NODES
      YS(1)=0.0
      YS(2)=-0.25
      YS(3)=-0.5
      YS(4)=-0.7
      YS(5)=-0.85
      YS(6)=-0.95
      YS(7)=-0.96
      YS(8)=-1.0
      YS(9)=-1.05
      YS(10)=-1.06
      YS(11)=-1.13
      YS(12)=-1.24
      YS(13)=-1.4
C*     PROPAGATE GRID
      DO 15 I=1,13
      X(I)=XS(I)
```

```
   15 Y(I)=YS(I)
      K=NN
      HIT=STEP
      L=0
      DO 1 I=1,NREP
      DO 2 J=1,NN
      K=K+1
      X(K)=XS(J)+HIT
    2 Y(K)=YS(J)
C*     MODIFICATION OF HORIZONTAL INTERNODAL SPACING
      IF(I.GT.6) STEP=0.1
      HIT=HIT+STEP
      DO 3 J=1,NE2
      L=L+1
      DO 4 M=1,3
    4 NODEL(L,M)=NS(J,M)+(I-1)*NN
    3 CONTINUE
    1 CONTINUE
      NNOD=K
      NEL=L
      NHOL=0
      NBNOD=2*(NREP+NN-2)
C      ASSIGN ELASTIC CONSTANTS
      DO 200 I=1,NEL
      X0=(X(NODEL(I,1))+X(NODEL(I,2))+X(NODEL(I,3)))/3.0
      Y0=(Y(NODEL(I,1))+Y(NODEL(I,2))+Y(NODEL(I,3)))/3.0
C*     ROCK PROPERTIES
      VISC(I)=1.0E60
      P(I)=0.35
      E(I)=1.0E11
      DEN(I)=2.7
      IF(Y0.GT.-1.06.AND.Y0.LT.-1.05) GOTO 25
      IF(Y0.GT.-0.96.AND.Y0.LT.-0.95) GOTO 26
      GOTO 30
   26 IF(X0.GT.20.0.AND.X0.LT.0.35) GOTO 35
      IF(X0.GT.0.0.AND.X0.LT.0.15) GOTO 35
      GOTO 30
   25 IF(X0.LT.0.15) GOTO 35
      GOTO 30
C*     INSERT HARD LAYER
      E(I)=1.0E12
      P(I)=.25
      DEN(I)=2.7
      GOTO 30
C*     INSERT VOID
   35 DEN(I)=0.001
      E(I)=1.0E6
      P(I)=0.45
   30 CONTINUE
      IF(Y0.GE.-0.95.OR.Y0.LE.-0.96) GOTO 40
C      VISC(I)=1.0E17
      P(I)=0.45
   40 DEN(I)=DEN(I)-DENSUB
  200 CONTINUE
      WRITE(6,100) NNOD,NEL,NBNOD,NHOL,DENSUB
      WRITE(6,101) (I,X(I),Y(I),FORST(2*I-1),FORST(2*I),I=1,NNOD)
      WRITE(6,102) (I,(NODEL(I,J),J=1,3),E(I),P(I),DEN(I),VISC(I),
     1 I=1,NEL)
      WRITE(6,103) TTS,IDIM,XMIN,XMAX,YMIN,YMAX
  100 FORMAT(4I10,F10.3)
```

```
  101 FORMAT(I10,2F10.3,2E10.3)
  102 FORMAT(4I10,E10.3,2F10.3,E10.3)
  103 FORMAT(E10.3,I10,4F10.3)
      STOP
      END
****
```

APPENDIX 2

Preparation of the Finite Element Program

Program PREPFE listed in this Appendix reads the grid data produced by program GRDGEN (Appendix 1) from stream 5, and calculates the dimensions of all the arrays of variable size in the finite-element program FERBIS. It also prints the grid dimensions and the appropriate time steps to be used in the case of a visco-elastic analysis (stream 6). The grid data is listed to file CHDAT (stream 4) for possible subsequent plotting of the grid.

```
C******PROGRAM TO PRODUCE PARAMETERS AND ARRAY DIMENSIONS
C       PRIOR TO F.E. RUN
      PROGRAM PREPFE(OUTPUT,F5,CHDAT,TAPE5=F5,TAPE6=OUTPUT,TAPE4=CHDAT)
      DIMENSION X(500),Y(500),FORST(1000),NODEL(800,3),
     +E(800),P(800),DN(800),VISCOS(800)
      READ(5,1000) NNOD,NEL,NBNOD,NHOL,DS
 1000 FORMAT(2I10,2I10,F10.3)
      NNOD2=NNOD*2
      DO 5 I=1,NNOD
    5 READ(5,1005) K,X(K),Y(K),FORST(2*K-1),FORST(2*K)
 1005 FORMAT(I10,2E10.3,2E10.3)
      READ(5,1010) (L,(NODEL(I,J),J=1,3),E(I),P(I),DN(I),VISCOS(I),
     +I=1,NEL)
 1010 FORMAT(4I10,E10.3,2F10.3,E10.3)
      DEV=0.0
      XMAX=0.0
      XMIN=0.0
      YMAX=0.0
      YMIN=0.0
      TCRIT=1.0E60
      TCRIT1=0.0
      NBW=0
      DO 10 I=1,NNOD
      XMAX=AMAX1(XMAX,X(I))
      XMIN=AMIN1(XMIN,X(I))
      YMAX=AMAX1(YMAX,Y(I))
      YMIN=AMIN1(YMIN,Y(I))
   10 CONTINUE
      DO 15 I=1,NEL
      TEVIS=VISCOS(I)/E(I)/3600.0/24.0/365.5
      TCRIT=AMIN1(TCRIT,TEVIS)
      TCRIT1=AMAX1(TCRIT1,TEVIS)
      KB1=IABS(NODEL(I,1)-NODEL(I,2))
      KB2=IABS(NODEL(I,2)-NODEL(I,3))
      KB3=IABS(NODEL(I,3)-NODEL(I,1))
      MBW=MAX0(KB1,KB2,KB3,NBW)
      IF(MBW.NE.NBW) JEL=I
   15 NBW=MBW
      NBW=2*NBW+2
      NBW=2*NBW-1
      WRITE(6,1040)
      WRITE(6,1015)
 1015 FORMAT(2X,'FINITE ELEMENT GRID'/)
      NN=((NBW+1)*3)/2
      WRITE(4,1020) NNOD,NEL,DEV
 1020 FORMAT(2I10,F10.3)
      DO 20 I=1,NNOD
      WRITE(6,1030) I,X(I),Y(I)
   20 WRITE(4,1025) X(I),Y(I)
 1025 FORMAT(2E10.3)
 1030 FORMAT(I10,2F10.3)
      WRITE(6,1105)
      DO 25 I=1,NEL
      WRITE(6,1010) I,(NODEL(I,J),J=1,3),E(I),P(I),DN(I),VISCOS(I)
   25 WRITE(4,1035)(NODEL(I,J),J=1,3)
 1035 FORMAT(3I10)
      NBOR=1
      IBOR=1
      WRITE(6,1040)
 1040 FORMAT('1')
```

```
      WRITE(6,1045)
 1045 FORMAT(2X,'FINITE ELEMENT PROGRAM DIMENSIONS'/)
      WRITE(4,1050) NBOR
      WRITE(4,1050) IBOR
 1050 FORMAT(I10)
      WRITE(4,1055) XMAX,XMIN,YMAX,YMIN
 1055 FORMAT(4E10.3)
      WRITE(6,1060) NNOD2,NN
 1060 FORMAT(10X,'AT(',I3,',',I3,')'/)
      WRITE(6,1065) NNOD2
 1065 FORMAT(2X,'STIN,FORST,DISP ETC (',I3,')'/)
      WRITE(6,1070) NNOD,NNOD
 1070 FORMAT(10X,'X(',I3,'),Y(',I3,')'/)
      WRITE(6,1075) NEL
 1075 FORMAT(2X,'NODEL,DN,XXX,STRAY,DLIB ETC (',I3,
     +')'/)
      WRITE(6,1080) XMIN,XMAX,YMIN,YMAX
 1080 FORMAT(2X,'X RANGES FROM',F8.3,' TO',F8.3,' AND Y'
     +,' FROM',F8.3,' T0',F8.3/)
      WRITE(6,1085) TCRIT
 1085 FORMAT(2X,'CRITICAL MAX TIME STEP = ',E10.3,' YEARS'/)
      WRITE(6,1090) TCRIT1
 1090 FORMAT(2X,'MINIMUM TOTAL TIME = ',E10.3,' YEARS'/)
      WRITE(6,1095) JEL,MBW
 1095 FORMAT(2X,'MAX. NODAL DIFFERENCE IS IN ELEMENT',I4,
     +' AND EQUALS',I4/)
      WRITE(6,1100)
 1100 FORMAT(/2X,'DATA HAS BEEN WRITTEN TO FILE CHDAT FOR POSSIBLE PLOTT
     +ING'/)
 1105 FORMAT('0')
      STOP
      END
****
```

APPENDIX 3

Program to Reduce Stiffness Matrix Bandwidth

Reduction of the bandwidth of the body stiffness matrix will result in smaller computing times, and may even in some cases make the difference between being able or not being able to fit the finite element grid into the available computer storage. The program listed here, IMPNBW, is based on that presented by Dean (1972), but has been considerably extended to take advantage of nodal exchanges which do not directly improve the bandwidth but may allow another exchange to do so. The program attempts the improvement using two different methods, the results of which are compared in order to choose the best on each occasion. The two methods differ only in the particular swaps that occur if no improvment is immediately possible. Further improvement can sometimes be obtained by resubmitting the data produced on stream 8. A flow diagram for the main program and one subroutine is given in Fig. A3.1.

Input Data (Stream 5)

1. NNOD,NEL (2I10)

NNOD	number of nodes in the finite element grid.
NEL	number of elements in the finite element grid.

2. N, X(N), Y(N) (I10,2F10.3)

N	node numbers.
X,Y	x and y co-ordinates of the nodes (km).

3. (IREFEO (J,I), I=1,3) (3I10)

IREFEO	node numbers corresponding to each element.

4. NWRITE (I10)

NWRITE	equal to 0 if only final grids are to be printed, and equal to 1 if a step-by-step description of the process is also to be printed.

Output Data

1. The original input data and the corresponding bandwidth (stream 5).

2. The nodal distributions resulting from both methods and their corresponding bandwidths (stream 6).

3. A step-by-step description of the swapping process, if NWRITE=1 (stream 6).

4. The new co-ordinates for each node, corresponding to the best of the two methods (stream 6).

5. New grid data identical in format to the original grid input data (stream 8).

Reference

Dean, D. S., 1972. Stress Analysis of the Lithosphere. Unpublished Ph.D. Thesis, University of Durham.

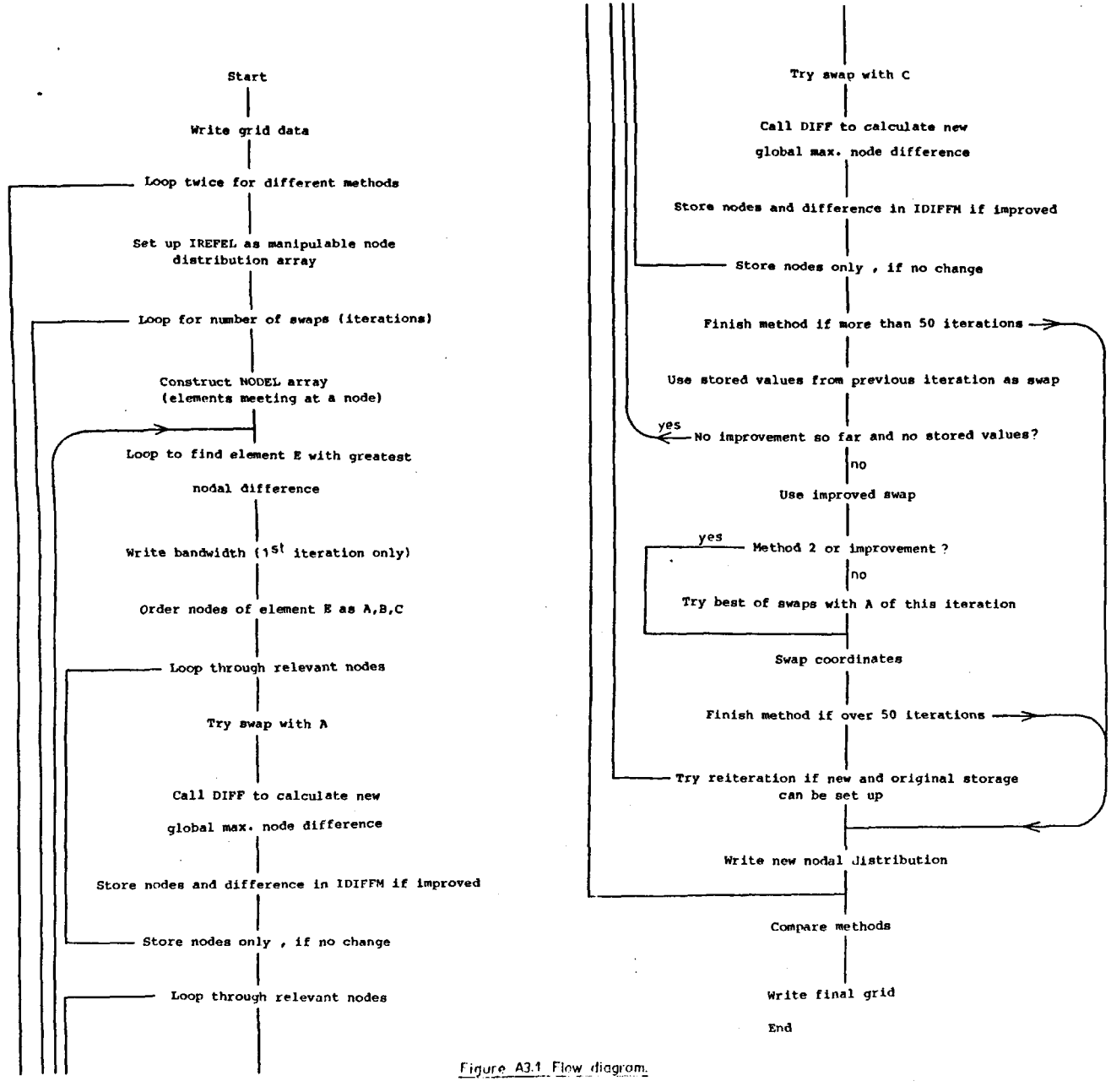

Figure A3.1 Flow diagram.

```
C ****** PROGRAM TO IMPROVE BANDWIDTH OF FINITE ELEMENT GRID
C       BY TWO DIFFERENT METHODS
C
      PROGRAM IMPNBW (NBWDAT,OUTPUT,F5,F6,F7,NBW0,NEWDAT,
     +TAPE5=NBWDAT,TAPE6=OUTPUT,TAPE7=NBW0,TAPE8=NEWDAT)
      COMMON IDIFFM,NODEL(500,10),IREFEL(1000,3),NDEV
      DIMENSION IREFEX(1000,3),IREFEO(1000,3),X(500),Y(500)
     +,X2(500),Y2(500)
C
C****** READ AND STORE DATA
C*      1ST LINE : NO. OF NODES, NO. OF ELEMENTS - (2I10)
C*      2ND LINE : NODE NOS. AND COORDINATES - (I10,2E10.3)
C*      THEN : CORRESPONDING NODE NOS. - (3I10)
C*      LASTLY 'NWRITE' IN (I10) - IF THIS IS 0 THEN ONLY
C*      RESULTS ARE PRINTED, OTHERWISE A STEP BY STEP
C*      DESCRIPTION OF THE MANIPULATION IS ALSO GIVEN.
C
      READ(5,2000) NNOD,NEL
      IF(NNOD.GT.500) STOP9000
      IF(NEL.GT.1000) STOP9000
      IBEST=1000
      NDEV=6
      IF(NWRITE.EQ.0) NDEV=7
      WRITE(6,1010)
C ****** START METHOD
C       SET UP NODE DISTRIBUTION(S) AND COORDINATES
      DO 40 NIT=1,2
      IF(NIT.EQ.2) WRITE(NDEV,1020)
      IF(NIT.EQ.2) GOTO 2
      WRITE(6,1017)
      DO 100 J=1,NNOD
      READ(5,1007) N,X(N),Y(N)
      WRITE(6,1007) J,X(J),Y(J)
      X2(J)=X(J)
  100 Y2(J)=Y(J)
      WRITE(6,3001)
      DO 1 J=1,NEL
      READ(5,3000) (IREFEO(J,I),I=1,3)
    1 WRITE(6,1016) J,(IREFEO(J,I),I=1,3)
      READ(5,3002) NWRITE
      IAB=0
      JB=0
    2 IT=1
      NIAB=0
      NJB=0
      NIABX=0
      NJBX=0
      NSTOR1=0
      NSTOR2=0
      NSTOR3=0
      NSTOR4=0
      NS1=1001
      NS3=1001
      IELX=0
      IND=1
      DO 3 J=1,NEL
      DO 3 I=1,3
      IREFEL(J,I)=IREFEO(J,I)
      IF(NIT.EQ.1) GOTO 3
      IREFEO(J,I)=IREFEX(J,I)
```

```
    3 CONTINUE
      IF(NIT.NE.2) GOTO 4
      DO 325 I=1,NNOD
      XX=X2(I)
      X2(I)=X(I)
      X(I)=XX
      YY=Y2(I)
      Y2(I)=Y(I)
      Y(I)=YY
  325 CONTINUE
C
C ****** START ITERATIONS
C
C****** COMPILE LIST OF ALL THE ELEMENTS TO WHICH EACH NODE BELONGS
    4 DO 8 I=1,NNOD
      N=1
      DO 5 J=1,10
    5 NODEL(I,J)=0
      DO 8 J1=1,NEL
C      DOES NODE I BELONG TO ELEMENT J1 ?
      DO 6 J2=1,3
      IF(I.EQ.IREFEL(J1,J2)) GOTO 7
    6 CONTINUE
      GOTO 8
    7 NODEL(I,N)=J1
      N=N+1
      IF(N.GT.10) WRITE(6,3003) (NODEL(I,K),K=1,10)
      IF(N.GT.10) STOP9000
    8 CONTINUE
C****** FIND ELEMENT WITH GREATEST NODAL DIFFERENCE
    9 NDIFF=0
      IEL=IELX
      DO 10 I=1,NEL
      IF(IND.EQ.3.AND.I.EQ.IEL) GOTO 10
      IA=IABS(IREFEL(I,1)-IREFEL(I,2))
      IB=IABS(IREFEL(I,2)-IREFEL(I,3))
      IC=IABS(IREFEL(I,1)-IREFEL(I,3))
      N=MAX0(IA,IB,IC)
      IF(N.LE.NDIFF) GOTO 10
      IELX=I
      NDIFF=N
C      NDIFF IS ORIGINAL MAX. NODE DIFF. FOR THIS ITERATION
   10 CONTINUE
      IF(IT.GT.1.OR.NIT.EQ.2) GOTO 11
      NBW=(4*NDIFF)+3
      WRITE(6,1011) NBW,IELX
   11 WRITE(NDEV,1001) IT
      WRITE(NDEV,1000) IELX,NDIFF
C
C****** ORDER THE NODES OF THE ELEMENT WITH GREATEST DIFFERENCE
C       IN NODAL NOS. IN DESCENDING ORDER A,B,C
      IA=MAX0(IREFEL(IELX,1),IREFEL(IELX,2),IREFEL(IELX,3))
      IC=MIN0(IREFEL(IELX,1),IREFEL(IELX,2),IREFEL(IELX,3))
      IB=(IREFEL(IELX,1)+IREFEL(IELX,2)+IREFEL(IELX,3)-IA-IC)
C
C****** SWAP NODES A AND J WHERE J IS (A-1),(A-2),.....(B+1) IN TURN
C      IDIFFB IS MAX. NODE DIFF. TO BE IMPROVED IF POSSSIBLE
      IDIFFB=NDIFF
      NSWAP=IA-IB-1
      WRITE(NDEV,9000) IA,IB,IC
```

```
      IF(NSWAP.EQ.0) GOTO 15
      DO 14 I=1,NSWAP
      J=IA-I
C****** CALC. NEW MAX. DIFF. AFTER THIS SWAP
      CALL DIFF(IA,J)
C****** WE ARE AFTER THE SWAP THAT GIVES THE LEAST MAX. DIFF.
C       IDIFFM IS MAX. NODE DIFF. FOR THIS PARTICULAR SWAP
      WRITE(NDEV,9001) IDIFFM
      IF(IDIFFM.NE.IDIFFB) GOTO 12
C       STORE NODES FOR POSSIBLE USE
      NSTOR1=IA
      NSTOR2=J
   12 IF(IDIFFM.GE.IDIFFB) GOTO 13
C****** STORE PARAMETERS FOR BEST SWAP SO FAR
      IDIFFB=IDIFFM
      IAB=IA
      JB=J
      IC1=IA
      JW=J
      WRITE(NDEV,1003) IAB,JB
      WRITE(NDEV,1004) IDIFFB
      GOTO 14
   13 WRITE(NDEV,1008) IDIFFB
   14 CONTINUE
C
C****** NOW SWAP NODE C WITH J WHERE J IS (C+1),(C+2),....(B-1) IN TURN
   15 NSWAP=IB-IC-1
      IF(NSWAP.EQ.0) GOTO 19
      DO 18 I=1,NSWAP
      J=IC+I
C****** CALC. NEW MAX. DIFF. AFTER THIS SWAP
      CALL DIFF(IC,J)
C****** WHICH SWAP GIVES THE LEAST MAX.DIFF. ?
      WRITE(NDEV,9001) IDIFFM
      IF(IDIFFM.NE.IDIFFB) GOTO 16
C       STORE NODES FOR POSSIBLE USE
      NSTOR3=IA
      NSTOR4=J
   16 IF(IDIFFM.GE.IDIFFB) GOTO 17
C****** STORE PARAMETERS FOR BEST SWAP SO FAR
      IDIFFB=IDIFFM
      IAB=IC
      JB=J
      WRITE(NDEV,1003) IAB,JB
      WRITE(NDEV,1004) IDIFFB
      GOTO 18
   17 WRITE(NDEV,1008) IDIFFB
   18 CONTINUE
C
C****** USE STORED VALUES IF NO IMPROVEMENT SO FAR
   19 IF(IDIFFB.LT.NDIFF) GOTO 24
      IF(NSTOR3.EQ.NS3) GOTO 21
   20 IAB=NSTOR3
      JB=NSTOR4
      GOTO 22
   21 IF(NS1.EQ.NSTOR1) GOTO 32
      IAB=NSTOR1
      JB=NSTOR2
   22 IF(IAB.EQ.0.OR.JB.EQ.0) IND=3
      IF(IND.EQ.3) WRITE(NDEV,1002)
```

```
      IF(IND.EQ.3) IT=IT+1
      IF(IT.GT.50) GOTO 33
      IF(IND.EQ.3) GOTO 9
C
C****** INSTIGATE SWAP AND START AGAIN
C       SWAP NODE DISTRIBUTION
   24 DO 27 I=1,NEL
      DO 27 J=1,3
      IREFEX(I,J)=IREFEL(I,J)
      IF(IREFEX(I,J).EQ.IAB) GOTO 25
      IF(IREFEX(I,J).EQ.JB) GOTO 26
      GOTO 27
   25 IREFEX(I,J)=JB
      GOTO 27
   26 IREFEX(I,J)=IAB
   27 CONTINUE
      N=0
      IF(IDIFFB.LT.NDIFF) GOTO 29
      IF(NIT.EQ.2) GOTO 29
C       RECALCULATE MAX. NODE DIFF.
      DO 28 I=1,NEL
      IA=IABS(IREFEX(I,1)-IREFEX(I,2))
      IB=IABS(IREFEX(I,2)-IREFEX(I,3))
      IC=IABS(IREFEX(I,3)-IREFEX(I,1))
   28 N=MAX0(IA,IB,IC,N)
      IF(N.LE.NDIFF) IDIFFB=N
      IF(N.LE.NDIFF) GOTO 29
      IF(IAB.EQ.IC1.OR.JB.EQ.JW) IDIFFB=N
      IF(IAB.EQ.IC1.OR.JB.EQ.JW) GOTO 29
C       USE FIRST NODE BEST SWAP INSTEAD
      IAB=IC1
      JB=JW
      GOTO 24
   29 DO 30 I=1,NEL
      DO 30 J=1,3
   30 IREFEL(I,J)=IREFEX(I,J)
C       SWAP COORDINATES
      XX=X(JB)
      X(JB)=X(IAB)
      X(IAB)=XX
      YY=Y(JB)
      Y(JB)=Y(IAB)
      Y(IAB)=YY
      IF(IDIFFB.GE.NDIFF)WRITE(NDEV,9002) IAB,JB
      IF(IAB.NE.0.AND.JB.NE.0)WRITE(6,1006) IAB,JB
      IF(IAB.EQ.0.OR.JB.EQ.0) WRITE(6,1019)
C
C****** HAVE A FURTHER GO AT IMPROVEMENT
      IF(N.GE.NDIFF) GOTO 31
      WRITE(NDEV,1012)
   31 IF(IT.EQ.1) IND=0
      IT=IT+1
      IF(IT.GT.50) GOTO 33
      NS1=NSTOR1
      NS3=NSTOR3
      IF(NIABX.EQ.IAB.AND.NJBX.EQ.JB) GOTO 315
      GOTO 316
  315 IF(NIAB.EQ.IAB.AND.NJB.EQ.JB) GOTO 33
  316 NIABX=NIAB
      NJBX=NJB
```

```
      NIAB=IAB
      NJB=JB
      GOTO 4
   32 WRITE(NDEV,1009)
C
C       PRINT IMPROVED DATA
   33 WRITE(6,1005)
      DO 39 N=1,NEL
      WRITE(6,1016) N,(IREFEL(N,I),I=1,3)
      IF(NIT.EQ.1) GOTO 39
      IF(IBEST.GE.IDIFFB) GOTO 35
      DO 34 I=1,3
   34 IREFEX(N,I)=IREFEO(N,I)
      GOTO 37
   35 DO 36 I=1,3
   36 IREFEX(N,I)=IREFEL(N,I)
   37 IF(N.GT.1) GOTO 38
      WRITE(8,2000) NNOD,NEL
      DO 101 I=1,NNOD
      IF(IBEST.LT.IDIFFB) X(I)=X2(I)
      IF(IBEST.LT.IDIFFB) Y(I)=Y2(I)
  101 WRITE(8,1007) I,X(I),Y(I)
   38 WRITE(8,3000) (IREFEX(N,I),I=1,3)
      IF(N.LT.NEL) GOTO 39
      WRITE(8,3002) NWRITE
   39 CONTINUE
      NBW=(4*IDIFFB)+3
      WRITE(6,3010) NBW
      IF(NIT.EQ.2) GOTO 40
C       IBEST IS FINAL BANDWIDTH FROM FIRST METHOD
      IBEST=IDIFFB
   40 CONTINUE
      WRITE(6,1018)
      WRITE(6,1007) (I,X(I),Y(I),I=1,NNOD)
      IF(IT.GT.5) WRITE(NDEV,1013)
      IF(IBEST.GE.IDIFFB) WRITE(6,1014)
      IF(IBEST.LT.IDIFFB) WRITE(6,1015)
C
 1000 FORMAT(/2X,'GREATEST NODE DIFF.IS NOW IN ELEMENT',I4,
     +' AND IS EQUAL TO',I4/)
 1001 FORMAT(/2X,'ITERATION',I4/)
 1002 FORMAT(/2X,'NO IMPROVEMENT POSSIBLE WITH THIS ELEMENT',
     +' - TRY ANOTHER'/)
 1003 FORMAT(/2X,'SO THE MAX. NODE DIFF. IS IMPROVED BY SWAPPING NODES',
     +I4,' AND',I4/)
 1004 FORMAT(/2X,'BEST MAX. NODE DIFF. NOW EQUALS',I4/)
 1005 FORMAT(/2X,'HERE IS THE IMPROVED NODAL DISTRIBUTION'/)
 1006 FORMAT(/2X,'NODES',I4,' AND',I4,' HAVE BEEN SWOPPED'/)
 1007 FORMAT(I10,2F10.3)
 1008 FORMAT(/2X,'SO MAX. NODE DIFF. UNIMPROVED AND STILL EQUALS',I4/)
 1009 FORMAT(/2X,'NO FURTHER IMPROVEMENT POSSIBLE'/)
 1010 FORMAT('1')
 1011 FORMAT(/2X,'BANDWIDTH =',I4,'  E.G. IN ELEMENT ',I4/)
 1012 FORMAT(/2X,'SO THE LOCAL BANDWIDTH HAS BEEN IMPROVED'/)
 1013 FORMAT(/2X,'FURTHER IMPROVEMENT MAY BE POSSIBLE'/)
 1014 FORMAT(/2X,'THIS LATTER GRID HAS BEEN STORED IN FILE NEWDAT')
 1015 FORMAT(/2X,'THE FIRST NEW GRID HAS BEEN STORED IN',
     +' FILE NEWDAT')
 1016 FORMAT(4I10)
 1017 FORMAT(/2X,'HERE ARE THE ORIGINAL COORDINATES'/)
```

```
 1018 FORMAT(/2X,'THE FINAL COORDINATES ARE '/)
 1019 FORMAT(/2X,'NO IMPROVEMENT POSSIBLE WITH THIS METHOD'/)
 1020 FORMAT(/2X,'***** TRY A DIFFERENT WAY -'/)
 2000 FORMAT(2I10)
 3000 FORMAT(3I10)
 3001 FORMAT(/2X,'HERE IS THE ORIGINAL NODE DISTRIBUTION -'/)
 3002 FORMAT(I10)
 3003 FORMAT(/2X,'THE ELEMENTS INVOLVED ARE -',10I4/)
 3010 FORMAT(/2X,'NEW BANDWIDTH =',I4/)
 9000 FORMAT(/2X,'THE NODE NOS. ARE',I4,' , ',I4,' AND',I4/)
 9001 FORMAT(/10X,'THIS GIVES A MAX. NODE DIFF. OF',I4/)
 9002 FORMAT(/2X,'NO OVERALL IMPROVEMENT SO FAR, BUT TRY '
     +,'SWAPPING NODES ',I4,' AND',I4,' AND START AGAIN'/)
      STOP
      END


      SUBROUTINE DIFF(N1,N2)
      COMMON IDIFFM,NODEL(500,10),IREFEL(1000,3),NDEV
C****** CALC. THE NEW GREATEST NODAL DIFF. OVER ALL THE ELEMENTS
C       CONTAINING NODES N1 AND N2 WHEN THESE NODAL NUMBERS ARE INTERCHANGED
      NMO=0
      J=N2
      IA=N1
      I=0
      N=1
      WRITE(NDEV,5000) IA,J
 5000 FORMAT(/10X,'TRY SWOPPING NODES',I4,' AND',I4/)
    1 IF(IREFEL(NODEL(J,N),1).EQ.J) GOTO 2
      IF(IREFEL(NODEL(J,N),2).EQ.J) GOTO 3
      JA=IREFEL(NODEL(J,N),1)
      JB=IREFEL(NODEL(J,N),2)
      GOTO 4
    2 JA=IREFEL(NODEL(J,N),2)
      JB=IREFEL(NODEL(J,N),3)
      GOTO 4
    3 JA=IREFEL(NODEL(J,N),1)
      JB=IREFEL(NODEL(J,N),3)
    4 IF(JA.EQ.IA) JA=J
      IF(JB.EQ.IA) JB=J
      I1=IABS(JA-IA)
      I2=IABS(JB-IA)
      I3=IABS(JA-JB)
      M=MAX0(I1,I2,I3)
      IF(M.GT.NMO) NMO=M
      N=N+1
      IF(NODEL(J,N).EQ.0) GOTO 5
      GOTO 1
    5 IF(I.EQ.1) GOTO 6
      N=1
      J=N1
      IA=N2
      I=1
      GOTO 1
    6 IDIFFM=NMO
      RETURN
      END
****
```

APPENDIX 4

Visco-elastic Finite Element Program

The program FERBIS listed in this Appendix consists of a main program and eight subroutines.

Main Program

A flow diagram of the main program is shown in Fig. A4.1.

Subroutine PLOT

This subroutine produces a line printer alphanumeric representation of the final stress distribution. Five separate diagrams are printed (on stream 6), showing the three principal stresses, the maximum shear stress, and the Coulomb-Mohr strength (see Subroutine SLIPS). The diagrams are of fixed size, and so the horizontal and vertical scales will usually be different.

Subroutine GMPRD

This subroutine multiplies two matrices together to form a third matrix. The dimensions of the matrices have to be fed into the subroutine as parameters. The subroutine is adapted from an I.B.M. scientific subroutine package.

Subroutine GMTRA

This subroutine calculates the transpose of one matrix. The dimensions of the matrix have to be fed in as parameters. This subroutine is adapted from an I.B.M. scientific subroutine package.

Subroutine MATSOL

This subroutine is used to solve the equilibrium equation of finite element, $[K]\{\delta\} = \{F\}$ for displacement $\{\delta\}$, where $[K]$ is the stiffness matrix and $\{F\}$ is the total force vector. The subroutine is available on the Harwell scientific subroutine package MA07BD (Hopper, 1973), and uses Gaussian elimination.

Subroutine MATHEL

This subroutine is called by Subroutine MATSOL.

Subroutine PLOTS

This subroutine plots the final solutions using the GHOST graphical output system. Three diagrams are plotted, showing the total, deviatoric and maximum shear stresses. The latter diagram shows the element divisions as well. The portion of the grid plotted in each depends on the values selected in the preliminary program GRDGEN (see Appendix 1) and the scaling is automatic. Scaling of the stresses is also automatic, and uses one of five standard scales to facilitate comparison between separate plots. The scales of the total and deviatoric stresses on the same plot, however, will often be different because of their difference in magnitude. Values for shear stress are not printed in elements which leave a Young's Modulus below 10^8dynes/cm^2, nor in elements which are too small.

Subroutine FAIL

This subroutine uses the principal stresses to test for rock fracture using the Modified Griffiths Criterion as described in Section 2.4. If fracture occurs, a value for Q is assigned, which indicates the particular fracture region (Fig. 2.9).

Subroutine SLIPS

This subroutine uses the principal stresses to test for slippage along a pre-formed fault plane using the Coulomb-Mohr Criterion. A value C is calculated which represents the distance (in kilobars) between the Mohr circle and the failure criterion. C is put equal to -1.0 if failure is calculated.

Input Data

All data are in C.G.S. unless otherwise specified. The following are internally set parameters, assigned values before the READ statements,which are not explicitly explained in the listing.

1. RNODEF

Equals 1 if final displacements are to be written to stream 2 with the stresses, and 0 otherwise.

2. OUT

Stress convergence tolerance of cycle for solution within time increment.

The following are read in on streams 5 and 1. Stream 5 usually contains data written by program GRDGEN (Appendix 1).

1. NNOD, NEL, NBNOD, NHOL, DENSUB (Stream 5) (4IO,F10.3)

NNOD	number of nodes of finite element grid.
NEL	number of elements of finite element grid.
NBNOD	number of boundary nodes of finite element grid. If this is negative, then element strengths are contoured instead of shear stresses.
NHOL	number of internal holes in the finite element grid.
DENSUB	density subtracted from whole grid.

2. K,X(K),Y(K),FORST(2*K-1),FORST(2*K) (stream 5) (I10,2F10.3,2E10.3)

K	node numbers.
X,Y	co-ordinates of nodes (mm).
FORST	x and y components of applied stress vectors.

3. K,(NODEL(K,J),J=1,3),E(K),P(K),DN(K),VISCOS(K) (stream 5)
(4I10,E10.3,2F10.3,E10.3)

K	element numbers
NODEL	node numbers associated with each triangular element.
E,P,DN,VISCOS	element Young's Moduli, Poisson's Ratios, densities and viscosities.

4. XTTS,IDIM,XMN,XMX,YMN,YMX (stream 5) (E10.3,I10,4F10.3)

XTTS	horizontal tectonic stress added to solution (negative compressional) for every element.
IDIM	equal to 0 if whole grid to be used for plotting, and 1 if the following limits are imposed:
XMN,XMX, YMN,YMX	the minimum and maximum values in the x and y directions of the final stress plots.

5. NTIM,TIMC (stream 5) (I10,E10.3)

NTIM	number of time increments.
TIMC	length of each time increment (years).

6. NOYES (stream 5) (I10)

NOYES	equal to 1 if stresses and displacements are to be read from stream 1, and 0 otherwise.

7. NDD2 (stream 1) (I10)

NDD2	number of initial stress and displacement records on stream 1 [if NOYES = 0], or equal to NNOD2 [if NOYES = 1].

8. PREDIP(I),(STREN(I,J),J 1,4) (stream 1) (2X,5E15.7)

PREDIP	initial displacements of nodes (x and y components on consecutive records).
STREN	initial stresses for each element (x and y components on consecutive records).

Note that these input records need not be present if NOYES 0, but will be anyhow if subgrid displacements have been written to this file by a previous run of FERBIS.

9. ND (stream 5) (I10)

ND	number of nodes with prescribed displacements.

10. LD(I),(ISP(I,J)PDIS(I,J),J=1,2) (stream 5) (I10,2(I10,F10.3))

LD	node number at which displacements are specified.
ISP	equal to 1 if this component of displacement is specified (x followed by y components, on same record).
PDIS	the prescribed displacement for the particular direction.

11. NY (stream 5) (I10)

NY	equal to 1 if additional prescribed displacements are to be read from primary grid, and 0 otherwise.

12. NDD2 (stream 1) (I10)

Already described under no. 7.

13. (CREEP(I),I=1,4) (stream 1) (2X,5E15.7)

A dummy READ statement, in order to arrive at the correct record for primary grid prescribed displacements.

14. NND2 (stream 5) (I10)

NND2 number of primary grid prescribed displacements.

15. LD(I),(ISP(I,J),PDIS(I,J),J=1,2) (stream 1) (I10,2(I10,E15.7))

See no. 10. Additional prescribed displacements from primary grid run.

16. NBOR (stream 5) (I10)

NBOR number of boundary corner nodes (joined up in plotting in the given order to form model boundary.

17. IBOR(I) (stream 5) (8I10)

IBOR node numbers of boundary nodes.

18. NDAT (stream 5) (I10)

NDAT see listing for explanation - controls nature of output.

19. NFILE2 (stream 5) (I10)

NFILE2 if equal to 1 final stresses and displacements are written to stream 2, and if equal to 0 they are not.

20. NDD (stream 5) (I10)

NDD number of prescribed displacements to write to stream 2 for subgrid run.

21. LDD(I) (stream 5) (8I10)

LDD node numbers of nodes whose displacements are to be prescribed to corresponding subgrid nodes.

22. LD2(I) (stream 5) (8I10)

LD2 node numbers of subgrid nodes which will receive the primary grid displacements.

Output Data

Various combinations of the output blocks listed below will be produced, depending on the value assigned to NDAT.

1. All input data, specifying grid, boundary conditions and time increment information (stream 6).

2. Final nodal displacements, element stresses and results of failure tests for each element (stream 6).

3. Nodal displacements, element stresses, and any further prescribed displacements (stream 2).

4. Fault slippage results (element strengths) or maximum shear stresses for use in a contouring routine (not specified) in format (2F6.2, F5.1) (stream 3). If IDIM=1, however, the values are limited to elements between the limits XMN, XMX, YMN, YMX, and are written to stream 7.

5. Full grid and final principal stresses for possible plotting in external program (stream 4) or for use in pore pressure program (Appendix 8).

6. Maximum and minimum shear stresses, and total strain energy (stream 6).

7. Alphanumeric representation of principal and shear stresses, and element strengths.

8. Graphical output of total, deviatoric and maximum shear stresses.

Reference

Hopper, M. J., 1973. Harwell subroutine library, H.M.S.O.

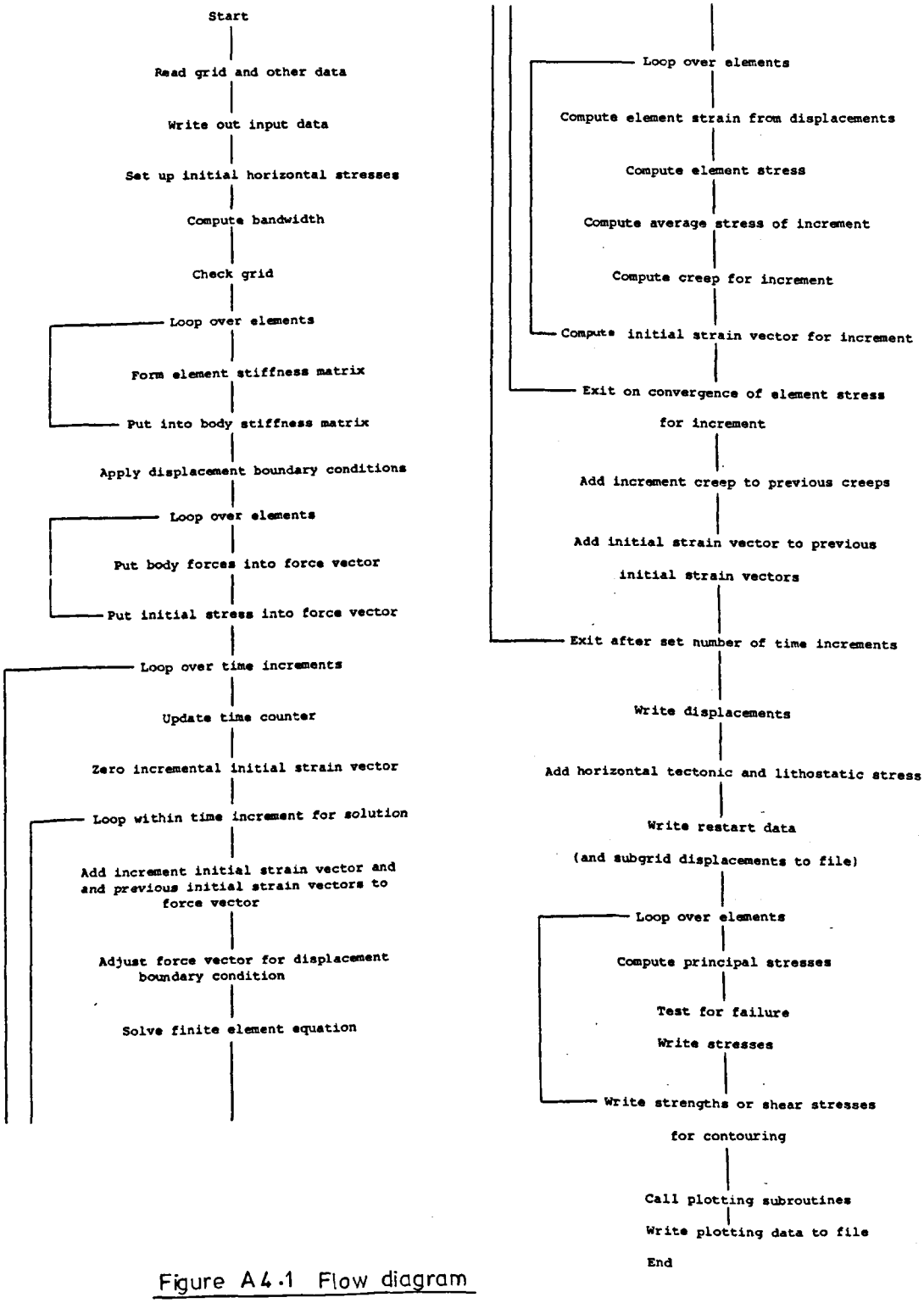

Figure A4.1 Flow diagram

```
C******    PLANE-STRAIN VISCO-ELASTIC FINITE ELEMENT PROGRAM
C
      PROGRAM FERBIS(OUTPUT,F1,F2,F5,F4,BBFILE,F3,F7,RDAT,
     1 TAPE1=BBFILE,TAPE4=RDAT,TAPE5=F5,TAPE2=F2,TAPE3=F3,
     2 TAPE6=OUTPUT,TAPE7=F7)
C******MAIN PROGRAM*************************************************
      COMMON/K/ AT,DLIB,BLIB,DELIB
      COMMON/L/ STIN,CSTIN,STREN,TRAY
      COMMON/M/ DN,XXX,YYY,STRAY
      COMMON/N/ E,P,FORST,FIST,VISCOS,PREDIP
C*****DIMENSION STATEMENTS*****************************************
C***** DIMENSION AT(2*NNOD,(NBW+1)*1.5)
      DIMENSION AT(256,96)
C****** DIMENSION.GT.(2*NNOD)
      DIMENSION CSTIN(256,4),FIST(256),STREN(256,4),PREDIP(256),
     +          DISP(256),STRAY(256,5),FORST(256),STIN(256,4)
C****** DIMENSION.GE.NNOD
      DIMENSION X(128),Y(128)
C****** DIMENSION.GE.NEL
      DIMENSION NODEL(214,3),E(214),P(214),DN(214),VISCOS(214),
     +          XXX(214),YYY(214),TRAY(214,5),
     +          DELIB(214),DLIB(9,214),BLIB(18,214)
C****** DIMENSIONS FIXED
      DIMENSION LD(50),LD2(50),ISP(50,2),
     +          PDIS(50,2),IBOR(10),T(36),D(9),B(18),V(6),
     +          F(18),H(18),W(3),QQ(3),CC(3),CREEP(4),DISEL(6),
     +          STRESS(4),LDD(50),STRAIN(4),STEL(4),DFS(4)
C
C     N.B. DIMENSIONS OF STRAY IN S.R. PLOT AND STRAY AND NODEL
C     IN S.R. PLOTS MUST AGREE
C
C****** SPECIFY LARGE CORE MEMORY STORAGE
      LEVEL 2,AT,DLIB,BLIB,DELIB
      LEVEL 2,STIN,CSTIN,STREN,TRAY
      LEVEL 2,DN,XXX,YYY,STRAY
      LEVEL 2,E,P,FORST,FIST,VISCOS,PREDIP
      DATA G/-981.0/
C*****TRANSFERRED DISPLACEMENTS INDICATOR
      RNODEF=0.0
C*****STRESS CONVERGENCE CONDITION
      OUT=1.0D6
C******INTERNAL FRICTION
      XMU=0.7
C*****SHEAR STRENGTH
      SS=0.2E9
C*****TENSILE STRENGTH
      TS=-0.2E9
C*****DEPTH INCREASE OF HORIZONTAL INITIAL STRESS ABOVE LITHOSTATIC (BARS
/KM)
      DBPK=70.0
C
C*****READ IN INPUT DATA IN CGS EXCEPT FOR X ,Y , TIMC AND XMX ETC **********
C*****READ NO. OF NODES ,ELEMENTS, BOUNDARY NODES, HOLES AND SUBTRACTED D
ENSITY
C      NBNOD NEGATIVE MEANS ELEMENT STRENGTHS CONTOURED
C      INSTEAD OF SHEAR STRESSES
      READ(5,1000) NNOD,NEL,NBNOD,NHOL,DENSUB
      NNOD2=NNOD*2
      NEST=NBNOD
      NBNOD=IABS(NBNOD)
```

```
 1000 FORMAT(4I10,F10.3)
      DO 5 I=1,NNOD
C***** READ NODE COORDINATES (KMS) + APPLIED STRESSES
    5 READ(5,1005) K,X(K),Y(K),FORST(2*K-1),FORST(2*K)
 1005 FORMAT(I10,2F10.3,2E10.3)
      TCRIT=0.0
      TCRIT=1.0E20
      DO 10 I=1,NEL
      READ(5,1010) K,(NODEL(K,J),J=1,3),E(K),P(K),DN(K),VISCOS(K)
      IF(E(I).LT.1.0E8.OR.VISCOS(I).GT.1.0E40) GOTO 10
      TEVIS=VISCOS(I)/E(I)/3600.0/24.0/365.5
      TCRIT1=AMAX1(TCRIT1,TEVIS)
      TCRIT=AMIN1(TCRIT,TEVIS)
   10 CONTINUE
 1010 FORMAT(4I10,E10.3,2F10.3,E10.3)
C******READ TECTONIC STRESS AND REDUCED PLOT DIMENSIONS (KM)
C*       IDIM=0 MEANS WHOLE GRID PLOTTED
      READ(5,1015) XTTS,IDIM,XMN,XMX,YMN,YMX
 1015 FORMAT(E10.3,I10,4F10.3)
C*****READ NUMBER OF TIME INCREMENTS AND STEP LENGTH (YEARS)
      READ(5,1030) NTIM,TIMC
C*****SET INITIAL STRAINS ,STRESSES AND DISPLACEMENTS TO ZERO
      DO 15 I=1,NNOD2
      DO 12 J=1,4
      STIN(I,J)=0.0
   12 STREN(I,J)=0.0
   15 PREDIP(I)=0.0
C****** NOYES=1 TO READ INIT. DISPS AND STRESSES FROM BBFILE
      READ(5,1020) NOYES
      IF(NOYES.EQ.0) GO TO 25
 1020 FORMAT(I10)
      READ(1,1020) NDD2
      DO 20 I=1,NNOD2
   20 READ(1,1025) PREDIP(I),(STREN(I,J),J=1,4)
 1025 FORMAT(2X,5E15.7)
 1030 FORMAT(I10,E10.3)
C***** TAKE PREDIP OFF X,Y TO PERTURBATE GRID POSITION
   25 DO 30 I=1,NNOD
      KY=2*I
      KX=KY-1
      X(I)=X(I)+PREDIP(KX)/1.0E5
   30 Y(I)=Y(I)+PREDIP(KY)/1.0E5
C*****READ BOUNDARY CONDITIONS  (PRESCRIBED DISPLACEMENTS = PDIS)
      READ(5,1020) ND
      ND2=ND
      DO 33 I=1,ND
   33 READ(5,1040) LD(I),(ISP(I,J),PDIS(I,J),J=1,2)
C*****IF NY IS NOT ZERO READ PRIMARY GRID DISPLACEMENTS ALSO
      READ(5,1020) NY
      IF(NY.EQ.0) GOTO 37
      IF(NOYES.NE.0) GOTO 35
      READ(1,1020) NDD2
      DO 34 J=1,NDD2
   34 READ(1,1025)(CREEP(I),I=1,4)
   35 READ(5,1020) NND2
      ND1=ND+1
      ND=NND2+ND
      DO 36 I=ND1,ND
   36 READ(1,1042) LD(I),(ISP(I,J),PDIS(I,J),J=1,2)
 1040 FORMAT(I10,2(I10,F10.3))
```

```
 1042 FORMAT(I10,2(I10,E15.7))
C***** READ PLOTTING DATA
C***** READ BOUNDARY CORNER NODES.
   37 READ(5,1020) NBOR
      READ(5,1045) (IBOR(I),I=1,NBOR)
 1045 FORMAT(8I10)
C***** READ OUTPUT CONTROL DATA
C       NDAT
C  -3 GRID ONLY : -2 PLOT ONLY : -1 STRESSES ONLY
C   3 ALL BUT PLOT : 2 DISPS + STRESSES : 1 PLOT + STRESSES
C       NFILE2
C   1 WRITE PREDIP + STRAY TO 2 :  0 DON'T
      READ(5,1020) NDAT
      READ(5,1020) NFILE2
      MNDAT=IABS(NDAT)
C     WRITE PRESCRIBED SUBGRID DISPLACEMENTS TO FILE 2 UNLESS NDD = 0
      READ(5,1020) NDD
      IF(NDD.EQ.0) GOTO 38
      READ(5,1045)(LDD(I),I=1,NDD)
      READ(5,1045)(LD2(I),I=1,NDD)
C
C*****WRITE OUT INPUT DATA**********************************************
   38 WRITE(6,1075)
      WRITE(6,1050)
 1050 FORMAT(30X,'FINITE ELEMENT ANALYSIS'//)
      IF(NFILE2.EQ.1) WRITE(6,1055)
 1055 FORMAT(10X,'THIS RUN HAS WRITTEN SOLUTION DATA TO FILE 2'/)
      IF(NOYES.EQ.1) WRITE(6,1057)
 1057 FORMAT(10X,'THIS RUN HAS READ INITIAL STRESSES FROM FILE 1'/)
      IF(DBPK.NE.0.0) WRITE(6,1058) DBPK
 1058 FORMAT(10X,'ADDITIONAL INITIAL HORIZONTAL STRESS INCREASES AT '
     +,F6.0,' BARS/KM'/)
      WRITE(6,1060) NNOD,NEL
 1060 FORMAT(2X,'NUMBER OF NODES =',I4,10X,'NUMBER OF ELEMENTS =',I4)
      WRITE(6,1065)
 1065 FORMAT('0')
      WRITE(6,1070) XTTS
 1070 FORMAT(10X,'TECTONIC STRESS = ',E10.3,' DYNES/CM2'/)
 1075 FORMAT('1')
      IF(MNDAT.NE.3) GOTO 45
      WRITE(6,1080)
 1080 FORMAT(10X,'COORDINATES (KM) AND APPLIED STRESSES (CGS)'/)
      WRITE(6,1085)
 1085 FORMAT(4X,'NODE',7X,'X(I)',7X,'Y(I)',
     +3X,'APPL. STRESS(X) APPL. STRESS(Y)'/)
      DO 40 I=1,NNOD
   40 WRITE(6,1090) I,X(I),Y(I),FORST(2*I-1),FORST(2*I)
 1090 FORMAT(2X,I4,4X,2F10.3,5X,2E12.3)
   45 WRITE(6,1065)
      IF(MNDAT.NE.3) GOTO 55
      WRITE(6,1095)
 1095 FORMAT(/10X,'NODAL DISTRIBUTION , MECHANICAL PROPERTIES (CGS)',
     +' AND INITIAL STRESS'/)
      WRITE(6,1098)
 1098 FORMAT(/31X,'YOUNGS',3X,'POISSON',26X,'INITIAL STRESSES')
      WRITE(6,1100)
 1100 FORMAT(4X,'ELEMENT',6X,'NODES',9X,'MODULUS',
     +3X,'RATIO',2X,'DENSITY',3X,'VISCOSITY',8X,'X',11X,'Y'/)
      DO 50 I=1,NEL
   50 WRITE(6,1105) I,(NODEL(I,J),J=1,3),E(I),P(I),DN(I),VISCOS(I)
```

```
     +,(STREN(I,J),J=1,2)
 1105 FORMAT(5X,I4,2X,I4,1X,I4,1X,I4,3X,E10.3,F7.3,2X,F6.3,3(3X,E10.3))
   55 WRITE(6,1065)
      IF(NTIM.EQ.1) WRITE(6,1110)
 1110 FORMAT(10X,'ELASTIC SOLUTION'/)
      IF(NTIM.NE.1) WRITE(6,1115) NTIM
 1115 FORMAT(2X,'VISCO-ELASTIC SOLUTION, NUMBER OF TIME ITERATIONS=',I4)
      WRITE(6,1065)
      WRITE(6,1120) TIMC
 1120 FORMAT(2X,'TIME INCREMENT =',E10.3,' YEARS'/)
C***** CONVERT TIMC FROM YEARS TO SECONDS
      TIMC=TIMC*365.5*24.0*60.0*60.0
      WRITE(6,1125) TCRIT
 1125 FORMAT(2X,'CRITICAL MAX TIME STEP = ',E10.3,' YEARS'/)
      WRITE(6,1130) TCRIT1
 1130 FORMAT(2X,'MINIMUM TOTAL TIME = ',E10.3,' YEARS'/)
      WRITE(6,1065)
      IF(MNDAT.NE.3.AND.NDAT.NE.1) GOTO 65
      WRITE(6,1135)
 1135 FORMAT(10X,'PRESCRIBED DISPLACEMENTS'/)
      WRITE(6,1138)
 1138 FORMAT(/12X,'NODE',6X,'X - DISPLACEMENT',5X,'Y - DISPLACEMENT'
     +,5X,'(KMS)'/)
      DO 62 I=1,ND
      WRITE(6,1140) LD(I),((ISP(I,J),PDIS(I,J)),J=1,2)
      DO 60 J=1,2
   60 PDIS(I,J)=PDIS(I,J)*1.0E5
   62 CONTINUE
 1140 FORMAT(I16,I9,3X,F10.3,I8,3X,F10.3)
   65 DO 68 I=1,4
   68 CREEP(I)=0.0
C****** SCALE DIMENSIONS FROM KM TO CM
      XMAX=-1.0E20
      YMAX=-1.0E20
      XMIN=1.0E20
      YMIN=1.0E20
      DO 70 I=1,NNOD
      XMAX=AMAX1(XMAX,X(I))
      YMAX=AMAX1(YMAX,Y(I))
      XMIN=AMIN1(XMIN,X(I))
      YMIN=AMIN1(YMIN,Y(I))
      XDIF=XMAX-XMIN
      YDIF=YMAX-YMIN
      X(I)=X(I)*1.0E5
   70 Y(I)=Y(I)*1.0E5
C*****SET UP INITIAL HORIZONTAL STRESSES
      ICQ=0
      DO 72 I=1,NEL
      STR1=STREN(I,1)
      STR2=STREN(I,2)
      Y0=(Y(NODEL(I,1))+Y(NODEL(I,2))+Y(NODEL(I,3)))/3.0
      STREN(I,1)=STREN(I,2)
      STREN(I,4)=STREN(I,2)
      STR=-DBPK*((YMAX*1.0E5)-Y0)*10.0
      STREN(I,1)=STREN(I,1)+STR
      IF(STR1.NE.STREN(I,1)) ICQ=1
      IF(STR2.NE.STREN(I,2)) ICQ=1
   72 CONTINUE
      I=NNOD/2
      IF(ICQ.EQ.1)WRITE(6,1142) I,STREN(I,1),STREN(I,2)
```

```
 1142 FORMAT(/10X,'INITIAL STRESSES HAVE BEEN ALTERED SO THAT ',
     +,'FOR EXAMPLE, IN ELEMENT ',I4,' THEY ARE NOW ',E10.3,
     +' AND ',E10.3)
C*****TO CALC BANDWIDTH (NBW) =4*(MAX. NODEL DIF.)+3********************
      NBW=0
      DO   75 I=1,NEL
      KB1=IABS(NODEL(I,1)-NODEL(I,2))
      KB2=IABS(NODEL(I,2)-NODEL(I,3))
      KB3=IABS(NODEL(I,3)-NODEL(I,1))
   75 NBW=AMAX0(KB1,KB2,KB3,NBW)
      NBW=2*NBW+2
      NBW=2*NBW-1
      WRITE(6,1145) NBW
 1145 FORMAT(/2X,'BANDWIDTH=',I10/)
C****** CHECK GRID
      NTX=2*(NNOD+NHOL-1)-NBNOD
      IF(NTX.EQ.NEL) GOTO 80
      WRITE(6,1150)
 1150 FORMAT(//2X,'*****  GRID IS FAULTY  *****'//)
   80 CONTINUE
C
C*****TO FORM ELEMENT STIFNESS MATRIX ***********************************
      DO 115 I=1,NEL
C***** SET H AND T TO ZERO
      DO 85 LIT=1,36
   85 T(LIT)=0.0
      DO 90 LIT=1,18
   90 H(LIT)=0.0
C*****FORM D (ELASTICITY) MATRIX*****************************************
***********
      A=E(I)*(1.0-P(I))/((1.0+P(I))*(1.0-2*P(I)))
      Q=P(I)/(1.0-P(I))
      D(1)=A
      D(2)=A*Q
      D(3)=0.0
      D(4)=A*Q
      D(5)=A
      D(6)=0.0
      D(7)=0.0
      D(8)=0.0
      D(9)=A*(1.0-Q)/2.0
      I1=NODEL(I,1)
      I2=NODEL(I,2)
      I3=NODEL(I,3)
C*****DELTA = ELEMENT AREA
      DELTA=Y(I3)*X(I2)
     1     -Y(I2)*X(I3)
     2     -X(I1)*Y(I3)
     3     +X(I1)*Y(I2)
     4     +Y(I1)*X(I3)
     5     -Y(I1)*X(I2)
C*****FORM B MATRIX*****************************************************
      QQ(1)=(Y(I2)-Y(I3))/DELTA
      CC(1)=(X(I3)-X(I2))/DELTA
      QQ(2)=(Y(I3)-Y(I1))/DELTA
      CC(2)=(X(I1)-X(I3))/DELTA
      QQ(3)=(Y(I1)-Y(I2))/DELTA
      CC(3)=(X(I2)-X(I1))/DELTA
      B(1)=QQ(1)
      B(2)=0.0
```

```
      B(3)=CC(1)
      B(4)=0.0
      B(5)=CC(1)
      B(6)=QQ(1)
      B(7)=QQ(2)
      B(8)=0.0
      B(9)=CC(2)
      B(10)=0.0
      B(11)=CC(2)
      B(12)=QQ(2)
      B(13)=QQ(3)
      B(14)=0.0
      B(15)=CC(3)
      B(16)=0.0
      B(17)=CC(3)
      B(18)=QQ(3)
      DELTA=ABS(DELTA)
C****** STORE ELEMENT B MATRIX,D MATRIX AND UNPERTURBED AREA
      DO 95 KK=1,18
   95 BLIB(KK,I)=B(KK)
      DELIB(I)=DELTA
      DO 100 KK=1,9
  100 DLIB(KK,I)=D(KK)
      N=3
      M=6
      CALL GMTRA(B,F,N,M)
C*****B IS TRANSPOSED TO F
C*****MULTIPLY D BY B TO GIVE H
      N=3
      M=3
      L=6
      CALL GMPRD(D,B,H,N,M,L)
C*****MULTIPLY F BY H TO GIVE T
      N=6
      M=3
      L=6
      CALL GMPRD(F,H,T,N,M,L)
C*****TO MULTIPLY BY DELTA/2
      DO 105 NI=1,36
  105 T(NI)=T(NI)*DELTA/2.0
C*****WE NOW HAVE ELEMENT STIFFNESS MATRIX = T**************************
C
C*****TO PUT T INTO BODY STIFFNESS MATRIX = AT**************************
      K=1
      DO 110 MS=1,3
      DO 110 NS=1,2
      DO 110 KS=1,3
      DO 110 LS=1,2
      JX=NODEL(I,MS)
      JX=2*JX-2+NS
      IY=NODEL(I,KS)
      IY=2*IY-2+LS
      LOC=JX-IY+0.5*(NBW+1)
      IF(LOC.LT.1) GO TO 110
      IF(LOC.GT.NBW) GO TO 110
      AT(IY,LOC)=AT(IY,LOC)+T(K)
  110 K=K+1
  115 CONTINUE
      WRITE(6,1155)
 1155 FORMAT(2X,'TOTAL STIFFNESS FORMED')
```

```
C***** INTRODUCE PRESCRIBED DISPLACEMENTS = PDIS **********************
      DO 125 II=1,ND
      DO 120 J=1,2
      LIK=ISP(II,J)
      IF(LIK.EQ.0) GO TO 120
      I=LD(II)
      N=2*I+J-2
      FORST(N)=PDIS(II,J)*1.0D 24
      LOC=0.5*(NBW+1)
      AT(N,LOC)=1.0D 24
  120 CONTINUE
  125 CONTINUE
      WRITE(6,1160)
 1160 FORMAT(2X,'PRESCRIBED DISPLACEMENTS INTRODUCED')
C
C*****TO PUT BODY FORCES AND INITIAL STRESS INTO FORCE VECTOR=FORST*****
C*****TO INCORPORATE BODY FORCES = A
      DO 150 I=1,NEL
C***** SET INITIAL FLUID STRESSES TO ZERO
      IF(E(I).GT.1.0E7) GOTO 135
      DO 130 J=1,3
  130 STREN(I,J)=0.0
  135 I1=NODEL(I,1)
      I2=NODEL(I,2)
      I3=NODEL(I,3)
      I11=2*I1-1
      I12=2*I1
      I21=2*I2-1
      I22=2*I2
      I31=2*I3-1
      I32=2*I3
      X(I1)=X(I1)-PREDIP(I11)
      Y(I1)=Y(I1)-PREDIP(I12)
      X(I2)=X(I2)-PREDIP(I21)
      Y(I2)=Y(I2)-PREDIP(I22)
      X(I3)=X(I3)-PREDIP(I31)
      Y(I3)=Y(I3)-PREDIP(I32)
      DELTA=Y(I3)*X(I2)
     1      -Y(I2)*X(I3)
     2      -X(I1)*Y(I3)
     3      +X(I1)*Y(I2)
     4      +Y(I1)*X(I3)
     5      -Y(I1)*X(I2)
      DELTA=ABS(DELTA)
      X(I1)=X(I1)+PREDIP(I11)
      Y(I1)=Y(I1)+PREDIP(I12)
      X(I2)=X(I2)+PREDIP(I21)
      Y(I2)=Y(I2)+PREDIP(I22)
      X(I3)=X(I3)+PREDIP(I31)
      Y(I3)=Y(I3)+PREDIP(I32)
      A=DELTA/6.0*G*DN(I)
      K1=2*I1
      K2=2*I2
      K3=2*I3
      L1=K1-1
      L2=K2-1
      L3=K3-1
      FORST(K1)=FORST(K1)+A
      FORST(K2)=FORST(K2)+A
      FORST(K3)=FORST(K3)+A
```

```
C*****TO INCORPORATE INITIAL STRESSES
      DO 140 KK=1,18
  140 B(KK)=BLIB(KK,I)
      DELTA=DELIB(I)
C*****TRANSPOSE B TO F
      N=3
      M=6
      CALL GMTRA(B,F,N,M)
C*****SET UP W (INITIAL STRESS) MATRIX
      W(1)=STREN(I,1)
      W(2)=STREN(I,2)
      W(3)=STREN(I,3)
C*****MULTIPLY F BY W TO GIVE V
      N=6
      M=3
      L=1
      CALL GMPRD(F,W,V,N,M,L)
      DO 145 KK=1,6
  145 V(KK)=V(KK)*DELTA/2.0
      FORST(L1)=FORST(L1)-V(1)
      FORST(K1)=FORST(K1)-V(2)
      FORST(L2)=FORST(L2)-V(3)
      FORST(K2)=FORST(K2)-V(4)
      FORST(L3)=FORST(L3)-V(5)
      FORST(K3)=FORST(K3)-V(6)
  150 CONTINUE
C
C
C*****START ITERATIONS FOR TIME INCREMENTS*****************************
      TIMTOT=0.0
      PT=1.0
      ENER=0.0
      DO 250 IN=1,NTIM
      TIMTOT=TIMTOT+TIMC
C*****SET INCREMENTAL CREEP AND FORCE TO ZERO
      DO 155 J=1,NNOD2
      FIST(J)=0.0
      DO 155 IJ=1,4
  155 CSTIN(J,IJ)=0.0
C
C*****START SOLUTION CYCLES WITHIN TIME STEP**********************
      DO 230 J=1,4
      DIFSTR=0.0
C*****ADD INITIAL STRAIN FORCE(FIST) TO FORCE VECTOR = DISP
      DO 160 K=1,NNOD2
  160 DISP(K)=FIST(K)+FORST(K)
C*****TO SET FORCE VECTOR TO ZERO FOR PRESCRIBED DISPLACEMENTS
      DO 170 KOD=1,ND
      DO 165 LOD=1,2
      MOD=ISP(KOD,LOD)
      IF(MOD.EQ.0) GO TO 165
      NID=LD(KOD)
      MID=2*NID+LOD-2
      KID=2*NNOD*(MID-1)+MID
      DISP(MID)=PDIS(KOD,LOD)*1.0D 24
  165 CONTINUE
  170 CONTINUE
C
C*****TO SOLVE THE EQUATION   AT*DISP=DISP*****************************
C*****CALL SOLUTION SUBROUTINE HARWELL LIBRARY GAUSSIAN ELIMINATION****
```

```
      NUM=NNOD2
      CALL MATSOL(AT,DISP,NUM,NNOD2,NBW,PT)
      PT=0.0
C*****RESET INITIAL STRAIN FORCE INCREMENT TO ZERO
      DO 175 LI=1,NNOD2
  175 FIST(LI)=0.0
C*****WE NOW HAVE DISPLACEMENTS = DISP*******************************
C
C*****TO OBTAIN STRAINS FROM DISPLACEMENTS*****************************
C****** ALLOW FOR CREEP
      DO 220 I=1,NEL
      I1=NODEL(I,1)
      I2=NODEL(I,2)
      I3=NODEL(I,3)
      DO 180 KK=1,18
  180 B(KK)=BLIB(KK,I)
      DO 185 KK=1,9
  185 D(KK)=DLIB(KK,I)
      DELTA=DELIB(I)
      J1=2*I1
      K1=J1-1
      J2=2*I2
      K2=J2-1
      J3=2*I3
      K3=J3-1
      DISEL(1)=DISP(K1)
      DISEL(2)=DISP(J1)
      DISEL(3)=DISP(K2)
      DISEL(4)=DISP(J2)
      DISEL(5)=DISP(K3)
      DISEL(6)=DISP(J3)
C*****MULTIPLY B BY DISEL TO GIVE INCREMENTAL STRAINS
      N=3
      M=6
      L=1
      CALL GMPRD(B,DISEL,STRAIN,N,M,L)
      STRAIN(4)=0.0
C*****  SUBTRACT INITIAL STRAIN TO GIVE ELASTIC STRAIN
      DO 190 IK=1,4
  190 STEL(IK)=STRAIN(IK)-STIN(I,IK)-CSTIN(I,IK)
C*****MULTIPLY D BY STRAINS TO GET STRESS
      N=3
      M=3
      L=1
      CALL GMPRD(D,STEL,STRESS,N,M,L)
      THET=0.0
      IF(IN.GT.1) GOTO 192
      IF(STEL(1).EQ.STEL(2)) GOTO 191
      THET=ATAN(2.0*STEL(3)/(STEL(1)-STEL(2)))*0.5
      IF(THET.LE.0.0) THET=THET+90.0/57.29
  191 STELP1=(STEL(1)*(COS(THET))**2)+
     +(STEL(2)*(SIN(THET))**2)+
     +(STEL(3)*(SIN(2.0*THET)))
      STELP2=STEL(1)+STEL(2)-STELP1
      STRP1=(STRESS(1)*(COS(THET))**2)+
     +(STRESS(2)*(SIN(THET))**2)+
     +(STRESS(3)*(SIN(2.0*THET)))
      STRP2=STRESS(1)+STRESS(2)-STRP1
      ENER=ENER+(((STRP1*STELP1)+(STRP2+STELP2))*DELIB(I)*0.5)
C***** AMEND STRESS TO ALLOW FOR ELEMENT CREEP IN 3RD DIMENSION = ELC
```

```
  192 ELC=E(I)/((1.0+P(I))*(1.0-2.0*P(I)))
      STRESS(1)=STRESS(1)+ELC*P(I)*STEL(4)
      STRESS(2)=STRESS(2)+ELC*P(I)*STEL(4)
      STRESS(4)=(ELC*P(I)*(STEL(1)+STEL(2)))+ELC*(1.0-P(I))*STEL(4)
C***** ADD INITIAL STRESS TO CALC STRESS
      DO 195 IK=1,4
  195 STRESS(IK)=STRESS(IK)+STREN(I,IK)
      IF(J.GT.1) GO TO 205
C***** PUT STRESSES INTO TRAY FOR INITIAL CYCLE
      DO 200 IK=1,4
  200 TRAY(I,IK)=STRESS(IK)
  205 CONTINUE
      AS=STRESS(1)-TRAY(I,1)
      BS=STRESS(2)-TRAY(I,2)
      CS=STRESS(3)-TRAY(I,3)
      DS=STRESS(4)-TRAY(I,4)
C***** STRESS ALTERATIONS ARE ZERO FOR INITIAL CYCLE
      ZAS=ABS(AS)
      ZBS=ABS(BS)
      ZCS=ABS(CS)
      DIFSTR=AMAX1(ZAS,ZBS,ZCS,DIFSTR)
      STRAY(I,1)=STRESS(1)
      STRAY(I,2)=STRESS(2)
      STRAY(I,3)=STRESS(3)
      STRAY(I,4)=STRESS(4)
C***** CALCULATE NEW ESTIMATE OF INCREMENT STRESS
      AS=TRAY(I,1)+AS/2.0
      BS=TRAY(I,2)+BS/2.0
      CS=TRAY(I,3)+CS/2.0
      DS=TRAY(I,4)+DS/2.0
C*****TO OBTAIN VALUE OF CREEP FROM STRESS AND STRAIN******************
C*****FOR PLANE STRAIN
      STRM=(AS+BS+DS)/3.0
      S1=AS-STRM
      S2=BS-STRM
      S3=CS
      S4=DS-STRM
      CREEP(1)=S1*TIMC/(VISCOS(I)*2.0)
      CREEP(2)=S2*TIMC/(VISCOS(I)*2.0)
      CREEP(3)=S3*TIMC/(VISCOS(I))
      CREEP(4)=S4*TIMC/(VISCOS(I)*2.0)
C***** AMEND MATRIX W FOR CREEP(4)
      AW1=ELC*P(I)*CREEP(4)
C*****PUT ELEMENT CREEP INTO CSTIN FOR NEXT CYCLE
      DO 210 NIL=1,4
  210 CSTIN(I,NIL)=CREEP(NIL)
C*****TO INCORPERATE INITIAL CREEP BY EXPRESSING AS INITIAL STRAIN
C*****TO MULTIPLY D BY CREEP
      N=3
      M=3
      L=1
      CALL GMPRD(D,CREEP,W,N,M,L)
      W(1)=W(1)+AW1
      W(2)=W(2)+AW1
C*****TO TRANSPOSE B TO F
      N=3
      M=6
      CALL GMTRA(B,F,N,M)
C*****TO MULTIPLY F BY W TO GIV
      N=6
```

```
      M=3
      L=1
      CALL GMPRD(F,W,V,N,M,L)
      DO 215 NERG=1,6
  215 V(NERG)=V(NERG)*DELTA/2.0
C*****TO MAKE FIST
      FIST(J1)=FIST(J1)+V(2)
      FIST(K1)=FIST(K1)+V(1)
      FIST(J2)=FIST(J2)+V(4)
      FIST(K2)=FIST(K2)+V(3)
      FIST(J3)=FIST(J3)+V(6)
      FIST(K3)=FIST(K3)+V(5)
  220 CONTINUE
C
C*****TO TEST FOR CONVERGENCE*********************************************
      IF(NTIM.LE.2.OR.IN.GT.1) GOTO 225
      WRITE(6,1165) DIFSTR
 1165 FORMAT(/2X,'DIFSTR=',E10.3)
  225 DFS(J)=DIFSTR
      IF(J.EQ.1) GO TO 230
      JH=J-1
      DIFSTR=DFS(J)-DFS(JH)
      DIFSTR=ABS(DIFSTR)
      IF(J.LE.2) DIFSTR=1.0E10
      IF(DIFSTR.LE.OUT) GO TO 235
  230 CONTINUE
  235 CONTINUE
C
C***** ADD CSTIN TO STIN TO FIND TOTAL INC. STRAIN
      DO 240 IJ=1,NEL
      DO 240 IK=1,4
  240 STIN(IJ,IK)=STIN(IJ,IK)+CSTIN(IJ,IK)
C***** ADD FIST TO FORST
      DO 245 IJ=1,NNOD2
  245 FORST(IJ)=FORST(IJ)+FIST(IJ)
  250 CONTINUE
C
C
C*****WRITE RESULTS FOR FINAL STATE***************************************
      IF(NDAT.LT.1) GOTO 255
      WRITE(6,1170)
 1170 FORMAT(/10X,'DISPLACEMENTS IN CMS, COORDINATES IN KMS'/)
      WRITE(6,1175)
 1175 FORMAT(/4X,'NODE',7X,'X DISPL.',5X,'Y DISPL.',7X,'X COORD.'
     +,2X,'Y COORD'/)
  255 DO 265 I=1,NNOD
      IJ=2*I
      IK=IJ-1
C****** CONVERT FROM CM TO KM
      X(I)=X(I)/1.0E5
      Y(I)=Y(I)/1.0E5
C*****SET INITIAL DISPLACEMENTS
      PREDIP(IK)=PREDIP(IK)+DISP(IK)*RNODEF
      PREDIP(IJ)=PREDIP(IJ)+DISP(IJ)*RNODEF
      IF (NDAT.LT.1) GOTO 265
      WRITE(6,1180) I,DISP(IK),DISP(IJ),X(I),Y(I)
 1180 FORMAT(4X,I4,5X,E10.3,3X,E10.3,3X,2F10.3)
  265 CONTINUE
C****** ADD HORIZONTAL TECTONIC AND LITHOSTATIC STRESS
      DO 266 I=1,NEL
```

```
      Y0=(Y(NODEL(I,1))+Y(NODEL(I,2))+Y(NODEL(I,3)))/3.0
      FF=(YMAX-Y0)*1.0E5*DENSUB*981.0
      IF(E(I).GT.1.0E8) STRAY(I,2)=STRAY(I,2)-FF
      IF(E(I).GT.1.0E8) STRAY(I,4)=STRAY(I,4)-FF
  266 IF(E(I).GT.1.0E8) STRAY(I,1)=STRAY(I,1)+XTTS-FF
C***** WRITE PREDIP AND STRAY*****************************************
C*****SEND TO FILE (DEVICE 2) FOR RESTART OPTION
      WRITE(2,1020) NNOD2
      IF(NDD.NE.0) GOTO 268
      IF (NFILE2.EQ.0) GOTO 275
  268 DO 270 IC=1,NNOD2
  270 WRITE(2,1025) PREDIP(IC),(STRAY(IC,JC),JC=1,4)
C****** WRITE PRESCRIBED SUBGRID DISPLACEMENTS TO FILE 2
  275 IF(NDD.EQ.0) GOTO 278
      WRITE(6,1185)
 1185 FORMAT(/2X,'THE FOLLOWING PRESCRIBED DISPLACEMENTS HAVE',
     +' BEEN WRITTEN TO FILE 2')
      WRITE(6,1187)
 1187 FORMAT(/4X,'FROM NODE',3X,'TO NODE',6X,'X - DISPLACEMENT',5X,
     +'Y - DISPLACEMENT',5X,'(KMS)'/)
      DO 277 I=1,NDD
      ISP2=1
      IJ=2*(LDD(I))
      IK=IJ-1
      DISP(IJ)=DISP(IJ)/1.0E5
      DISP(IK)=DISP(IK)/1.0E5
      WRITE(6,1188) LDD(I),LD2(I),ISP2,DISP(IK),ISP2,DISP(IJ)
 1188 FORMAT(I9,I11,3X,2(I10,F10.3))
  277 WRITE(2,1042) LD2(I),ISP2,DISP(IK),ISP2,DISP(IJ)
  278 WRITE(6,1065)
C
C***** TO CALCULATE THE PRINCIPAL STRESSES*****************************
      STMXD=0.0
      STMAX=0.0
      TAUX=0.0
      TAUN=1.0E20
      IFL=0
      NC=0
      NQ=0
      IF(NDAT.LT.-1) GOTO 285
      WRITE(6,1190)
 1190 FORMAT(/20X,'STRESSES IN CGS, COORDINATES IN KMS'/)
      WRITE(6,1195)
 1195 FORMAT(/11X,'PRINCIPAL STRESSES'6X,'ANGLE',6X,
     +'DEVIATORIC STRESSES'9X,'MAX SHEAR',4X,'CENTROID',6X,
     +'COULOMB',2X,'GRIFFITHS')
      WRITE(6,1200)
 1200 FORMAT(9X,'S1',8X,'S2',8X,'S3',3X,'TO HORIZ',3X,'S1',8X,'S2',
     +8X,'S3',8X,'STRESS',6X,'X',6X,'Y',5X,'STRENGTH   FRACTURE?'/)
  285 DO 310 I=1,NEL
      ANZA=0.0
      ANZB=0.0
      SC4=0.0
      IF(E(I).LT.1.0E5) GOTO 292
      SC1=STRAY(I,1)
      SC2=(STRAY(I,2))
      SC3=(STRAY(I,3))
      THET=0.0
      IF(SC1.EQ.SC2) GOTO 290
      THET=2.0*SC3/(SC1-SC2)
```

```
      THET=ATAN(THET)
      THET=THET/2.0
      THET=57.29*THET
      IF(THET.GT.0.0) GO TO 290
      THET=THET+90.0
  290 ALPHA=THET/57.29
      ANZA=(SC1*(COS(ALPHA))**2)+
     1 (SC2*(SIN(ALPHA))**2)+
     2 (SC3*(SIN(2.0*ALPHA)))
      ANZB=SC1+SC2-ANZA
      SC4=STRAY(I,4)
  292 AVER=(ANZA+ANZB+SC4)/3.0
      BXB=X(NODEL(I,1))+X(NODEL(I,2))+X(NODEL(I,3))
      BYB=Y(NODEL(I,1))+Y(NODEL(I,2))+Y(NODEL(I,3))
      BXB=(BXB)/3.0
      BYB=(BYB)/3.0
      Q=0.0
      C=0.0
      S1=ANZA-AVER
      S2=ANZB-AVER
      SC4Z=SC4-AVER
      ANZAA=ABS(ANZA)
      ANZBA=ABS(ANZB)
      SC4A=ABS(SC4)
      SA1=ABS(S1)
      SA2=ABS(S2)
      SAC4=ABS(SC4Z)
C****** CALCULATE MAX TOTAL AND DEVIATORIC STRESSES
      STMAX=AMAX1(STMAX,ANZAA)
      STMAX=AMAX1(STMAX,ANZBA)
      STMAX=AMAX1(STMAX,SC4A)
      STMXD=AMAX1(STMXD,SA1)
      STMXD=AMAX1(STMXD,SA2)
      STMXD=AMAX1(STMXD,SAC4)
      IF(DN(I)+DENSUB.LT.1.1) GOTO 295
C****** TEST FOR FAILURE
      IFL=1
      CALL FAIL(ANZA,ANZB,I,TS,XMU,Q)
      CALL SLIPS(ANZA,ANZB,XMU,SS,I,C)
      IF(C.LE.0.0) NC=1
      IF(Q.NE.0.0) NQ=1
  295 TAU=0.5*(ABS(ANZA-ANZB))
      IF (NDAT.LT.-1) GOTO 300
      WRITE(6,1205)I,ANZA,ANZB,SC4,THET,S1,S2,SC4Z,TAU,BXB,BYB,C,Q
 1205 FORMAT(I5,3E10.3,F5.1,1X,3E10.3,1X,1X,E10.3,2F7.3,5X,F4.2,6X,F4.1)
  300 TAU=TAU/1.0E6
      IF(E(I).LT.1.0E8) GOTO 305
      IF(NEST.LT.0) TAU=C
      TAUX=AMAX1(TAUX,TAU)
      TAUN=AMIN1(TAUN,TAU)
C****** WRITE STRENGTHS OR SHEAR STRESSES FOR CONTOURING
      WRITE(3,1210) BXB,BYB,TAU
 1210 FORMAT(2F6.2,F5.1)
      IF(IDIM.EQ.0) GOTO 305
      IF(BXB.LT.XMN.OR.BXB.GT.XMX) GOTO 305
      IF(BYB.LT.YMN.OR.BYB.GT.YMX) GOTO 305
      WRITE(7,1210) BXB,BYB,TAU
  305 XXX(I)=BXB
      YYY(I)=BYB
      STRAY(I,1)=ANZA
```

```
      STRAY(I,2)=ANZB
      STRAY(I,3)=THET
      STRAY(I,4)=SC4
      STRAY(I,5)=C
      VISCOS(I)=Q
  310 CONTINUE
C
C****** SET UP PLOTTING ***********************************************
      WRITE(3,1065)
      WRITE(7,1065)
      ENER=ABS(ENER)*1.0E-7
      IF(NTIM.EQ.1) WRITE(6,1212) ENER
 1212 FORMAT(/2X,'TOTAL ELASTIC STRAIN ENERGY EQUALS ',E10.3,' JOULES')
      IF(NEST.GE.0) WRITE(6,1215) TAUN,TAUX
 1215 FORMAT(/2X,'SHEAR STRESS RANGES FROM',F6.1,' BARS TO ',F6.1
     +,' BARS'/)
      IF(NEST.LT.0) WRITE(6,1218) TAUN,TAUX
 1218 FORMAT(/2X,'STRENGTH RANGES FROM',F6.2,' TO',F6.2/)
      IF(DENSUB.GT.0.0) WRITE(6,1216)DENSUB
 1216 FORMAT(60X,'A DENSITY OF ',F5.2,' WAS SUBTRACTED DURING'
     +,' CALCULATION'/)
      IF(NC.EQ.1) WRITE(6,1220)
      IF(NQ.EQ.1) WRITE(6,1225)
 1220 FORMAT(/2X,'K=1 MEANS TENSIONAL FAILURE, K=4 MEANS COLOMB-M'
     +,'OHR FAILURE'/)
 1225 FORMAT(/2X,'STRESS REGION 1= TENSIONAL'/2X,'STRESS REGION 2'
     +,'= OPEN CRACKS'/2X,'STRESS REGION 3= INTERMEDIATE'/2X,'STRESS'
     +,' REGION 4= CLOSED CRACKS'/)
      IF(IFL.EQ.0) WRITE(6,1228)
 1228 FORMAT(/2X,'NO TESTS FOR FAILURE HAVE BEEN CONDUCTED'/)
      XM=XMAX
      YM=YMAX
      XN=XMIN
      YN=YMIN
      YYMX=YMAX
      IF(NDAT.EQ.-2) GOTO 315
      IF(NDAT.EQ.1) GOTO 315
      GOTO 325
  315 IF(IDIM.EQ.0) GOTO 320
      XMAX=XMX
      XMIN=XMN
      YMAX=YMX
      YMIN=YMN
  320 CALL PLOTS(X,Y,NODEL,STRAY,NNOD,NEL,VISCOS,STMAX,
     +XMAX,YMAX,XMIN,YMIN,STMXD,NBOR,IBOR,E)
  325 CONTINUE
C***** SEND DATA TO CHANNEL 4 FOR POSSIBLE PLOTTING
      WRITE(4,1230) NNOD,NEL,DEV
      DO 335 I=1,NNOD
  335 WRITE(4,1235) X(I),Y(I)
      DO 340 I=1,NEL
      NM=1
  340 WRITE(4,1240) (STRAY(I,J),J=1,4)
      DO 345 I=1,NEL
      STRAY(I,3)=(STRAY(I,1)-STRAY(I,2))*0.5
  345 WRITE(4,1245)(NODEL(I,J),J=1,3)
 1230 FORMAT(2I10,F10.3)
 1235 FORMAT(2F10.3)
 1240 FORMAT(4E11.3)
 1245 FORMAT(3I10)
```

```
      WRITE(4,1020) NBOR
      WRITE(4,1250)(IBOR(I),I=1,NBOR)
      WRITE(4,1240) XMAX,XMIN,YMAX,YMIN
 1250 FORMAT(8I10)
  350 CALL PLOT(NEL,XXX,YYY,STRAY,XDIF,YDIF,YYMX)
      STOP
      END
C
      SUBROUTINE PLOT(N,XP,YP,STRAY,XDIF,YDIF,YMAX)
      DIMENSION K(101,56),ICHAR(26),XP(1),YP(1),STRAY(256,5)
      LEVEL 2,XP,YP,STRAY
      DATA IB/1H /,ICHAR/
     + 1HA,1HB,1HC,1HD,1HE,1HF,1HG,1HH,1HI,1HJ,1HK,1HL,
     + 1HM,1HN,1HO,1HP,1HQ,1HR,1HS,1HT,1HU,1HV,1HW,1HX,1HY,1HZ/
     +,IN/1H-/
      DO 4 L=1,5
      WRITE(6,1000)
 1000 FORMAT(1H1)
      DO 1 I=1,100
      DO 1 J=1,55
    1 K(I,J)=IB
      DO 2 I=1,N
      STR1=STRAY(I,1)
      STR2=STRAY(I,2)
      IF(STR1.GT.STR2) GOTO 6
      STR=STRAY(I,2)
      STRAY(I,2)=STRAY(I,1)
      STRAY(I,1)=STR
    6 Y=(YMAX-YP(I))/YDIF*55.0
      IY=Y+1.0
      X=XP(I)/XDIF*100.0
      IX=X+1.0
      IQ=0
      IF(STRAY(I,L).LT.0.0)IQ=1
      IF(L.EQ.1)STRAY(I,1)=STRAY(I,1)**2.0
      IF(L.EQ.2)STRAY(I,2)=STRAY(I,2)**2.0
      IF(L.EQ.3)STRAY(I,3)=STRAY(I,3)**2.0
      IF(L.EQ.4)STRAY(I,4)=STRAY(I,4)**2.0
      IF(L.EQ.5)STRAY(I,5)=(STRAY(I,5)*1.0E10)**2.0
      Z=ABS(STRAY(I,L))
      IZ=1
      IF(Z.GT.1.0) IZ=INT(ALOG10(Z))+1
      IF(Z.GT.1.0E25) IZ=26
      K(IX,IY)=ICHAR(IZ)
      IF(IQ.EQ.0) GOTO2
      IX=IX-1
      K(IX,IY)=IN
    2 CONTINUE
      IF(L.EQ.1) WRITE(6,1010)
      IF(L.EQ.2) WRITE(6,1011)
      IF(L.EQ.3) WRITE(6,1012)
      IF(L.EQ.4) WRITE(6,1013)
      IF(L.EQ.5) WRITE(6,1014)
 1010 FORMAT(10X,'SIGHMA1**2'/)
 1011 FORMAT(10X,'SIGHMA2**2'/)
 1012 FORMAT(10X,'MAX TAU**2'/)
 1013 FORMAT(10X,'SIGHMA3**2'/)
 1014 FORMAT(10X,'STRENGTH'/)
      DO 3 I=1,56
    3 WRITE(6,1001)(K(J,I),J=1,101)
```

```
 1001 FORMAT(10X,101A1)
    4 CONTINUE
      RETURN
      END
C
      SUBROUTINE GMPRD(A,B,R,N,M,L)
      DIMENSION A(1),B(1),R(1)
      IR=0
      IK=-M
      DO 10 K=1,L
      IK=IK+M
      DO 10 J=1,N
      IR=IR+1
      JI=J-N
      IB=IK
      R(IR)=0
      DO 10 I=1,M
      JI=JI+N
      IB=IB+1
   10 R(IR)=R(IR)+A(JI)*B(IB)
      RETURN
      END
C
C*****  SUBROUTINE MATRIX TRANSPOSITION**********************************
      SUBROUTINE GMTRA(A,R,N,M)
      DIMENSION A(1),R(1)
      IR=0
      DO 10 I=1,N
      IJ=I-N
      DO 10 J=1,M
      IJ=IJ+N
      IR=IR+1
   10 R(IR)=A(IJ)
      RETURN
      END
C
      SUBROUTINE MATSOL(A,B,IA,N,NW,PT)
      DIMENSION  A(IA,1),B(N)
      EQUIVALENCE (IP,I,NEX,KIB,NCO),(NR12,NS,J,LBO),
     +(AMAXT,TBEST,TEMP)
      LEVEL 2,A
      NR=(NW-1)/2
      NR1=NR+1
      NR2=NR1+NR
      NR32=NR2+NR1
      IF(PT.EQ.0.) GOTO 50
      DO 5 ISET=1,N
      NR12=MIN0(NR2+1,N-ISET+NR1+1)
      DO 5 JSET=NR12,NR32
    5 A(ISET,JSET)=0.0
      DO 45 K=1,N
      IP=K
      NS=NR1
      BEST=ABS(A(IP,NS))
      DO 10 NFT=1,NR
      IPT=K+NFT
      IF(IPT.GT.N) GOTO 10
      NT=NR1-NFT
      TBEST=ABS(A(IPT,NT))
      IF(BEST.GE.TBEST) GOTO 10
```

```
      BEST=TBEST
      NS=NT
      IP=IPT
   10 CONTINUE
      IF(K.EQ.1)PT=BEST
      PT=AMIN1(BEST,PT)
      IF(BEST.NE.0.) GOTO 20
      WRITE(6,1000)
 1000 FORMAT(///' ZERO PIVOT FOUND IN MATSOL.  ATTEMPT TO SOLVE THE SYST
     +EM OF EQUATIONS ABANDONED.'///)
      RETURN
   20 A(K,NR32)=IP
      IF(IP.EQ.K) GOTO 30
      DO 25 NV=1,NR2
      TEMP=A(K,NR+NV)
      A(K,NR+NV)=A(IP,NS+NV-1)
   25 A(IP,NS+NV-1)=TEMP
C     ELIMINATION AND COEFF. STORAGE
   30 IF(K+NR.LE.N) GOTO 35
      NL=N-K
      IF(NL)45,45,40
   35 NL=NR
   40 CONTINUE
      CALL MATHEL (A,NL,K,NR,IA)
   45 CONTINUE
C     NOW B IS PROCESSED
   50 DO 60 KB=1,N
      NEX= A(KB,NR32)
      IF(NEX.EQ.KB) GOTO 55
      TEMP=B(KB)
      B(KB)=B(NEX)
      B(NEX)=TEMP
   55 DO 60 IB=1,NR
      KIB=KB+IB
      IF(KIB.GT.N) GOTO 60
      B(KIB)=B(KIB)-B(KB)*A(KB,IB)
   60 CONTINUE
C     BACK SUBSTITUTE
      DO 70 NBACK=1,N
      NCO=N+1-NBACK
      BNCO=B(NCO)
      L2=MIN0(NR2,NBACK)
      IF(L2.EQ.1)GO TO 70
      DO 65 LCO=2,L2
   65 BNCO=BNCO-B(LCO+NCO-1)*A(NCO,LCO+NR)
   70 B(NCO)=BNCO/A(NCO,NR1)
      RETURN
      END
C
      SUBROUTINE MATHEL(A,NL,K,NR,IA)
      DIMENSION A(1)
      LEVEL 2,A
      NR1 = NR + 1
      NR3 = 3*NR
      J4 = K + NR*IA
      PIVT = A(J4)
      DO 9 IK =1,NL
      I = IK + K
      J1 = I + (NR-IK)*IA
      TEMP = -A(J1)/PIVT
```

```
      A(K + (IK-1)*IA) = - TEMP
      J2 = I + (NR3-IK)*IA
      J3 = J4
      DO 9 J=J1,J2,IA
      A(J) = A(J) + A(J3)*TEMP
      J3 = J3 + IA
9     CONTINUE
      RETURN
      END
C
      SUBROUTINE PLOTS(X,Y,NODEL,STRAY,NNOD,NEL,VISCOS,
     + STMAX,XMAX,YMAX,XMIN,YMIN,STMXD,NB,IB,E)
      DIMENSION X(1),Y(1),NODEL(214,3),STRAY(256,5),DISP(1)
     +,IB(10),E(1),VISCOS(1)
      LEVEL 2,STRAY,VISCOS,E
      XDIF=XMAX-XMIN
      YDIF=YMAX-YMIN
      CMAX=AMAX1(XDIF,YDIF)
      FAC=CMAX/10.0
      XL=XMIN
      XU=XMIN+CMAX+FAC/2.0
      YL=YMIN-(FAC/2.0)
      YU=YMIN+CMAX
      STMXD=0.0
      STMAX=0.0
      DO 5 I=1,NEL
      XXC=(X(NODEL(I,1))+X(NODEL(I,2))+X(NODEL(I,3)))/3.0
      YYC=(Y(NODEL(I,1))+Y(NODEL(I,2))+Y(NODEL(I,3)))/3.0
      IF(XXC.GT.XMAX.OR.XXC.LT.XMIN) GOTO 5
      IF(YYC.GT.YMAX.OR.YYC.LT.YMIN) GOTO 5
      STMAX=AMAX1(STMAX,ABS(STRAY(I,1)))
      STMAX=AMAX1(STMAX,ABS(STRAY(I,2)))
      AVER=(STRAY(I,1)+STRAY(I,2)+STRAY(I,4))/3.0
      STD1=STRAY(I,1)-AVER
      STD2=STRAY(I,2)-AVER
      STD4=STRAY(I,4)-AVER
      STMXD=AMAX1(STMXD,ABS(STD1),ABS(STD2),ABS(STD4))
    5 CONTINUE
      CALL PAPER(1)
      CALL PSPACE(0.1,0.75,0.1,0.75)
      CALL MAP(XL,XU,YL,YU)
      CMAXX=CMAX
      DO 40 IDEV=1,2
      CMAX=CMAXX
      STSC=2.2E11/CMAX
      IF(IDEV.EQ.2) STMXD=STMAX
      IF(STMXD.LT.0.5E10) STSC=1.0E11/CMAX*2.0
      IF(STMXD.LT.2.5E9) STSC=5.0E10/CMAX*2.0
      IF(STMXD.LT.1.0E9) STSC=2.0E10/CMAX*2.0
      IF(STMXD.LT.0.25E9) STSC=5.0E9/CMAX*2.0
      IF(STMXD.LT.0.5E8) STSC=1.0E9/CMAX*2.0
      STSC=STSC*0.85
      XOR=XL+(FAC/4.0)
      YOR=YMAX+(FAC/8.0)
      CALL CTRORI (0.0)
      CALL CTRMAG(8)
      IF(IDEV.EQ.1) CALL PLOTCS(XOR,YOR,20H DEVIATORIC STRESSES,20)
      IF(IDEV.EQ.2) CALL PLOTCS(XOR,YOR,15H TOTAL STRESSES,15)
      YQ=YMIN-(FAC/6.0)
      YQ1=YQ-(FAC/5.0)
```

```
      CMAX2=XMIN+(CMAX/9.0)
      CMAX3=CMAX2+1.0
      MQ=0
      IF(CMAX3.GT.(0.8*XMAX)) MQ=1
      IF(MQ.EQ.1) CMAX3=CMAX2+0.5
      IF(CMAX3.GT.(0.8*XMAX)) MQ=2
      IF(MQ.EQ.2) CMAX3=CMAX2+0.1
      CALL POSITN(CMAX2,YQ)
      CALL JOIN(CMAX3,YQ)
      CMAX8=(CMAX2+CMAX3)*0.3
      IF(MQ.EQ.0) CALL PLOTCS(CMAX8,YQ1,5H 1 KM,5)
      IF(MQ.EQ.1) CALL PLOTCS(CMAX8,YQ1,7H 0.5 KM,7)
      IF(MQ.EQ.2) CALL PLOTCS(CMAX8,YQ1,7H 0.1 KM,7)
      CMAX4=CMAX3+(CMAX/7.0)
      CMAX5=CMAX4+(2.0E10/STSC)
      IF(CMAX5.GT.XU) CMAX5=CMAX4+(2.0E9/STSC)
      IF(CMAX5.GT.XU) MQ=3
      IF(MQ.EQ.3) CMAX5=CMAX4+(2.0E8/STSC)
      IF(CMAX5.GT.XU) GOTO 15
      CALL POSITN(CMAX4,YQ)
      CALL JOIN(CMAX5,YQ)
      CALL POSITN(CMAX4,YQ1)
      CALL TYPECS(3H 10,3)
      CALL SUPFIX
      CMAX5=CMAX4+(2.0E10/STSC)
      IF(MQ.EQ.3) CALL TYPECS(1H8,1)
      IF(MQ.EQ.3) GOTO 10
      IF(CMAX5.GT.XU) CALL TYPECS(1H9,1)
      IF(CMAX5.LE.XU) CALL TYPECS(2H10,2)
   10 CALL NORMAL
      CALL SPACE(2)
      CALL TYPECS(9H DYNES/CM,9)
      CALL SUPFIX
      CALL TYPECS(1H2,1)
   15 CALL NORMAL
      DO 30 I=1,NEL
      IF(E(I).LT.1.0E10) GOTO 30
      AVER=(STRAY(I,1)+STRAY(I,2)+STRAY(I,4))/3.0
      IF(IDEV.EQ.2) AVER=0.0
      X1=X(NODEL(I,1))
      Y1=Y(NODEL(I,1))
      X2=X(NODEL(I,2))
      Y2=Y(NODEL(I,2))
      X3=X(NODEL(I,3))
      Y3=Y(NODEL(I,3))
      XXC=(X1+X2+X3)/3.0
      YYC=(Y1+Y2+Y3)/3.0
      IF(XXC.GT.XMAX.OR.XXC.LT.XMIN) GOTO 30
      IF(YYC.GT.YMAX.OR.YYC.LT.YMIN) GOTO 30
      ST1=STRAY(I,1)-AVER
      ST2=STRAY(I,2)-AVER
      ST4=STRAY(I,4)-AVER
      TA=COS(STRAY(I,3)/57.29)*ST1/STSC
      TB=SIN(STRAY(I,3)/57.29)*ST1/STSC
      TX=COS(STRAY(I,3)/57.29)*ST2/STSC
      TY=SIN(STRAY(I,3)/57.29)*ST2/STSC
      XN1=XXC+TA
      XN2=XXC-TA
      YN1=YYC+TB
      YN2=YYC-TB
```

```
      XS1=XXC-TY
      XS2=XXC+TY
      YS1=YYC+TX
      YS2=YYC-TX
      CALL POSITN(XN1,YN1)
      CALL JOIN(XN2,YN2)
      CALL POSITN(XS1,YS1)
      CALL JOIN(XS2,YS2)
      TA=ST1
      TX=ST2
      QUAD=(STRAY(I,3)/90.0)-1.0
      IF(TA.LT.0.0) QUAD=QUAD+2.0
      IF(TA.LT.0.0) GOTO 20
      CALL CTRORI(QUAD)
      CALL PLOTNC(XN1,YN1,54)
      QUAD=QUAD+2.0
      CALL CTRORI(QUAD)
      CALL PLOTNC(XN2,YN2,54)
   20 CONTINUE
      IF(TX.LT.0.0) GOTO 25
      QUAD=QUAD-1.0
      CALL CTRORI(QUAD)
      CALL PLOTNC(XS1,YS1,54)
      QUAD=QUAD+2.0
      CALL CTRORI(QUAD)
      CALL PLOTNC(XS2,YS2,54)
   25 RAD=ABS(ST4)/STSC
      CALL POSITN(XXC,YYC)
      CALL CIRCLE(RAD)
   30 CONTINUE
      XBOR=X(IB(1))
      YBOR=Y(IB(1))
      CALL POSITN(XBOR,YBOR)
      DO 35 I=2,NB
      XB=X(IB(I))
      YB=Y(IB(I))
   35 CALL JOIN(XB,YB)
      CALL JOIN(XBOR,YBOR)
      CALL FRAME
   40 CONTINUE
      CALL PSPACE(0.1,0.75,0.1,0.75)
      CALL MAP(XL,XU,YL,YU)
      YQ1=YQ+(FAC/5.0)
      CALL WINDOW(XL,XU,YQ1,YU)
      CALL CTRORI(0.0)
      CALL CTRMAG(8)
      CALL PLOTCS(CMAX2,YQ,27H MAX. SHEAR STRESSES (BARS),27)
      DO 60 I=1,NEL
      CALL CTRMAG(8)
      X1=X(NODEL(I,1))
      Y1=Y(NODEL(I,1))
      X2=X(NODEL(I,2))
      Y2=Y(NODEL(I,2))
      X3=X(NODEL(I,3))
      Y3=Y(NODEL(I,3))
      CALL POSITN(X1,Y1)
      CALL JOIN(X2,Y2)
      CALL JOIN(X3,Y3)
      CALL JOIN(X1,Y1)
      IF(E(I).LT.1.0E8) GOTO 60
```

```
      A=ABS(Y3*X2-Y2*X3-X1*Y3+X1*Y2+Y1*X3-Y1*X2)*625.0/
     +(CMAX**2)
      IF(A.LT.0.3) GOTO 60
      IF(A.LT.0.6) CALL CTRMAG(4)
      XXC=(X1+X2+X3)/3.0
      IF(A.LT.1.2) CALL CTRMAG(6)
      YUP=0.0
      YDO=0.0
      DO 45 J=1,3
      YUP=AMAX1(YUP,Y(NODEL(I,J)))
   45 YDO=AMIN1(YDO,Y(NODEL(I,J)))
      YY=YUP-YDO
      YYC=(Y1+Y2+Y3)/3.0
      IF(XXC.GT.XMAX.OR.XXC.LT.XMIN) GOTO 60
      IF(YYC.GT.YMAX.OR.YYC.LT.YMIN) GOTO 60
      RDT=STRAY(I,1)-STRAY(I,2)
      RDT=RDT/2.0
      RDT=ABS(RDT)
      RDT=RDT/1.0E6
      CALL PLOTNF(XXC,YYC,RDT,1)
      YYC=YYC-(YY/50.0)
      C=STRAY(I,5)
      Q=VISCOS(I)
      IF(C.LT.1.0) GOTO 50
      IF(Q.LT.0.0) CALL PLOTCS(XXC,YYC,4H* + ,4)
      IF(Q.EQ.0.0) CALL PLOTCS(XXC,YYC,4H *  ,4)
      GOTO 55
   50 IF(Q.LT.0.0) CALL PLOTCS(XXC,YYC,4H +  ,4)
   55 CONTINUE
   60 CONTINUE
      CALL GREND
      END
C
      SUBROUTINE FAIL(S1,S2,I,TS,MU,Q)
      REAL MU,IFC,L
      DATA A,B,C,D,E,BLANK/1HA,1HB,1HC,1HD,1HE,1H /
      S1=-S1
      S2=-S2
C      +VE STRESSES ARE COMPRESSIONAL
C      SO P IS SIGHMA2 AND R IS SIGHMA1
      T=TS
      FAC=-4.19
      L=BLANK
      P=AMAX1(S1,S2)
      R=AMIN1(S1,S2)
      SC=FAC*T
C      FAILURE CRITERIA
      OCFC=(P-R)*(P-R)+8.0*T*(P+R)
      IFC=P*P+P*(6.0*R-4.0*SC)+(R*R-4.0*R*SC)
      ALPHA=(SQRT(1.0+MU**2))/MU
      BETA=(4.0*T*SQRT(1.0-(SC/T))/MU)+2.0*SC
      CCFC=BETA/(1.0-ALPHA)-R*(1.0+ALPHA)/(1.0-ALPHA)
C      DEFINE POSSIBLE CLOSED CRACK REGION
      THETA=0.5*ATAN(1.0/MU)
      DE=SC/(COS(THETA)**2)-R*(TAN(THETA)**2)
C      FIND INTERSECTION OF OCFC AND CCFC
      AA=(ALPHA+1.0)/(ALPHA-1.0)
      BB=BETA/(1.0-ALPHA)
      CC=8.0*T
      F=(AA-1.0)**2
```

```
      G=2.0*BB*(AA-1.0)+CC*(AA+1.0)
      H=BB*(BB+CC)
      DC=(-G+SQRT(G**2-4.0*F*H))/2.0/F
C      DEFINE MIN. SIG1 FOR IFC TO BE EFFECTIVE
      DB=SC-2.0*T+2.0+SQRT(T*(2.0*T-SC))
C      DEFINE MAX. SIG1 FOR IFC TO BE EFFECTIVE
      DD=SC*((2.0*ALPHA*(ALPHA+1.0))/(2.0*ALPHA**2-1.0))
C      TEST FOR FAILURE REGION
      D=P+3.0*R
      IF(D.LT.0.0) GOTO 2
      IF(P.LT.SC) GOTO 3
      IF(R-SC) 4,4,9
C
C      TENSIONAL REGION
    2 CONTINUE
      K=1
      IF(R.LT.T) K=-1
      GOTO 100
C
C      OPEN CRACK REGION
    3 K=2
      IF(OCFC.GT.0.0) K=-2
      GOTO 100
C
C      INTERMEDIATE REGION
    4 K=3
C      TEST FOR SUBREGION
      IF(P.GT.DE) GOTO 5
C      OPEN CRACK
      L=A
      IF(OCFC.GT.0.0) K=-3
      GOTO 100
C      TEST FOR SUBREGION
    5 IF(R.GT.DC) GOTO 6
C      CLOSED CRACK
      L=B
      IF(P.GT.CCFC) K=-3
      GOTO 100
C      TEST FOR SUBREGION
    6 IF(P.GT.DB) GOTO 7
C      OPEN CRACK
      L=C
      IF(OCFC.GT.0.0) K=-3
      GOTO 100
C      TEST FOR SUBREGION
    7 IF(P.GT.DD) GOTO 8
C      INTERMEDIATE
      L=D
      IF(IFC.GT.0.0) K=-3
      GOTO 100
C      CLOSED CRACK
    8 L=E
      IF(P.GT.CCFC) K=-3
      GOTO 100
C
C      CLOSED CRACK REGION
    9 K=4
      L=BLANK
      IF(P.GT.CCFC) K=-4
C
```

```
  100 CONTINUE
C       NEGATIVE VALUES OF K DENOTE FAILURE
      IF(K.GT.0) GOTO 2001
      WRITE(6,2000)I, K,L
      IF(K.LT.0.0)Q=FLOAT(K)
 2000 FORMAT(2X,'ELEMENT',I4,' FAILED IN STRESS REGION',I4,2X,A1)
 2001 CONTINUE
      S1=-S1
      S2=-S2
      RETURN
      END
C
      SUBROUTINE SLIPS(SS1,SS2,XMU,SS,I,C)
      BETA=0.0
      S1=-SS1
      S2=-SS2
      K=0
      XINT=-SS/XMU
      IF(S1.LT.XINT.OR.S2.LT.XINT) K=1
      IF(K.EQ.4) GOTO 1
      SUM=S1+S2
      IF(S1.GT.S2) GOTO 2
      SSX=S1
      S1=S2
      S2=SSX
    2 DIF=S1-S2
      SMU=2.0*SS*XMU
      XMU2=1.0+(XMU*XMU)
      W1=SMU-SUM
      TRM1=(SMU-SUM)*(SMU-SUM)
      W2=S2*S1
      W3=SS*SS+(S1*S2)
      TRM2=4.0*XMU2*(SS*SS+(S1*S2))
C       TEST IF MOHR CIRCLE INTERSECTS ENVELOPE
      DIF2=TRM1-TRM2
      IF(DIF2.LT.0.0) GOTO 5
      SQ=SQRT(TRM1-TRM2)
      SIGMA1=(SUM-SMU+SQ)/2.0/XMU2
      SIGMA2=(SUM-SMU-SQ)/2.0/XMU2
      COSB1=(2.0*SIGMA1-SUM)/DIF
      COSB2=(2.0*SIGMA2-SUM)/DIF
      BETA1=0.5*ACOS(COSB1)
      BETA2=0.5*ACOS(COSB2)
      DO 10 N=1,19
      ANG=BETA*57.29
      IF(BETA.LE.BETA1.AND.BETA.GE.BETA2)K=4
      IF(BETA.GE.BETA1.AND.BETA.LE.BETA2)K=4
    1 IF(K.EQ.0) GOTO 10
      WRITE(6,1000) ANG,I,K
       C=-1.0
      GOTO 5
   10 BETA=BETA+(5.0/57.29)
 1000 FORMAT (2X,'FAULT AT',F4.0,' DEGREES TO SIGMA 1 FAILED IN ELEMENT
     +',I4,' ,K=',I3)
    5 H=SUM*0.5
      R=DIF*0.5
      DIST=((XMU*H)+SS)/SQRT(XMU**2+1.0)
      C=(ABS(DIST)-R)/1.0E9
      RETURN
      END
```

APPENDIX 5

Visco-Elastic Finite Element Formulation

The rate at which visco-elastic creep strains develop depends both on the current state and the past history of stress and strain. However, in linear visco-elasticity, e.g. that of a Maxwell substance described by:

$$\dot{\varepsilon} = 1/E\ \dot{\sigma} + \frac{1}{2\eta}\sigma \qquad \text{(A5.1)}$$

where the creep strains are explicitly separated from the elastic strains, it is possible to equate the constitutive law with that of an elastic relationship (Zienkiewicz, 1971):

$$\{\sigma\} = [D](\{\varepsilon\}-\{\varepsilon_o\}) \qquad \text{(A5.2)}$$

by using the viscous creep as an initial strain. Thus the finite-element equation becomes:

$$[K]\{\delta\} = \{F\}_{TOT} + \{F\}_{\varepsilon_o} \qquad \text{(A5.3)}$$

where

$$\{F\}_{\varepsilon_o} = \int [B]^T [D]' \{\varepsilon_o\}_v d(vol)$$

and, integrating A5.1,

$$\{\varepsilon_o\}_v = \begin{Bmatrix} \varepsilon_{ox} \\ \varepsilon_{oy} \\ \varepsilon_{oxy} \\ \varepsilon_{oz} \end{Bmatrix} = \frac{\Delta t}{2\eta} \begin{Bmatrix} \sigma_x - \sigma_{av} \\ \sigma_y - \sigma_{av} \\ 2\sigma_{xy} \\ \sigma_z - \sigma_{av} \end{Bmatrix} \qquad \text{(A5.4)}$$

where $\sigma_{av} = 1/3(\sigma_x + \sigma_y + \sigma_z)$.

The final solution is thus approached by the iteration of small time steps, Δt, during which the stress and strain are assumed to remain constant. The

stress value for a particular step is unknown before it is begun, but is initially approximated to by the stress at the end of the previous increment. After the stress state at the end of the increment has been calculated using equation A5.2 and the constitutive equations, a better estimate of the average stress state for the increment is calculated. The finite element process can thus be repeated until only small changes in stress occur - usually this is achieved within only two or three cycles.

Despite the assumption of overall plane strain, the viscous strain in the third direction, $\{\varepsilon_z\}_v$, is not equal to zero (Kusznir, 1976), and so:

$$[D]'\{\varepsilon_o\}_v = \frac{E(1-\nu)}{(1+\nu)(1-2\nu)} \begin{bmatrix} 1 & \nu/1-\nu & \nu/1-\nu & 0 \\ \nu/1-\nu & 1 & \nu/1-\nu & 0 \\ 0 & 0 & 0 & \frac{1-2\nu}{2(1-\nu)} \end{bmatrix} \begin{Bmatrix} \varepsilon_x \\ \varepsilon_y \\ \varepsilon_z \\ \varepsilon_{xy} \end{Bmatrix} \quad \text{(A5.5)}$$

It follows that the elastic creep, $\{\varepsilon_z\}_e = -\{\varepsilon_z\}_v$, and the constitutive equations thus become:

$$\begin{Bmatrix} \sigma_x \\ \sigma_y \\ \sigma_{xy} \\ \sigma_z \end{Bmatrix} = \frac{E(1-\nu)}{(1+\nu)(1-2\nu)} \begin{bmatrix} 1 & \nu/1-\nu & \nu/1-\nu & 0 \\ \nu/1-\nu & 1 & \nu/1-\nu & 0 \\ \nu/1-\nu & \nu/1-\nu & 1 & 0 \\ 0 & 0 & 0 & \frac{1-2\nu}{2(1-\nu)} \end{bmatrix} (\{\varepsilon\}-\{\varepsilon_o\}) \quad \text{(A5.6)}$$

The stiffness matrix is of course still identical to that formulated for the elastic case, since $\{\varepsilon_z\}_{TOT} = 0$. It is thus convenient to partially invert the solution matrices for permanent use throughout the time steps. The propagation of the visco-elastic process through time is demonstrated in Fig. A5.1.

The numerical process has been found to be stable as long as the incremental viscous creep is less than the incremental elastic strain. This corresponds to a maximum time step given by:

$$\Delta t = \frac{2\eta}{E} \qquad (A5.7)$$

Total relaxation is usually achieved within a total time equal to $10\Delta t$.

References

1. Kusznir, N. J., 1976. Theoretical Studies of the Geodynamics of Accretion Boundaries in Plate Tectonics. Unpublished Ph.D. Thesis, University of Durham.

2. Zienkiewicz, O. C., 1971. The Finite Element Method in Engineering Science, McGraw-Hill, London, 521 pp.

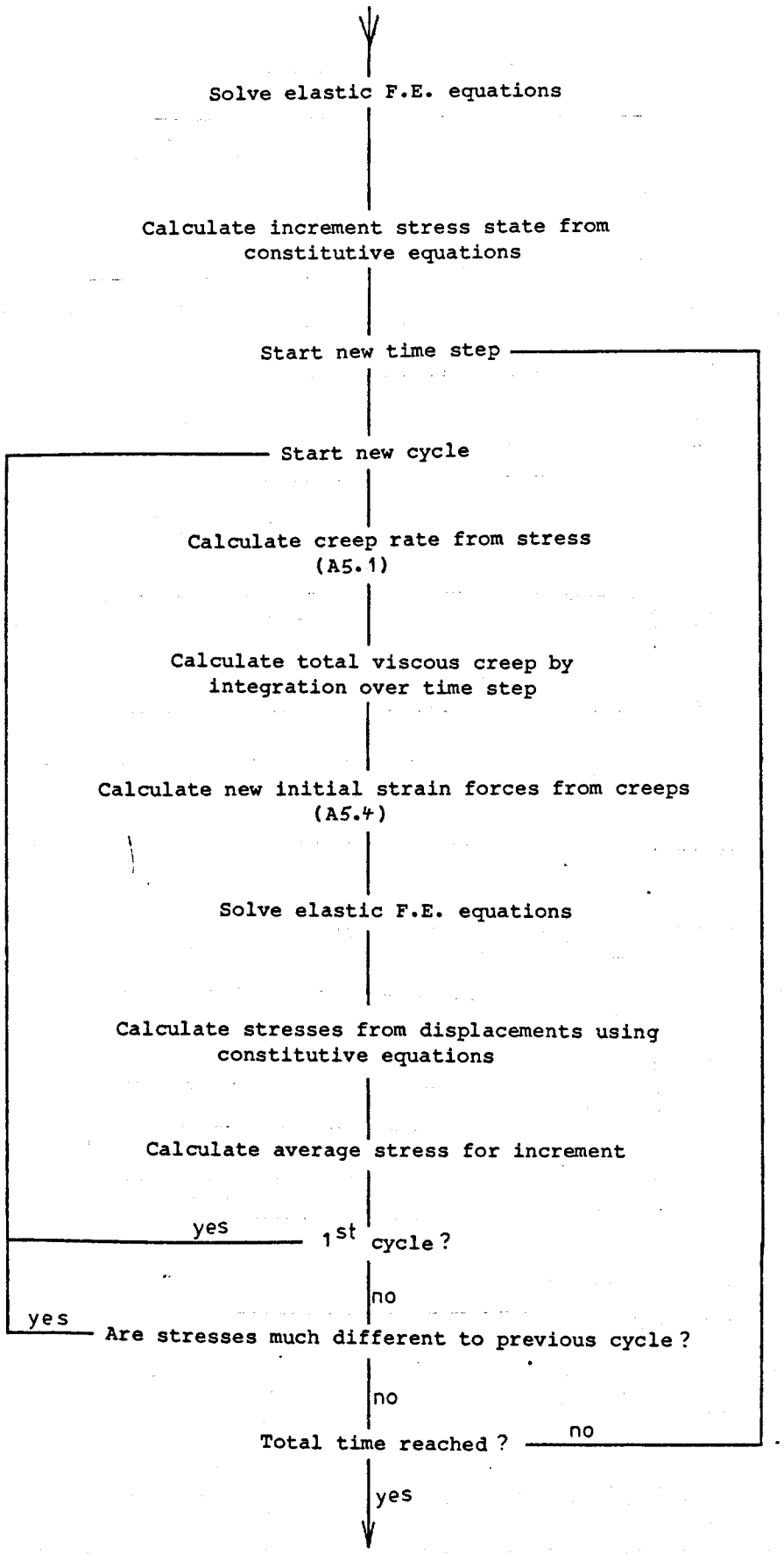

Figure A5.1 Visco-Elastic Algorithm

APPENDIX 6

Initial Stress Transfer

As a useful test of the correct transfer of stresses between the visco-elastic and subsequent elastic finite-element computations, it is possible to check the stresses and displacements resulting from the elastic run whose initial topography, boundary conditions etc., are identical to those of the visco-elastic run.

The original run can be described by:

$$[K]\{\delta_1\} = \{F\}_p + [B]^T[D]\{\varepsilon_\cdot\} \qquad (A6.1)$$

where the notation is the same as that of #2.2. The stresses can then be calculated by using:

$$\{\sigma_1\} = [D][B]\{\delta_1\} - [D]\{\varepsilon_\cdot\} \qquad (A6.2)$$

after a large number of iterations, since initial stresses are zero. These stresses then become the initial stresses in the elastic run ($\sigma_0 = \sigma_1$):

$$[K]\{\delta_2\} = \{F\}_p - \{F\}\sigma_0 \qquad (A6.3)$$

where

$$\{F\}\sigma_0 = [B]^T\{\sigma_0\}$$

The stiffness matrix, elasticity matrix, [B] matrix and body forces are of course the same as that in A6.1, and so, equating A6.2 and A6.3:

$$[K]\{\delta_2\} = \{F\}_p - [B]^T[D][B]\{\delta_1\} + [B]^T[D]\{\varepsilon_\cdot\} \qquad (A6.4)$$

Now as $[K] = [B]^T[D][B]$, the right hand sidebecomes zero by A6.1, so $\{\delta_2\}$ must also be zero. The stresses in the elastic run are calculated by:

$$\{\sigma_2\} = [D][B]\{\delta_2\} + \{\sigma_0\} \qquad (A6.5)$$

i.e. $\{\sigma_2\} = \{\sigma_1\}$

The displacements produced by the elastic run must therefore be zero, and the stresses equal to the initial stresses.

APPENDIX 7

A Test for the Visco-Elastic Finite-Element Program FERBIS

The program was tested by comparing the results with the analytical solution obtained by Lee et al. (1959) for a hollow visco-elastic cylinder subjected to internal pressure and reinforced by an external steel sheet. Only one quarter of the cylinder was modelled as there is axial symmetry. Both the analytical and finite-element solutions assume plane-strain conditions. The dimensions and the mechanical constants of the cylinder are shown in Fig. A7.1, along with the finite-element subdivision used.

The analytical results are compared with the finite element solutions in Fig. A7.2. As can be seen, there is good agreement between the two. The tangential stresses are measured in terms of the applied pressure P_o, and the times in terms of the Maxwell relaxation time, τ_o, for the cylinder. τ_o has been made equal to 1 sec. by appropriate selection of the mechanical constants, and corresponds to 8/3 times the elemental time constant for the finite-element process. Each iteration was actually conducted over 3/8 x 0.01 sec., so that, for example, it took 27 iterations to cover a time equal to $0.1\tau_o$.

Reference

Lee, E. H., Radok, J. R. M., and Woodward, W. B., 1959. Stress Analysis for Linear Viscoelastic Materials. Trans. Soc. Rheology, 3, 41-59.

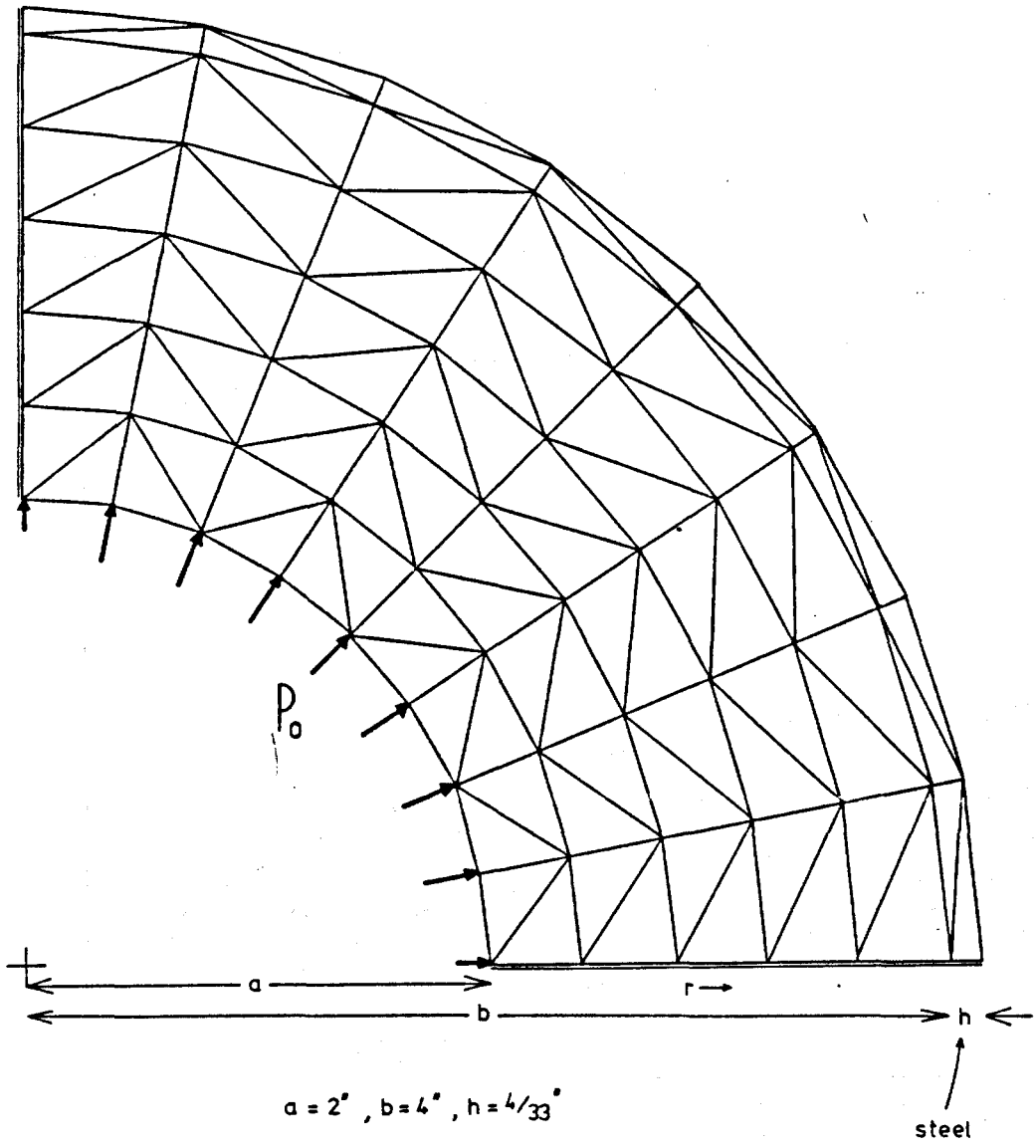

	V/E material	Steel
E	10^5 psi	3×10 psi
ν	$1/3$	$1/\sqrt{\tau}$
η	$3/8 \times 10^5$ psi.sec.	10^{60} psi.sec.

condition of zero displacement perpendicular to boundary.

Figure A7.1 Grid for test of visco-elastic finite element program.

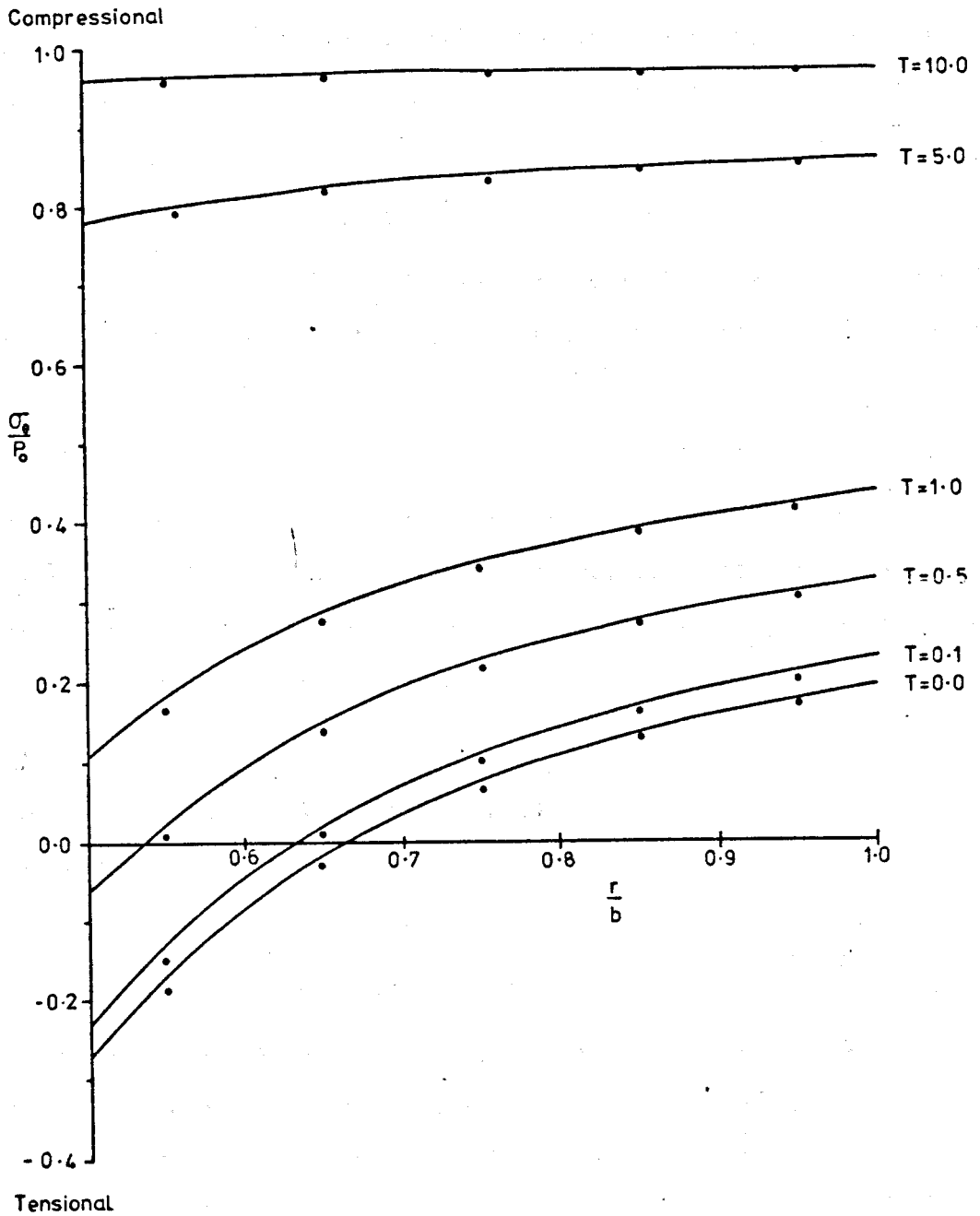

Figure A7.2 Visco-elastic finite element solutions (dots) compared to analytical solution for internally pressurised cylinder.

APPENDIX 8

Finite Difference Pore Pressure Diffusion Program

The program listed in this Appendix effectively calculates the diffusion of pore pressure over a finite element grid. It achieves this by superposing a rectangular finite difference grid over it, and assigning and initial and/or constant pressures on particular finite element grid nodes to the near finite difference node. Pressures and boundary conditions may be also read directly into the finite difference grid if desired, although knowledge of the size and shape of this grid has to be obtained beforehand for this to be possible, by using a preliminary run of the program. After calculation of the pressure diffusion over the stated time, the pressures are assigned to the centroid of each finite element using a weighted average of the three closest finite difference grid points. The program then calculates the effective stresses, using stresses written on stream 4 of the finite element program FERBIS (Appendix 4), and then uses four different failure criteria with these.

Main Program

A flow diagram is given in Fig. A8.1.

Subroutine FAIL

This subroutine uses the principal effective stresses to test for rock fracture using the Modified Griffiths Criterion as described in Section 2.4. If fracture occurs, a value for Q is assigned, corresponding to the particular fracture region (Fig. 2.9).

Subroutine SLIPS

This subroutine uses the principal effective stresses to test for slippage along a pre-formed fault plane using the Coulomb-Mohr criterion.

Subroutine PLPRNT

This subroutine writes the values of the pressures of the top ten rows of nodes. It is called for the first ten iterations, and then on a further ten equally spaced occasions during the remaining iterations.

Subroutine PLOT

This subroutine produces a line printer alphanumeric representation of the final pressure distribution. As the size of the diagram is fixed, the vertical and horizontal scales are usually not the same.

Subroutine ANGCAL

This subroutine calculates the angle subtended at a node by two ready nodes in the finite difference grid.

Subroutine DISCAL

This subroutine calculates the distance between two finite difference nodes, and compares it with a previously set minimum distance.

Subroutine CLCMP

This subroutine plots the finite element grid in black, with the finite difference nodes superposed in red.

Subroutine PLCONT

This subroutine produces contours of the pressure distribution on ten equally spaced occasions during the iteration process.

Subroutine SAFAIL

This subroutine tests for failure using the two criteria due to Murrell (see Section 2.4).

Input Data

The data is in C.G.S. units, unless otherwise stated. The following are internal parameters set in the program:-

TS	tensile strength
XMU	coefficient of internal friction
SS	shear strength
TEND	length of time for which diffusion process is to take place.

The following data are read in on streams 4, 5 and 1. Stream 4 is output from FERBIS on stream 4, and stream 5 is output from GRDGEN.

1. NNOD,NEL,DEV (stream 4) (2I10,F10.3)

NNOD,NEL	overwritten by statement 4.
DEV	a dummy parameter.

2. X(I),Y(I) (stream 4) (2F10.3)

X,Y	dummy parameters.

3. (STRAY(I,J),J=1,4) (stream 4) (4E11.3)

STRAY(J=1,2)	principal stresses at the centroids of each finite element.
STRAY(J=3,4)	dummy parameters.

4. NNOD,NEL,NBNOD,NHOL (stream 5) (4I10)

NNOD	number of finite element nodes.
NEL	number of finite elements.
NBNOD,NHOL	dummy parameters.

5. K,X2(I),Y2(I),G1,G2 (stream 5) (I10,2F10.3,2E10.3)

K,G1,G2	dummy parameters.
X2,Y2	co-ordinates of finite element nodes (km).

6. K,(NODEL(I,J),J=1,3),E,P,DEN,VISC (stream 5) (4I10,E10.3,2F10.3,E10.3)

K,E,P,DEN,VISC	dummy parameters.
NODEL	finite element nodes corresponding to each element.

7. NTBC (stream 1) (I10)

NTBC	controls boundary conditions on finite difference grid. Details are given in the listing.

8. NDAT (stream 1) (I10)

NDAT	equal to 0 if contours of pressures to be plotted, equal to 1 if superposed grids are to be plotted, and takes other values for no plotter output to be produced.

9. NBC4 (stream 1) (I10)

NBC4	number of finite element node permeabilities and diffusion storages to be read in and transferred to finite difference grid.

10. K,PERM(K),STOR(K) (stream 1) (I10,2E10.3)

K	number of finite element node.
PERM	permeability at node.
STOR	diffusion storage at node.

11. NBC5 (stream 1) (I10)

NBC5	number of finite difference permeabilities and diffusion storages to be read in.

12. K,PERM2(K),STOR2(K) (stream 1) (I10,2E10.3)

K	finite difference grid point.
PERM2	finite difference grid point permeability.
STOR2	finite difference grid point diffusion storage.

13. NBC (stream 1) (I10)

NBC	number of finite element initial pressures.

14. K,PPX(K) (stream 1) (I10,E10.3)

K	finite element node.
PPX	finite element node initial pressure.

15. NBC (stream 1) (I10)

NBC	number of finite element constant pressure conditions.

16. K,PPX(K) (stream 1) (I10,E10.3)

K	finite element node.
PPX	finite element node constant pressure condition.

17. NBC2 (stream 1) (I10)

NBC2	number of finite difference constant pressure conditions.

18. K,PP(K) (stream 1) (I10,E10.3)

K	number of finite difference grid point.
PP	constant pressure condition.

19. NBC3 (stream 1) (I10)

NBC3	number of finite difference initial pressures.

20. K,PP(K) (stream 1) (I10,E10.3)

K	number of finite difference grid point.
PP	grid point initial pressure.

Output Data (stream 6)

1. Details of the transfers from finite element to finite difference nodes of initial pressures and constant pressure conditions.

2. Finite difference grid data.

3. Information regarding the state of the pressure field during the iteration process (top ten rows of nodes only). N.B. The upper boundary of the grid forms the right-hand boundary in these plots.

4. An alphanumeric representation of the final pressure distribution.

5. Information regarding the calculation of the final pressure at each finite element centroid.

6. Finite element effective stresses, and the results of failure tests that prove positive.

7. Plotter output (according to the value of NDAT).

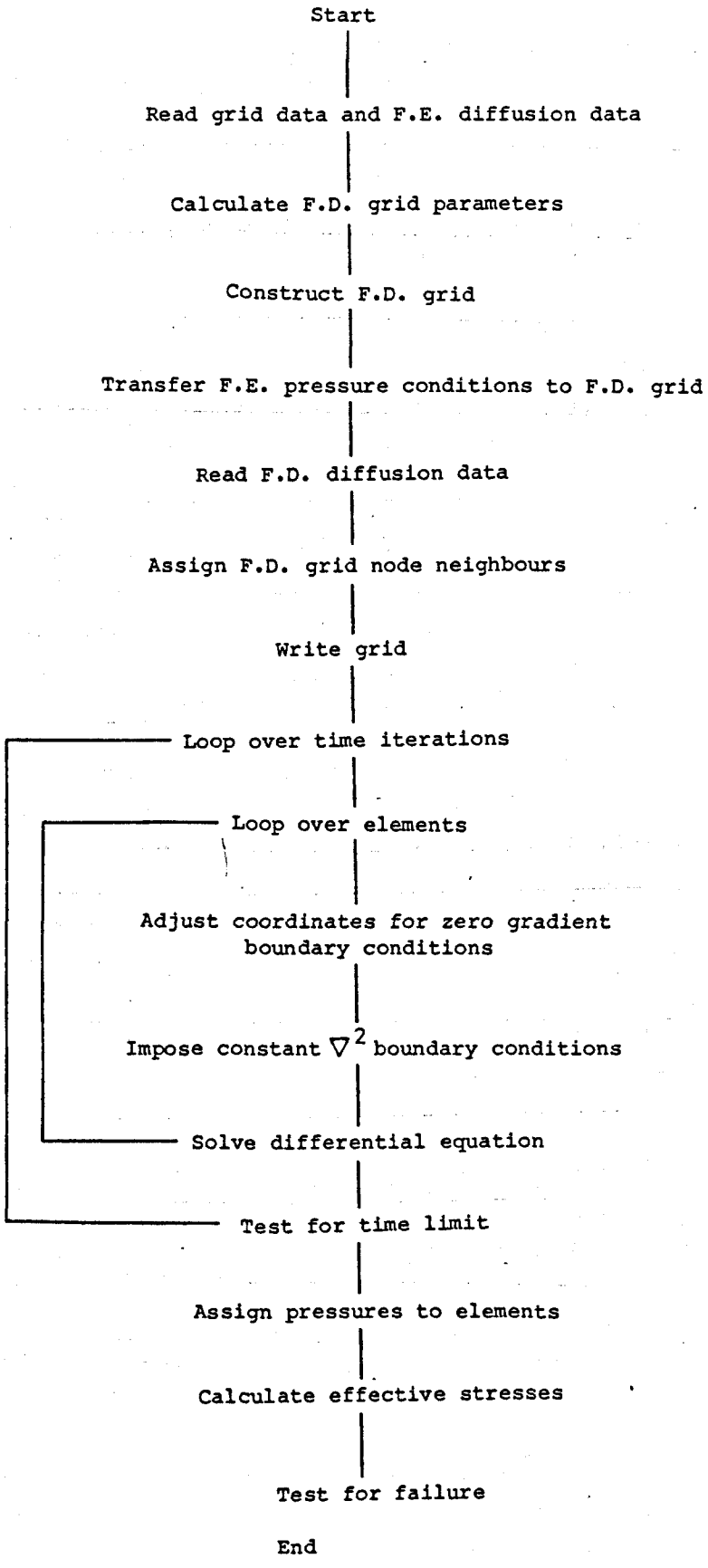

Figure A8.1 Flow diagram

```
C****** FINITE DIFFERENCE PROGRAM SUPERPOSES REGULAR GRID OVER
C       F.E. GRID, CALCULATES PORE PRESSURES AND ASSIGNS VALUES
C       TO F.E. ELEMENTS . COULOMB-MOHR AND MODIFIED GRIFFITH
C       FAILURE CRITERIA ARE THEN APPLIED WITH THE
C       EFFECTIVE STRESSES
C
      PROGRAM PRES(INPUT,OUTPUT,F1,F2,F6,F5,F4,TAPE1=F5,TAPE2=F2,
     1 TAPE6=OUTPUT,TAPE3=INPUT,TAPE5=F1,TAPE4=F4)
      COMMON MR
      DIMENSION X(500),DEL2A(500),Y(500),T(500),KDJ(10,500),IBC(500)
     1,PP(500),STOR(500),PERM2(500),PPX(500),IND(500),INDA(500)
     2,PERM(500),NODEL(1000,3),IBNOD(100),STRAY(1000,4),STRAY1(1000,2)
     3,DEL2(500),X2(500),STOR2(500),Y2(500),ANGLE(2),DISTAN(3),KK(3)
C*     READ NO. OF NODES AND ELEMENTS
      READ(4,1000) NNOD,NEL,DEV
 1000 FORMAT(2I10,F10.3)
C*     READ COORDS (KM)
      READ(4,1005) (X(I),Y(I),I=1,NNOD)
 1005 FORMAT(2F10.3)
C*     READ STRESSES (CGS)
      READ(4,1010)(((STRAY(I,J),J=1,4),I=1,NEL))
 1010 FORMAT(4E11.3)
C*     READ NO. OF NODES,ELEMENTS AND INITIAL PRESSURES
      READ(5,1015) NNOD,NEL,NBNOD,NHOL
C*     READ COORDS (KM)
      READ(5,1020) (K,X2(I),Y2(I),G1,G2,I=1,NNOD)
C*     READ NODAL DISTRIBUTION
      READ(5,1025) (K,(NODEL(I,J),J=1,3),E,P,DEN,VISC,I=1,NEL)
 1015 FORMAT(4I10)
 1020 FORMAT(I10,2F10.3,2E10.3)
 1025 FORMAT(4I10,E10.3,2F10.3,E10.3)
C*      FAILURE PARAMETERS
      TS=-0.5E9
      XMU=0.7
      SS=1.0E9
C      TOTAL TIME IN SECS
      TEND=2.0E7
C*      SURFACE BOUNDARY HAS ZERO PRESSURE GRADIENT B.C.S.
C*      NTBC=1 MEANS BOTH REMOTE BOUNDARIES HAVE CONSTANT DEL2P B.C.S.
C*      NTBC=2 ALL SUBSURFACE BOUNDARIES HAVE CONSTANT DEL2P B.C.S.
C*      OTHER VALUES GIVE ZERO PRESSURE GRADIENT B.C.S ON L.H.S. BOUNDARY
C*      AND CONSTANT PRESSURE B.C.S ON OTHER SUBSURFACE BOUNDARIES
      READ(1,1050) NTBC
C*      NDAT=0 MEANS CLCMP PRESSURE PLOTS PRODUCED
C*      NDAT=1 MEANS  CLCMP GRID PLOT PRODUCED
      READ(1,1050) NDAT
      DO 5 I=1,500
      PERM2(I)=0.0
      STOR(I)=0.0
      DEL2A(I)=0.0
      DEL2(I)=0.0
      STOR2(I)=0.0
    5 PERM(I)=0.0
      NLP=1
C
C***** READ F.E. PERMEABILITIES AND DIFFUSION STORAGES OF ELEMENTS
      READ(1,1050) NBC4
      IF(NBC4.EQ.0) GOTO 10
      READ(1,1035) (K,PERM(K),STOR(K),I=1,NBC4)
   10 CONTINUE
```

```
 1030 FORMAT(10I10)
 1035 FORMAT(I10,2E10.3)
C
C***** CALCULATE F.D. GRID
      XMAX=0.0
      YMAX=0.0
      YMIN=0.0
      XMIN=0.0
      DO 15 I=1,NNOD
      XMAX=AMAX1(XMAX,X2(I))
      YMAX=AMAX1(YMAX,Y2(I))
      XMIN=AMIN1(XMIN,X2(I))
   15 YMIN=AMIN1(YMIN,Y2(I))
      DMAX=AMAX1(XMAX,YMAX)
      EX=DMAX*2.4
      N1=0
      N2=0
      N3=0
      N4=0
      XAV=(XMIN+XMAX)/2.0
      YAV=(YMAX+YMIN)/2.0
      XDIF=XMAX-XMIN
      YDIF=YMAX-YMIN
      DO 35 I=1,NNOD
      IF(X2(I).GT.XAV) GOTO 25
      IF(Y2(I).LT.YAV) GOTO 20
      N1=N1+1
      GOTO 35
   20 N3=N3+1
      GOTO 35
   25 IF(Y2(I).LT.YAV) GOTO 30
      N2=N2+1
      GOTO 35
   30 N4=N4+1
   35 CONTINUE
      RAT=XDIF/YDIF
      AV=SQRT(FLOAT(NNOD))
      NNXX=IFIX((2.0*AV*RAT)/(RAT+1.0)*1.25)+1
      NNYY=IFIX((2.0*AV)/(RAT+1.0)*1.25)+1
      NN=NNXX*NNYY
      RAT=FLOAT(N1+N3)/FLOAT(NNOD)
      IF(RAT.LT.0.25) RAT=0.25
      IF(RAT.GT.0.75) RAT=0.75
      NX1=IFIX(RAT*FLOAT(NNXX))
      NX2=NNXX-NX1
      RAT=FLOAT(NNOD)/FLOAT(N1+N2)
      IF(RAT.GT.4.0) RAT=4.0
      IF(RAT.LT.1.34) RAT=1.33
      NY2=IFIX(FLOAT(NNYY)/RAT)
      NY1=NNYY-NY2
      SCAX=(XAV-XMIN)/(NX1)
      SCAY=(YMAX-YAV)/(NY2)
      SCAX1=(XMAX-XAV)/(NX2)
      SCAY1=(YAV-YMIN)/(NY1)
      DT=AMIN1(SCAX,SCAY,SCAX1,SCAY1)
      DT=DT*1.0E5
      DO 40 I=1,NNOD
      X2(I)=X2(I)*1.0E5
   40 Y2(I)=Y2(I)*1.0E5
      DO 45 I=1,500
```

```
      X(I)=0.0
      Y(I)=0.0
      IND(I)=0
      INDA(I)=0
      PP(I)=0.0
      PPX(I)=0.0
   45 IBC(I)=0
C****  CONSTRUCT GRID IN CM
      XC=XMIN
      XCL=SCAX*5.0
      K=1
      NX2A=NX1-1
      NY2A=NY2-1
      NX1B=NX2+1
      NY1B=NY1+1
      XNL=EXP(ALOG(EX)/(FLOAT(NX1B)-SCAX))
      XAL=XNL**SCAX
      YNL=EXP(ALOG(EX)/(FLOAT(NY1B)-SCAY))
      YAL=YNL**SCAY
      MM=0
      DO 55 I=1,NNXX
      NI=I+MM
      YC=YMAX
      YCL=SCAY*5.0
      PWDX=XNL**(NI-NX1+2)-XNL**(NI-NX1+1)
      M=0
      DO 50 J=1,NNYY
      N=J+M
      X(K)=XC*1.0E5
      Y(K)=YC*1.0E5
      K=K+1
      PWD=YNL**(N-NY2+2)-YNL**(N-NY2+1)
      IF(J.GE.NY2A) SCAY1=PWD/YAL
      IF(J.GE.(NY2)) YCZ=YC-SCAY1
      IF(J.LT.(NY2)) YCZ=YC-SCAY
      IF(J.EQ.1) YCZ=YCZ+(SCAY)/3.0
      YCT=YC-YCZ
      IF(YCL.LT.YCT) YCZ=YC-YCL
      IF(YCT.GT.(2.0*YCL)) M=M+1
      YCL=(YC-YCZ)*5.0
   50 YC=YCZ
      IF(I.GE.NX2A) SCAX1=PWDX/XAL
      IF(I.GE.(NX1)) XCZ=XC+SCAX1
      IF(I.LT.(NX1)) XCZ=XC+SCAX
      IF(I.EQ.1) XCZ=XCZ-(SCAX/3.0)
      XCT=XCZ-XC
      IF(XCL.LT.XCT) XCZ=XCL+XC
      IF(XCT.GT.(2.0*XCL)) MM=MM+1
      XCL=(XCZ-XC)*5.0
   55 XC=XCZ
C*      READ F.D. PERMEABILITIES AND DIFFUSION STORAGES
      READ(1,1050) NBC5
      IF(NBC5.EQ.0) GOTO 60
      READ(1,1035)(K,PERM2(K),STOR2(K),I=1,NBC5)
C*      TRANSFER F.E. DIFFUSION PARAMETERS
   60 IF(NBC4.EQ.0) GOTO 75
      L=0
   65 L=L+1
      IF(PERM(L).EQ.0.0.AND.STOR(L).EQ.0.0) GOTO 65
      XCC=(X2(NODEL(L,1))+X2(NODEL(L,2))+X2(NODEL(L,3)))/3.0
```

```
      YCC=(Y2(NODEL(L,1))+Y2(NODEL(L,2))+Y2(NODEL(L,3)))/3.0
      DIST=1.0E20
      DO 68 J=1,NN
      CALL DISCAL(X,Y,XCC,YCC,J,JJ,DIST,MR)
   68 IF(MR.EQ.1) GOTO 70
   70 PERM2(JJ)=PERM(L)
      STOR2(JJ)=STOR(L)
      IF(L.LT.NEL) GOTO 65
   75 DO 80 L=1,NN
      PERM(L)=PERM2(L)
   80 STOR(L)=STOR2(L)
C******
C*     READ F.E. INITIAL PRESSURES AND CONSTANT PRESSURE BOUNDARY
C*     CONDITIONS APPLIED AT NODES, IN ASCENDING ORDER OF PRESSURE
      PPMAX=0.0
      WRITE(6,1038)
 1038 FORMAT('1')
      DO 110 LK=1,2
      READ(1,1050) NBC
      IF(NBC.EQ.0) GOTO 110
      DO 105 I=1,NBC
      READ(1,1055) K,PPX(K)
      PPMAX=AMAX1(PPMAX,PPX(K))
      DIST=1.0E20
      DO 95 J=1,NN
      CALL DISCAL(X,Y,X2(K),Y2(K),J,JJ,DIST,MR)
   95 IF(MR.EQ.1) GOTO 100
  100 PP(JJ)=PPX(K)
      IF(LK.EQ.2) WRITE(6,1040) K,X2(K),Y2(K),JJ,X(JJ),Y(JJ)
 1040 FORMAT(/2X,'INITIAL PRESSURE ON F.E. NODE',I4,' AT ',
     +2E10.3,' WILL BE PLACED ON F.D. NODE',I4,' AT',2E10.3/)
      IF(LK.EQ.1) WRITE(6,1045) K,X2(K),Y2(K),JJ,X(JJ),Y(JJ)
 1045 FORMAT(/2X,'CONSTANT PRESSURE CONDITION ON F.E. NODE',I4,' AT',
     +2E10.3,' WILL BE PLACED ON F.D. NODE',I4,' AT ',2E10.3/)
      IF(LK.EQ.2) GOTO 105
      IBC(JJ)=1
  105 CONTINUE
  110 CONTINUE
 1050 FORMAT(I10)
 1055 FORMAT(I10,E10.3)
C*      READ EXTRA F.D. CONSTANT PRESSURE BOUNDARY CONDITIONS
      READ(1,1050) NBC2
      IF(NBC2.EQ.0) GOTO 120
      DO 115 I=1,NBC2
      READ(1,1055) K,PP(K)
      PPMAX=AMAX1(PP(K),PPMAX)
  115 IBC(K)=1
C*      READ EXTRA F.D. INITIAL PRESSURES
  120 READ(1,1050) NBC3
      IF(NBC3.EQ.0) GOTO 130
      DO 125 I=1,NBC3
      READ(1,1055) K,PP(K)
  125 PPMAX=AMAX1(PP(K),PPMAX)
  130 PPMAX=PPMAX*1.1
      STORX=0.0
      PERMX=0.0
C      ASSIGN NODE NEIGHBOURS
      DO 175 K=1,NN
      KDJ(1,K)=K-1
      KDJ(2,K)=K+1
```

```
      KDJ(3,K)=K-NNYY
      KDJ(4,K)=K+NNYY
      IF(K.EQ.1) GOTO 160
      IF(K.EQ.NN) GOTO 165
      IF((Y(K-1)-Y(K)).GT.0.0) GOTO 140
      KDJ(1,K)=KDJ(2,K)
      IND(K)=1
  140 IF((Y(K)-Y(K+1)).GT.0.0) GOTO 145
       KDJ(2,K)=KDJ(1,K)
      IBC(K)=1
      IND(K)=-1
  145 IF((K-NNYY).GT.0) GOTO 150
      KDJ(3,K)=KDJ(4,K)
      INDA(K)=1
  150 IF((K+NNYY).LE.NN) GOTO 155
      KDJ(4,K)=KDJ(3,K)
      IBC(K)=1
      INDA(K)=-1
  155 GOTO 170
  160 KDJ(1,K)=KDJ(2,K)
      KDJ(3,K)=KDJ(4,K)
      IND(K)=1
      INDA(K)=1
      GOTO 170
  165 KDJ(2,K)=KDJ(1,K)
      KDJ(4,K)=KDJ(3,K)
      IND(K)=-1
      INDA(K)=-1
      IBC(K)=1
  170 PERM(K)=PERM(K)*10.0
      IF(NLP.EQ.17) NLP=0
      NLP=NLP+1
      STORX=AMAX1(STORX,STOR(K))
  175 PERMX=AMAX1(PERMX,PERM(K))
      FAC1=PERMX*STORX
C******
C       PRINT GRID
      WRITE(6,1060)
 1060 FORMAT(50X,'FINITE DIFFERENCE GRID'/)
      WRITE(6,1065)
 1065 FORMAT(/8X,'NODE',5X,'X',9X,'Y',15X,'NODE NEIGHBOURS',3X,
     +2X,'PERM',6X,'STOR',5X,'PRESSURE',4X,'CONSTANT?'/)
      DO 180 I=1,NN
  180 WRITE(6,1070) I,X(I),Y(I),(KDJ(J,I),J=1,4),PERM(I),STOR(I),
     +PP(I),IBC(I)
 1070 FORMAT(I10,2X,2E10.3,2X,4I6,3E10.3,I10)
      IF(NDAT.EQ.1) CALL CLCMP(X,Y,X2,Y2,NODEL,XMAX,XMIN,YMAX,
     +YMIN,NNOD,NN,NEL)
C
C*****
C       START TIME ITERATIONS
      IOF=0
      TIME=0.0
      IT=0
      NIT=0
      IF(NDAT.EQ.0) CALL PAPER(1)
      IF(NDAT.EQ.0) CALL CTRMAG(10)
      NC=-1
      NC1=NC
      NC2=0
```

```
C****** SOLVE DIFFERENTIAL EQUATION
  185 DO 200 L=1,NN
      DEL2(L)=DEL2A(L)
      PPX(L)=0.0
      IJ=IBC(L)
 1075 FORMAT(2I10)
      IF(IJ.NE.1) GO TO 190
      PPX(L)=PP(L)
      GOTO 200
  190 IA=KDJ(1,L)
      IB=KDJ(2,L)
      IC=KDJ(3,L)
      ID=KDJ(4,L)
      PA=PP(IA)
      PB=PP(IB)
      PC=PP(IC)
      PD=PP(ID)
      P0=PP(L)
      YA=Y(IA)
      YB=Y(IB)
      XC=X(IC)
      XD=X(ID)
      X0=X(L)
      Y0=Y(L)
C***** ADJUST COORDINATES FOR ZERO GRADIENT B.C.'S
      IF(IND(L).EQ.1) YA=2.0*Y0-YB
      IF(INDA(L).EQ.1) XC=2.0*X0-XD
      FAC=PERM(L)*STOR(L)
      DELT=(DT**2.0)/10.0/FAC1
      GRAD2=((PA-P0)/(YA-Y0)-(P0-PB)/(Y0-YB))/
     +((YA-YB)/2.0)+
     +((PC-P0)/(XC-X0)-(P0-PD)/(X0-XD))/
     +((XC-XD)/2.0)
      IF(NTBC.NE.1.AND.NTBC.NE.2) GOTO 195
      IF(NTBC.EQ.1.AND.INDA(L).EQ.1) GOTO 195
C***** IMPOSE CONSTANT DEL2 B.C.'S
      IF(IND(L).EQ.0.AND.INDA(L).EQ.0) GOTO 195
      IF(INDA(L).EQ.1) GRAD2=DEL2(L+NNYY)
      IF(INDA(L).EQ.-1) GRAD2=DEL2(L-NNYY)
      IF(IND(L).EQ.1) GRAD2=DEL2(L+1)
      IF(IND(L).EQ.-1) GRAD2=DEL2(L-1)
      IF(L.EQ.1) GRAD2=DEL2(NNYY+2)
      IF(L.EQ.NNYY) GRAD2=DEL2(2*NNYY-1)
      N6=NN-NNYY-1
      N7=N6+2
      N8=NN-2*(NNYY)+2
      IF(L.EQ.NN) GRAD2=DEL2(N6)
      IF(L.EQ.N7) GRAD2=DEL2(N8)
  195 IF(GRAD2.LT.0.0.AND.GRAD2.GT.-1.0E-9) GRAD2=0.0
      DEL2A(L)=GRAD2
      DEL=GRAD2*DELT
      DEL=DEL*FAC
      PPX(L)=PP(L)+DEL
  200 CONTINUE
      DO 205 I=1,NN
      PP(I)=0.0
      PP(I)=PPX(I)
      IF(PP(I).GT.PPMAX) IOF=1
      PPX(I)=0.0
  205 IF(PP(I).LT.1.0E-70) PP(I)=0.0
```

```
      TIME=TIME+DELT
 1085 FORMAT(10E10.3)
      NIT=NIT+1
      IT=IT+1
      NPR=TEND/DELT/20.0
      IF(IT.LT.11) GOTO 210
      IF(NIT.NE.NPR) GOTO 215
      NIT=0
  210 DTIME=TIME/60.0/60.0/24.0
      NC1=NC1*NC
      CALL PLPRNT(NNXX,PP,NNYY,IT,DTIME)
      IF(NC1.LT.0.AND.NDAT.EQ.0) CALL PLCONT(NNXX,PP,NNYY,PPMAX,DTIME,
     +XMAX,XMIN,YMAX,YMIN,X,Y,NC2)
      IF(NC2.EQ.4) NC2=0
  215 IF(IOF.EQ.1) GOTO 220
      IF(TIME.LT.TEND) GOTO 185
C
C*****
  220 CALL PLPRNT(NNXX,PP,NNYY,IT,DTIME)
      TINC=DELT/60.0/60.0/24.0
      IF(NDAT.EQ.0) CALL GREND
      WRITE(6,1090) TINC
 1090 FORMAT(10X,'TIME INCREMENT= ',E10.3,'  DAYS')
C       SOLUTION FOUND
      WRITE(6,1095) IT
 1095 FORMAT(2X,'NUMBER OF ITERATIONS=',I10)
      TIME=TIME/60.0/60.0/24.0
      WRITE(6,1100) TIME
 1100 FORMAT(10X,'TOTAL TIME = ',E10.3,'  DAYS'//)
      CALL PLOT(NN,X,Y,PP,XDIF,YDIF,XMIN,YMIN,PPMAX)
      NNOD1=NNOD1+1
      IF(IOF.EQ.1) GOTO 265
C       ASSIGN PRESSURES TO ELEMENTS
      JJ=0
      ANG=0.0
      WRITE(6,1105)
 1105 FORMAT(//73X,'FINAL')
      WRITE(6,1110)
 1110 FORMAT(6X,'ELEMENT',7X,'BASED ON PP NODES:',8X,
     +'WHOSE PRESSURES ARE:',6X,'PRESSURE'/)
      DO 250 I=1,NEL
      PPX(I)=0.0
      X1=X2(NODEL(I,1))
      X2A=X2(NODEL(I,2))
      X3=X2(NODEL(I,3))
      Y1=Y2(NODEL(I,1))
      Y2A=Y2(NODEL(I,2))
      Y3=Y2(NODEL(I,3))
      XXC=(X1+X2A+X3)/3.0
      YYC=(Y1+Y2A+Y3)/3.0
      DO 235 K=1,2
      DIST=1.0E10
      DO 230 J=1,NN
      XD=X(J)/1.0E5
      YD=Y(J)/1.0E5
      IF(XD.GT.XMAX.OR.XD.LT.XMIN) GOTO 230
      IF(YD.GT.YMAX.OR.YD.LT.YMIN) GOTO 230
      IF(K.EQ.1) GOTO 225
      IF(J.EQ.KK(1)) GOTO 230
  225 CALL DISCAL(X,Y,XXC,YYC,J,JJ,DIST,MR)
```

```
  230 CONTINUE
      CALL ANGCAL(X,Y,XXC,YYC,ANG,JJ)
      ANGLE(K)=ANG
      DISTAN(K)=DIST
      KK(K)=JJ
  235 CONTINUE
      AVANG=(ANGLE(1)+ANGLE(2))/2.0
      IF(ABS((AVANG-ANGLE(1))).LT.90.0) AVANG=AVANG+180.0
      AVA1=AVANG-45.0
      AVA2=AVANG+45.0
      IF(AVA1.GE.360.0) AVA1=AVA1-360.0
      IF(AVA1.LT.0.0) AVA1=AVA1+360.0
      IF(AVA2.GE.360.0) AVA2=AVA2-360.0
      AVAN1=AMIN1(AVA1,AVA2)
      AVAN2=AMAX1(AVA1,AVA2)
      DIST=1.0E20
      DO 240 L=1,NN
      XD=X(L)/1.0E5
      YD=Y(L)/1.0E5
      IF(XD.GT.XMAX.OR.XD.LT.XMIN) GOTO 240
      IF(YD.GT.YMAX.OR.YD.LT.YMIN) GOTO 240
      L2=L
      IF(L.EQ.KK(1).OR.L.EQ.KK(2)) GOTO 240
      CALL ANGCAL(X,Y,XXC,YYC,ANG,L2)
      IF(ANG.LT.AVAN1) GOTO 240
      IF(ANG.GT.AVAN2) GOTO 240
      CALL DISCAL(X,Y,XXC,YYC,L,LL,DIST,MR)
  240 CONTINUE
      DISTAN(3)=DIST
      KK(3)=LL
      DO 245 M=1,3
  245 DISTAN(M)=1.0/DISTAN(M)
      PPX(I)=(PP(KK(1))*DISTAN(1)+PP(KK(2))*DISTAN(2)+PP(KK(3))*DISTAN(3
     +))/(DISTAN(1)+DISTAN(2)+DISTAN(3))
  250 WRITE(6,1115) I,KK(1),KK(2),KK(3),PP(KK(1)),PP(KK(2)),
     +PP(KK(3)),PPX(I)
 1115 FORMAT(4I10,4E10.3)
C***** PRINT PRESSURES
C***** APPLY PRESSURES TO FAILURE CRITERIA
      WRITE(6,1120)
 1120 FORMAT(/3X,'ELEMENT PORE PRESSURE  MAX + MIN STRESSES',
     +5X,'EFFECTIVE STRESSES'/)
      DO 260 I=1,NEL
      STRAY1(I,1)=STRAY(I,1)+PPX(I)
      STRAY1(I,2)=STRAY(I,2)+PPX(I)
      WRITE(6,1125) I,PPX(I),STRAY(I,1),STRAY(I,2),STRAY1(I,1)
     +,STRAY1(I,2)
 1125 FORMAT(I6,6X,E10.3,2X,E10.3,3(1X,E10.3))
      IF(STRAY(I,1).GT.0.0.OR.STRAY(I,2).GT.0.0) GOTO 255
      CALL SAFAIL(STRAY1(I,1),STRAY1(I,2),TS,I)
  255 CALL FAIL(STRAY1(I,1),STRAY1(I,2),I,TS,XMU,Q)
  260 CALL SLIPS(STRAY1(I,1),STRAY1(I,2),XMU,SS,I,C)
      WRITE(6,1130)
 1130 FORMAT(/2X'PROGRAM COMPLETED'/)
      GOTO 270
  265 WRITE(6,1135)
 1135 FORMAT(/2X,'TIME STEP TOO LARGE'/)
  270 CONTINUE
      STOP
      END
```

```
C
      SUBROUTINE FAIL(S1,S2,I,TS,MU,Q)
      REAL MU,IFC,L
      DATA A,B,C,D,E,BLANK/1HA,1HB,1HC,1HD,1HE,1H /
      S1=-S1
      S2=-S2
C      +VE STRESSES ARE COMPRESSIONAL
C      SO P IS SIGHMA2 AND R IS SIGHMA1
      T=TS
      FAC=-4.19
      L=BLANK
      P=AMAX1(S1,S2)
      R=AMIN1(S1,S2)
      SC=FAC*T
C      FAILURE CRITERIA
      OCFC=(P-R)*(P-R)+8.0*T*(P+R)
      IFC=P*P+P*(6.0*R-4.0*SC)+(R*R-4.0*R*SC)
      ALPHA=(SQRT(1.0+MU**2))/MU
      BETA=(4.0*T*SQRT(1.0-(SC/T))/MU)+2.0*SC
      CCFC=BETA/(1.0-ALPHA)-R*(1.0+ALPHA)/(1.0-ALPHA)
C      DEFINE POSSIBLE CLOSED CRACK REGION
      THETA=0.5*ATAN(1.0/MU)
      DE=SC/(COS(THETA)**2)-R*(TAN(THETA)**2)
C      FIND INTERSECTION OF OCFC AND CCFC
      AA=(ALPHA+1.0)/(ALPHA-1.0)
      BB=BETA/(1.0-ALPHA)
      CC=8.0*T
      F=(AA-1.0)**2
      G=2.0*BB*(AA-1.0)+CC*(AA+1.0)
      H=BB*(BB+CC)
      DC=(-G+SQRT(G**2-4.0*F*H))/2.0/F
C      DEFINE MIN. SIG1 FOR IFC TO BE EFFECTIVE
      DB=SC-2.0*T+2.0+SQRT(T*(2.0*T-SC))
C      DEFINE MAX. SIG1 FOR IFC TO BE EFFECTIVE
      DD=SC*((2.0*ALPHA*(ALPHA+1.0))/(2.0*ALPHA**2-1.0))
C      TEST FOR FAILURE REGION
      D=P+3.0*R
      IF(D.LT.0.0) GOTO 2
      IF(P.LT.SC) GOTO 3
      IF(R-SC) 4,4,9
C
C      TENSIONAL REGION
    2 CONTINUE
      K=1
      IF(R.LT.T) K=-1
      GOTO 100
C
C      OPEN CRACK REGION
    3 K=2
      IF(OCFC.GT.0.0) K=-2
      GOTO 100
C
C      INTERMEDIATE REGION
    4 K=3
C      TEST FOR SUBREGION
      IF(P.GT.DE) GOTO 5
C      OPEN CRACK
      L=A
      IF(OCFC.GT.0.0) K=-3
      GOTO 100
```

```
C       TEST FOR SUBREGION
    5 IF(R.GT.DC) GOTO 6
C       CLOSED CRACK
        L=B
        IF(P.GT.CCFC) K=-3
        GOTO 100
C       TEST FOR SUBREGION
    6 IF(P.GT.DB) GOTO 7
C       OPEN CRACK
        L=C
        IF(OCFC.GT.0.0) K=-3
        GOTO 100
C       TEST FOR SUBREGION
    7 IF(P.GT.DD) GOTO 8
C       INTERMEDIATE
        L=D
        IF(IFC.GT.0.0) K=-3
        GOTO 100
C       CLOSED CRACK
    8 L=E
        IF(P.GT.CCFC) K=-3
        GOTO 100
C
C       CLOSED CRACK REGION
    9 K=4
        L=BLANK
        IF(P.GT.CCFC) K=-4
C
  100 CONTINUE
C       NEGATIVE VALUES OF K DENOTE FAILURE
        IF(K.GT.0) GOTO 2001
        WRITE(6,2000)I, K,L
        IF(K.LT.0.0)Q=FLOAT(K)
 2000 FORMAT(2X,'ELEMENT',I4,' FAILED IN STRESS REGION',I4,2X,A1)
 2001 CONTINUE
        S1=-S1
        S2=-S2
        RETURN
        END
C
        SUBROUTINE SLIPS(SS1,SS2,XMU,SS,I,C)
        BETA=0.0
        S1=-SS1
        S2=-SS2
C****** COMPRESSIONAL STRESSES ARE NOW POSITIVE
        ANG=0.0
        K=0
        XINT=-SS/XMU
        IF(S1.LT.XINT.OR.S2.LT.XINT) K=4
        IF(K.EQ.4) GOTO 1
        SUM=S1+S2
        IF(S1.GT.S2) GOTO 2
        SS1=S1
        S1=S2
        S2=SS1
    2 CONTINUE
        DIF=S1-S2
        SMU=2.0*SS*XMU
        XMU2=1.0+(XMU*XMU)
        W1=SMU-SUM
```

```
      TRM1=(SMU-SUM)*(SMU-SUM)
      W2=S2*S1
      W3=SS*SS+(S1*S2)
      TRM2=4.0*XMU2*(SS*SS+(S1*S2))
C      TEST IF MOHR CIRCLE INTERSECTS ENVELOPE
      DIF2=TRM1-TRM2
      IF(DIF2.LT.0.0) GOTO 3
      SQ=SQRT(TRM1-TRM2)
      SIGMA1=(SUM-SMU+SQ)/2.0/XMU2
      SIGMA2=(SUM-SMU-SQ)/2.0/XMU2
      DIF3=(2.0*SIGMA1-SUM)/DIF
      DIF4=(2.0*SIGMA2-SUM)/DIF
      IF(DIF3.GT.1.0.OR.DIF4.GT.1.0) K=10
      IF(DIF3.LT.-1.0.OR.DIF4.LT.-1.0) K=10
      IF(K.EQ.10) GOTO 1
      COSB1=(2.0*SIGMA1-SUM)/DIF
      COSB2=(2.0*SIGMA2-SUM)/DIF
      BETA1=0.5*ACOS(COSB1)
      BETA2=0.5*ACOS(COSB2)
      DO 10 N=1,19
      ANG=BETA*57.29
      IF(BETA.LE.BETA1.AND.BETA.GE.BETA2)K=1
      IF(BETA.GE.BETA1.AND.BETA.LE.BETA2)K=1
    1 CONTINUE
      IF(K.EQ.0) GOTO 10
      WRITE(6,1000) ANG,I,K
      IF(K.NE.0) C=-1.0
      GOTO 3
   10 BETA=BETA+(5.0/57.29)
 1000 FORMAT (2X,'FAULT AT',F4.0,' DEGREES TO SIGMA 1 FAILED IN ELEMENT
     +',I4,' ,K=',I3)
    3 CONTINUE
      RETURN
      END
C

      SUBROUTINE PLPRNT(NNXX,PP,NNYY,IT,DTIME)
      DIMENSION GRAD2(500),DEL(500),PP(500)
C      WRITE UPPER 10 ROWS OF PRESSURES
C      SURFACE IS RIGHT VERTICAL SIDE
      WRITE(6,1000) IT,DTIME
 1000 FORMAT(/10X,'ITERATION',I10,10X,'TIME=',E10.3,' DAYS'/)
      WRITE(6,1005)
 1005 FORMAT(35X,'UPPER 10 ROWS OF PRESSURES:'/)
      DO 5 I=1,500
      GRAD2(I)=0.0
    5 DEL(I)=0.0
      K=1
      L=10
      DO 15 M=1,NNXX
      DO 10 N=K,L
      I=2*K+9-N
   10 GRAD2(I)=PP(N)
      WRITE(6,1010) (GRAD2(J),J=K,L)
      K=K+NNYY
   15 L=K+9
 1010 FORMAT(10E10.3)
      RETURN
      END
C
```

```
      SUBROUTINE PLOT(N,XP,YP,P,XDIF,YDIF,XMIN,YMIN,PMAX)
      DIMENSION K(101,56),ICHAR(26),XP(500),YP(500),P(500)
      DATA IB/1H /,ICHAR/
     + 1HA,1HB,1HC,1HD,1HE,1HF,1HG,1HH,1HI,1HJ,1HK,1HL,
     + 1HM,1HN,1HO,1HP,1HQ,1HR,1HS,1HT,1HU,1HV,1HW,1HX,1HY,1HZ/
     +,IN/1H-/
C      WRITE(6,1000)
 1000 FORMAT(1H1)
      WRITE(6,1010)
 1010 FORMAT(10X,'ALPHANUMERIC REPRESENTATION OF PRESSURES')
      DO 1 I=1,101
      DO 1 J=1,56
    1 K(I,J)=IB
      DO 2 I=1,N
      XP(I)=XP(I)/1.0E5
      YP(I)=YP(I)/1.0E5
      Y=(YP(I)-YMIN)/YDIF*55.0
      IY=56-Y
      IF(IY.GT.56.OR.IY.LT.1) GOTO 4
      X=(XP(I)-XMIN)/XDIF*100.0
      IX=X+1
      IF(IX.GT.101.OR.IX.LT.1) GOTO 4
      IZ=IFIX(P(I)/PMAX*52.0)
      IF(IZ.LT.1) IZ=1
      IF(IZ.GT.26) IZ=26
      K(IX,IY)=ICHAR(IZ)
    4 XP(I)=XP(I)*1.0E5
      YP(I)=YP(I)*1.0E5
    2 CONTINUE
      DO 3 I=1,56
    3 WRITE(6,1001)(K(J,I),J=1,101)
 1001 FORMAT(10X,101A1)
      RETURN
      END
C

      SUBROUTINE ANGCAL(X,Y,XXC,YYC,ANG,JJ)
      DIMENSION X(500),Y(500)
      YDIF=Y(JJ)-YYC
      XDIF=X(JJ)-XXC
      IF(XDIF.EQ.0.0) XDIF=1.0E-10
      IF(YDIF.EQ.0.0) YDIF=1.0E-10
      ANG=ATAN(ABS(YDIF)/ABS(XDIF))*57.29
      IA=0
      IB=0
      IF((X(JJ)-XXC).LT.0.0) IA=1
      IF((Y(JJ)-YYC).LT.0.0) IB=1
      IF(IA.EQ.0) GOTO 5003
      IF(IB.EQ.1) ANG=270.0-ANG
      IF(IB.EQ.0) ANG=270.0+ANG
      GOTO 5004
 5003 IF(IB.EQ.0) ANG=90.0-ANG
      IF(IB.EQ.1)ANG=ANG+90.0
 5004 CONTINUE
      RETURN
      END
C

      SUBROUTINE DISCAL(G,H,XGC,YGC,IJ,IJJ,GDIST,IMR)
```

```
      DIMENSION G(500),H(500)
      IMR=0
      IF(H(IJ).EQ.YGC.AND.G(IJ).EQ.XGC) IMR=1
      IF(IMR.EQ.1) GDIST=0.0
      IF(IMR.EQ.1) IJJ=IJ
      IF(IMR.EQ.1) GOTO 1
      GYDIF=ABS(H(IJ)-YGC)
      GXDIF=ABS(G(IJ)-XGC)
      D0=(GYDIF*GYDIF)+(GXDIF*GXDIF)
      D1=SQRT(D0)
      D2=AMIN1(GDIST,D1)
      IF(D2.EQ.D1) IJJ=IJ
      IF(D2.EQ.D1) GDIST=D2
    1 CONTINUE
      RETURN
      END
C

      SUBROUTINE CLCMP(X,Y,X2,Y2,NODEL,XMAX,XMIN,YMAX,YMIN,
     +NNOD,NN,NEL)
      DIMENSION X(1),Y(1),X2(1),Y2(1),NODEL(1000,3)
      DO 5 I=1,NN
      X(I)=X(I)/1.0E5
    5 Y(I)=Y(I)/1.0E5
      DO 7 I=1,NNOD
      X2(I)=X2(I)/1.0E5
    7 Y2(I)=Y2(I)/1.0E5
      CALL PAPER(1)
      CALL MAP(XMIN,XMAX,YMIN,YMAX)
C*      PLOT F.E. GRID
      DO 1 I=1,NEL
      CALL POSITN(X2(NODEL(I,1)),Y2(NODEL(I,2)))
      DO 2 J=2,3
    2 CALL JOIN(X2(NODEL(I,J)),Y2(NODEL(I,J)))
    1 CALL JOIN(X2(NODEL(I,1)),Y2(NODEL(I,1)))
      CALL CTRMAG(6)
C*      LABEL F.E. NODES
      DO 3 I=1,NNOD
      NP=NNOD+1-I
      CALL POSITN(X2(NP),Y2(NP))
      CALL HSPACE(-1)
      CALL HLINFD(-1)
    3 CALL TYPENI(NP)
C*      PLOT F.D. NODES
      CALL REDPEN
      CALL PTPLOT(X,Y,1,NN,43)
C*      LABEL F.D. NODES
      DO 4 I=1,NN
      NP=NN-I+1
      IF(X(NP).GT.XMAX.OR.X(NP).LT.XMIN) GOTO 4
      IF(Y(NP).GT.YMAX.OR.Y(NP).LT.YMIN) GOTO 4
      CALL POSITN(X(NP),Y(NP))
      CALL HSPACE(1)
      CALL HLINFD(1)
      CALL TYPENI(NP)
    4 CONTINUE
      CALL GREND
      DO 6 I=1,NN
      X(I)=X(I)*1.0E5
    6 Y(I)=Y(I)*1.0E5
```

```
      DO 8 I=1,NNOD
      X2(I)=X2(I)*1.0E5
    8 Y2(I)=Y2(I)*1.0E5
      RETURN
      END
C

      SUBROUTINE PLCONT(NX,PP,NY,PMAX,TIME,XMAX,XMIN,YMAX,YMIN,
     +X,Y,NC)
      DIMENSION PP(1),XX(50),YY(50),H(10),X(1),Y(1),P(40,40)
      NC=NC+1
      NN=NX*NY
      DO 10 I=1,NN
      X(I)=X(I)/1.0E5
   10 Y(I)=Y(I)/1.0E5
      XM=(XMAX-XMIN)/7.0+XMAX
      YX=(YMAX-YMIN)/7.0+YMAX
      YP=(YMAX+YX)/2.0
      XP=(XMAX-XMIN)*0.3+XMIN
      H(1)=PMAX/10.0
      DO 1 I=2,10
    1 H(I)=H(I-1)+H(1)
      I=0
      K=0
      DO 2 M=1,NX
      I=I+1
      J=0
      DO 3 L=1,NY
      J=J+1
    4 K=K+1
      IF(X(K).GT.XMAX.OR.X(K).LT.XMIN) GOTO 4
      IF(Y(K).GT.YMAX.OR.Y(K).LT.YMIN) GOTO 4
      P(I,J)=PP(K)
      XX(I)=X(K)
      YY(J)=Y(K)
      NNY=J
    3 CONTINUE
      NNX=I
    2 CONTINUE
      IF(NC.EQ.1) CALL PSPACE(0.1,0.5,0.5,0.9)
      IF(NC.EQ.2) CALL PSPACE(0.5,0.9,0.5,0.9)
      IF(NC.EQ.3) CALL PSPACE(0.1,0.5,0.1,0.5)
      IF(NC.EQ.4) CALL PSPACE(0.5,0.9,0.1,0.5)
      CALL MAP(XMIN,XM,YMIN,YX)
 1001 FORMAT(3E10.3)
      CALL CONTIA(P,1,NNX,NNX,1,NNY,NNY,H,1,10,XX,YY)
      CALL BOX(XMIN,XMAX,YMIN,YMAX)
      CALL POSITN(XP,YP)
      CALL TYPENE(TIME,3)
      CALL TYPECS(5H DAYS,5)
      IF(NC.EQ.4) CALL FRAME
    5 CONTINUE
      DO 20 I=1,NN
      X(I)=X(I)*1.0E5
   20 Y(I)=Y(I)*1.0E5
      RETURN
      END
C

      SUBROUTINE SAFAIL(P,R,SS,N)
```

```
      ST=SQRT(-4.0*SS)
      S1=AMAX1(P,R)
      S2=AMIN1(P,R)
      DO 10 I=1,19
      DEG=FLOAT(I*5)
      ANG=DEG/57.29
      TAU=ABS((S1-S2)*0.5*SIN(2.0*ANG))
      SIGN=ABS((S1*COS(ANG)*COS(ANG))+(S2*SIN(ANG)*SIN(ANG)))
      SIGNA=(SIGN**0.61)*ST
      SIGNB=(SIGN**0.9)*2.0
      IF(TAU.GE.SIGNA) WRITE(6,1000)N
 1000 FORMAT(2X,'ROCK FAILED IN ELEMENT',I4,
     +' - MURRELL FAILURE CRITERION')
      IF(TAU.GE.SIGNB) WRITE(6,2000) N,DEG
 2000 FORMAT(2X,'ROCK FAILED IN ELEMENT',I4,' ON FAULT AT ANGLE '
     +,F4.0,' DEGREES TO SIGHMA2 - MURRELL-EDMOND FAILURE CRITERION')
   10 IF(TAU.GE.SIGNA.OR.TAU.GE.SIGNB) GOTO 20
   20 CONTINUE
      RETURN
      END
C

****
```

APPENDIX 9

A Test for the Pore Pressure Program

As a test for the computer program PP, its results were compared to the analytical solution given by Howells (1974) for one-dimensional dispersion. As a solution for the flow equation in a homogeneous continuum.

$$\frac{\delta^2 p}{\delta z^2} = 1/k\lambda \ \frac{\delta p}{\delta t} \qquad \text{(A9.1)}$$

where $p = p_o$ at $z = 0$ for all time values, Jaeger (1951) gives:

$$p(z,t) = p_o\left(1-\text{erf}\ \frac{z}{2\sqrt{ct}}\right) \qquad \text{(A9.2)}$$

where

$$\text{erf}\ \beta = 1 - \frac{2}{\sqrt{\pi}} \int_o^{\beta} e^{-u^2}\, du$$

Following Howells and using a value for c (= $k\lambda$) of 1.16×10^5 cm^2 sec^{-1} (equivalent to a permeability, k = 1.16 darcy, and a specific storage, $\lambda = 10^5$ bar), the increase of pore-water pressure with time for two depths has been plotted in Fig. A5.1. The finite-difference pore pressure dispersion behaviour was made effectively one-dimensional by applying a permanent pressure, p_o, all along the upper surface of the rectangular grid, and using zero pressure gradient conditions at the side boundaries. The bottom boundary was made remote, at a depth of 65 kms. The finite-difference grid contained 380 nodes, and the internodal spacing varied between 33 m near the surface to 31.5 km at depth. A time step of 4.63×10^{-3} days (400 secs) was used. The finite difference solutions have also been plotted in Fig. A9.1, and can be seen to correspond almost exactly with the analytical solutions for times and distances typical of induced seismicity.

References

1. Howells, D. A., 1974. The Time for a Significant Change of Pore Pressure. Eng.Geol., 8, 135-138.

2. Jaeger, J. C., 1951. An Introduction of Applied Mathematics. Clarendon Press, Oxford, pp.364-369.

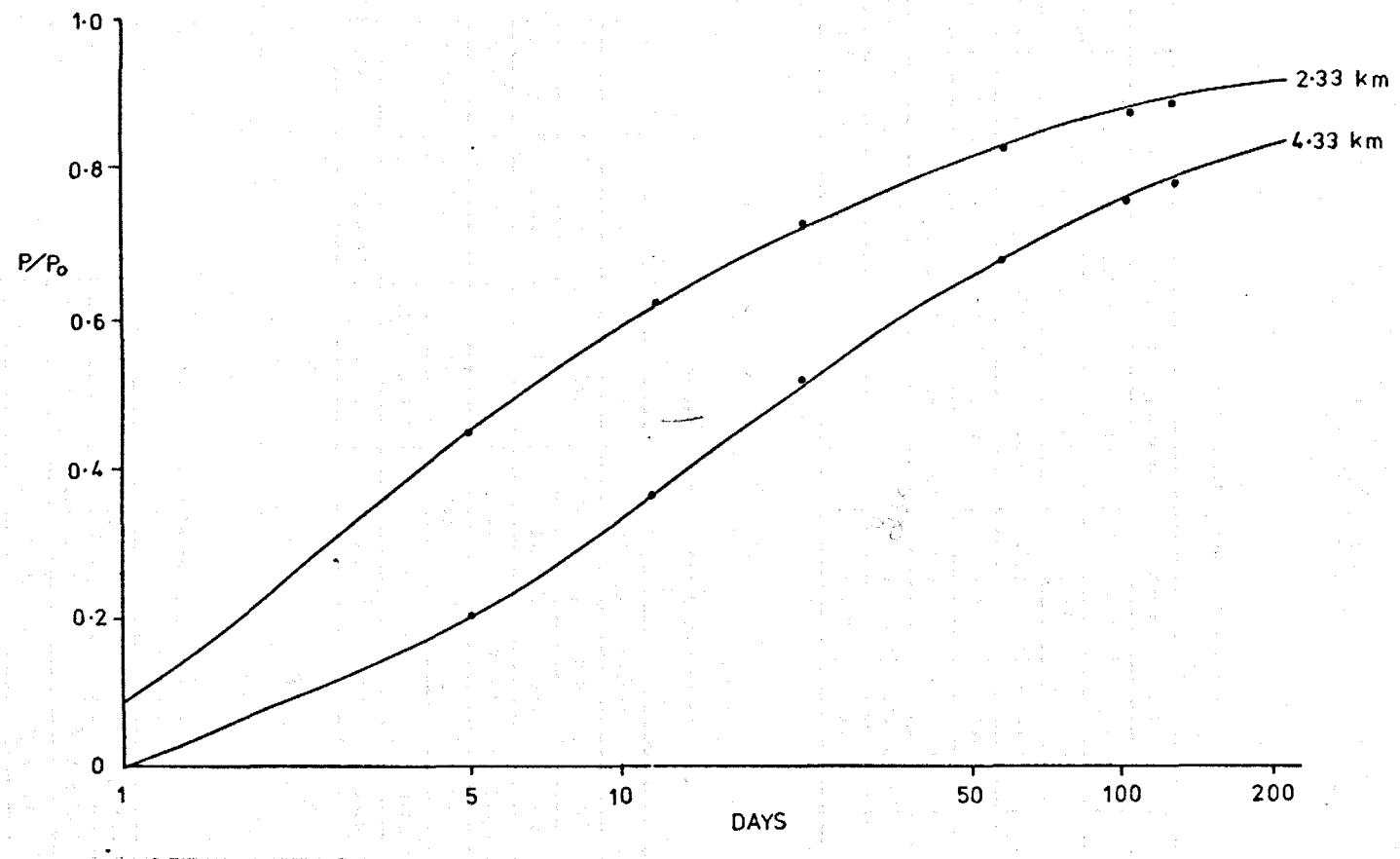

Figure A9.1 Finite difference solutions (dots) compared to the analytical solutions for the increase of pore pressure (P) with time beneath an infinite reservoir of head P .

APPENDIX 10

Conversion table for stress units

	Bars	Kbars	Dynes/cm^2	Kg/cm^2	P.s.i.	Pascals	MPascals
Bars	1.0	0.001	10^6	1.020	14.50	10^5	0.1
Kbars	1000	1.0	10^9	1020	14500	10^8	100
Dynes/cm^2	10^{-6}	10^{-9}	1.0	1.020×10^{-6}	1.450×10^{-5}	0.1	10^{-7}
Kg/cm^2	0.9807	9.807×10^{-4}	0.9807×10^6	1.0	14.22	9.807×10	9.807×10^{-2}
P.s.i.	0.06895	6.895×10^{-5}	6.895×10^4	0.07031	1.0	6895	6.895×10^{-3}
Pascals	10^{-5}	10^{-8}	10	1.020×10^{-5}	1.450×10^{-4}	1.0	10^{-6}
MPascals	10	10^{-2}	10^7	10.20	145.0	10	1.0

Conversion table for length units

	Cm	Inches	Feet	Metres	Km	Miles
Cm	1.0	0.2937	0.0328	0.01	10^{-5}	6.215×10^{-6}
Inches	2.540	1.0	0.0833	0.0254	2.54×10^{-5}	1.578×10^{-5}
Feet	30.48	12.0	1.0	0.3048	3.048×10^{-4}	1.894×10^{-4}
Metres	100.0	39.37	3.281	1.0	10^{-3}	6.215×10^4
Km	10^5	3.937×10^4	3281	10^3	1.0	0.6215
Miles	1.609×10^5	6.336×10^4	5280	1609	1.609	1.0

Conversion table for energy units

	Ergs	Joules	Foot pounds
Ergs	1.0	10^{-7}	7.37×10^{-8}
Joules	10^7	1.0	0.737
Foot pounds	1.356×10^7	1.356	1.0